



**UNIVERSITÀ DEGLI STUDI DI MILANO**

Doctorate School in Chemical Science and Technologies

Doctorate in Industrial Chemistry, Cycle XXVIII

**HYDROPHOBIC COATINGS BASED ON COMMERCIAL  
PERFLUOROPOLYETHERS FOR FOULING MITIGATION  
APPROACH ON A PILOT HEAT EXCHANGER PLANT**

**PhD student: Valeria Oldani, R10152**

**Tutor: Prof. Claudia L. Bianchi**

**Co-Tutor: Dr. Carlo Pirola**

**Coordinator: Prof. Maddalena Pizzotti**

**Prof. Dominique Roberto**

**A.Y. 2014/2015**



A Miriam, Sveva e Ioli



“καί τόδ ἄνωγα, τά μή πατέουσιν ἀμαξαι τά στείβειν, ἐτέρων ἶχνια μή καθ’ομά  
δίφρον ἔλαν μηδ’οίμον ἀνά πλατύν, ἀλλά κελεύθους ατρίπτους εἰ καί  
στειγοτέρην ἐλάσεις.”

Callimaco, Ἄιτια, I, 25-28

...e inoltre, anche a questo ti esorto: a battere le vie che non percorrono i carri  
pesanti, a non spingere il cocchio sulle medesime orme degli altri, né sulla via  
maestra, ma attraverso strade non battute, anche se dovrai guidare lungo una via  
più angusta.

(Trad. C. Carena)



# TABLE OF CONTENTS

GENERAL ABSTRACT .....	I
LIST OF FIGURES.....	XV
LIST OF TABLES .....	XIII
NOMENCLATURE.....	XXVII
PREFACE .....	1
<i>Research motivations</i> .....	1
<i>Research objectives and original contribution</i> .....	2
1 INTRODUCTION.....	5
<i>1.1 The problem of fouling in heat exchangers</i> .....	6
<i>1.2 Heat transfer principles and fouling resistance definition</i> .....	10
<i>1.3 Fouling mitigation strategies</i> .....	15
<i>1.4 Modification of the surface free energy for fouling mitigation</i> .....	18
<i>1.5 Hydrophobic coatings for fouling mitigation</i> .....	22
<i>1.5.1 Hydrophobic fluorinated polymers: perfluoropolyethers</i> .....	25
<i>1.5.2 Perfluoropolyethers/inorganic composite coatings</i> .....	29
2. MATERIALS AND COATINGS PREPARATION .....	39
<i>2.1 Metal substrates</i> .....	40
<i>2.2 Perfluoropolyethers coatings</i> .....	43
<i>2.3 Multilayer coatings</i> .....	48

2.4 Organic/inorganic hybrid coatings.....	50
2.4.1 Two steps preparation method.....	53
2.4.2 One step preparation method.....	57
3. CHARACTERIZATION PROCEDURES .....	63
3.1 Contact angle measurements .....	64
3.2 Coating morphology determination.....	68
3.3 Coating composition and thickness determination.....	69
4. EXPERIMENTAL PROCEDURES AND EQUIPMENT .....	71
4.1 Resistance tests .....	72
4.2 Particulate fouling tests .....	75
4.3 Heat exchanger pilot plant.....	79
4.3.1 Pilot plant- I layout.....	85
4.3.2 Pilot plant- II layout.....	90
4.3.3 Choice of the operating conditions .....	93
4.3.4 Fouling conditions .....	95
5. RESULTS AND DISCUSSION: PERFLUOROPOLYETHERS COATINGS .....	97
5.1 Optimization of the formulation and of the deposition procedures .....	98
5.2 Characterization results.....	102
5.2.1 Morphology, composition and thickness.....	102
5.2.2 Hydrophobicity assessment.....	108
5.3 Coating resistance against erosion.....	112



5.4 Particulate fouling mitigation.....	122
5.5 Pilot plant experimentation.....	124
5.5.1 Anti-fouling assessment of Fluorolink <sup>®</sup> S10.....	124
5.5.2 Anti-fouling assessment of Fluorolink <sup>®</sup> F10.....	142
6. RESULTS AND DISCUSSION: MULTILAYER COATINGS .....	153
6.1 Characterization results.....	154
6.1.1 Morphology, composition and thickness.....	154
6.1.2 Hydrophobicity assessment.....	158
6.2 Coating resistance against erosion.....	159
6.3 Particulate fouling mitigation.....	166
7. RESULTS AND DISCUSSION: HYBRID COATINGS.....	171
7.1 Optimization of the formulation and of the deposition procedures ...	172
7.2 Characterization results.....	176
7.2.1 Morphology, composition and thickness.....	176
7.2.2 Hydrophobicity assessment.....	187
7.3 Coating resistance against erosion.....	190
7.4 Particulate fouling mitigation.....	205
7.5 Pilot plant experimentation.....	208
8. COMPARISON BETWEEN PFPE COATINGS AND COMPOSITE COATINGS.....	219
9. CONCLUSIONS .....	223







# GENERAL ABSTRACT

## Introduction

Heat exchangers are process equipment used for the industrial transmission of heat from a hot fluid to a cold one, across a solid wall, generally indicated as the heat transfer surface [1]. Fouling in heat exchangers consists in the deposition, on the heat transfer surfaces, of particles, solid materials or biological substances, usually dissolved or dispersed in the operating fluids. These unwanted deposits act as thermal insulators, thus provoking a decrease in the heat transfer efficiency of the plants, and may occlude the cross sectional flow areas, inducing consistent increases of pressure drop, which compromise the plant operation as well [2]. To control the fouling phenomenon in heat exchangers, several mitigation strategies are usually applied, at the same time, in industrial plants. These strategies involve the plant design, the treatment of the operating fluids for the removal of the foulant precursors, the mechanical removal of the fouling deposit, etc. [3]. Among all the possible fouling mitigation strategies, the modification of the surface properties of the heat transfer materials is clearly the most interesting one for chemical research. This strategy belongs from the physical methods of fouling control, which aims to interfere with the interactive mechanisms between the foulant precursors dispersed in the operating fluid and the heat transfer surfaces, thus reducing the foulant adhesion [4]. The modification of surface wettability, targeted to make the heat transfer surfaces hydrophobic, emerged as an interesting strategy to control fouling on solid surfaces; it has been in fact demonstrated the less propensity of foulant precursors, dispersed or dissolved in water media, to

interact with such a surface [5]. Several researches applied this concept to the mitigation of fouling in heat exchangers, demonstrating the influence of the hydrophobic surfaces on foulant deposition, in particular during the fouling induction period. The hydrophobic surfaces are in fact able to alter the mechanism of deposition and removal of the foulant particles, occurring during the fouling induction period, acting on the physical forces that regulate these mechanisms [6, 7].

## **Aim of the work**

This PhD research concerns the use of commercial perfluoropolyethers,  $\alpha,\omega$ -substituted with inorganic groups, for the preparation of hydrophobic coatings, targeted to the deposition on stainless steel substrates, for the mitigation of fouling on heat transfer surfaces. Fluoropolymer, in particular polytetrafluoroethylene, have been already considered for the preparation of hydrophobic coatings for fouling mitigation in heat exchangers, however due to their poor stickiness to the substrates and poor resistance against mechanical and chemical stresses, their industrial use was inhibited [4]. New types of fluoropolymer coatings were developed, exploiting novel deposition techniques, able to confer the desired properties to the film [8-10]; however, these coatings procedure are more complex and expensive. Perfluoropolyethers, functionalized at the chain-ends, were never considered for fouling mitigation in heat exchangers. Hence, this PhD research aimed to investigate the possible application of these materials for the preparation of hydrophobic coatings, suitable for fouling mitigation on heat transfer surfaces. We developed three typologies of hydrophobic coatings, all containing perfluoropolyethers (PFPE). Our research was in particular focused on the improvement of the mechanical properties of the polymeric coatings. To achieve our goal we combined the

PFPE with inorganic materials, by means of a multilayer approach or by the synthesis of inorganic-organic composites (hybrid coatings). These reinforcing procedures are surely well-known in literature [11-12], however the combinations proposed in this PhD research are innovative, and above all easy to handle and cost-effective. During the research, in fact, we had to face with preparation of large amounts of the coatings formulations, to coat the heat transfer surfaces of a heat exchanger on pilot scale. The experimentation on the heat exchanger pilot plant represents an important step of the whole research. It permitted the evaluation of the anti-fouling ability of the coatings technology developed on real heat transfer surfaces, with the aim of a possible scale-up at industrial level of the hydrophobic anti-fouling coatings based on the chosen perfluoropolyethers.

## Results and discussion

At first, we investigated the fouling mitigation effect of simple  $\alpha,\omega$ -functionalized PFPE coatings, selecting in particular two PFPE derivatives, commercialized with the names of Fluorolink<sup>®</sup>S10 and Fluorolink<sup>®</sup>F10. These polymers possess chain-ends functional groups consisting of triethoxysilane groups and ammonium phosphate groups. The inorganic chain-ends were exploited to form covalent or polar interactions with functional groups present at the surface of metal surfaces [13]. We optimized a polymer formulation in water. Stainless steel was used as substrate for coating deposition, by the dip-coating technique. Hence, the coatings obtained (of  $\sim 5$   $\mu\text{m}$  thickness) were highly hydrophobic (contact angle CA varying in the range  $120^\circ$ - $140^\circ$ ), but not homogeneous, neither continuous on the substrate. We firstly investigated the erosion tendency of the PFPE coatings when exposed to aggressive liquid environments, or wall shear stresses induced by the liquid flowing. The

resistance tests highlighted the low resistance of the PFPE coatings toward alkaline solutions, which are responsible of a coating deterioration due to hydrolysis reactions, involving the bonds between the polymer and the metal surface. On the other hand, the polymeric coatings were not greatly eroded by acidic solutions (HCl, pH=2) or disinfectant solutions containing chlorine (normally used for the cleaning of the heat transfer surfaces). However, we observed scarce resistance against water at high temperature (323-343 K) and shear stresses (flowrate 0.13-0.17 m/s), in particular if long periods of exposition were considered (months). The anti-fouling efficiency of the PFPE coatings was firstly investigated in a small test ring, by depositing the PFPE film on the internal surfaces of a stainless steel tube sample (internal diameter 8 mm, length 100 mm). In the test rig a solution of CaSO<sub>4</sub> (4 g/L) was continuously recirculated in the tube sample at a flowrate of 0.05 m/s, in order to recreate particulate fouling conditions. We observed that the presence of the hydrophobic PFPE coatings permitted a reduction of the fouling rate (express as mg of CaSO<sub>4</sub> deposits, normalized by the duration of the test and the surface area exposed in cm<sup>2</sup>) of the 90%, if compared to an uncoated and hydrophilic surface. Eventually, we investigate the effect of the coatings on fouling occurring on real heat transfer surfaces. Both Fluorolink<sup>®</sup>S10 and Fluorolink<sup>®</sup>F10 were employed to coat the tube bundle of a shell and tube heat exchanger in pilot scale (length 700 mm). The two coatings were investigated in separate pilot plant experiments. In each experiment the heat transfer performances of the coated pilot plant were compared with the ones of an identical, but uncoated, heat exchanger, operating in parallel, at the same conditions. Figure GA-1 illustrates the pilot plant scheme and some design specifications. The heat exchangers operated in continuous, 24/24 hours; as operating fluid we used sweet water rich in Ca and Mg carbonate, responsible



of crystallization fouling phenomena. During the operation, a transient flow regime (in part laminar and in part turbulent) was kept inside the shells and tubes of the heat exchangers.

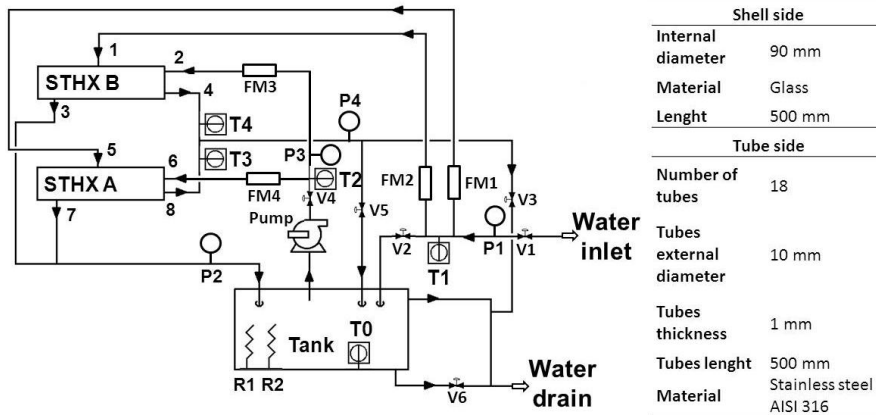


Figure GA-1. Schematic diagram of the pilot plant I. FM= flowmeter; P=manometer; R= Heating element; T=thermocouple; V= valve. STHX B= shell and tube heat exchanger B (not coated): 1= Shell side inlet; 2= tube side inlet; 3= shell side outlet; 4 =tube side outlet. STHX A= shell and tube heat exchanger A (coated): 5= shell side inlet; 6= tube side inlet; 7= shell side outlet; 8= tube side outlet.

Both the hydrophobic coatings permitted a reduction of the fouling incidence, as demonstrated by the trend of the fouling resistance  $R_f$  (Figure GA-2 and Figure GA-3). The pilot plant experimentation involving the Fluorolink<sup>®</sup>S10 coating lasted for 6 months, but data are presented only 60 days of work. During this period we observed a progressive increase of the fouling resistance, due to the formation of scale deposits. However, the fouling resistance of the uncoated heat exchanger increased more rapidly in respect to the coated one. At the end of the experimentation, the  $R_f$  value calculated for the coated heat

exchanger was  $0.0018 \text{ m}^2\text{K/W}$ , and  $0.0051 \text{ m}^2\text{K/W}$  for the uncoated heat exchanger (see Figure GA-2) [14].

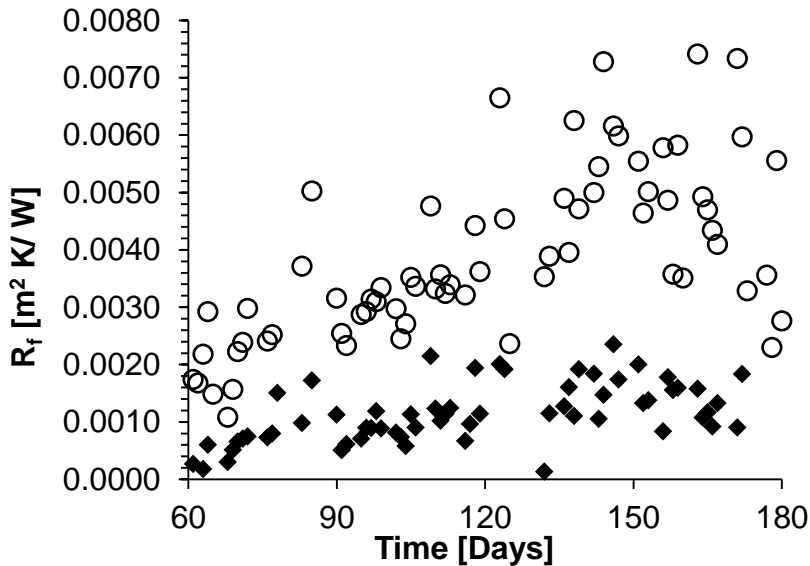


Figure GA-2. Fouling resistance  $R_f$  vs time.  $\blacklozenge$  Fluorolink®S10 coated heat exchanger (STHX A);  $\circ$  Uncoated heat exchanger (STHX B).

We observed a similar result for the F10 coating. In that case, in the first period of operation, we observed the ability of the hydrophobic coating to delay the formation of the fouling deposits. From Figure GA-3 it is possible to observe an increase of the fouling resistance after 15 days of operation for the uncoated heat exchanger; the same increase of  $R_f$  was observed for the coated heat exchanger 10 days later. Moreover, in the last period of operation (from the 50<sup>th</sup> to the 55<sup>th</sup> day of operation) the fouling resistance of the uncoated heat exchanger increased more (until the value of  $0.00023 \text{ m}^2\text{K/W}$ ), while decreased for the coated heat exchanger ( $0.000031 \text{ m}^2\text{K/W}$ ), indicating a possible removal of the foulant deposits thanks to the presence of the hydrophobic coating.

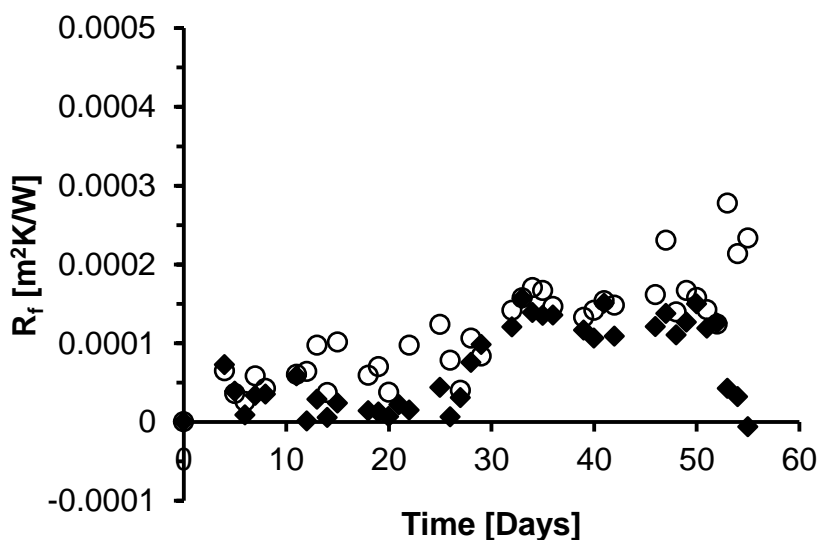


Figure GA-3. Fouling resistance  $R_f$  vs time.  $\blacklozenge$  Fluorolink® F10 coated heat exchanger (STHX A);  $\circ$  Uncoated heat exchanger (STHX B).

The results of the pilot plant experimentations confirmed the ability of perfluoropolyethers coatings to mitigate fouling on heat transfer surfaces. However their low resistance against high temperatures and shear stresses compromised the integrity of the coatings and at the end of the pilot plant experimentation the surfaces were no longer hydrophobic.

The first attempt to improve the mechanical and physical properties of the PFPE based coatings involved the preparation of the multilayer coatings, characterized by the overlapping of PFPE films with films of ceramic oxides nanopowders ( $\text{TiO}_2$  or  $\text{ZrO}_2$ ) impregnated with a silane (triethoxy(octyl)silane OTES). The best multilayer coating prepared was constituted by a  $\text{ZrO}_2$  film, overlapped by a S10 film (named  $\text{ZrO}_2$ -OTES/S10). The multilayer coatings showed an improvement in mechanical resistance against shear stresses, but were still sensitive to the immersion in high temperature liquids, which greatly

eroded the hydrophobic coating. Moreover, the multilayer coatings were characterized by a very high thickness (25-30  $\mu\text{m}$ ), which inhibited their use on heat transfer surfaces, since they can have an insulator effect comparable to the one determined by the fouling deposits [15]. The investigation on multilayer coatings, however, confirmed us the possibility to improve the mechanical properties of PFPE by the combination with metal oxides. For this reason, we considered the preparation of hybrid coatings. It has been demonstrated that the interpenetration of a fluoropolymer with a metal oxide, permits to increase the hardness and the mechanical properties of fluoropolymers [16]. Therefore, we developed hybrid coatings by combining the commercial  $\alpha,\omega$ -functionalized perfluoropolyethers with sol-gel networks of  $\text{SiO}_2$  or  $\text{ZrO}_2$ . In particular, we observed that the polymer Florolink®S10 was able to interact with silica network, forming stable formulations in which the organic part and the inorganic one were interspersed. The hybrid coatings thus obtained had an average thickness of 7  $\mu\text{m}$  and were homogeneous and well dispersed on the stainless steel substrate. The resistance tests pointed out a great increase of the resistance against chemical and mechanical erosion induced by liquids for these hybrid coatings. Figure GA-4 and GA-5 compares the decrease of contact angle (CA), observed for PFPE, multilayer and hybrid coatings, when immersed in high temperature water or when exposed to shear stress (7 days tests). In both the cases, the CA decrease of the hybrid coatings was inferior to the 10%, and the final CA value was about  $140^\circ$ . Moreover, for longer time of exposition (1 month) we observed a progressive erosion of both the PFPE and multilayer coatings until their complete removal. On the other hand, the  $\text{SiO}_2/\text{S10}$  coated surfaces maintained almost unaltered the CA value, confirming the high resistance of the hybrid coating.

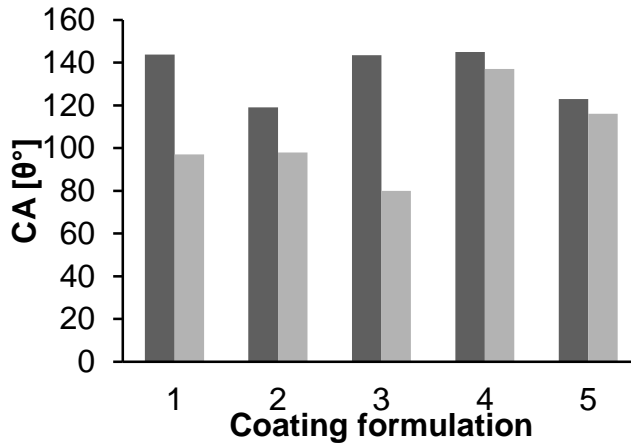


Figure GA-4. Coatings resistance against water at high temperature (343 K): comparison between the starting CA (■) and the CA at the end of test (■). Legend: 1= Fluorolink<sup>®</sup>S10; 2= Fluorolink<sup>®</sup>F10; 3= multilayer coating ZrO<sub>2</sub>-OTES/S10; 4= hybrid coating SiO<sub>2</sub>/S10-20/80\_1; 5= hybrid coating SiO<sub>2</sub>/F10-20/80\_1.

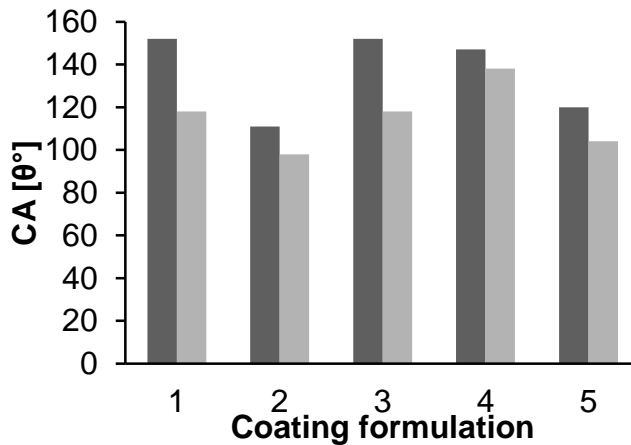


Figure GA-5. Coatings resistance against wall shear stresses: comparison between the starting CA (■) and the CA at the end of test (■). Legend: 1= Fluorolink<sup>®</sup>S10; 2= Fluorolink<sup>®</sup>F10; 3= multilayer coating ZrO<sub>2</sub>-OTES/S10; 4= hybrid coating SiO<sub>2</sub>/S10-20/80; 5= hybrid coating SiO<sub>2</sub>/F10-20/80.

The experimentation on pilot plant, confirmed, one more time, the ability of the hydrophobic coatings containing PFPE to mitigate the crystallization fouling phenomenon induced in the operating conditions adopted. Figure GA-6 illustrates the trend of the fouling resistance of an uncoated heat exchanger, compared to a heat exchanger coated by the SiO<sub>2</sub>/S10 hybrid coating.

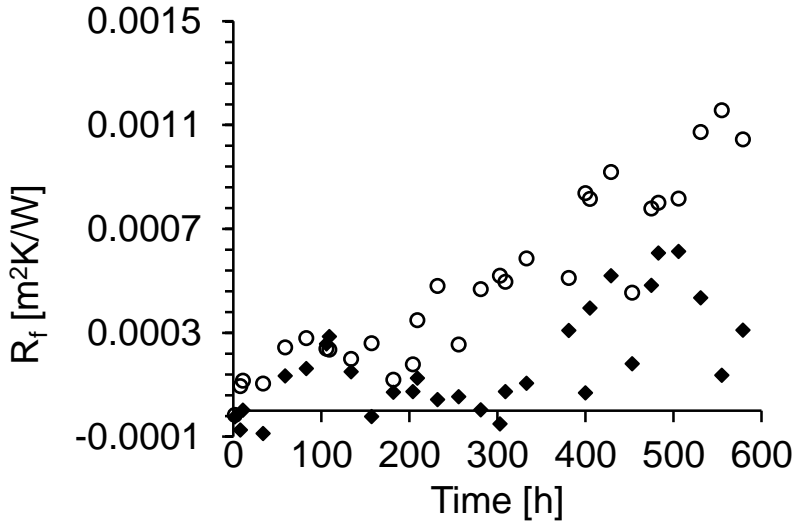


Figure GA-6. Fouling resistance  $R_f$  vs time.  $\blacklozenge$  heat exchanger coated by the hybrid SiO<sub>2</sub>/S10 coating (STHX A);  $\circ$  Uncoated heat exchanger (STHX B).

Until 200 hours of operation, the fouling resistances were very similar, and very low, for both the coated and uncoated heat exchanger (the average values were 0.00006 and 0.0001  $\text{m}^2\text{K/W}$  respectively). From that period, however we observed a progressive increase of the  $R_f$  values for the uncoated heat exchanger, indicating the formation of the firsts fouling deposits. On the contrary, the fouling resistance remained stable at very low values until 400 hours of operation for the coated heat exchanger. Therefore, we assumed the ability of the hybrid coating to delay the fouling of the heat transfer surfaces

and to prolong the fouling induction period of about 200 hours, in the conditions adopted. Moreover, in the last period of operation we observed a progressive decrease of the  $R_f$  for the coated heat exchanger ( $0.0003 \text{ m}^2\text{K/W}$ ), indicating a possible removal of the foulant deposits from the hydrophobic heat transfer surfaces. On the other hand, the fouling resistance further increased on the uncoated heat exchanger ( $0.001 \text{ m}^2\text{K/W}$ ).

## Conclusions

The current PhD research focused the attention on the preparation of hydrophobic coatings for stainless steel surfaces, with the aim to produce a coating technology available at the industrial scale and targeted to the mitigation of fouling in very complex systems, as the heat exchangers. We decided to use a particular family of polymers, the inorganic  $\alpha,\omega$ -substituted perfluoropolyethers, as backbone for the preparation of the anti-fouling coatings, since these materials were not deeply investigated for such a type of application, thus contributing to enrich the state of the art concerning the applications of PFPE. Moreover, we prepared novel typology of hydrophobic coatings by the combination of commercial PFPE with metal oxides networks, with the aim to obtain a final product characterized by both the properties of the organic part and the inorganic one, i.e., high hydrophobicity, and high mechanical properties. The design and use of a heat exchanger pilot plant contributed to make more interesting and complete the current research. We could demonstrate, in fact, the effective ability of the perfluoropolyether based coatings to mitigate crystallization fouling phenomena on real heat transfer surfaces. At last, the best hydrophobic coating prepared, in terms of morphology, surface properties, and mechanical and physical properties, were obtained by the combination in a hybrid coating of a sol-gel silica network, with

the commercial polymer Fluorolink®S10. This coating demonstrated high resistance against erosion induced by aggressive liquid environments and the ability to prolong the fouling induction period in the heat exchanger pilot plant. Is not possible to ensure a fully industrial applicability of the coatings prepared, however is surely interesting the possibility to obtain from commercial products, not designed for fouling mitigation, an efficient anti-fouling coating. Moreover, we may assume that the combined use of the hydrophobic coating studied in this research with other fouling mitigation strategies, can contribute to prolong the shelf life of those industrial heat exchangers working in mild conditions but affected by particulate or crystallization fouling.

## References

- [1] A. Dimian, C. Bildea and A. Kiss, Eds., Integrated design and simulation of chemical processes, Second Edition, Amsterdam: Elsevier, 2014, pp. 780-784.
- [2] H. Muller-Steinhagen and H. Zettler, Eds., Heat exchanger fouling. Mitigation and cleaning technologies, Israel: PP Publico Publications, 2011.
- [3] H. Muller-Steinhagen, M.R. Malayeri, and A.P. Watkinson, Fouling of heat exchanger-New approaches to solve an old problem, *Heat Transfer Engineering*, 26, pp. 1-4, 2005.
- [4] H. Muller-Steinhagen, M. Malayeri and A.P. Watkinson, Heat exchanger fouling: mitigation and cleaning strategies, *Heat Transfer Engineering*, Vols. 32(3-4), pp. 189-196, 2011.
- [5] C. Magin, S. Cooper and A. Brennan, Non-toxic antifouling strategies, *Material Today*, vol. 10, pp. 36-44, 2010.



- [6] M. Forster and M. Bohnet, Modification of molecular interactions at the interface crystal/heat transfer surface to minimize heat exchanger fouling, *International Journal of Thermal Science* , vol. 39, pp. 697-708, 2000.
- [7] R. Oliveira, Understanding adhesion: a means for preventing fouling, *Experimental Thermal and Fluid Science*, vol. 14, pp. 316-322, 1997.
- [8] A. Marmur, Super-hydrophobicity fundamentals: implications to biofouling prevention, *Biofouling: The Journal of Bioadhesion and Biofilm Research*, vol. 22, pp. 107-115, 2007.
- [9] Cheng, Y.H.; Chen, H.Y.; Zhu, Z.C.; Jen, T.C.; Peng, Y.X., Experimental study on the anti-fouling effects of Ni-Cu-P-PTFE deposit surface of heat exchangers, *Applied Thermal Engineering* , vol. 68, pp. 20-25, 2014.
- [10] Y. Cai, M. Liu and L. Hui, Observations and mechanism of CaSO<sub>4</sub> fouling on hydrophobic surfaces, *Industrial Engineering Chemical Research* , vol. 53, p. 3509–3527, 2014.
- [11] R. Taurino, E. Fabbri, D. Pospiech, A. Synytska, M. Messori, Preparation of scratch resistant superhydrophobic hybrid coatings by sol-gel process, *Progress in Organic Coatings*, vol. 77, p. 1635-1641, 2014.
- [12] H. Fischer, Polymer nanocomposites: from fundamental research to specific applications, *Materials Science and Engineering*, vol. 23, p. 763–772, 2003.
- [13] E. Fabbri, P. Fabbri, M. Messori, M. Montecchi and F. Pilati, Perfluoropolyethers-silica hybrids: preparation and surface characterization, *Journal of Sol-Gel Science and Technology*, vol. 34, pp. 155-163, 2005.

- [14] V. Oldani, C.L. Bianchi, S. Biella, C. Pirola and G. Cattaneo, Perfluoropolyethers coatings design for fouling reduction on heat transfer stainless steel surfaces, *Journal of Heat Transfer Engineering*, DOI: 10.1080/01457632.2015.1044417.
- [15] V. Oldani, R. del Negro, C.L. Bianchi, R. Suriano, S. Turri, C. Pirola, B. Sacchi, surface properties and anti-fouling assessment of coatings obtained from perfluoropolyethers and ceramic oxides nanopowders deposited on stainless steel, *Journal of Fluorine Chemistry*, vol. 180, p. 7-14, 2015.
- [16] R. Suriano, V. Oldani, C.L. Bianchi, S. Turri, AFM nanomechanical properties and durability of new hybrid fluorinated sol-gel coatings, *Surface & Coatings Technology*, vol. 264, p. 87-96 (2015).

## LIST OF FIGURES

FIGURE 1-1. EXAMPLE OF CRYSTALLIZATION FOULING IN A SHELL AND TUBE HEAT EXCHANGER .....	9
FIGURE 1-2. SCHEMATIC REPRESENTATION OF THE HEAT FLOW ACROSS A WALL BY CONDUCTION. ....	11
FIGURE 1-3. HEAT CONDUCTION ACROSS A METAL WALL COVERED BY FOULING DEPOSITS. THE PRESENCE OF FOULING LAYERS STRONGLY AFFECTS THE TEMPERATURE DISTRIBUTION, AND THE FOULING LAYERS OFFER A FURTHER RESISTANCE TO THE HEAT TRANSFER.....	14
FIGURE 1-4. SUM-UP OF THE ON-LINE CLEANING STRATEGIES FOR FOULING MITIGATION IN HEAT EXCHANGERS. ....	16
FIGURE 1-5. ILLUSTRATIONS OF CONTACT ANGLES FORMED BY A SESSILE LIQUID DROP ON A FLAT (IDEAL) SURFACE.....	19
FIGURE 1-6. EXAMPLES OF COMMERCIAL PERFLUOROPOLYETHERS FORMULAE WITH THEIR CORRESPONDING FLUORINATED MONOMERS.....	27
FIGURE 1-7. GENERIC CHEMICAL STRUCTURE OF A SILOXANE AND SILOXANE INTERACTION WITH A METAL OXIDE SURFACE. R' AND R REPRESENT GENERIC ALIPHATIC GROUPS.....	33
FIGURE 2-1. CHEMICAL STRUCTURES OF FLUOROLINK®S10 AND FLUOROLINK®F10.....	44
FIGURE 2-2. DIP-COATER USED FOR THE PFPE COATINGS DEPOSITION ON STAINLESS STEEL PLAIN SAMPLES.....	47
FIGURE 3-1. ILLUSTRATION OF THE INTERACTIONS BETWEEN A LIQUID DROP AND A SOLID SURFACE ACCORDING TO YOUNG'S EQUATION. DESCRIPTION OF THE ELEMENTS NECESSARY FOR THE DETERMINATION OF CA ( $\theta$ ) FROM THE DROP SHAPE ANALYSIS.....	65
FIGURE 3-2. ILLUSTRATION OF THE ADVANCING AND RECEDING CONTACT ANGLES.....	66
FIGURE 3-3. DROP SHAPE ON HETEROGENEOUS AND ROUGH SURFACES. A) WENZEL STATE ILLUSTRATION; B) CASSIE-BAXTER STATE ILLUSTRATION.....	67
FIGURE 3-4. LABORATORY INSTRUMENTATION FOR CONTACT ANGLES MEASUREMENTS (A), AND XPS ANALYSES (B).....	70
FIGURE 4-1. EXPERIMENTAL APPARATUS FOR SHEAR STRESS TESTS. ....	75
FIGURE 4-2. EFFECT OF THE FLOW VELOCITY ON THE FOULING RESISTANCE FOR DIFFERENT TYPES OF FOULING .....	76

FIGURE 4-3. EFFECT OF THE SURFACE TEMPERATURE ON THE FOULING RESISTANCE FOR DIFFERENT TYPES OF FOULING .....77

FIGURE 4-4. SCHEMATIC OF THE TEST RIG FOR THE EVALUATION OF PARTICULATE FOULING RATE ON COATED STAINLESS STEEL TUBES. TC=THERMOCOUPLE; R= HEATING ELEMENT; P=PUMP; FM= FLOAT FLOWMETER.....78

FIGURE 4-5. MAIN COMPONENTS OF A SHELL AND TUBES HEAT EXCHANGER, WORKING IN COUNTER FLOW. ....80

FIGURE 4-6. FLOWS DIRECTION AND CORRESPONDING TEMPERATURES PROFILES FOR SHELL AND TUBES HEAT EXCHANGERS. PARALLEL FLOW (A); COUNTER FLOW (B).....81

FIGURE 4-7. POSSIBLE BAFFLES TYPES IN SHELL AND TUBES HEAT EXCHANGERS LAY-OUT (A); POSSIBLE PITCH TUBE LAY-OUTS (B).....82

FIGURE 4-8. MULTIPASS FLOW ARRANGEMENT FOR SHELL AND TUBES HEAT EXCHANGERS. ONE SHELL-PASS AND TWO TUBE-PASSES (A); TWO SHELL-PASSES AND 4 TUBE-PASSES (B).....83

FIGURE 4-9. TEMA TYPES FOR CLASSIFICATION OF SHELL AND TUBES HEAT EXCHANGERS.....84

FIGURE 4-10. PICTURE OF THE PILOT PLANT I.....86

FIGURE 4-11. SCHEMATIC DIAGRAM OF THE PILOT PLANT I. FM= FLOWMETER; P=MANOMETER; R= HEATING ELEMENT; T=THERMOCOUPLE; V= VALVE. STHX B= SHELL AND TUBE HEAT EXCHANGER B (NOT COATED): 1= SHELL SIDE INLET; 2= TUBE SIDE INLET; 3= SHELL SIDE OUTLET; 4 =TUBE SIDE OUTLET. STHX A= SHELL AND TUBE HEAT EXCHANGER A (COATED): 5= SHELL SIDE INLET; 6= TUBE SIDE INLET; 7= SHELL SIDE OUTLET; 8= TUBE SIDE OUTLET. ....86

FIGURE 4-12. PICTURE OF THE PILOT PLANT II. ....90

FIGURE 4-13. SCHEMATIC DIAGRAM OF THE PILOT PLANT II. FM= FLOWMETER; P=MANOMETER; R= HEATING ELEMENT; T=THERMOCOUPLE; V= VALVE. STHX B= SHELL AND TUBE HEAT EXCHANGER B (NOT COATED): 1= SHELL SIDE INLET; 2= TUBE SIDE INLET; 3= SHELL SIDE OUTLET; 4= TUBE SIDE OUTLET. STHX A= SHELL AND TUBE HEAT EXCHANGER A (COATED): 5= SHELL SIDE INLET; 6= TUBE SIDE INLET; 7= SHELL SIDE OUTLET; 8= TUBE SIDE OUTLET. ....91







FIGURE 5-1. OPTIMIZATION OF THE COATINGS DEPOSITION PROCEDURE FOR S10 (A, B) AND F10 (C, D) COATINGS. A, C) VARIATION OF THE IMMERSION TIME, HEAT TREATMENT PERFORMED AT 393 K FOR 3 HOURS; B, D) VARIATION OF THE TEMPERATURE AND DURATION FOR THE HEAT TREATMENT, IMMERSION TIME 24 HOURS. LEGEND:  353 K;  373 K;  383 K;  393 K;  403 K;  413 K. .... 101

FIGURE 5-2. SEM PICTURES OF A STAINLESS STEEL PLAIN SUBSTRATE (A, B); S10 COATING (C, D) AND F10 COATING (D, E). ON THE LEFT MAGNIFICATION OF 500X; ON THE RIGHT MAGNIFICATION OF 2000X. .... 104

FIGURE 5-3. XPS SURVEY SPECTRUM FOR THE S10 COATING. .... 106

FIGURE 5-4. XPS SURVEY SPECTRUM FOR THE F10 COATING. .... 106

FIGURE 5-5. IMAGES OF WATER DROPLET DEPOSITED ON AN UNCOATED STAINLESS STEEL SURFACE (A), AND A FLUOROLINK®S10 COATED STAINLESS STEEL SURFACE (B). .... 109

FIGURE 5-6. ILLUSTRATION OF THE ADVANCING AND RECEDING CA TREND ( ● ), COMPARED WITH THE VOLUME OF THE WATER DROPLET ( ◆ ), WHICH WAS INCREASED AND CONTRACTED ACCORDINGLY. S10 COATING (A); F10 COATING (B). .... 111

FIGURE 5-7. COATING RESISTANCE AGAINST EROSION IN LIQUID ENVIRONMENTS: COMPARISON BETWEEN THE STARTING CA ( ■ ) AND THE CA AT THE END OF THE TEST ( ■ ). S10 COATING ON UNPOLISHED STAINLESS STEEL SUBSTRATES (A); S10 COATING ON POLISHED STAINLESS STEEL SUBSTRATES (B). 1= NH<sub>2</sub>CL/NHCL<sub>2</sub> SOLUTION, T= 323 K; 2= NAOH SOLUTION, T= 323 K; 3= HCL SOLUTION, T=323 K; 4= WATER, T=298 K; 5= WATER, T=343 K; 6= WATER FLUX, T=313 K, FLOWRATE=0.13 M/S. .... 113

FIGURE 5-8. TREND OF CA DECREASE DURING RESISTANCE TESTS FOR S10 COATINGS DEPOSITED ON UNPOLISHED STAINLESS STEEL SURFACES (A,B) AND POLISHED SURFACES (C,D). LEGEND: ✖ = NH<sub>2</sub>CL/NHCL<sub>2</sub> SOLUTION, T= 323 K; ◆ = NAOH SOLUTION, T= 323 K; □ = HCL SOLUTION, T=323 K; ▲ = WATER, T=298 K; ✖ = WATER, T=343 K; ● = WATER FLUX, T=313 K, FLOWRATE=0.13 M/S. .... 116

FIGURE 5-9. COATING RESISTANCE AGAINST EROSION IN LIQUID ENVIRONMENTS: COMPARISON BETWEEN THE STARTING CA ( ■ ) AND THE CA AT THE END OF THE TEST ( ■ ). F10 COATING ON UNPOLISHED STAINLESS STEEL SUBSTRATES (A); F10 COATING ON POLISHED STAINLESS STEEL SUBSTRATES (B). 1= NH<sub>2</sub>CL/NHCL<sub>2</sub> SOLUTION, T= 323 K; 2= NAOH SOLUTION, T= 323 K; 3= HCL SOLUTION, T=323 K; 4= WATER, T=298 K; 5= WATER, T=343 K; 6= WATER FLUX, T=313 K, FLOWRATE=0.13 M/S. .... 118

FIGURE 5-10 TREND OF CA DECREASE DURING RESISTANCE TESTS OF F10 COATINGS DEPOSITED ON UNPOLISHED STAINLESS STEEL SURFACES (A,B) AND POLISHED SURFACES (C,D). LEGEND: ✖ = NH<sub>2</sub>CL/NHCL<sub>2</sub> SOLUTION, T= 323 K; ◆ = NAOH SOLUTION, T= 323 K; □ = HCL

SOLUTION, T=323 K;  $\blacktriangle$  = WATER, T=298 K;  $\times$  = WATER, T=343 K;  $\bullet$  = WATER  
 FLUX, T=313 K, FLOWRATE=0.13 M/S. .... 119

FIGURE 5-11. RESULTS OF COATING RESISTANCE AGAINST EROSION IN SYNTHETIC SEAWATER: TEST  
 PERFORMED AT ROOM TEMPERATURE (A); TEST PERFORMED AT 323 K (B).  $\blacksquare$  INITIAL WATER CA;  
 $\blacksquare$  WATER CA AT THE END OF THE TEST. .... 122

FIGURE 5-12. PICTURES OF TUBES SECTION AFTER THE FOULING TEST (48 HOURS): UNCOATED SURFACE  
 (A); S10 COATED SURFACE (B); F10 COATED SURFACE (C)..... 125

FIGURE 5-13. SHELL-SIDE AND TUBE-SIDE FILM COEFFICIENTS OF S10 COATED (STHX A) AND  
 UNCOATED (STHX B) HEAT EXCHANGERS.  $\blacklozenge$   $H_H$  OF STHX A;  $\circ$   $H_H$  FOR UNCOATED HEAT  
 EXCHANOF STHX B;  $\triangle$   $H_C$  OF STHX A;  $\times$   $H_C$  OF STHX B. .... 131

FIGURE 5-14. ABSOLUTE VALUE OF THE HEAT TRANSFERRED ( $Q$ ) VS TIME.  $\blacklozenge$  S10 COATED HEAT  
 EXCHANGER (STHX A);  $\circ$  UNCOATED HEAT EXCHANGER (STHX B). .... 132

FIGURE 5-15. OVERALL HEAT TRANSFER COEFFICIENT ( $U$ ) VS TIME.  $\blacklozenge$  S10 COATED HEAT EXCHANGER  
 (STHX A);  $\circ$  UNCOATED HEAT EXCHANGER (STHX B); — LINEAR TREND STHX A; - - - -  
 LINEAR TREND STHX B. .... 133

FIGURE 5-16. FOULING RESISTANCE VS TIME.  $\blacklozenge$  S10 COATED HEAT EXCHANGER (STHX A);  $\circ$   
 UNCOATED HEAT EXCHANGER (STHX B)..... 136

FIGURE 5-17. PICTURES OF THE TUBE BUNDLES OF THE HEAT EXCHANGERS AT THE END OF THE  
 EXPERIMENTATION. A = TUBE BUNDLE OF THE STHX A, COATED WITH FLUOROLINK®S10; B =  
 TUBE BUNDLE OF THE STHX B, UNCOATED..... 138

FIGURE 5-18. SECTIONS OF TUBE SAMPLES COLLECTED FROM THE TUBE BUNDLE OF THE HEAT  
 EXCHANGERS AT THE END OF THE PILOT PLANT OPERATION. A = TUBE SAMPLE FROM THE STHX A  
 (COATED WITH FLUOROLINK®S10); B = TUBE SAMPLE FROM STHX B (NOT COATED). .... 139

FIGURE 5-19. FOULING DEPOSITS COLLECTED FROM THE REAR HEADS OF THE HEAT EXCHANGERS. A =  
 DEPOSIT COLLECTED ON STHX A (COATED WITH FLUOROLINK®S10); B = DEPOSIT COLLECTED IN  
 STHX B (UNCOATED). .... 139

FIGURE 5-20 SEM PICTURES OF FOULING DEPOSITS FORMED ON THE INTERNAL TUBE SURFACE OF THE  
 S10 COATED HEAT EXCHANGER (A) AND UNCOATED HEAT EXCHANGER (B)..... 142

FIGURE 5-21. ABSOLUTE VALUE OF THE HEAT TRANSFERRED ( $Q$ ) VS TIME.  $\blacklozenge$  F10 COATED HEAT  
 EXCHANGER (STHX A);  $\circ$  UNCOATED HEAT EXCHANGER (STHX B). .... 146

FIGURE 5-22. OVERALL HEAT TRANSFER COEFFICIENT ( $U$ ) VS TIME.  $\blacklozenge$  F10 COATED HEAT EXCHANGER (STHX A);  $\circ$  UNCOATED HEAT EXCHANGER (STHX B)..... 148

FIGURE 5-23. FOULING RESISTANCE VS TIME.  $\blacklozenge$  COATED HEAT EXCHANGER;  $\circ$  UNCOATED HEAT EXCHANGER ..... 151

FIGURE 5-24. PICTURES OF INTERNAL TUBES SURFACES, COLLECTED IN CORRESPONDENCE OF THE REAR HEAD. A) TUBE OF THE COATED HEAT EXCHANGER (STHX A); B) TUBE OF THE UNCOATED HEAT EXCHANGER (STHX B). ..... 152

FIGURE 6-1. SEM IMAGES OF A  $\text{TiO}_2$ -OTES LAYER (A, B, C) AND OF A  $\text{ZrO}_2$ -OTES LAYER (D, E, F). MAGNIFICATION OF 200X FOR PICTURES A AND D, 2000X FOR PICTURES B AND E; 5000X FOR PICTURES C AND F. .... 156

FIGURE 6-2. HIGH RESOLUTION SPECTRA OF TI 2P DOUBLET (A) AND ZR 3D DOUBLET. PEAK-FIT TABLE A: A=459.3, B=461.6, C=464.9, D=467.1; PEAK-FIT TABLE B: A=182.8, B=184.5, C=185.5, D=187.2. .... 158

FIGURE 6-3. COATING RESISTANCE AGAINST EROSION IN LIQUID ENVIRONMENTS: COMPARISON BETWEEN THE STARTING CA ( $\blacksquare$ ) AND THE CA AT THE END OF THE TEST ( $\blacksquare$ ). S10/ $\text{TiO}_2$ -OTES MULTILAYER COATING (A); S10/ $\text{ZrO}_2$ -OTES MULTILAYER COATING (B). 1=  $\text{NH}_2\text{CL}/\text{NHCL}_2$  SOLUTION, T= 323 K; 2=  $\text{NAOH}$  SOLUTION, T= 323 K; 3=  $\text{HCL}$  SOLUTION, T=323 K; 4= WATER, T=298 K; 5= WATER, T=343 K; 6= WATER FLUX, T=313 K, FLOWRATE=0.13 M/S. .... 163

FIGURE 6-4. TREND OF CA DECREASE DURING RESISTANCE TESTS. S10/ $\text{TiO}_2$ -OTES MULTILAYER COATING (A, B); S10/ $\text{ZrO}_2$ -OTES MULTILAYER COATING (C, D). LEGEND:  $\text{---}^*$  =  $\text{NH}_2\text{CL}/\text{NHCL}_2$  SOLUTION, T= 323 K;  $\text{---}\blacklozenge$  =  $\text{NAOH}$  SOLUTION, T= 323 K;  $\text{---}\square$  =  $\text{HCL}$  SOLUTION, T=323 K;  $\text{---}\blacktriangle$  = WATER, T=298 K;  $\text{---}\times$  = WATER, T=343 K;  $\text{---}\bullet$  = WATER FLUX, T=313 K, FLOWRATE=0.13 M/S. .... 164

FIGURE 6-5. COATING RESISTANCE AGAINST EROSION IN LIQUID ENVIRONMENTS: COMPARISON BETWEEN THE STARTING CA ( $\blacksquare$ ) AND THE CA AT THE END OF THE TEST ( $\blacksquare$ ).  $\text{TiO}_2$ -OTES/S10 MULTILAYER COATING (A);  $\text{ZrO}_2$ -OTES/S10 MULTILAYER COATING (B). 1=  $\text{NH}_2\text{CL}/\text{NHCL}_2$  SOLUTION, T= 323 K; 2=  $\text{NAOH}$  SOLUTION, T= 323 K; 3=  $\text{HCL}$  SOLUTION, T=323 K; 4= WATER, T=298 K; 5= WATER, T=343 K; 6= WATER FLUX, T=313 K, FLOWRATE=0.13 M/S. .... 166

FIGURE 6-6. TREND OF CA DECREASE DURING RESISTANCE TESTS.  $\text{TiO}_2$ -OTES/S10 MULTILAYER COATING (A, B);  $\text{ZrO}_2$ -OTES/S10 MULTILAYER COATING (C, D). LEGEND:  $\text{---}^*$  =  $\text{NH}_2\text{CL}/\text{NHCL}_2$  SOLUTION, T= 323 K;  $\text{---}\blacklozenge$  =  $\text{NAOH}$  SOLUTION, T= 323 K;  $\text{---}\square$  =  $\text{HCL}$


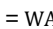
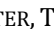
SOLUTION, T=323 K;  = WATER, T=298 K;  = WATER, T=343 K;  = WATER FLUX, T=313 K, FLOWRATE=0.13 M/S. .... 167

FIGURE 6-7. INTERNAL SURFACES OF TUBES SAMPLES AFTER PARTICULATE FOULING TEST LASTED FOR 48 HOURS. TiO<sub>2</sub>-OTES/S10 COATED SAMPLE (A) AND ZRO<sub>2</sub>-OTES/S10 COATED SAMPLE (B).  
..... 170

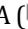
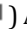
FIGURE 7-1. COATING RESISTANCE AGAINST EROSION IN WATER AT 323 K: COMPARISON BETWEEN THE STARTING CA () AND THE CA AT THE END OF TEST (). A) HYBRID COATINGS SiO<sub>2</sub>/S10 AND TiO<sub>2</sub>/S10 PREPARED WITH THE TWO-STEPS PROCEDURE: 1= SiO<sub>2</sub>/S10-50/50\_2; 2= SiO<sub>2</sub>/S10-30/70\_2; 3= SiO<sub>2</sub>/S10-20/80\_2; 4= TiO<sub>2</sub>/S10-50/50\_2; 5= TiO<sub>2</sub>/S10-30/70\_2; 6= TiO<sub>2</sub>/S10-20/80\_2. B) HYBRID COATINGS SiO<sub>2</sub>/S10 PREPARED WITH THE ONE STEP PROCEDURE: 1= SiO<sub>2</sub>/S10-50/50\_1; 2= SiO<sub>2</sub>/S10-30/70\_1; 3= SiO<sub>2</sub>/S10-20/80\_1.  
..... 176

FIGURE 7-2. SEM IMAGES OF HYBRID COATINGS CONTAINING THE POLYMER FLUOROLINK®S10. ON THE LEFT MAGNIFICATION OF 500X, ON THE RIGHT MAGNIFICATION OF 2000X. LEGEND: SiO<sub>2</sub>/S10-20/80\_2 (A, B); SiO<sub>2</sub>/S10-30/70\_1 (C, D); ZRO<sub>2</sub>/S10-30/70\_1 (E, F). .... 179

FIGURE 7-3. SEM IMAGES OF HYBRID COATINGS CONTAINING THE POLYMER FLUOROLINK®F10. ON THE LEFT, MAGNIFICATION OF 50X, ON THE RIGHT MAGNIFICATION OF 200X, IN THE FRAMED PICTURE MAGNIFICATION OF 2000X. LEGEND: SiO<sub>2</sub>/F10-20/80\_2 (A, B); SiO<sub>2</sub>/F10-20/80\_1 (C, D); ZRO<sub>2</sub>/F10-20/80\_1 (E, F). .... 181

FIGURE 7-4. XPS HIGH RESOLUTION SPECTRA OF Si 2P SINGLET (A, B) AND Zr 3D DOUBLET (C, D) OF HYBRID COATINGS CONTAINING FLUOROLINK®S10. SiO<sub>2</sub>/S10-20/80\_2 (A); SiO<sub>2</sub>/S10-30/70\_1 (B); ZRO<sub>2</sub>/S10-20/80\_2 (C); ZRO<sub>2</sub>/S10-30/70\_1 (D). .... 185

FIGURE 7-5. SEM MAGNIFICATION OF A CUT SECTION OF THE COATING ZRO<sub>2</sub>/S10-30/70\_1, DEPOSITED ON A STAINLESS STEEL PLAIN SAMPLE, FOR THE DETERMINATION OF THE COATING THICKNESS.. 188





FIGURE 7-6. COATING RESISTANCE AGAINST EROSION IN LIQUID ENVIRONMENTS: COMPARISON BETWEEN THE STARTING CA () AND THE CA AT THE END OF THE TEST (). COATINGS: 1= SiO<sub>2</sub>/S10-20/80\_2; 2= SiO<sub>2</sub>/S10-50/50\_1; 3= SiO<sub>2</sub>/S10-30/70\_1; 4= SiO<sub>2</sub>/S10-20/80\_1. LEGEND: A) HCL, PH=2, 323 K; B) NH<sub>2</sub>CL-NHCL<sub>2</sub>, PH=7, 323 K; C) WATER AT 343 K; D) WATER FLUX, 0.17 M/S, 323 K. .... 193

FIGURE 7-7. TREND OF CA DECREASE DURING RESISTANCE TESTS. COATINGS: SiO<sub>2</sub>/S10-20/80\_2 (A, B); SiO<sub>2</sub>/S10-20/80\_1 (C, D). LEGEND:  = NH<sub>2</sub>CL/NHCL<sub>2</sub> SOLUTION, T= 323 K;  =



HCL SOLUTION, T=323 K;  $\bullet\bullet\times\bullet\bullet$  = WATER, T=323 K;  $\bullet\bullet\bullet\bullet$  = WATER FLUX, T=343 K,  
 FLOWRATE=0.17 M/S..... 194

FIGURE 7-8. COATING RESISTANCE AGAINST EROSION IN LIQUID ENVIRONMENTS: COMPARISON BETWEEN THE STARTING CA (■) AND THE CA AT THE END OF THE TEST (■). COATINGS: 1= SiO<sub>2</sub>/F10-20/80\_2; 2= SiO<sub>2</sub>/F10-50/50\_1; 3= SiO<sub>2</sub>/F10-30/70\_1; 4= SiO<sub>2</sub>/F10-20/80\_1. LEGEND: A) HCL, PH=2, 323 K; B) NH<sub>2</sub>CL-NHCL<sub>2</sub>, PH=7, 323 K; C) WATER AT 323 K; D) WATER FLUX, 0.17 M/S, 323 K. .... 196

FIGURE 7-9. TREND OF CA DECREASE DURING RESISTANCE TESTS. COATINGS: SiO<sub>2</sub>/F10-20/80\_2 (A, B); SiO<sub>2</sub>/F10-20/80\_1 (C, D). LEGEND:  $\times$  = NH<sub>2</sub>CL/NHCL<sub>2</sub> SOLUTION, T= 323 K;  $\square$  = HCL SOLUTION, T=323 K;  $\bullet\bullet\times\bullet\bullet$  = WATER, T=343 K;  $\bullet\bullet\bullet\bullet$  = WATER FLUX, T=323 K, FLOWRATE=0.17 M/S..... 198

FIGURE 7-10. COATING RESISTANCE AGAINST EROSION IN LIQUID ENVIRONMENTS: COMPARISON BETWEEN THE STARTING CA (■) AND THE CA AT THE END OF THE TEST (■). COATINGS: 1= ZRO<sub>2</sub>/S10-20/80\_2; 2= ZRO<sub>2</sub>/S10-50/50\_1; 3= ZRO<sub>2</sub>/S10-30/70\_1. LEGEND: A) HCL, PH=2, 323 K; B) NH<sub>2</sub>CL-NHCL<sub>2</sub>, PH=7, 323 K; C) WATER AT 343 K; D) WATER FLUX, 0.17 M/S, 323 K. .... 201

FIGURE 7-11. TREND OF CA DECREASE DURING RESISTANCE TESTS. COATINGS: ZRO<sub>2</sub>/S10-20/80\_2 (A, B); ZRO<sub>2</sub>/S10-30/70\_1 (C, D). LEGEND:  $\times$  = NH<sub>2</sub>CL/NHCL<sub>2</sub> SOLUTION, T= 323 K;  $\square$  = HCL SOLUTION, T=323 K;  $\bullet\bullet\times\bullet\bullet$  = WATER, T=323 K;  $\bullet\bullet\bullet\bullet$  = WATER FLUX, T=343 K, FLOWRATE=0.17 M/S..... 202

FIGURE 7-12. COATING RESISTANCE AGAINST EROSION IN LIQUID ENVIRONMENTS: COMPARISON BETWEEN THE STARTING CA (■) AND THE CA AT THE END OF THE TEST (■). COATING: ZRO<sub>2</sub>/F10-20/80\_1. TEST CONDITIONS: 1= WATER FLUX, 0.17 M/S, 323 K; 2= WATER, 323 K; 3= HCL, PH=2, 323 K; 4= NH<sub>2</sub>CL-NHCL<sub>2</sub>, PH=7, 323 K..... 203

FIGURE 7-13. COATING RESISTANCE AGAINST EROSION DUE TO SYNTHETIC SEAWATER: COMPARISON BETWEEN THE STARTING CA (■) AND THE CA AT THE END OF THE TEST (■). COATING: 1= SiO<sub>2</sub>/S10-20/80\_2; 2= SiO<sub>2</sub>/S10-20/80\_1..... 204

FIGURE 7-14. TREND OF CA DECREASE DURING IMMERSION IN SYNTHETIC SEAWATER. LEGEND:  $\blacktriangleleft$  SiO<sub>2</sub>/S10-20/80\_2 COATING;  $\blacktriangleright$  SiO<sub>2</sub>/S10-20/80\_1 COATING. .... 205

FIGURE 7-15. PHOTOGRAPHS OF THE WATER DROPLET DEPOSITED ON THE INTERNAL SURFACES OF THE TUBES AFTER THE PARTICULATE FOULING TEST. SiO<sub>2</sub>/S10-20/80\_1 (A); SiO<sub>2</sub>/S10-20/80\_2 (B).....208

FIGURE 7-16. QUANTITY OF HEAT TRANSFERRED ( $Q$ ) VS TIME. ◆ HEAT EXCHANGER COATED BY THE HYBRID SiO<sub>2</sub>/S10 FORMULATION (STHX A); ○ UNCOATED HEAT EXCHANGER (STHX B); — LINEAR TREND STHX A; - - - - LINEAR TREND STHX B.....212

FIGURE 7-17. OVERALL HEAT TRANSFER COEFFICIENT ( $U_{LM}$ ) VS TIME. ◆ HEAT EXCHANGER COATED BY THE HYBRID SiO<sub>2</sub>/S10 FORMULATION (STHX A); ○ UNCOATED HEAT EXCHANGER (STHX B). .....215

FIGURE 7-18. FOULING RESISTANCE ( $R_f$ ) VS TIME. ◆ HEAT EXCHANGER COATED BY THE HYBRID SiO<sub>2</sub>/S10 FORMULATION (STHX A); ○ UNCOATED HEAT EXCHANGER (STHX B). .....217

## LIST OF TABLES

TABLE 1-1. FOULING OF HEAT EXCHANGERS OBSERVED IN SOME IMPORTANT INDUSTRIES. ....	7
TABLE 1-2. THERMAL CONDUCTIVITIES OF METALS TYPICALLY USED FOR THE MANUFACTURE OF HEAT TRANSFER SURFACES, IN COMPARISON WITH THE THERMAL CONDUCTIVITIES OF SOME FOULANT MATERIALS.....	8
TABLE 2-1. CHEMICAL COMPOSITION OF STAINLESS STEEL AISI 316, REPORTED ON TECHNICAL SHEET.	41
TABLE 2-2. MECHANICAL AND PHYSICAL PROPERTIES OF STAINLESS STEEL AISI 316 AT ROOM TEMPERATURE, REPORTED ON THE TECHNICAL SHEET.....	42
TABLE 2-3. PHYSICAL AND MECHANICAL PROPERTIES OF STAINLESS STEEL TYPE SAF 2205 AND TYPE SMO 254 AT ROOM TEMPERATURE, FROM TECHNICAL SHEET. ....	43
TABLE 2-4. CHEMICAL COMPOSITION OF FLUOROLINK®S10 AND FLUOROLINK®F10 COATINGS FORMULATION AND WEIGHT PERCENTAGES OF EACH CONSTITUENT.....	46
TABLE 2-5. LABELS OF MULTILAYER COATINGS AND SPECIFICATIONS OF COMPOSITION.....	50
TABLE 2-6. LIST OF INORGANIC/ORGANIC HYBRID COATINGS. THE COATING LABEL, THE TYPE OF PREPARATION PROCEDURE AND THE REACTANT USED ARE REPORTED. ....	52
TABLE 2-7. REACTANTS AND CORRESPONDING MOLAR RATIOS FOR THE SOL-GEL SYNTHESIS OF TiO <sub>2</sub> AND SiO <sub>2</sub> NETWORKS. ....	54
TABLE 2-8. REACTANTS AND CORRESPONDING MOLAR RATIO FOR THE SOL-GEL SYNTHESIS OF ZrO <sub>2</sub> NETWORK.....	55
TABLE 2-9. COMPOSITION OF FLUOROLINK®S10 AND FLUOROLINK®F10 FORMULATIONS FOR THE TWO STEPS SYNTHESIS OF ORGANIC/INORGANIC HYBRID COATINGS. ....	55
TABLE 2-10. ORGANIC/INORGANIC HYBRID COATINGS PREPARED WITH THE TWO STEPS PROCEDURE. ....	57
TABLE 2-11. CHEMICALS USED FOR THE PREPARATION OF SiO <sub>2</sub> /PFPE HYBRID COATINGS AND CORRESPONDING MOLAR RATIOS. ....	58
TABLE 2-12. CHEMICALS USED FOR THE PREPARATION OF ZrO <sub>2</sub> /PFPE HYBRID COATINGS AND CORRESPONDING MOLAR RATIOS. ....	59
TABLE 2-13. ORGANIC/INORGANIC HYBRID COATINGS PREPARED BY THE ONE STEP PROCEDURE AND USED IN THE EXPERIMENTAL SECTION.....	60
TABLE 4-1. SPECIFICATION AND CHEMICAL COMPOSITION OF TAP WATER USED FOR THE RESISTANCE TESTS. ....	72

TABLE 4-2. SYNTHETIC SEAWATER PREPARATION. LISTS OF REAGENTS FOR THE PREPARATION OF SOLUTION 1 AND SOLUTION 2 IN DISTILLED WATER. ....73

TABLE 4-3. DESIGN SPECIFICATIONS OF THE SHELL AND TUBES HEAT EXCHANGERS CONSTITUTING THE PILOT PLANT I. ....88

TABLE 4-4. SPECIFICATIONS OF THE OPERATING UNITS AND OF THE MEASURING DEVICES, WORKING ON THE PILOT PLANT I. THE SYMBOLS USED FOR REFERRING TO THE DEVICES ARE THE SAME USED IN THE FLOWSHEET OF THE PLANT.....89

TABLE 4-5. DESIGN SPECIFICATIONS OF THE SHELL AND TUBES HEAT EXCHANGERS CONSTITUTING THE PILOT PLANT II.....92

TABLE 5-1. VARIABLES FOR THE OPTIMIZATION OF THE COATINGS DEPOSITION AND CORRESPONDING VALUES USED IN THE EXPERIMENTATION ..... 100

TABLE 5-2. FORMULATION AND COATING CONDITIONS ADOPTED FOR THE OBTAINMENT OF THE S10 AND F10 COATINGS. .... 102

TABLE 5-3. RELATIVE ATOMIC ABUNDANCE (%) OF THE S10 AND F10 COATINGS, DETECTED BY XPS ANALYSES. .... 105

TABLE 5-4. PROFILOMETRY RESULTS FOR THE S10 AND F10 COATINGS DEPOSITED ON STAINLESS STEEL PLAIN SAMPLES. .... 107

TABLE 5-5. WETTING PROPERTIES OF THE STAINLESS STEEL PLAIN SAMPLES BEFORE AND AFTER THE COVERAGE WITH S10 AND F10. .... 110

TABLE 5-6. CASO<sub>4</sub> FOULING DEPOSITS AMOUNTS, FORMED ON UNCOATED TUBES SAMPLES AND ON TUBES SAMPLES COATED WITH FLUOROLINK®S10 OR F10. .... 123

TABLE 5-7. OPERATING CONDITIONS OF THE HEAT EXCHANGERS, MAINTAINED DURING THE INVESTIGATION OF THE FOULING MITIGATION ABILITY OF FLUOROLINK®S10 COATING. .... 127

TABLE 5-8. COMPARISON BETWEEN THE AVERAGE OVERALL HEAT TRANSFER COEFFICIENTS AND THE AVERAGE FOULING RESISTANCE CALCULATED (MONTHLY) FOR THE S10 COATED HEAT EXCHANGER AND THE UNCOATED HEAT EXCAHNGER..... 135

TABLE 5-9. ELEMENTAL COMPOSITION (RELATIVE ATOMIC CONTENT %), OBTAINED FROM EDX ANALYSES, OF FOULANT DEPOSITS ON THE STAINLESS STEEL HEAT TRANSFER SURFACE OF THE COATED (FLUOROLINK®S10) AND UNCOATED HEAT EXCHANGER. .... 141

TABLE 5-10. OPERATING CONDITIONS OF THE PILOT PLANT I USED FOR THE INVESTIGATION OF FLUOROLINK®F10 ABILITY IN FOULING MITIGATION ..... 144

TABLE 5-11. COMPARISON BETWEEN THE AVERAGE DAILY VALUES OF Q OF STHX A (COATED BY THE F10 POLYMER) AND STHX B, FOR SOME INDICATIVE DAYS OF WORKING. .... 147

TABLE 5-12. COMPARISON BETWEEN THE OVERALL HEAT TRANSFER COEFFICIENTS ( $U_{LM}$ ) AND THE FOULING RESISTANCE ( $R_f$ ) OF FLUOROLINK®F10 COATED HEAT EXCHANGER (STHX A) AND THE UNCOATED HEAT EXCHANGER (STHX B). .... 150

TABLE 6-1. ATOMIC COMPOSITION OF THE TiO<sub>2</sub>-OTES/S10 AND ZrO<sub>2</sub>-OTES/S10 COATINGS, DETERMINED BY XPS SURVEY ANALYSES. .... 157

TABLE 6-2. SURFACE WETTING PROPERTIES OF THE CERAMIC OXIDES SINGLE LAYERS DEPOSITED ON STAINLESS STEEL SUBSTRATES AND MULTILAYER COATINGS. .... 160

TABLE 6-3. CASO<sub>4</sub> FOULING DEPOSITS AMOUNTS, FORMED ON UNCOATED TUBES SAMPLES AND ON TUBES SAMPLES COATED WITH TiO<sub>2</sub>-OTES/S10 AND ZrO<sub>2</sub>-OTES/S10 MULTILAYER COATINGS. .... 169

TABLE 7-1. COMPARISON BETWEEN THE STATIC CONTACT ANGLE VALUES OF HYBRID COATING, PREPARED VARYING THE RELATIVE WEIGHT COMPOSITION OF PERFLUOROPOLYETHER (FLUOROLINK®S10) AND THE ORGANOMETALLIC PRECURSOR (TTIP, TEOS OR ZP), FOR THE PREPARATION OF THE SOL-GEL INORGANIC NETWORK (TiO<sub>2</sub>, SiO<sub>2</sub> OR ZrO<sub>2</sub> RESPECTIVELY). .... 174

TABLE 7-2. RELATIVE ATOMIC ABUNDANCE (%) OF THE HYBRID COATINGS CONTAINING THE POLYMER FLUOROLINK®S10 AND THE INORGANIC NETWORK OF SiO<sub>2</sub> OR ZrO<sub>2</sub>, PREPARED WITH THE TWO-STEPS OR THE ONE-STEP PROCEDURE. .... 183

TABLE 7-3. RELATIVE ATOMIC ABUNDANCE (%) OF THE HYBRID COATINGS CONTAINING THE POLYMER FLUOROLINK®F10, AND THE ORGANIC NETWORK OF SiO<sub>2</sub> OR ZrO<sub>2</sub>, PREPARED WITH THE TWO-STEPS OR THE ONE-STEP PROCEDURE. .... 186

TABLE 7-4. PROFILOMETRY RESULTS FOR THE SiO<sub>2</sub>/S10-20/80\_2 AND SiO<sub>2</sub>/S10-20/80\_1 HYBRID COATING DEPOSITED ON STAINLESS STEEL PLAIN SAMPLES. .... 187

TABLE 7-5. CA MEASUREMENTS OF HYBRID COATINGS CONTAINING THE INORGANIC NETWORK BASED ON SiO<sub>2</sub> OR ZrO<sub>2</sub>, AND THE POLYMER FLUOROLINK®S10 OR FLUOROLINK®F10. .... 189

TABLE 7-6. CASO<sub>4</sub> FOULING DEPOSITS AMOUNTS, FORMED ON UNCOATED TUBES SAMPLES AND ON TUBES SAMPLES COATED WITH SiO<sub>2</sub>/S10-20/80\_2 AND SiO<sub>2</sub>/S10-20/80\_1 HYBRID COATINGS. .... 207

TABLE 7-7. OPERATING CONDITIONS OF THE PILOT PLANT II USED FOR THE INVESTIGATION OF THE FOULING MITIGATION ABILITY OF THE HYBRID COATING NAMED SiO<sub>2</sub>/S10-20/80\_1. .... 210

TABLE 7-8. COMPARISON BETWEEN THE AVERAGE DAILY Q VALUE OF THE HEAT EXCHANGER COATED BY SiO<sub>2</sub>/S10-20/80\_1 (STHX A) AND THE UNCOATED HEAT EXCHANGER (STHX B), AT SELECTED TIME OF OPERATION.....214

TABLE 7-9. COMPARISON OF THE AVERAGE  $U_{LM}$  AND  $R_f$  VALUES, CORRESPONDING TO THREE SUB-PERIODS OF OPERATION OF THE PILOT PLANT, BETWEEN THE COATED HEAT EXCHANGER (STHX A) AND THE UNCOATED HEAT EXCHANGER (STHX B). .....216

## NOMENCLATURE

$A$ = superficial area	[m <sup>2</sup> ]
$A_c$ = cross sectional flow area	[m <sup>2</sup> ]
$A_{lm}$ = logarithmic mean of the internal and external superficial area of a cylindrical duct	[m <sup>2</sup> ]
$C_p$ = specific heat duty	[J/kgK]
$D$ = diameter	[m]
$D_{in}$ = internal diameter	[m]
$D_{out}$ = external diameter	[m]
$h$ = film coefficient	[W/hKm <sup>2</sup> ]
$k$ = Thermal conductivity	[W/mK]
$N_T$ = Number of tubes	
$Q$ = quantity of heat	[W]
Ra = average roughness	[m $\mu$ ]
$R_f$ = Fouling resistance or fouling factor	[hKm <sup>2</sup> /W]
$R_{wall}$ = wall resistance	[hKm <sup>2</sup> /W]
$S$ = tube section	[m <sup>2</sup> ]

*Nomenclature*

$S_b$  = shell section in correspondence of the baffle [m<sup>2</sup>]

$S_d$  = shell section in correspondence of the shell diameter [m<sup>2</sup>]

$T$  = Temperature [K]

$T_b$  = bulk temperature [K]

$T_w$  = wall temperature [K]

$U$  = Overall heat transfer coefficient [W/hKm<sup>2</sup>]

$U_{lm}$  = Overall heat transfer coefficient calculated on the logarithmic mean of the internal and external heat transfer surface [W/hKm<sup>2</sup>]

$u_m$  = fluid velocity [m/s]

$x$  = length [m]

$x_p$  = baffle spacing [m]

$y_L$  = tubes spacing [m]

$y_T$  = tubes pitch [m]

$W$  = mass flowrate [kg/h]

[m<sup>3</sup>/h]



Greek symbols

$\gamma$ = interfacial tension	[mN/m]
$\Delta T$ = temperature difference	[K]
$\Delta T_{lm}$ = logarithmic mean of the temperature difference	[K]
$\varepsilon_F$ = shell void fraction	[m]
$\theta$ = contact angle degrees	[°]
$\lambda$ = linear thermal expansion coefficient	[m/mK]
$\mu$ = fluid viscosity	[P]
$\mu_b$ = fluid viscosity in the bulk	[P]
$\mu_w$ = fluid viscosity in correspondence of the a tube wall	[P]
$\rho$ = fluid density	[g/cm <sup>3</sup> ]

Dimensionless numbers

$Nu$ = Nusselt number	$\frac{hD}{k}$
$Pr$ = Prandtl number	$\frac{C_p \mu}{k}$
$Re$ = Reynold number	$\frac{u_m D \rho}{\mu}$

$Re_G$  = Reynold number defined by Gnielinski

$$\frac{W x_S}{\varepsilon_F D_S \mu_b x_p}$$

# PREFACE

## Research motivations

One of the fundamental features of a chemical process is surely the ability to transfer heat efficiently; therefore, heat exchangers result the backbone of most of the industrial processes. However, the heat transfer efficiency of an industrial heat exchanger is highly affected by fouling phenomena. Usually, several strategies are simultaneously adopted to mitigate fouling in heat exchangers. Beside the engineering approach, related to the correct design of the plant, many other techniques have been developed and applied for fouling control. The use of protective coatings can be included in the “chemical approach” to mitigate fouling, even if it’s not sufficient to remediate fouling by itself. In the wide market of anti-fouling coatings, only a few of them were developed and successfully commercialized for fouling mitigation in heat exchangers. The extreme complexity of the heat transfer mechanism, together with the plant design requirements and the final cost, make, in fact, the choice of the coating not trivial. It’s still impossible to find the “perfect” coating for fouling

limitation on heat transfer surfaces, since, generally, a robust and effective fouling-release coating is characterized by a very low thermal conductivity, which compromises the overall heat transfer efficiency of the plant.

Fouling in heat exchangers is, thus, an historical problem and beside the deep knowledge of the mechanisms that regulate the fouling phenomena, the research of new strategies for fouling mitigation is still active. In the field of coating technology, the academic, but also the industrial research, is mainly focused on the development of specific solution for determined work conditions. The complexity of the topic makes the research very hard and the results obtained not always fulfil all the requirements needed, however the importance of the problem encourages industries to invest money in this research field.

## Research objectives and original contribution

This PhD research focused the attention on the mitigation of particulate and crystallization fouling phenomena on stainless steel heat transfer surfaces. The surface modification, targeted to make hydrophobic the solid substrates, emerged as an interesting strategy to control fouling on heat transfer metal surfaces. We prepared “easy to handle”, and cost-effective coatings, toward a possible utilization of the coatings at a real industrial scale. The main properties that we aimed to confer to the coatings were: hydrophobicity, thermal resistance, liquid erosion resistance and chemical resistance. In parallel, we designed a heat exchanger pilot plant for directly evaluate the fouling mitigation performance of the coatings in real conditions, but also to explore their applicability on a larger scale compared to the laboratory one.

In this research, the main materials used for coating formulations are available at industrial scale and consist of commercial perfluoropolyethers; likewise, the coating deposition procedures adopted are well-known in industries and easy to perform. The choice of use commercial products and simple deposition techniques is strictly related to the will of applying the coating technology developed on a pilot plant scale heat exchanger, which obviously implies larger quantities and more difficult operations in respect to a laboratory scale. From that standpoint, the originality of this research does not lie on the development of novel coating materials or new coating strategies, but mostly lies on the new application of old ideas in a field still open to investigation, such as the research of anti-fouling coatings for heat transfer surfaces. Moreover, we targeted our research to a possible scale-up of the coatings production and utilization. Obviously, in order to obtain a final coating conformed to all the requirements desired, we had to deal with the clear limitations of available commercial products, developed for completely different applications. For this reason, the research was directed also toward an implementation of the starting materials, i.e., the commercial polymers, by the development of new formulations and the combination with reinforcing inorganic components.



# 1 INTRODUCTION

*In this Chapter, the concept of fouling in heat exchangers is introduced, considering the effects and the remediation methods. The reduction of surface free energy is proposed as the best approach to physically mitigate fouling in heat exchangers. We made an overview of the state of the art regarding the preparation of hydrophobic coatings for fouling mitigation in heat exchangers. Finally, the materials and strategies used during this PhD research are considered in respect to the recent scientific innovations reported in literature.*

## 1.1 The problem of fouling in heat exchangers

Fouling consists in the formation of deposits of unwanted materials on solid surfaces. The term “materials” includes any type of substance or molecule, organic, inorganic or biologic, that can be dispersed or either dissolved in a fluidic media. This phenomenon is very common in heat exchangers, since operating fluids are usually rich in foulant precursors, and the normal working conditions of these plants favor the main mechanism of adhesion of the matter contained in the operating fluids on the heat transfer surfaces. Moreover, any type of processing industry, from the petrochemical to the food production, employees heat transfer units; as a result, facing the problem of fouling in heat exchangers means facing any type of fouling, due to the incredible variety of fluids composition and operating conditions involved in these processes [1]. Table 1-1 lists some examples of fouling of heat exchangers observed in different industries; it has been estimated that the 90% of heat exchangers suffer from fouling, it's thus clear the complexity and the extent of the problem [2].



Table 1-1. Fouling of heat exchangers observed in some important industries.

Industry group	Type of fouling
Chemical (generic)	Crystallization; particulate; biological; chemical reactions; corrosion.
Food	Chemical reaction; crystallization; biological; particulate.
Petroleum refineries	Chemical reaction; crystallization; particulate; biological; corrosion.
Electricity generation	Biological; crystallization; particulate; freezing; corrosion.

Fouling is a major problem in heat exchangers since the foulant layers formed on the heat transfer surfaces have in general thermal conductivity much lower than the one of the material composing the heat transfer surface (Table 1-2). The main effect of fouling is thus a reduction of the overall heat transfer efficiency of the plant. Moreover, the unwanted deposits can cause an increase of the surface roughness, hence altering the flow regime inside the tubes, or a restriction of the cross-sectional flow area, leading to higher pressure drops.

Table 1-2. Thermal conductivities of metals typically used for the manufacture of heat transfer surfaces, in comparison with the thermal conductivities of some foulant materials.

<b>Material</b>	<b>Thermal conductivity</b>
Copper	400
Brass	114
Mild steel	27.6
Titanium	21
Calcium carbonate	2.9
Calcium sulphate	2.3
Milk components	0.5-0.7
Hematite	0.6
Wax	0.24

These drawbacks have to be quantified in terms of costs, however, only few studies have been focused on the accurate determination of the economic penalties of fouling in industries and they are all dated back to 80s. No matter which is the actual cost of fouling in industries, it is possible to understand the economical extent of the problem simply considering the following aspects:

- The heat exchangers are over-dimensioned to deal with the reduction in heat transfer efficiency. An excessive heat transfer surface area corresponds to an additional capital cost and a major cost of transportation and installation, due to the bigger dimension and the high weights.
- In order to mitigate or limit fouling, it is necessary to arrange on-line or off-line cleaning strategies, which include: instruments for fluid pre-treatments, cleaning in place equipments, sophisticated anti-fouling materials, anti-fouling coatings, ecc.
- When the heat transfer efficiency of a plant decreases or the pressure drop increases due to fouling, the energetic and fuel consumption drastically rears.
- Planned or unplanned shut-downs of the plant for permitting the removal of the foulant deposits bring to production losses [2].



Figure 1-1. Example of crystallization fouling in a shell and tube heat exchanger .

## 1.2 Heat transfer principles and fouling resistance definition

The drastic nature of the fouling problem in heat exchangers obliged engineers and technologists to develop a mathematical factor able to represent the extent of the negative effect of fouling on the heat transfer efficiency of a plant. This factor is defined as the fouling resistance ( $R_f$ ) and sometimes is referred to as *fouling factor*. The traditional methods of design of heat exchangers take in consideration the potential problem of fouling and use the fouling factor for calculating the overall heat transfer coefficient  $U$ , whose value is the starting point for the correct dimensioning of the plant.

In order to understand the impact of the fouling factor on the overall heat transfer efficiency of heat exchangers, let's consider at first the mechanisms of the heat transfer across a wall and the basic principles for the determination of the heat transfer capacity of a heat exchanger.

The transfer of heat across a stationary wall is defined as *conduction* (Figure 1-2). This heat transfer mode consists in the transfer of energy, at molecular level, from the most energetic body to the lowest energetic body. Therefore, is regulated by the existence of a temperature gradient. In accordance with these considerations, the quantity of heat ( $Q$ ) transferred instantaneously across a wall (with a thickness  $x$ ), is directly proportional to the temperature difference ( $dT$ ) between the two sides of the wall and the wall area  $A$ ; this proportion is express by Equation (1-1).

$$dQ = kA - \frac{dT}{dx} \quad W \quad (1-1)$$

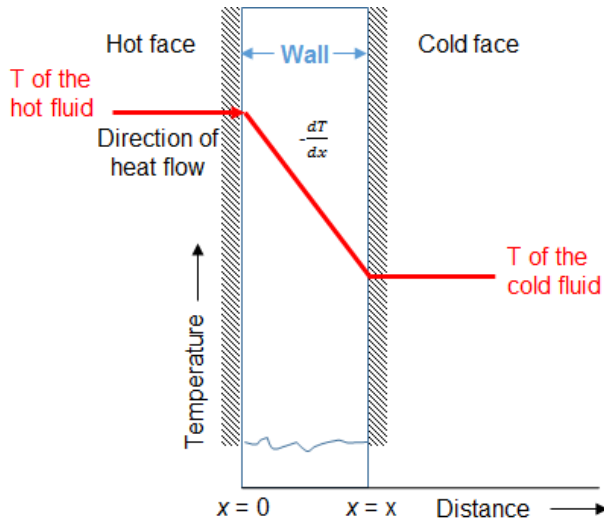


Figure 1-2. Schematic representation of the heat flow across a wall by conduction.

In Equation (1-1) the term  $-\frac{dT}{dx}$  is the temperature gradient and formally has a negative sign when the temperature is assumed higher in correspondence of  $x = 0$ . The term  $k$  denotes the thermal conductivity of the wall (expressed in W/mK). The value of  $k$  depends from the wall material; some materials (see Table 1-2) show very high thermal conductivity values and are employed for the manufacture of heat exchangers, other materials (as the foulant particles) show very low values of thermal conductivity and work as *insulators* [3].

The heat transfer from a solid wall to a fluid, or vice-versa, is favored by the fluid motion. The cold fluid adjacent to the hot solid surface receives heat, then, mixing with the bulk, transfers the heat to the whole fluid mass. This phenomenon is called *convection*, and occurs naturally, by means of fluid density gradient, or artificially, by means of mechanical agitation. The quantity

of heat  $Q$  transferred per unit time between a solid wall and a fluid by convection is expressed as follows:

$$dQ = hdA T_w - T_b \quad (1-2)$$

In Equation (1-2),  $dA$  is the surface area of contact between the fluid and the wall,  $T_w$  and  $T_b$  are the wall temperature and the bulk temperature of the fluid respectively, and  $h$  is the film coefficient, which corresponds to the reciprocal of the heat transfer resistance (dimension:  $W/hKm^2$ ). The film coefficient indicates the rate of heat transfer of a fluid under a certain agitation. This coefficient depends from the physical properties of the fluid, but also from the size and the shape of the solid wall, from the temperature difference between the fluid and the wall and even from the potential phase transition of the fluid. Due to the huge number of variables it's not possible to derive rationally the value of the fluid coefficient. Thus, in the industrial practice, the fluid coefficients are determined from a dimensional analysis (method of correlating many variables into a single Equation), followed by basic experiments, performed with a wide range of variables in order to get a general model available for any other combination of variables.

From the dimensional analysis, three fundamental dimensionless numbers have been obtained for the film coefficient determination; they are listed below:

- *Nusselt* number

$$Nu = \frac{hD}{k} \quad (1-3)$$

- *Reynolds* number

$$Re = \frac{DU_m\rho}{k} \quad (1-4)$$

- *Prandtl* number

$$Pr = \frac{C_p\mu}{k} \quad (1-5)$$

Several Equations, based on the use of these three dimensionless numbers and experimental constant values, have been proposed for the film coefficients determination, in correlation with various conditions.

The principle of the heat transfer in heat exchanger lays primarily on the conduction and convection phenomena (the radiative heat transfer is here not discussed). Indeed, the fundamental Equation of heat exchangers, describing the heat transfer efficiency of the plant, was derived as follow (Equation (1-6)):

$$Q = UA\Delta T_{lm} \quad (1-6)$$

$Q$  is the heat transferred per unit time,  $U$  is the overall heat transfer coefficient and  $\Delta T_{lm}$  is the logarithmic mean temperature difference, expressed by Equation (1-7).

$$\Delta T_{ml} = \frac{\Delta T_{hot} - \Delta T_{cold}}{\ln \frac{\Delta T_{hot}}{\Delta T_{cold}}} \quad (1-7)$$

The reciprocal of the overall heat transfer coefficient  $U$  is the overall heat transfer resistance, which is expressed as the sum of the individual resistances opposed to the heat transfer (Equation (1-8)):

$$\frac{1}{U} = \frac{1}{h_1} \frac{A_2}{A_1} + \frac{x}{k} + \frac{1}{h_2} \quad (1-8)$$

The terms  $h_1$  and  $h_2$  represent the film coefficient of the two fluids, one flowing on the external side of the heat transfer surface, and one flowing on the internal side.  $A_1$  and  $A_2$  are the heat transfer areas (external and internal) and  $\frac{x}{k}$  is the wall resistance, also expressed as  $R_{wall}$  [4].

In presence of a fouling deposit, the Equation (1-8) should be corrected. The foulant deposits, in fact, offer a further resistance to the heat transfer, as represented in Figure 1-3.

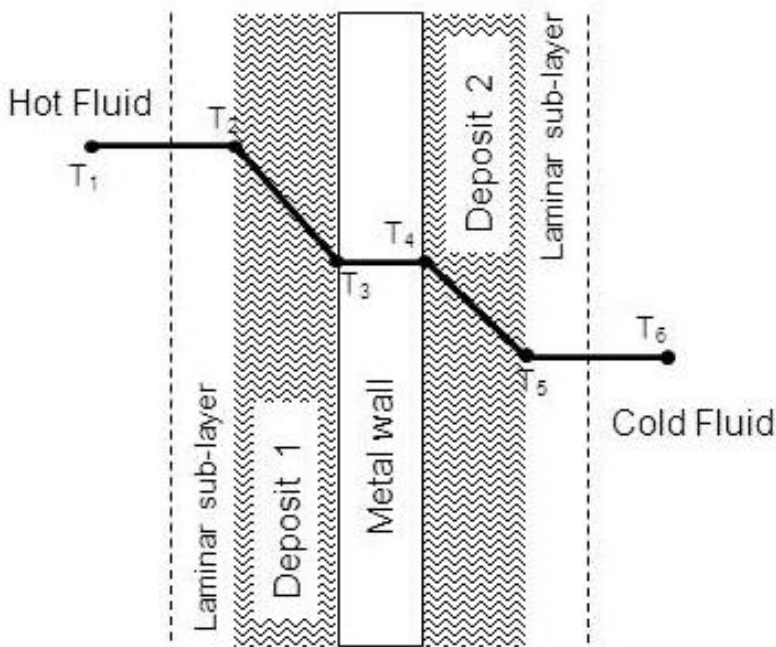


Figure 1-3. Heat conduction across a metal wall covered by fouling deposits. The presence of fouling layers strongly affects the temperature distribution, and the fouling layers offer a further resistance to the heat transfer.



Equation (1-9) is used in industrial practice for the calculation of the overall heat transfer coefficient. In this Equation, the fouling resistance ( $R_f$ ) terms are introduced:

$$\frac{1}{U} = \frac{1}{h_1} + R_{f1} \frac{A_2}{A_1} + R_{wall} + \frac{1}{h_c} + R_{f2} \quad (1-9)$$

The fouling resistance contributes to the reduction of the value of the overall heat transfer coefficient, and, hence, reduces the heat duty of the heat exchanger. In the design of a new heat exchanger, the fouling resistance can be used for determining the correct dimension of the heat transfer surface area, to achieve the desired heat duty, even in presence of fouling deposits. For this reason, the Tubular Exchanger Manufacturers Association (TEMA) provided a list of fouling resistance values for different types of fluid, which can be used as general guideline for the correct dimensioning of shell and tubes heat exchangers [2].

### 1.3 Fouling mitigation strategies

The correct design of heat exchangers is the first step to mitigate fouling. Beside the evaluation of the fouling resistance, there are other important parameters to be considered during this stage:

- Heat exchanger type and geometry.
- Operating conditions able to disadvantage fouling (adequate choose of fluid velocities in accordance with the heat exchanger geometry, in order to avoid hot spots or dead zones).
- Materials.
- Design for an easy cleaning.

However, in most cases, the correct design of the heat exchanger is not enough for permitting an efficient limitation of fouling. For this reason, on-line mitigation techniques are generally employed. A general breakdown of these methodologies has been outlined by Müller-Steinhagen et al. [5] and is briefly summed up in Figure 1-4.

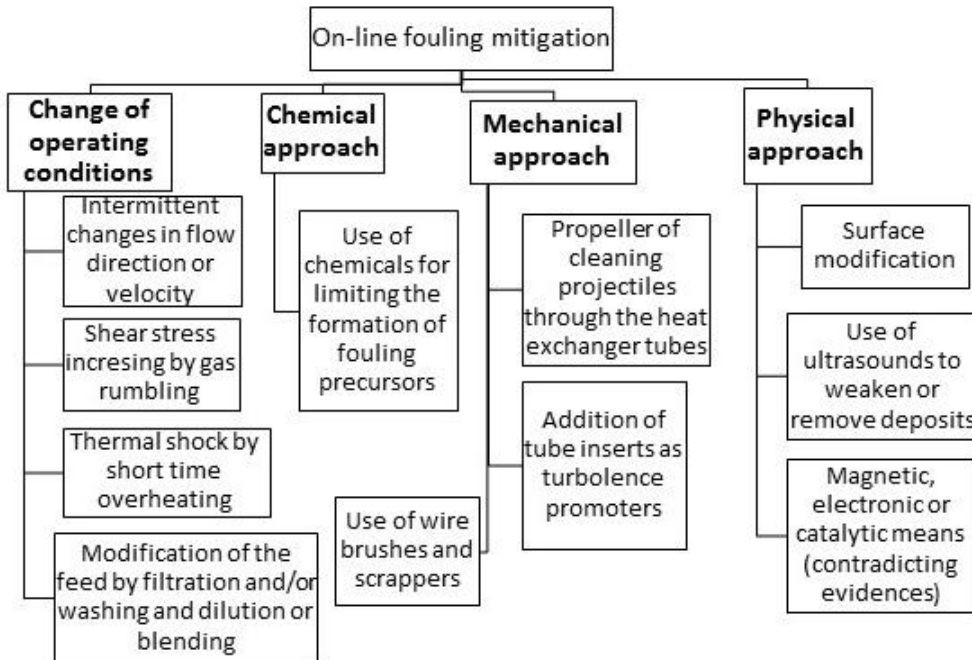


Figure 1-4. Sum-up of the on-line cleaning strategies for fouling mitigation in heat exchangers.

The chemical and the mechanical approaches are the most used in the industrial practice for the on-line mitigation of fouling. Usually these techniques are very effective, especially if applied to an initially clean heat exchanger; however, they show also many drawbacks. For example, they can be environmentally hazardous, or very expensive; they can bring to corrosion phenomena, increase

the pressure drop or require modification of the heat exchanger layout, with further operating costs.

Anyway, despite all the efforts to reduce foulant deposition in heat exchangers, it is not possible to avoid it altogether, above all considering the possible formation of different types of fouling at the same time, the different operating conditions, which varies from plant to plant, and the possible deviation from the expected operating conditions. For this reason, off-line cleaning strategies are always necessary [6]. Off-line cleaning of heat exchangers relies on chemical or mechanical methods (such as the use of projectiles or shot blasting). However, off-line cleaning may remove not only the foulant layer, but also protective layers deposited on the heat transfer surfaces, inducing further problems, such as corrosion [5].

Coming back to the on-line mitigation strategies, the physical approach is still at the early development, however, in respect to the other approaches, it tries to limit or avoid fouling without modifying the plant layout or the operating conditions, as the other approaches do. The surface modification represents a very desirable solution to mitigate fouling, since it does not imply the modification of the lay-out of the plant or the use of hazardous substances. The surface modification of a heat transfer material is easily obtained by a coating procedure; thanks to coatings it is possible to impart to the surfaces those properties needed for fouling mitigation. The modern approach to limit fouling by the modification of the surface properties of solids finds an example in nature; as demonstrated by the leaves of the flowers or the skin of some fishes, it is possible to reduce the deposition of unwanted materials by modifying the surface free energy. Even fundamental models, such as the DLVO theory, provide important correlations between the surface free energy and the

deposition rate of foulant particles on solid surfaces. In section 1.4, the topic of the free surface energy modification for fouling mitigation is more deeply discussed.

## 1.4 Modification of the surface free energy for fouling mitigation

Historically, anti-fouling coatings or paints were used in bio-fouling prevention in the marine industry. The anti-fouling paints were usually made of poisoning agents (like lead or tributyltin); however, recent environmental legislations forbade the use of biocides in coatings and paints, promoting the research and development of new anti-fouling coatings strategies, more environmental friendly [7]. In 1980', Baier [8] introduced a novel concept that brought to the development of non-toxic and environmental friendly anti-fouling coatings. It was observed a correlation between the surface free energy of a solid surface and the retention strength of some bio-foulant. Baier observed that the critical minimum surface energy to minimize foulant adhesion was 22 mN/m and this observation was validate in many natural environments, like blood, tissue, sea water or bacterial suspensions.

The Baier's observations are related to the wettability of the solid surface [9]. Thermodynamically, the wetting phenomena can be explained by the classical theory of capillarity. The core of this theory is the notion of the interfacial tension (or surface energy)  $\gamma_{ij}$ , i.e., the free energy necessary to increase the contact area between two different phases,  $i$  and  $j$  [10]. Wettability is often quantified by an empirical parameter, the contact angle (CA). The CA is the angle formed by a pure liquid, with a known surface tension, at the interface of

a solid surface. The Young Equation (1-10) expresses the relationship between the contact angle and the interfacial tension:

$$\gamma_{LV}\cos\theta = \gamma_{SV} - \gamma_{SL} \quad (1-10)$$

Three interfacial tensions are involved in the definition of the contact angle ( $\theta$ ): the liquid-vapor ( $\gamma_{LV}$ ), the solid-vapor ( $\gamma_{SV}$ ) and the solid-liquid ( $\gamma_{SL}$ ) interfacial tension. A complete wettability occurs when the CA between a solid surface and the liquid is equal to zero ( $\theta = 0^\circ$ ); when the liquid is water, this condition is referred to as superhydrophilicity. Partial wetting occurs when the CA is higher than zero; if the CA formed by a water droplet on a solid flat surface is inferior than  $90^\circ$ , the solid is defined hydrophilic ( $\theta < 90^\circ$ ); if the contact angle is higher than  $90^\circ$  the surface is defined hydrophobic ( $\theta > 90^\circ$ ). In particular, if the CA value is higher than  $150^\circ$  the surface is superhydrophobic [11].

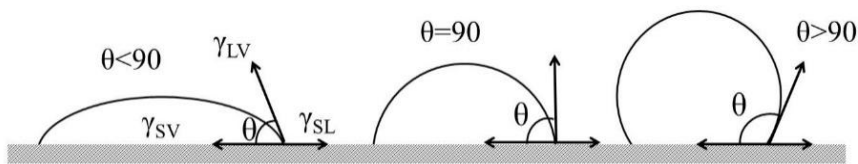


Figure 1-5. Illustrations of contact angles formed by a sessile liquid drop on a flat (ideal) surface.

In accordance with the Baier's theory, the adhesion strength or the shear strength of bio-foulants on solid surfaces is reduced when the surface free energy of the solid is 22 mN/m. That value is typical of those surfaces having a CA higher than  $90^\circ$ , i.e., hydrophobic surfaces. Marmur [12] offered a clear and simple explanation of the importance of surface wettability in fouling prevention. Since bio-foulants are suspended in water, the minimization of the contact between the solid and the water can be effective in bio-fouling

minimization, since the fouling particles dispersed in the water media do not have the possibility to get in touch with the solid surface. This can be achieved by generating an air film between the solid surface and the water, and this principle relates to the wettability of the solid surface in a solid-water-air system.

Therefore, the modification of the surface free energy of the solid material can be a possible way to minimize, at least, bio-fouling, but it was observed in literature the possibility to reduce the adhesion even of other types of fouling particles. Zhao et al. [13] studied the adhesion of  $\text{CaSO}_4$  particles on a stainless steel surface coated by an electroless-PTFE composite coating, characterized by a surface free energy value of 25-30 mN/m. They observed a potential ability of the low energy coating to reduce mineral fouling. The same result was observed by Malayeri et al. [14]. In this research, moreover, the authors pointed up the importance of the modification of the surface free energy of the solid materials, in respect to the modification of the surface roughness or geometry. According to Malayeri, the surface roughness and geometrical properties of a surface may influence the fouling phenomenon in two ways: by reducing the work of adhesion between the surface and the foulant particles, or by increasing the shear forces. Low energy surfaces are able to generate both this phenomena.

The ability of low energy surfaces to prevent fouling can be further explained considering the types of forces involved in the interactions between the foulant particles and the solid surfaces. The interfacial interactions can be either mechanic, or molecular. In this latter case, if the particles are suspended in a liquid medium, as often occurs in heat exchangers, the adhesion forces involved are mainly explained by the DLVO theory (from the names of the authors: Derjaguin, Landau, Verwey and Overbeek). The DLVO forces include *Van der*

*Waals* interactions, which are attractive forces, and the electrostatic double layer forces, which are repulsive forces. Therefore, in accordance with the DLVO theory, the adhesion of solid particles on a solid surface, across a liquid/solid interface, is a balance between attractive and repulsive forces. For preventing fouling, is thus possible to interfere with the attractive forces or favour the repulsive ones. Therefore, for example, surface finishing is very important, since the presence of cracks or crevices on the surfaces may favour the adhesion of particles, that, moving along the surface, find in these defects a position to settle [15]. Even the reduction of the free surface energy plays an important role, since hydrophilic surfaces can better interact with particles suspended in water media, in respect to hydrophobic surfaces, as demonstrated by Förster and Bohnet [16] [17]. In their works, the authors considered the crystallization fouling process in heat exchangers. Crystallization fouling occurs in heat exchangers in two steps, called the induction period and the fouling period. Both of these periods are characterized by adhesion and removal processes. The adhesion processes depends from the molecular interactions between the solid surfaces and the crystals, while the removal process primarily lays on the shear stress effect. The main difference between these periods is that in the first one (induction), the foulant particles start to form stable crystalline nuclei in the liquid media, able to adhere on the heat transfer surface, but at the same time characterized by low shear strength, and therefore easier to be removed by shear stresses. In the second period, on the other hand, occurs the formation of thick layers of deposits, which are much more difficult to be removed from the solid surface. In fact, is during the fouling period that is possible to observe the decrease of the overall heat transfer coefficient and the increase of the fouling resistance. The authors of this research demonstrated that low-energy surfaces are able to reduce the rate of nucleation of the crystals

on the solid surfaces during induction period, and to decrease the adhesive strength between crystals and the solid surfaces, promoting the removal processes, thus leading to longer fouling induction period.

In conclusion, the reduction of the surface free energy of a solid surface and the consequent variation of wettability of the surface, which becomes hydrophobic, has been deeply investigated as possible strategy to mitigate fouling by surface modification. The evidences obtained showed that hydrophobic surfaces are able to reduce bio-foulant or foulant deposition in many conditions and environments [18], even on heat transfer surfaces.

The reduction of the surface tension of a solid material can be achieved in various ways, by a coating procedure, or by the modification of the surface roughness or geometry; however it is important to highlight that in the case of application on heat transfer surfaces, the following requisites should be respected:

- The heat transfer ability of the surface should be preserved.
- The surface roughness should be not increased, since a smoother surface reduces foulant deposition.

## 1.5 Hydrophobic coatings for fouling mitigation

For practical reason, the use of coatings represents the best choice in industrial applications for surface modifications. As long as they can be easily applied, they are low costs and low toxic. In the field of heat exchangers protection from fouling, the main properties required for an anti-fouling coating, beside the hydrophobicity, are the chemical and the mechanical stability. The resistance of a coatings against erosion is clearly increased by the thickness, however the



high thickness is responsible of a reduction of the heat transfer ability of the materials, since usually these coatings, in particular if polymeric coatings, are characterized by a poor thermal conductivity. To not compromise the heat transfer capacity of the heat exchanging surfaces, the coatings thickness should be kept below  $\sim 5 \mu\text{m}$  [19]. In order to get a positive result is necessary to find a compromise between all these requirements. Currently the best commercial anti-fouling coatings are sold by Saekaphen®; these coatings are extremely effective, however their thickness ranges from 180 to 200  $\mu\text{m}$  (<http://www.saekaphen.de>). All these problems may be avoided by the use of novel coatings techniques, such as the ion implantation [19], the magnetron sputtering [20], or the cathodic vacuum arc plating [21]. All these techniques are able to mitigate fouling phenomena in heat exchangers, however their industrial application is inhibited by the cost and the complexity of the instrumentations [5]. Even the surface roughness of the coatings plays an important role in fouling control in heat exchangers. In fact, the more the surface is rough, the larger is the contact surface area for the foulant particles; therefore, a careful control of the roughness profile of the coated materials is required [2].

A part of the academic and industrial research is thus focused also on the development of novel organic or inorganic coatings, which can be applied by a common industrial coating procedure. Rosmaninho et al. [22] explored different types of hydrophobic coatings for fouling mitigation by milk components, on heat transfer surfaces. They evaluated the anti-fouling effect of diamond like carbon (DLC) sputtering, ion implantation, chemical vapour deposition of DLC and  $\text{SiO}_x$ , autocatalytic Ni-P-PTFE coatings and silica coatings. The Ni-P-PTFE coatings emerged to be the best solution for the mitigation of fouling, since they showed the lower surface energy value and the higher removal potential for

both the micro-biological deposits and the inorganic deposits due to milk. Similar conclusions were obtained by Cheng et al. [23]; the addition of PTFE particles into Ni-Cu-P matrixes permit the obtainment of low energy coatings able to mitigate mineral fouling ( $\text{CaSO}_4$ ) on heat transfer surfaces. Fluoroalkylsilane was positively employed for obtaining hydrophobic coatings on metal surfaces by simple dipping procedures. Experimentations on  $\text{CaCO}_3$  fouling mitigation on heat transfer surfaces showed lower foulant nucleation and adhesion on the solid surfaces in respect to hydrophilic surfaces; however, the poor mechanical properties of the fluoroalkylsilane coatings inhibit their application on heat transfer surfaces [24]. Cai et al. [25] [26] combined the hydrophobic properties of fluoroalkylsilane with  $\text{TiO}_2$  for obtaining composite coatings by a multilayer approach. The coatings showed good anti-fouling ability during mineral fouling in pool boiling, moreover, the heat transfer capacity of the metal surfaces was preserved. Either Yang et al. [27] investigated the  $\text{CaCO}_3$  fouling on pool boiling systems. They observed that ultrathin organic films with low surface energy (a copper-decosanoic acid self-assembled monolayer), deposited on copper substrates, reduced the fouling rate, generating a fouling induction period which was not observed on normal copper surfaces in that fouling conditions. Further evidences, regarding the ability of organic coatings to reduce fouling phenomena in heat exchangers, are presented in the work of Malayeri et al. [14]; they obtained unstructured and nano-structured organic coatings on stainless steel, with thickness in the range 1.5–50  $\mu\text{m}$  and contact angles higher than  $90^\circ$ . The authors observed that in crystallization fouling conditions, the fouling induction period on the hydrophobic surfaces was longer than the one calculated for uncoated surfaces, i.e., the fouling rate was reduced. On the other hand, Wang et al. [28] investigated inorganic nano-coatings made of  $\text{TiO}_2$  deposited on copper

substrates by vacuum coating technique. The TiO<sub>2</sub> coatings showed moderate hydrophobicity, however they were able to increase the fouling induction period of pool boiling heat transfer surfaces of 50 times, in presence of a crystallization fouling phenomenon, attesting the ability of inorganic coatings to protect from fouling, as long as they are able to modify the surface wettability of the substrates.

As previously stated, in this PhD research we decide to employ the surface modification strategy to mitigate fouling on heat exchangers, focusing the attention on the utilization of hydrophobic coatings. In particular, we decided to use organic coatings, due to their low costs, easy formulation and versatility in coating procedures. We directed our choice of materials towards commercial polymers, since they are easily available at industrial level with relatively low costs. Since we had to face with the problem of hydrophobicity, of wear resistance, and erosion resistance, we also explored the possibility to modify the organic coatings by creating organic-inorganic composite coatings. In particular, we investigated the reinforcing effect played by inorganic particles by means of a multi-layer approach or by directly adding the organic compounds into an inorganic sol-gel matrix. The following sections deal with an overview of the materials used and the strategy adopted in this PhD research.

### 1.5.1 Hydrophobic fluorinated polymers: perfluoropolyethers

Polymers containing C-F bonds are defined fluoropolymers. This family of polymers shows unique properties, which are strictly related to the nature of the fluorocarbon bond. Fluorine has in fact low polarizability and high electronegativity, which make the covalent bond with carbon highly energetic

and very strong. As a result, fluoropolymers show high thermal stability and high chemical resistance, low friction coefficient, low dielectric constant, low refractive index, and, above all, low surface tension [29]. Thanks to these properties, fluoropolymers found important applications in high temperature and chemical aggressive environments. The most common commercial fluoropolymer is the one derived from tetrafluoroethylene monomers, i.e., the PTFE or polytetrafluoroethylene. PTFE has been discovered more than 50 years ago, and since then, its application as coating for temperature resistant materials has never subsided. However, PTFE and similar fluoropolymers, even if possess incredible thermal and chemical endurance, show also many drawbacks; the main one is the incredibly high viscosity (about 10 billion poise), which limits their processability. The need to prepare polymers with an easier processability, led to the development of new classes of fluorinated polymers [30].

Perfluoropolymers represent a class of fluoropolymer with a good viscosity index, which makes them easier processable. They contain only C-F bonds and, beside having all the typical properties of fluoropolymers, they also show high repellency toward water and oil. Perfluoropolyethers (PFPE) belong from this family of polymers. The synthesis of PFPE starts from the homo-monomer, which is fluorinated or perfluorinated (see Figure 1-6 for some examples). PFPE are thermally and chemically inert, their glass transition temperature is very low (about 153 K), they have low coefficient of friction and low barrier properties. Moreover, they are both hydrophobic and oleophobic, and possess a very low surface tension, that, in accordance with the average molecular weight, can vary from 10 to 25 mN/m. A further and very interesting feature of

PFPE is the non-toxicity and biological inertness. PFPE, in fact, are employed also in food and pharmaceutical industries.

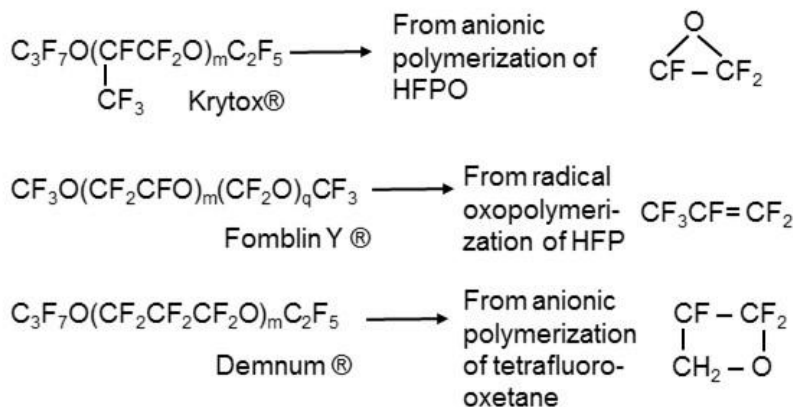


Figure 1-6. Examples of commercial perfluoropolyethers formulae with their corresponding fluorinated monomers.

PFPE are typically used as lubricants in aerospace and automotive devices, since they can resist at a wide range of temperatures and pressures and have a very high chemical stability and oxidation resistance [31]. However, some examples of the use of PFPE for the obtainment of anti-fouling coatings can be found in literature. Yarbrough et al. [32] prepared a series of cross-linkable PFPE graft terpolymers, containing different alkyl-(meth)acrylate monomers, for marine fouling prevention. In presence of *Alga Ulva* spores, the PFPE coatings exploited a promising fouling-release effect. The PFPE were also used to passivate gold substrates, obtaining micro-patterned hydrophobic surfaces; the anti-fouling activity was explored in presence of natural proteins (bovine serum albumin) and polymeric nanoparticles (latex). One more time, PFPE emerged to be capable to reduce bio-foulant adhesion [33].

The need to enhance the PFPE performances in certain fields, and above all the necessity to make them able to emulsify water, led to development of hybrid PFPE. In particular, the combination at a nano-metric scale of inorganic components with PFPE permit to obtain final products that possess both the typical properties of perfluoropolymers, and the ones of inorganic moieties, such as high modulus, low thermal expansion coefficients and chemical or thermal stability. Organic/inorganic perfluoropolyethers that possess inorganic functional groups at the ends of the polymeric chain are usually defined as  $\alpha,\omega$ -functionalized PFPE. The chemical-physical properties of these macromolecules usually reflect the properties of the polymeric backbone; however, the specific functional groups introduced are able to modify, to some extent, the general behaviour of the PFPE. Indeed, the polar ending groups are able to interact each other or generate hydrogen bonds, leading to a higher sensitivity of the viscosity toward temperature; as a result, the viscosity index is lowered. Moreover, the inorganic functional groups are able to interact with the functional groups (for example  $-\text{OH}$  groups) present at the surface of many materials. The  $\alpha,\omega$ -functionalized PFPE are, for these reasons, largely employed for coatings formulation. Yet, the influence of the inorganic functional groups on the polymer behaviour is strictly related to the molecular weight, the higher is the molecular weight, the lower is the effect of the inorganic group, since the perfluoropolyether backbone is predominant [34] [35].

We employed commercial  $\alpha,\omega$ -functionalized PFPE for the preparation of hydrophobic coatings for stainless steel substrates. The physical and chemical stability, together with the low surface tension and hydrophobicity of these materials make them perfect candidate for the formulation of anti-fouling

coatings for heat transfer surfaces. Moreover, in respect to other fluoropolymers, PFPE have a lower toxicity, and can be considered environmental friendly. In the experimental work, we optimized the coatings formulations and the deposition procedures, in order to obtain coatings with an average thickness inferior than 5  $\mu\text{m}$ , in order not to compromise the heat transfer capacity of the stainless steel. Furthermore, we explored the resistance of the coatings against erosion and wear played by liquid environments. Finally, we tested the anti-fouling ability of the coatings in a heat exchanger pilot-plant in presence of a crystallization fouling phenomena (scaling).

The results obtained were promising, since we observed in the pilot plant experimentation a reduction of the fouling rate on the PFPE coated surfaces. However, the resistance against physical erosion and wear induced by liquid environments was not satisfactory. For this reason, we explored the possibility to reinforce the organic coatings preparing organic/inorganic composites coatings.

### 1.5.2 Perfluoropolyethers/inorganic composite coatings

By mixing an organic material with an inorganic one, is possible to obtain a final product that shows superior properties in respect to the pure counterpart. Indeed, composite organic/inorganic materials have properties that are in between the original properties of the pure components, and offer the main advantageous properties of both the organic materials and inorganic ones. Organic materials can offer structural flexibility, tunable electronic properties, hydrophobic and oleophobic behaviour, enhanced optical properties, *etc.* On the other hand, inorganic materials possess important properties as thermal and

mechanical stability, wear resistance, band gap tunability and many magnetic or dielectric properties [36].

The use of inorganic compounds to improve the mechanical, chemical and physical properties of organic coatings is widely reported in literature. In the field of corrosion protection, sol-gels coatings of metal oxides play a predominant role, since they are chemically inert, very hard and poor electron conductors. However, these coatings are brittle, and often the surface is not crack-free. The addition of a polymeric component can impart to the final coating the flexibility required [37] [38]. The incorporation of aluminium powders in a polythiourethane matrix led to a final coating with improved adhesion on metal substrates and higher electrical conductivity in respect to the simple organic polyurethane coating [39]. The combination of silica and polymer matrices, like polyurethane, poly(methylmethacrylate) or poly(ethilen glycol), in nanocomposites, brought to the obtainment of novel coatings with higher modulus, increased strength and remarkable thermal stability [40]. In its review, Fisher [41] offered a general overview of the preparation methods and the applications of composite materials consisting of polymer matrices and natural or synthetic minerals. From this review emerged that almost any type of polymer building block can be combined with several inorganic compounds, as long as the preparation method is carefully performed. The result is the obtainment of materials that have enhanced desired properties, such as heat resistance, mechanical strength, or wear resistance, and have reduced undesired properties, such as gas permeability or brittleness. In the field of coating technology, the tunability of these properties is clearly outstanding. For this reason, we investigated the reinforcing effect played by inorganic materials on PFPE coatings, considering in particular the possibility to increase the



mechanical resistance of the polymeric coatings against shear stresses and the thermal stability.

We explored two possible approaches for the obtainment of composite inorganic/PFPE coatings: the multilayer deposition of inorganic and organic films and the synthesis of sol-gel organic/inorganic hybrids.

#### 1.5.2.1 Multilayer coatings made of TiO<sub>2</sub> or ZrO<sub>2</sub> nanoparticles and perfluoropolyethers

In general, the multilayer approach emerged to be a possible choice for the combination of organic and inorganic properties in coating processing. Taurino et al. investigated the scratch resistance of a multilayer coatings consisting of an organic binder, a silica precursor (organosilane) and a perfluoropolyether. The multilayer coating, deposited on glass substrates, was highly hydrophobic (CA ~150°) and, at the same time, the mechanical properties were improved. Thanks to the inorganic layer, in fact, the value of penetration resistance, together with the critical load value of the scratch tests, increased, in respect to the coatings not containing the inorganic layer. As previously reported, Cai et al. [25] explored the reinforcing effect of a TiO<sub>2</sub> nanoparticles film deposited onto a copper substrate covered by a fluoroalkylsilane layer, with consequent enhancing of the erosion resistance of the coatings employed for crystallization fouling mitigation in pool boiling. Organic/inorganic hybrid multilayer coatings were obtained on mild steel also for improving corrosion protection. The multilayer coating consisted of a layer of a conducting polymer, in which were dispersed CeO<sub>2</sub> nanoparticles loaded with a corrosion inhibitor, and an upper layer of a silica compound. Thanks to the combination of the organic polymer, the ceria nanoparticles and the silica layer, the multilayer coatings showed good

anti-corrosion properties and represented an alternative to the common chromium based anti-corrosion coatings, which have toxic effects on the environment [42].

Since the purpose of this research was to increase the resistance against erosion of the PFPE coatings, we selected as inorganic reinforcing compounds  $\text{TiO}_2$  (titania) and  $\text{ZrO}_2$  (zirconia) nanoparticles. Metal oxides nanoparticles are well-known for their hardness and chemical resistance [37]; in particular, zirconia is the material that best expresses such a properties [43]. On the other hand, titania is most used as pigment for paints production, or as a catalyst for photocatalytic reactions; however  $\text{TiO}_2$  possess also high chemical stability, high refractive index, low toxicity and can be produced at low cost, all properties that make it a multifunctional material, useful in many applications [44]. Usually,  $\text{TiO}_2$  or  $\text{ZrO}_2$  coatings are obtained by a sol-gel processes, starting from the organic precursors or from the metal halide. However, in this research, we preferred to employ the commercial nanoparticles for the preparation of the inorganic films on the metal substrates. The use of the nanoparticles, in fact, facilitates the preparation of the inorganic film, making the procedure easy to handle and low cost. The main problem related with the use of nanoparticles for coating preparation is the poor ability to disperse into solvents and the agglomeration effect. The surface modification, targeted to reduce the surface energy of the nanoparticles, can be an effective way to improve the dispersion ability of the nanoparticles in aqueous media or organic solvents and reduces their tendency to agglomerate [45]. To get a surface energy modification of the nanoparticles, we decided to impregnate  $\text{TiO}_2$  and  $\text{ZrO}_2$  with siloxanes. Siloxanes (see Figure 1-7 for chemical structure) are able to form strong bonds with inorganic compounds by the hydrolysis of the lateral  $-\text{OR}$  groups. The result of this

interaction is the reduction of the surface wettability and surface energy of the inorganic compounds, with a consequent improvement of the dispersion ability in organic solvents and a reduction of the agglomeration process [46].

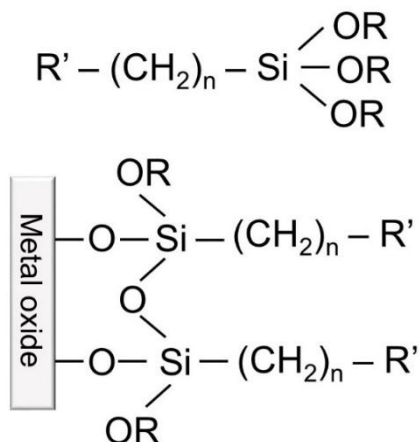


Figure 1-7. Generic chemical structure of a siloxane and siloxane interaction with a metal oxide surface. R' and R represent generic aliphatic groups.

We obtained multilayer coatings by overlapping the inorganic film with the organic one, or vice-versa. Multilayers coatings emerged to be more resistant than single PFPE coatings against chemical erosion, or shear stresses, but the stability against high temperature liquids was not improved at all. For this reason, we focused also on the preparation of organic/inorganic hybrid coatings following a different procedure; in that case, metal oxide sol-gel networks were employed for the preparation of the composite coatings.

### 1.5.2.2 Organic/inorganic hybrid sol-gel coatings

The sol-gel process has been positively employed for the preparation of organic/inorganic hybrid materials, since, in respect to other synthetic

processes, occurs at low temperature and pressure, can be easily controlled, and does not employ expensive reagents or solvents; therefore is normally considered as an environmental friendly synthetic route. Thanks to sol-gel processes, it is possible to obtain organic/inorganic hybrid materials in three ways:

- 1. By the incorporation of organic groups (polymers or oligomers) into an inorganic network.
- 2. By the co-condensation of functional groups, present on the polymers or oligomers, with metal oxides, forming stable interactions between the two components.
- 3. By the synthesis in situ of the inorganic components within an organic matrix [47].

A broader classification of the inorganic/organic hybrid coatings consider the types of interactions generated between the two phases, the first class encloses the hybrid materials in which the organic part is weakly connected to the inorganic one, by, for example, hydrogen bonds or Van der Waals interactions, leading to an interpenetration of the two components. The second class includes the hybrid systems characterized by strong bonds between the two phases, such as covalent or ionic-covalent interactions [48]. In this research, we incorporated physically the PFPE derivatives with the metal oxides by preparing the sol-gel network in co-presence with the polymer, with the aim to achieve an interpenetration of the two phases. The final features of the organic/inorganic hybrid materials obtained from this preparation route depend not only from the specific properties of the starting components, but also from the morphology of the two phases and the interfacial interactions between the two components.

The main problem of physical entrapment is the phase separation of the two components or the leaching, mainly due to the different polarity of the organic and inorganic parts [49]. However, it has been reported that this problem can be partially avoided by the functionalization of the organic molecules with triethoxysilane groups, which are able to interact with the inorganic network by co-condensation during the formation of the sol-gel [50]. The use of commercial PFPE with triethoxysilane  $\alpha,\omega$ -functionalization can be thus advantageous for the preparation of the organic/inorganic hybrid coatings.

Sol-gel preparation of inorganic networks usually starts from the metal alkoxides; silicon alkoxide is the most used precursor for the formation of a  $\text{SiO}_2$  (silica) inorganic networks, since this reagent is easy to be purified and permits a sol-gel reaction with a controlled rate. The hydrolysis and condensation of the silicon alkoxide occur in alcohols (solvent), and in presence of water. The molar ratio of the alkoxide/water plays an important role for the kinetic parameters, together with the quantity of catalyst (an acid or a base) used. The pH in fact regulates the gel point of the reaction. Beside the use of Si propoxide as chemical precursor for the formation of inorganic network, many other precursor can be employed, such as titanium(IV) propoxide, Zr(IV) propoxide or Al isopropoxide [49].

Some examples of the use of organic/inorganic hybrid coatings for fouling mitigation are reported in literature. Wouters et al. [51] explored the use of sol-gel chemistry for bio-fouling release coatings production. They obtained nanocomposite coatings by introducing sepiolite nanoparticles into an organic sol-gel matrix. Coatings were deposited on glass surfaces by spray procedure; they showed hydrophobic behaviour ( $\text{CA} \sim 90^\circ$ ) and improved bio-fouling release properties in comparison with common sol-gel coatings. Bergin et al.

[52] developed organic inorganic hybrid coatings by the interaction of polydimethylsiloxane (PDMS) with TEOS or (heptadecafluoro-1,1,2,2-tetrahydrodecyl)triethoxysilane (FTEOS). The coatings, deposited on polystyrene substrates, showed an improved and long lasting hydrophobicity. In particular, after immersion in water, the surface energy remained stable. The improvement of the PDMS organic coatings permits the application of this coatings as fouling-release coatings for marine fouling control. Organic/inorganic hybrid membrane were successfully employed for bio-fouling prevention in water filtration systems. The membrane were developed by incorporating into a sol-gel organic phase an antimicrobial drug with functionalized silica. The hybrid membrane appeared to be stable and resistant against chlorine, moreover, a suitable fouling experimentation in presence of *Escherichia Choli* bacteria did not provoke any deterioration or decrease in filtration efficiency of the membrane, attesting the ability to reduce bio-foulant adhesion [53].

In this work, titanium tetra-isopropoxide and tetraethylorthosilicate were used at first for the preparation of the inorganic networks. Both silica and titania in fact exhibit interesting properties for the reinforcement of the PFPE coatings, such as the chemical stability and the mechanical durability [54]. Furthermore, we investigated the incorporation of PFPE in zirconia networks, obtained by sol-gel process from Zirconium(IV) propoxide as a precursor. The physical incorporation of the PFPE inside the inorganic network was performed either at the end of the sol-gel process or during the hydrolysis and condensation reactions. All the formulations obtained were used for the preparation of coatings on stainless steel substrates. The resistance tests highlighted a sensitive increase of the resistance of the coatings, both against chemical erosion and

mechanical stresses, thanks to the presence of the inorganic part. The best organic/inorganic hybrid coatings were obtained from the incorporation of triethoxysilane  $\alpha,\omega$ -functionalized PFPE in silica network. Therefore, we coated the heat transfer surfaces of the heat exchanger pilot plant with one of these coatings, in order to evaluate the anti-fouling efficiency in presence of scaling. In respect to an uncoated heat exchanger, we observed a prolongation of the fouling induction period.





## 2 MATERIALS AND COATINGS PREPARATION

*This chapter deals with all the materials used during this research, starting from the metal substrates employed for the coating deposition. The main materials used for the preparation of the three different types of coatings, i.e., perfluoropolyethers coatings, multilayer coatings and hybrid coatings, are described in separate sections.*

Most of the chemicals used for coatings preparation or experimental tests, and cited in the following sections, were purchased from Sigma-Aldrich; the purity grade is  $\geq 99\%$ , where not specified. For chemicals or materials not purchased from Sigma-Aldrich, the producing company is mentioned with the material.

## 2.1 Metal substrates

Stainless steel type AISI 316 (provided by <sup>®</sup>Outokumpo) was used as metal substrate for the deposition of the hydrophobic coatings. This material is in fact the most used for the manufacture of heat exchangers, together with carbon steel and copper [1]. Type 316 is an austenitic stainless steel containing molybdenum; the specific chemical composition is reported in Table 2-1. The addition of molybdenum provides a high corrosion resistance in environments containing chlorides or other halides. Table 2-2 lists the main physical and mechanical properties of the material [55]. Different typology of stainless steel substrates were employed, depending on the experimental tests required. Plain samples with dimensions of  $30 \times 20$  mm were employed for coatings characterization and resistance tests. Tubes, with an internal diameter of 8 mm, thickness 1 mm and length 100 mm, were used for particulate fouling tests. Likewise, the heat transfer surfaces of the heat exchangers pilot plants were made of stainless steel AISI 316. All the stainless steel substrates were washed by immersion in sodium hydroxide and acetone, before the coating deposition. Moreover, some stainless steel plain samples were mechanically polished by using #40 and #80 abrasive paper and ultrasonically washed in methanol and water for 10 minutes.

Table 2-1. Chemical composition of stainless steel AISI 316, reported on technical sheet.

<b>Element</b>	<b>Maximum weight %</b>
Carbon	0.08
Manganese	2.00
Phosphorus	0.05
Sulfur	0.03
Silicon	0.75
Chromium	16.0-18.0
Nickel	10.0-14.0
Molybdenum	2.00-3.00
Nitrogen	0.10

Table 2-2. Mechanical and physical properties of stainless steel AISI 316 at room temperature, reported on the technical sheet.

<b>Properties</b>	<b>Value</b>
Density [g/cm <sup>3</sup> ]	7.889
Modulus of elasticity [psi]	$29 \times 10^6$
Coefficient of thermal expansion [293- 373 K]	$8.9 \times 10^{-6}$
Thermal conductivity [W/m K]	15.0
Heat capacity [J/kg K]	502
Ultimate tensile strength [ksi]	75 min
Hardness, Rockwell B	95 max

Other typologies of stainless steel substrates were employed for certain experiments. These materials were stainless steel type SAF 2205 and stainless steel type SMO 254 (both of them provided by <sup>©</sup>Outokumpo). The first one is a duplex stainless steel (ferritic-austenitic), characterized by a high content of chromium and nitrogen. The second one is an austenitic stainless steel containing high levels of chromium, molybdenum and nitrogen. These materials are specifically designed for operation in sea water, since they have excellent resistance against corrosion cracking in chlorine environments. The general properties of stainless steel SAF and SMO are reported in Table 2-3.

Both the substrates were rinsed in water and acetone before the coatings deposition.

Table 2-3. Physical and mechanical properties of stainless steel type SAF 2205 and type SMO 254 at room temperature, from technical sheet.

<b>Property</b>	<b>SAF 2205</b>	<b>SMO 254</b>
Thermal conductivity [W/m K]	15	13
Heat capacity [J/kg K]	500	502
Density [g/cm <sup>3</sup> ]	7.8	7.9
Tensile strength [ksi]	75 min	80 min

## 2.2 Perfluoropolyethers coatings

Two  $\alpha,\omega$ -functionalized perfluoropolyethers were selected among many commercial products for the preparation of the hydrophobic coatings. They were purchased from Solvay-Specialty Polymers, and their commercial names are Fluorolink<sup>®</sup>S10 and Fluorolink<sup>®</sup>F10 (in the following text they will be briefly expressed as S10 and F10). The selection was performed among a broader list of commercial perfluoropolyethers, containing or not functional groups at the chain ends. A preliminary investigation outlined as best candidates S10 and F10.

Fluorolink®S10 is a triethoxysilane  $\alpha,\omega$ -substituted PFPE. The general formula is presented in Figure 2-1. S10 appears as a clear liquid, with a pale yellow colour. The average molecular weight ranges between 1750-1950 g/mol; the specific density (at 293.15 K) is 1.51 g/cm<sup>3</sup> and the kinematic viscosity (293.15 K) is 173 cSt. The typical formulation of this polymer contains both water and an organic solvent; moreover, the use of a catalyst (an acid or an alkali) is required for polymer reticulation. The cross-linkage depends also from the curing conditions; at 423 K it is attested a complete cross-linkage reaction. The terminal functionalities of S10 are able to interact with –OH groups, forming covalent linkages. The –OH functional groups are generally formed at the surface of materials like glass, metals and plastics; indeed, S10 is a perfect candidate for the surface modification of stainless steel [56] [57] [58].

#### Fluorolink®S10



#### Fluorolink®F10

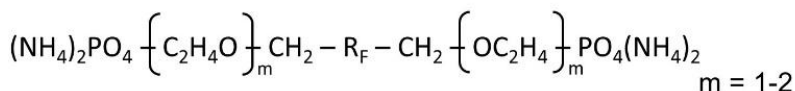


Figure 2-1. Chemical structures of Fluorolink®S10 and Fluorolink®F10.

Fluorolink® F10 possesses ammonium phosphate substitutions at the ends of the polymeric chain, as described in Figure 2-1. It is a pale brown, viscous liquid, characterized by a kinematic viscosity (at 293.15 K) of 18000 cSt. The density (at 293.15 K) is 1.73 g/cm<sup>3</sup> and the average molecular weight is comprised between 2400 and 3100 g/mol. F10 can be formulated either in organic solvents or in water (maximum weight percentage in the water formulation is 30%). In respect to S10, it does not need any catalyst for reticulation processes. The functional ammonium phosphate groups can form polar interactions with different surfaces, the data sheets suggests possible interactions with metals, stones and paper [56] [59].

Both the fluoropolymers S10 and F10 were applied on stainless steel substrates from a water containing formulation. Table 2-4 reports all the reagents used for each PFPE formulations and the relative weight percentage. The formulations containing S10 were obtained by adding the polymer to a solvent mix, made of distilled water and *iso*-propanol, adding in the end acetic acid for polymer reticulation, in the same weight percentage of the PFPE. The mixture was then stirred in a sonicated bath for 5 minutes, in order to get a pale yellow micro-emulsion. Likewise, the polymer F10 was formulated in a mix of *iso*-propanol and water, but the natural pH of the solution was not changed. The percentage of the PFPE varied from 10% to 20 wt %. The mixture was stirred in a sonicated bath for 5 minutes and a clear solution was obtained. Both the S10 and F10 formulations were freshly produced before the coating deposition on stainless steel substrates. Different formulations were prepared changing the relative weight content of each component (see Table 2-4).

Table 2-4. Chemical composition of Fluorolink®S10 and Fluorolink®F10 coatings formulation and weight percentages of each constituent.

<b>Fluorolink®S10 formulation</b>	<b>Weight %</b>
PFPE S10	0.5-5
<i>iso</i> -propanol	10-20
Water	70-89
Acetic acid (glacial – 99.9%)	0.5-5
<b>Fluorolink®F10 formulation</b>	<b>Weight %</b>
PFPE F10	10-20
<i>iso</i> -propanol	10-20
Water	60-80

A dip-coating procedure was employed for the deposition of the polymer formulation on the stainless steel substrates. At first, plain samples were coated by the aid of dip-coater instrumentation, controlling the velocity of insertion and removal from the coating bath. The dip-coating was repeated on the same sample, with the same formulation, from 5 to 10 times, at a rate of  $7.2 \cdot 10^{-3}$  m/s. Between the deposition of a PFPE layer and the subsequent, the samples were dried at room temperature for 1 hour, and heat treated at 373 K for 1 hour



(following the suggestions of the product technical sheet). This procedure permits the obtainment of very similar coatings on different samples, with a controlled thickness and uniformity. However, it required long time of preparation and implied the use of small samples.

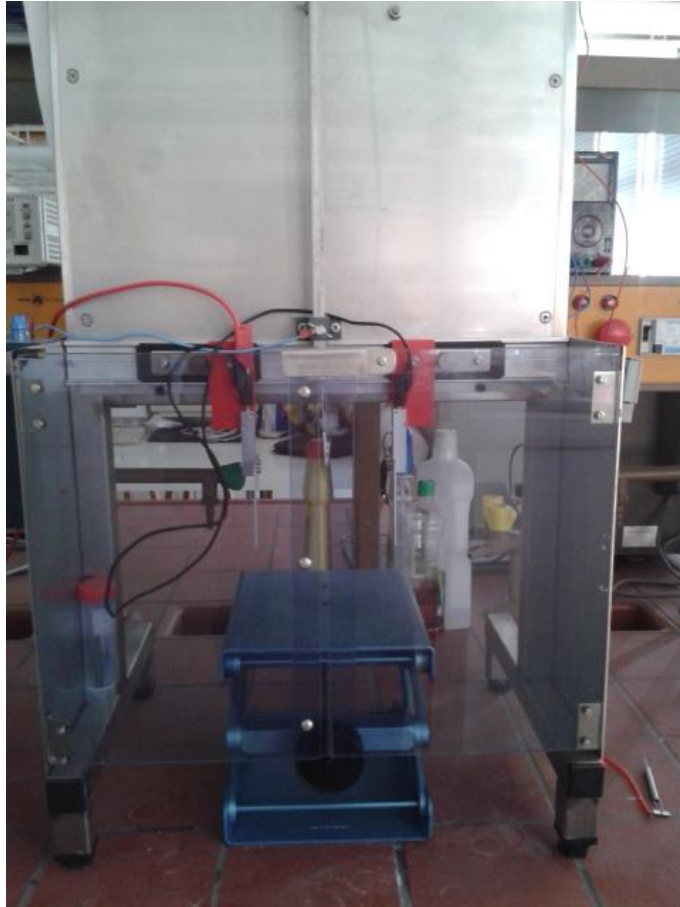


Figure 2-2. Dip-coater used for the PFPE coatings deposition on stainless steel plain samples.

Since we had to face with the necessity to coat bigger substrates, as the stainless steel tubes of the heat exchangers, we implemented a dip-coating procedure without using the dip-coater. In that case, the substrates were immersed in the

PFPE formulation without controlling the rate of insertion or removal, but prolonging the immersion time, from 5 minutes to 24 hours. After the immersion, the coated samples were dried in air at room temperature for several minutes and then heat treated in a static oven. Several heat treatment conditions were investigated varying the temperature from 353 K to 423 K and the duration from 1 hour to 48 hours.

### 2.3 Multilayer coatings

Multilayer coatings were prepared by overlapping inorganic and organic films on the stainless steel substrates. The organic films were obtained using fluorolink<sup>®</sup>S10; the PFPE formulation contained 1 wt % of S10 and 1 wt % of glacial acetic acid in a solvent solution made of 20 wt % of *iso*-propanol and 78 wt % of distilled water. The substrates were dipped inside the S10 formulation for 18 hours, dried in air, and afterward heat treated at 383 K for 3 hours. The inorganic films were obtained from the siloxane impregnated TiO<sub>2</sub> or ZrO<sub>2</sub> nanoparticles. Titanium dioxide (TiO<sub>2</sub>) nanopowders were purchased from Degussa (TiO<sub>2</sub>-P25); in this commercial product, the oxide is composed by 25% of the rutile phase and by 75% of the anatase phase. The particles size is about 25 nm and superficial area is 50 m<sup>2</sup>/g (manufacturer data). Zirconium dioxide (ZrO<sub>2</sub>) nanopowders were purchased from Sigma-Aldrich (99.99% purity). The particle size is inferior than 100 nm, and the specific surface area is  $\geq 25$  m<sup>2</sup>/g. The nanopowders were impregnated with triethoxy(octyl)silane (OTES). The impregnation step permits the reduction of the surface tension of the nanoparticles, with the aim to improve their dispersion in the organic solvent used for the coating deposition and reduce the agglomeration problems. The impregnation was carried out as follow: 0.5 g of nanopowders were

dispersed in 5 mL of dichloromethane and 0.1 g of OTES. The dispersion was stirred for 24 hours at room temperature; afterwards the solvent was evaporated by heating at 313 K for several hours. The inorganic films were obtained on the solid substrates by a spray technique. An amount of 0.05 g of the functionalized ZrO<sub>2</sub> or TiO<sub>2</sub> nanopowders were dispersed in 6 mL of *iso*-propanol by mixing in ultrasounds for 10 minutes. The metal oxide dispersion was then sprayed on the stainless steel surfaces (0.4 mL to coat 100 mm<sup>2</sup> of a plain surface). Coatings were dried in air, at room temperature, until the films were perfectly dry. Four types of multi-layer coatings were prepared, as Table 2-5 resumes. The inorganic films were deposited on the metal substrates and consequently coated with the PFPE film, or deposited on the PFPE film, previously obtained on the stainless steel substrate.

Table 2-5. Labels of multilayer coatings and specifications of composition.

Coating label	Characteristic
TiO <sub>2</sub> -OTES/S10	First film: suspension of TiO <sub>2</sub> nanoparticles, impregnated with OTES, in <i>iso</i> -propanol. Second film: S10 formulation.
S10/TiO <sub>2</sub> -OTES	First film: S10 formulation. Second film: suspension of TiO <sub>2</sub> nanoparticles, impregnated with OTES, in <i>iso</i> -propanol.
ZrO <sub>2</sub> -OTES/S10	First film: suspension of ZrO <sub>2</sub> nanoparticles, impregnated with OTES, in <i>iso</i> -propanol. Second film: S10 formulation.
S10/ZrO <sub>2</sub> -OTES	First film: S10 formulation. Second film: suspension of ZrO <sub>2</sub> nanoparticles, impregnated with OTES, in <i>iso</i> -propanol.

## 2.4 Organic/inorganic hybrid coatings

Inorganic/organic hybrid coatings were obtained by combining the PFPE and the inorganic network, obtained from sol-gel synthesis. We prepared three types of sol-gel inorganic networks; they differed from each other by the inorganic

precursor for the sol-gel synthesis, i.e., titanium tetra-isopropoxide (TTIP), silicon tetraethoxide (TEOS), and zirconium(IV) n-propoxide (ZP). Therefore the inorganic networks prepared contained  $\text{TiO}_2$ ,  $\text{SiO}_2$  and  $\text{ZrO}_2$  respectively. Each of these inorganic networks was combined, by physical incorporation, with Fluorolink<sup>®</sup>S10 or Fluorolink<sup>®</sup>F10. Two preparation procedures were implemented: the polymer was introduced in the sol-gel inorganic network after the hydrolysis and condensation process (two steps procedure); the polymer was introduced in the organic network during the sol-gel synthesis, i.e., during the hydrolysis and condensations process (one step procedure). Table 2-6 outlines the hybrid coatings optimized in this PhD research.

Table 2-6. List of inorganic/organic hybrid coatings. The coating label, the type of preparation procedure and the reactant used are reported.

<b>Coating label</b>	<b>Procedure</b>	<b>Reactants</b>
TiO <sub>2</sub> /S10_2	Two steps	Sol-gel network from TTIP precursor, incorporating the polymer S10
SiO <sub>2</sub> /S10_2	Two steps	Sol-gel network from TEOS precursor, incorporating the polymer S10
SiO <sub>2</sub> /S10_1	One step	Sol-gel network from TEOS precursor, incorporating the polymer S10
SiO <sub>2</sub> /F10_1	Two steps	Sol-gel network from TEOS precursor, incorporating the polymer F10
SiO <sub>2</sub> /F10_1	One step	Sol-gel network from TEOS precursor, incorporating the polymer F10
ZrO <sub>2</sub> /S10_2	Two steps	Sol-gel network from ZP precursor, incorporating the polymer S10
ZrO <sub>2</sub> /S10_1	One step	Sol-gel network from ZP precursor, incorporating the polymer S10
ZrO <sub>2</sub> /F10_1	One step	Sol-gel network from ZP precursor, incorporating the polymer F10

### 2.4.1 Two steps preparation method

The two steps preparation of the hybrid coatings implies the physical combination of the PFPE (Fluorolink<sup>®</sup>S10 or Fluorolink<sup>®</sup>F10) with the inorganic network at the end of the hydrolysis and condensation processes.

The inorganic networks from TTIP and TEOS were obtained following the procedure reported in [54]. Table 2-7 lists the chemical reactants used for the sol-gel synthesis of titania and silica networks, with the corresponding molar ratio. Titania sol-gel was prepared by introducing, drop-wise, the distilled water into a flask containing a solution of TTIP, *iso*-propanol, and acetic acid (glacial, 99.9% purity), previously stirred at room temperature for 10 minutes. After the addition of water, the solution was stirred for 30 minutes at room temperature, until a clear yellow sol-gel was obtained. The silica sol-gel was obtained by introducing, drop-wise, the water into a solution of TEOS and *iso*-propanol, previously mixed at room temperature for several minutes. Consequently hydrochloric acid (HCl, 37 wt % in water) was added in order to regulate the pH value at 2. The solution was then stirred under reflux at 353 K for 90 minutes; a transparent sol-gel was the final product.

Table 2-7. Reactants and corresponding molar ratios for the sol-gel synthesis of TiO<sub>2</sub> and SiO<sub>2</sub> networks.

<b>Chemicals for TiO<sub>2</sub> sol-gel network</b>				
	TTIP	<i>iso</i> -propanol	Water	Acetic acid
Molar ratio	1.0	30.6	4.0	0.3
<b>Chemicals for SiO<sub>2</sub> sol-gel network</b>				
	TEOS	<i>iso</i> -propanol	Water	Hydrochloric acid
Molar ratio	1.0	42.0	4.0	pH=2

The zirconia sol-gel was instead prepared following the procedure reported in [60]. In brief, the ZP precursor was mixed with *iso*-propanol in the molar ratio 1:15 at room temperature in a one neck flask. Glacial acetic acid was then added, drop-wise, in the molar ratio reported in Table 2-8. The solution was kept under agitation for 2 hours at room temperature. Afterwards, a solution made of *iso*-propanol, water and nitric acid (98% purity), in the molar ratio 7.5:1:0.6, was added drop-wise into the first solution, continuously stirred. After the addition of water, the solution was kept under stirring for further two hours at room temperature, until the formation of a transparent sol-gel. The



final molar ratio of all the reactants used for the sol-gel synthesis of  $ZrO_2$  network is reported in Table 2-8.

Table 2-8. Reactants and corresponding molar ratio for the sol-gel synthesis of  $ZrO_2$  network.

<b>Chemicals for <math>ZrO_2</math> sol-gel network</b>					
	ZP	<i>Iso</i> -propanol	Glacial acetic acid	Water	Nitric acid
Molar ratio	1	30	2	2	1.2

After the sol-gel synthesis, the PFPE, formulated in *iso*-propanol, was added into the inorganic-network. The PFPE formulations are listed in Table 2-9.

Table 2-9. Composition of Fluorolink®S10 and Fluorolink®F10 formulations for the two steps synthesis of organic/inorganic hybrid coatings.

<b>Components</b>		
	Fluorolink®S10	<i>Iso</i> -propanol
Content [weight %]	3	97
	Fluorolink®F10	<i>Iso</i> -propanol
Content [weight %]	7.2	92.8

The total amount of S10 or F10 introduced in the sol-gel network was optimized in accordance with the amount of the organic precursor (TTIP, TEOS or ZP) used for the sol-gel synthesis. The following weight ratios PFPE/organic precursors were investigated: 50/50; 70/30; 80/20. The solution obtained after the addition of the polymer formulation to the sol-gel inorganic network was kept under stirring at room temperature for 24 hours.

Coatings were obtained by a dip-coating procedure. The stainless steel substrates were immersed inside the hybrid formulation for 1-3 hours. The heat treatment was performed firstly at a temperature of 383 K in static oven for 3 hours; afterwards, the temperature was raised until 473 K and the sample was kept at this temperature for a further hour. Several types of coatings were obtained following this procedure, Table 2-10 resumes all the coatings prepared following the two steps procedure.

Table 2-10. Organic/inorganic hybrid coatings prepared with the two steps procedure.

Coating name	Components	Specification
TiO <sub>2</sub> /S10-20/80_2	TiO <sub>2</sub> inorganic network and S10	The weight ratio TTIP/S10 is 20/80
SiO <sub>2</sub> /S10-20/80_2	SiO <sub>2</sub> inorganic network and S10	The weight ratio TEOS/S10 is 20/80
SiO <sub>2</sub> /F10-20/80_2	SiO <sub>2</sub> inorganic network and F10	The weight ratio TEOS/S10 is 20/80
ZrO <sub>2</sub> /S10-20/80_2	ZrO <sub>2</sub> inorganic network and S10	The weight ratio TEOS/S10 is 20/80
ZrO <sub>2</sub> /F10-20/80_2	ZrO <sub>2</sub> inorganic network and F10	The weight ratio TEOS/S10 is 20/80

### 2.4.2 One step preparation method

In the one step procedure, the PFPE (Fluorolink<sup>®</sup>S10 or Fluorolink<sup>®</sup>F10) was mixed with the alkoxide in *iso*-propanol before the initiation of the hydrolysis and condensation process. In the one step preparation method, only SiO<sub>2</sub> and ZrO<sub>2</sub> networks were prepared.

The hybrid coatings containing SiO<sub>2</sub> inorganic networks and S10 or F10 were prepared as follows: a certain amount of PFPE was mixed with TEOS, glacial

acetic acid and *iso*-propanol in a one neck flask, stirring at room temperature for several minutes. The weight ratios PFPE/TEOS selected were 50/50, 70/30 and 80/20, while the molar ratio TEOS/acetic acid/*iso*-propanol was 1/1.2/41. A solution made of water, and *iso*-propanol (in the molar ratio 1/167) was then introduced dropwise and pH was adjusted by adding nitric acid in the molar ratio reported in Table 2-11. The solution obtained was stirred at room temperature for 24 hours; in that time the complete hydrolysis of the silica precursor occurred. Table 2-11 lists all the chemicals used for the sol-gel synthesis, and the corresponding molar ratios, for the one step preparation of SiO<sub>2</sub>/PFPE hybrid coatings. Considering the total amount of *iso*-propanol used for this preparation, the weight percentage of S10 in respect to the solvent was 1.5%, while the F10 was 6.6 wt %.

Table 2-11. Chemicals used for the preparation of SiO<sub>2</sub>/PFPE hybrid coatings and corresponding molar ratios.

<b>Chemicals for the one step preparation of SiO<sub>2</sub>/S10 hybrid coatings</b>					
	TEOS	<i>iso</i> -propanol	Nitric acid	Acetic acid	Water
Molar ratios	1.0	228.0	1.7	1.2	4.0
<b>Chemicals for the one step preparation of SiO<sub>2</sub>/F10 hybrid coatings</b>					
	TEOS	<i>iso</i> -propanol	Nitric acid	-	Water
Molar ratios	1.0	52.0	1.7	-	4.0

The hybrid coatings containing S10 and  $ZrO_2$  (in the weight ratios, 50/50 or 70/30 respectively), were prepared by mixing ZP and S10 in *iso*-propanol (with a molar ratio  $ZP/iso\text{-propanol} = 1/112$ ). Acetic acid was then added drop-wise, in the molar ratio reported in Table 2-12, and the solution was kept under stirring for 2 hours at room temperature. After this time, a solution made of water, *iso*-propanol and nitric acid (98% purity) in the molar ratio 1/100/0.7 was added drop-wise, the solution was mixed for further 24 hours at room temperature. At the end of the sol-gel synthesis, the weight percentage of S10 in respect to the total amount of solvent (*iso*-propanol) was 1.5%. The F10/ $ZrO_2$  hybrid formulation was obtained following the same procedure; however the molar ratio  $ZP/iso\text{-propanol}$  was changed, in order to obtain a final formulation containing 6.6 wt % of F10 in respect to the total amount of *iso*-propanol (see Table 2-12).

Table 2-12. Chemicals used for the preparation of  $ZrO_2$ /PFPE hybrid coatings and corresponding molar ratios.

---

**Chemicals for the one step preparation of  $ZrO_2$ /S10 hybrid coatings**

---

	ZP	<i>iso</i> -propanol	Acetic acid	Nitric acid	Water
Molar ratios	1	231.0	2	1.2	2

---

**Chemicals for the one step preparation of  $ZrO_2$ /F10 hybrid coatings**

	ZP	<i>iso</i> -propanol	Acetic acid	Nitric acid	Water
Molar ratios	1.0	52.0	2	1.2	2

---

Coatings were obtained on stainless steel substrates following the same procedure described in the previous paragraph (2.4.1 pp. 53). The list of the coatings prepared with the one step procedure and the corresponding labels is reported in Table 2-13.

Table 2-13. Organic/inorganic hybrid coatings prepared by the one step procedure and used in the experimental section.

<b>Coating name</b>	<b>Components</b>	<b>Specification</b>
SiO <sub>2</sub> /S10-30/70_1	SiO <sub>2</sub> inorganic network and S10	The weight ratio TEOS/S10 is 30/70
SiO <sub>2</sub> /S10-50/50_1	SiO <sub>2</sub> inorganic network and S10	The weight ratio TEOS/S10 is 50/50
SiO <sub>2</sub> /S10-20/80_1	SiO <sub>2</sub> inorganic network and S10	The weight ratio TEOS/S10 is 20/80
ZrO <sub>2</sub> /S10-30/70_1	ZrO <sub>2</sub> inorganic network and S10	The weight ratio ZP/S10 is 30/70
ZrO <sub>2</sub> /S10-50/50_1	ZrO <sub>2</sub> inorganic network and S10	The weight ratio ZP/S10 is 50/50
ZrO <sub>2</sub> /S10-20/80_1	ZrO <sub>2</sub> inorganic network and S10	The weight ratio ZP/S10 is 20/80
SiO <sub>2</sub> /F10-30/70_1	SiO <sub>2</sub> inorganic network and F10	The weight ratio TEOS/F10 is 30/70

Coating name	Components	Specification
SiO <sub>2</sub> /F10-50/50_1	SiO <sub>2</sub> inorganic network and F10	The weight ratio TEOS/F10 is 50/50
SiO <sub>2</sub> /F10-20/80_1	SiO <sub>2</sub> inorganic network and F10	The weight ratio TEOS/F10 is 20/80
ZrO <sub>2</sub> /F10-20/80_1	ZrO <sub>2</sub> inorganic network and F10	The weight ratio ZP/F10 is 20/80





## 3 CHARACTERIZATION PROCEDURES

*The chapter concerns the characterization procedures and the analytical instruments adopted for the study of the surface properties of the coatings. The determination of the surface free energy and hydrophobicity of the coatings were evaluated by contact angle measurements. The coatings morphology and distribution on stainless steel substrates were assessed by scanning electron microscopic analyses; X-ray photoelectron spectroscopy was used to assess the coatings composition and the chemical contour of the metal atoms constituting the inorganic part of the composite coatings. The coatings thickness and roughness were investigated by profilometry.*

### 3.1 Contact angle measurements

All the coatings prepared on plain stainless steel surfaces were characterized by contact angle (CA) measurements, in order to establish the surface wettability and the surface free energy. Contact angle measurements were performed on a Krüss Easy Drop instrument. We measured both static and dynamic CA, using water (milli-Q distilled water) as test liquid.

In static CA determination, the drop profile was extrapolated by using the conic section method for CA inferior than  $100^\circ$  and the Young-Laplace method for CA up to  $100^\circ$ . In the former method, the shape of the sessile drop is assumed to form an elliptical arc on the solid surface (yellow dotted line in Figure 3-1). The parameters for the conic section equation are matched to the drop shape, which is physically determined; the lines are tangential to the elliptical curve and pass through the point of intersection of the arc with the baseline. The contact angle ( $\theta$ ) is determined on both the sides of the drop in correspondence of the three phase contact point. In the latter method, the drop shape is assumed on the shape of an ideal sessile drop, considering also the effects of gravity and liquid weight on the drop curvature. The Young-Laplace Equation correlates the radii of a curvature ( $r_1$  and  $r_2$ ) with the surface tension ( $\sigma$ ) and the Laplace pressure ( $p$ ) as follows (Equation (3-1)):

$$\Delta p = \sigma \left( \frac{1}{r_1} + \frac{1}{r_2} \right) \quad (3-1)$$

The parameters of the Equations system which models the shape of the sessile drop are obtained from a numerical analysis. The contact angle is finally determined at the points of intersection of the modelled contour with the baseline [61].

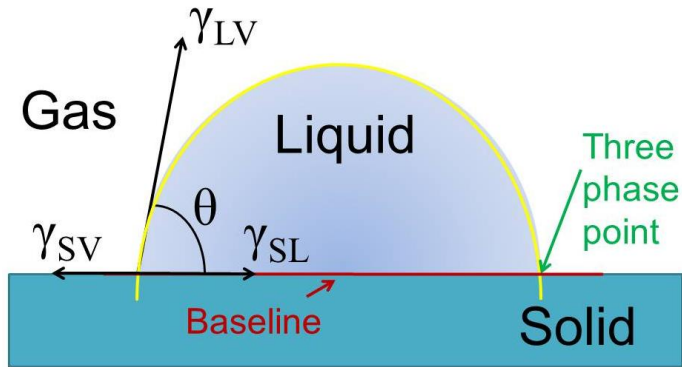


Figure 3-1. Illustration of the interactions between a liquid drop and a solid surface according to Young's Equation. Description of the elements necessary for the determination of CA ( $\theta$ ) from the drop shape analysis.

The Young Equation (1-10) expresses a single and unique value of contact angle. However, the wetting phenomenon is not static, in fact, once the drop is deposited on the solid surface, it can assume many metastable states, due to the tendency of the liquid to move and to expose its fresh surface to the solid. This phenomenon always occurs on real surfaces, which show asperities and inhomogeneity. In that sense, the measurement of a static CA is no longer correct; to obtain more accurate information about the wettability of a real solid, the measurement of the dynamic CA is of particular importance. In the dynamic contact angle measurements, the three phase point is in motion; this can be obtained by expanding and contracting the volume of the liquid, as shown in Figure 3-2. Hence, it is possible to obtain a range of CA values, whit advancing CA ( $\theta_{adv}$ ) approaching the maximum value, and receding CA ( $\theta_{rec}$ ) the minimum value.

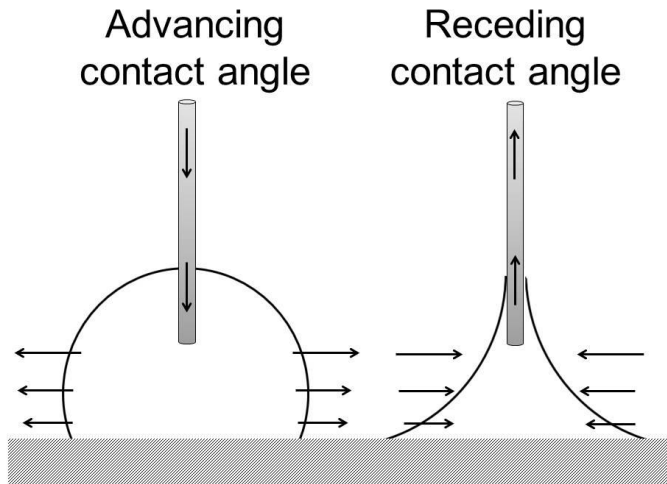


Figure 3-2. Illustration of the advancing and receding contact angles.

The difference between the advancing and receding CA is called hysteresis. On ideal smooth and homogeneous surfaces, no contact angle hysteresis is detectable, thus the static CA is equal to the advancing CA. On the other hand, in presence of heterogeneous surfaces, a contact angle hysteresis may occur. In particular, if the surface is rough, the  $\theta_{adv}$  and  $\theta_{rec}$  are different from the Young CA (determined in static conditions). The CA on rough and heterogeneous surfaces determined in thermodynamic equilibrium are called Wenzel and Cassie-Baxter contact angles [62]. The actual Wenzel or Cassie-Baxter contact angle is defined in Equation (3-2); the relationship between the ideal contact angle ( $\theta_Y$ , from Young's Equation) and the Wenzel or Cassie-Baxter contact angle ( $\theta_W$ ) is mediated by the roughness  $r$  of the surface, expressed as the ratio between the true surface area and the apparent one.

$$\cos\theta_W = r \cos\theta_Y \quad (3-2)$$

The Wenzel state (

Figure 3-3 a) occurs when the liquid spread follows the profile of the surface. In that case, during the measurement of the receding CA a part of the liquid remains into the cavities of the asperities. Thus, the receding drop gets in contact with the liquid left in the cavities, leading to a receding CA value lower than the advancing one. Consequently, the CA hysteresis may be very large. Otherwise, in the Cassie-Baxter state, when the liquid spreads on the surface, leaves air into the cavities (Figure 3-3 b); as a result, the liquid contacts the solid only at the top of the asperities both during advancing CA measurement and the receding measurement. Indeed, in this state, the CA hysteresis is very small [63].

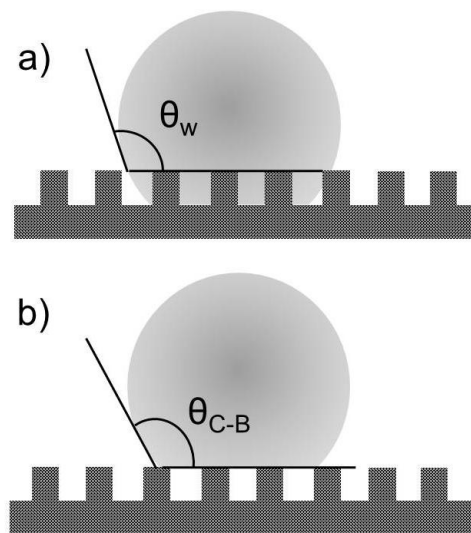


Figure 3-3. Drop shape on heterogeneous and rough surfaces. a) Wenzel state illustration; b) Cassie-Baxter state illustration.

In this work, advancing and receding contact angles were measured by increasing and reducing the volume of a sessile water drop during the drop

shape analysis, (maximum drop volume 8  $\mu\text{L}$ , flowrate: 15  $\mu\text{L}/\text{min}$ ). The values of  $\theta_{\text{adv}}$  and  $\theta_{\text{rec}}$  were recorded automatically by the instrument every 0.1 s, together with the drop volume. The profile of the sessile drop was measured by the conic section method; only the contact area was evaluated, thus this method is suitable for dynamic measurements where the needle remains in the drop.

The surface free energy (SFE) of coated samples was calculated by using the Oss and Good method [64]. This method is based on the Young's Equation (1-10) and calculates the solid-liquid tension ( $\gamma_{\text{LS}}$ ) in accordance with the Lewis acid-base theory, i.e., polar interactions take place when an electron acceptor impinges on an electron donor. According to this method, at least three liquids are required to determine the surface free energy of the solid, two liquids having an acid or a basic part and one purely dispersive liquid. For practical determination, three pairs of SFE-Theta values were obtained for each analysis by using as test liquids di-iodomethane, distilled water and formamide.

All the CA values reported in this paper are the average values obtained from at least five different determinations, depositing the liquid drops at different sample locations; only plain samples were used for contact angle determination.

### 3.2 Coatings morphology determination

The coatings morphology was observed by scanning electron microscopy (SEM). The SEM analyses were performed by using a LEO ZEISS instrument, model 1430, equipped with an EDX analyser (energy dispersive X-ray analyser), model Inca Oxford. The instrument was provided by a thermionic gun and the electron source was a tungsten filament. The experimental conditions kept for all the analyses provided a 20kV accelerating voltage in the

electron column, and a vacuum of  $10^{-5}$  torr. Before the SEM analyses, the samples were coated by a gold nanolayer (tents of Angstrom units), by sputtering technique. The gold sputter coating increases the sample conductivity without compromising the surface morphology of the underlying surface. The SEM analyses were performed to observe the coatings morphology and distribution on the metal surfaces. By tilting the sample stage ( $90^\circ$ ), it was possible to perform cross-sectional analyses of the coatings deposited on plain samples, in order to check the coating thickness. Moreover, foulant deposits obtained on the stainless steel heat transfer surfaces were characterized by SEM-EDX analyses.

### 3.3 Coatings composition and thickness determination

X-ray photoelectron spectroscopy (XPS) was employed to study the coatings atomic composition and the atoms interactions. The M-Probe apparatus (Surface Science Instruments) is equipped with a monochromatic source of Al- $K\alpha$  radiation (1486.6 eV). Both survey and high resolution analyses were performed on coated plain samples. Survey analysis permits the determination of the relative atomic composition of the top layer of the coatings (the depth of investigation of the instrument is about  $5\text{\AA}$ ). The high resolution analysis allows to examine the chemical contour of the atomic species, in order to determine the oxidation state or the chemicals bonds formed. The spot size of investigation for survey analyses is  $200\times 750\ \mu\text{m}$ , and pass energy of 1 eV/pt, while high resolution analyses were performed on a spot size of  $200\times 500\ \mu\text{m}$  and pass energy 0.03 eV/pt. The internal reference used for the peak shift correction was the 1s energy level of contaminant carbon, at 284.6 eV. The curve fittings were performed by using Gaussian's peaks and Shirley's baseline.

The coatings thickness was measured by the aim of an optical profilometer, UBM Microfocus Measurement System, on plain coated samples. The maximum resolution for the analyses on the vertical direction was  $0.006\ \mu\text{m}$ . The surface roughness was investigated on an area of  $0.3 \times 0.5\ \text{mm}$  and resolution of 500 points/mm.



Figure 3-4. Laboratory instrumentation for contact angles measurements (a), and XPS analyses (b).



## 4 EXPERIMENTAL PROCEDURES AND EQUIPMENT

*This chapter describes the experimental tests performed to assess the chemical and mechanical stability of the coatings prepared. The resistance tests were performed only in liquid environments, considering the specific application of the hydrophobic coatings for fouling mitigation in heat exchangers. The fouling mitigation activity of the hydrophobic coatings was primarily investigated in particulate fouling conditions, using a specific test-rig. Consequently, some coatings were selected for experimentation on a heat exchanger pilot plant. The equipment specifications are discussed in this chapter.*

## 4.1 Resistance tests

The coatings resistance against erosion was specifically studied in liquid environments, since the coatings were designed for application in heat exchangers, working with water. The resistance to chemical erosion was studied by dipping the plain stainless steel coated samples in different aggressive chemical solutions: alkaline solutions, prepared dissolving sodium hydroxide (NaOH) pellets in distilled water (pH=9). Acidic solutions, made by diluting hydrochloric acid (HCl, 37% wt) in distilled water (pH=2). Disinfectants solution containing chlorine (NH<sub>2</sub>Cl, NHCl<sub>2</sub> and NCl<sub>3</sub>, pH=7). The stability of the coatings was studied also by immersion in tap water (chemical composition in Table 4-1) at high temperature (343 K).

Table 4-1. Specification and chemical composition of tap water used for the resistance tests.

<b>Parameter</b>	<b>Value</b>	<b>Parameter</b>	<b>Value</b>
pH	7.8 mg/L	Potassium	1 mg/L
Calcium	87 mg/L	Sodium	14 mg/L
Magnesium	19 mg/L	Chlorides	25 mg/L
Ammonium	0.1 mg/L	Sulphites	47 mg/L
Fluorites	0.5 mg/L	Nitrates	23 mg/L

We also observed the erosion potential of synthetic seawater against the hydrophobic coatings. The synthetic seawater was prepared as follows: 245.34 g of NaCl and 92.86 g of Na<sub>2</sub>SO<sub>4</sub>·10H<sub>2</sub>O were dissolved in 8 L of distilled water. Then, 200 mL of the solution 1 (see Table 4-2) were slowly added, under vigorous stirring, and 100 mL of solution 2 (see Table 4-2). The solution thus obtained was diluted at 10 L with distilled water. The pH was regulated with a NaOH solution (0.1 M) at a value of 8.2.

Table 4-2. Synthetic seawater preparation. Lists of reagents for the preparation of solution 1 and solution 2 in distilled water.

<b>Solution 1 (for 2 L volume)</b>		<b>Solution 2 (for 1 L volume)</b>	
Reagent	Amount [g]	Reagent	Amount [g]
MgCl <sub>2</sub> ·6H <sub>2</sub> O	1111.14	KCl	69.5
CaCl <sub>2</sub> ·6H <sub>2</sub> O	229	NaHCO <sub>3</sub>	20.1
SrCl <sub>2</sub> ·6H <sub>2</sub> O	4.22	KBr	10.1
		H <sub>3</sub> BO <sub>3</sub>	2.7
		NaF	0.3

All the erosion tests previously described were performed by dipping, completely, the coated plain samples into the aggressive liquids, maintaining the solutions under moderate stirring. The effect of the aggressive environments with the temperature was also explored, thus the temperatures of the liquids

ranged from room temperature (298 K), to 323 K or 343 K. Each test lasted for 7 days in the case of simple PFPE coatings and multilayers coatings, while organic-inorganic hybrid coatings were kept immersed in the aggressive solutions even for longer periods (30 days). During the experimentation, the pH of alkaline and acidic solutions was checked and adjusted consequently, while disinfectant solutions and synthetic seawater were replaced every 1-2 days with fresh ones. During the chemical erosion tests, the coatings status was evaluated by static CA measurements. The CA values were measured each 2/3 days during the tests and compared to the one measured on the freshly coated surface. The uncoated sample surfaces had CA values inferior than  $90^\circ$  (hydrophilic surfaces), while the freshly coated samples had CA values higher than  $120^\circ$  (hydrophobic surfaces). Indeed, the decrease in CA indicated a progressive damage of the hydrophobic coatings, with a consequent restoration of the initial hydrophilicity of the stainless steel surface.

Beside the chemical erosion, we also investigated the effect of shear stresses on coatings integrity. The shear stress tests were performed by flowing tap water on the surface of the plain coated samples. In order to recreate conditions similar to the ones of a shell and tube heat exchanger, the plain samples were put inside a glass tubular sample holder (see Figure 4-1), with an internal diameter of 22 mm or 25.6 mm. The two sides of the tubular holder were connected by tubes at a thermostatic bath (temperature of the bath: 323 K), equipped with a water recirculating system, operating with a flowrate of 4 L/min. In that way the fluid velocity inside the tubular holder was kept stable at 0.13 m/s or 0.17 m/s, in accordance with the internal diameter of the tube. We estimated that in such a condition, the Re number corresponding to these water flows in the tubular sample holder was higher than 3000 (4898 and 5689

respectively); therefore, turbulent flow conditions were recreated in the test apparatus [4]. In that way, we could observe the physical erosion of the hydrophobic coatings due to shear stresses induced by the turbulent flow of water upon the surface. The shear stress tests were performed for a period of 7 days or 30 days. During the experimentation, only one side of the coated sample was directly exposed to the water flow, the other side leaned on the wall of the sample holder. CA measurements were performed on the side of the samples exposed to the water flow each 2/3 days.



Figure 4-1. Experimental apparatus for shear stress tests.

## 4.2 Particulate fouling tests

A preliminary evaluation of the anti-fouling potential of the hydrophobic coatings was performed in a specific apparatus, investigating the incidence of particulate fouling. The particulate fouling phenomenon consists in the deposition of small particles, suspended in the fluidic media, on the heat transfer surfaces, independently from their orientation. Also the settling of large particles due to gravity on horizontal heat transfer surfaces is considered particulate fouling. The particles involved in such a type of fouling are usually

inorganic particles, such as clay, silt, metal oxides or salts [65]. The particulate fouling phenomenon is dependant from the velocity of the fluidic media containing the suspended particles. As shown in Figure 4-2, the fouling resistance due to particulate fouling decreases whit increasing the water flow velocity. This is mainly due to the removal processes induced by the turbulent flow.

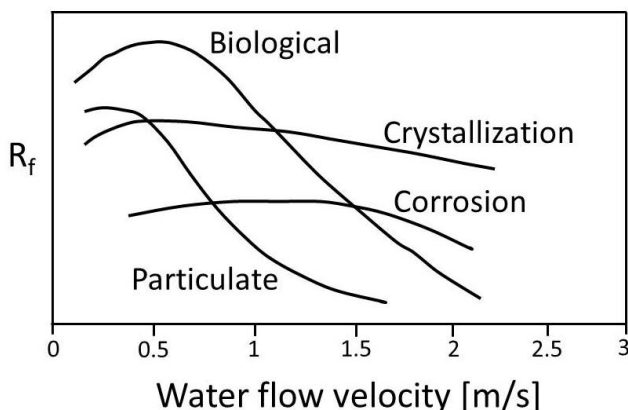


Figure 4-2. Effect of the flow velocity on the fouling resistance for different types of fouling

On the other hand, the particulate fouling phenomenon is independent from the temperature of the heat transfer surface (Figure 4-3). Thus, particulate fouling occurs on low temperature surfaces whit the same extent of high temperature surfaces [2].

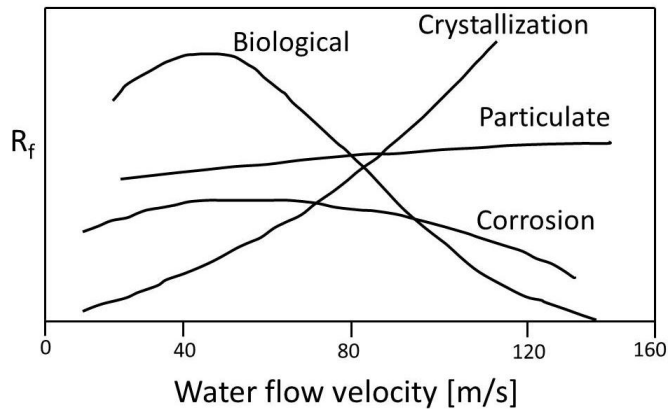
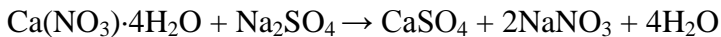


Figure 4-3. Effect of the surface temperature on the fouling resistance for different types of fouling

Figure 4-4 illustrates the test-rig designed for the particulate fouling test. In that case, stainless steel tubes were used as test samples; indeed, the experimentations were performed on tubes which internal surfaces were coated or not coated (internal reference). As foulant particles, we used calcium sulphate (CaSO<sub>4</sub>); specifically, 6 L of an aqueous solution of CaSO<sub>4</sub>, in concentration 4 g/L, was obtained by mixing a solution of calcium nitrate tetrahydrate (Ca(NO<sub>3</sub>)-4H<sub>2</sub>O) in distilled water, with a solution in distilled water of sodium sulphate (Na<sub>2</sub>SO<sub>4</sub>), in accordance with the following chemical reaction:



Thence, the solution was heated in a 6 L tank at a temperature of 313 K; in such a way, supersaturation conditions were kept inside the tank [14]. The supersaturated solution of CaSO<sub>4</sub> was pumped inside the coated tube sample, regulating the flowrate with a float flowmeter (standard accuracy ±5% of the full scale flow). Different tests were performed varying the flowrate from 0.04-

0.06 m/s to 0.13-0.15 m/s. In accordance with Figure 4-2, the water flowrate was kept relatively low to favour the particulates settling on the tube surfaces. Moreover, the tube sample was kept in horizontal position to permit the gravitational settling of the larger particles. Since the particulate fouling phenomenon is independent from the surface temperature, only the  $\text{CaSO}_4$  solution was heated at 313 K, while the metal surfaces were not heated; thus crystallization fouling phenomena inside the tube samples can be excluded.

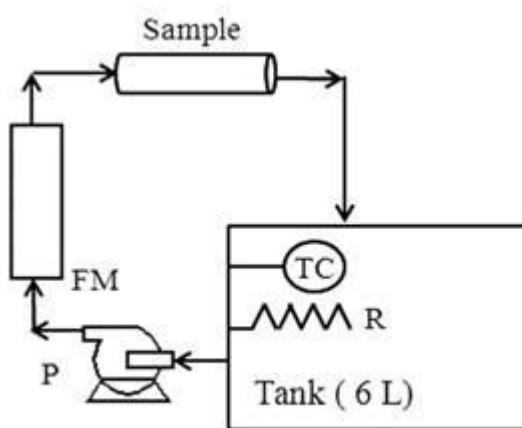


Figure 4-4. Schematic of the test rig for the evaluation of particulate fouling rate on coated stainless steel tubes. TC=thermocouple; R= heating element; P=pump; FM= float flowmeter.

The grade of particulate fouling inside the tubes was expressed as grams of  $\text{CaSO}_4$  particles deposited on the internal surface of the tube, in respect to the time of exposition and the total surface area involved in the fouling phenomenon ( $\text{g/m}^2\text{h}$ ). The grams of  $\text{CaSO}_4$  particles deposited inside the tubes samples were quantified by subtracting the initial weight of the sample to the



weight measured after the fouling test. Tests duration ranged from 24 hours to 40 days, in dependence from the type of coating involved in the fouling test.

### 4.3 Heat exchanger pilot plant

The anti-fouling efficiency of the hydrophobic coatings was eventually checked on real heat transfer surfaces, involved in fouling phenomena. This experimental part was carried out on a heat exchanger pilot plant. The pilot plant is constituted by two shell and tube heat exchangers, working in parallel. Shell and tubes heat exchangers (STHX) share the most part of the heat exchangers market (more than 60%) [66]; thanks to their robustness and reliability they are still the most important type of heat exchangers for industrial applications, despite the great technological advances of other types of heat exchangers. Moreover, the orientation of the tubes can be either vertical or horizontal, the pressures and pressures drops can be varied over a wide range of values, a great variety of materials can be used for the construction and in general the design is well established and regulated [67]. All these elements make STHX the most used heat exchanger type in the industrial practice. However, even if a good design practice may reduce fouling incidence in STHX, this equipment is highly involved in fouling phenomena [2].

The main components of STHX are briefly presented in Figure 4-5.

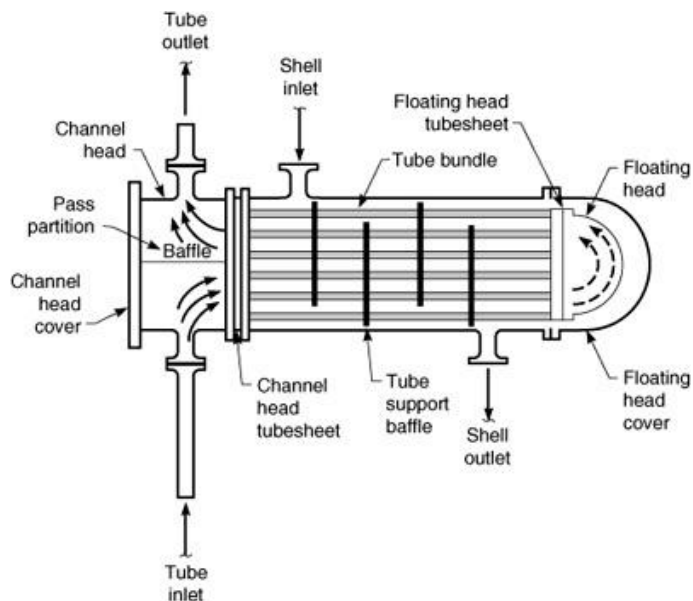


Figure 4-5. Main components of a shell and tubes heat exchanger, working in counter flow.

Shell and tubes heat exchangers are constituted by a tube bundle, usually containing a large number of tubes, packed inside a shell. The axes of the shell and the tubes are the same. Usually, the hot fluid, or the most aggressive fluid, is flowed inside the tubes, while the cold fluid is placed on the shell-side. Fluids can enter in the shell and tubes either on the same side, flowing on the same direction (parallel flow), or on opposite sides, thus flowing in opposite directions (counter flow), as shown in Figure 4-6.

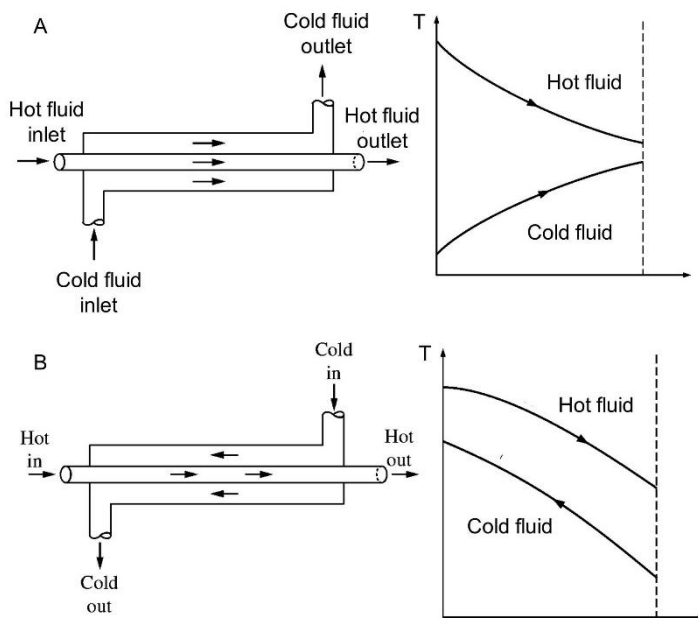


Figure 4-6. Flows direction and corresponding temperatures profiles for shell and tubes heat exchangers. Parallel flow (A); Counter flow (B).

To enhance the heat transfer, baffles are placed in the shell (Figure 4-7 A); in that way the shell-side fluid is forced to encounter the tube bundle both crosswise and lengthwise, flowing quickly across the shell. Moreover, the baffles maintain a uniform spacing between the tubes. Different tubes arrangement are possible in the shell and tubes heat exchangers, as illustrated in Figure 4-7 B. Shell and tubes heat exchangers can be further classified according to the number of shell and tubes passes, as it is explained in Figure 4-8.

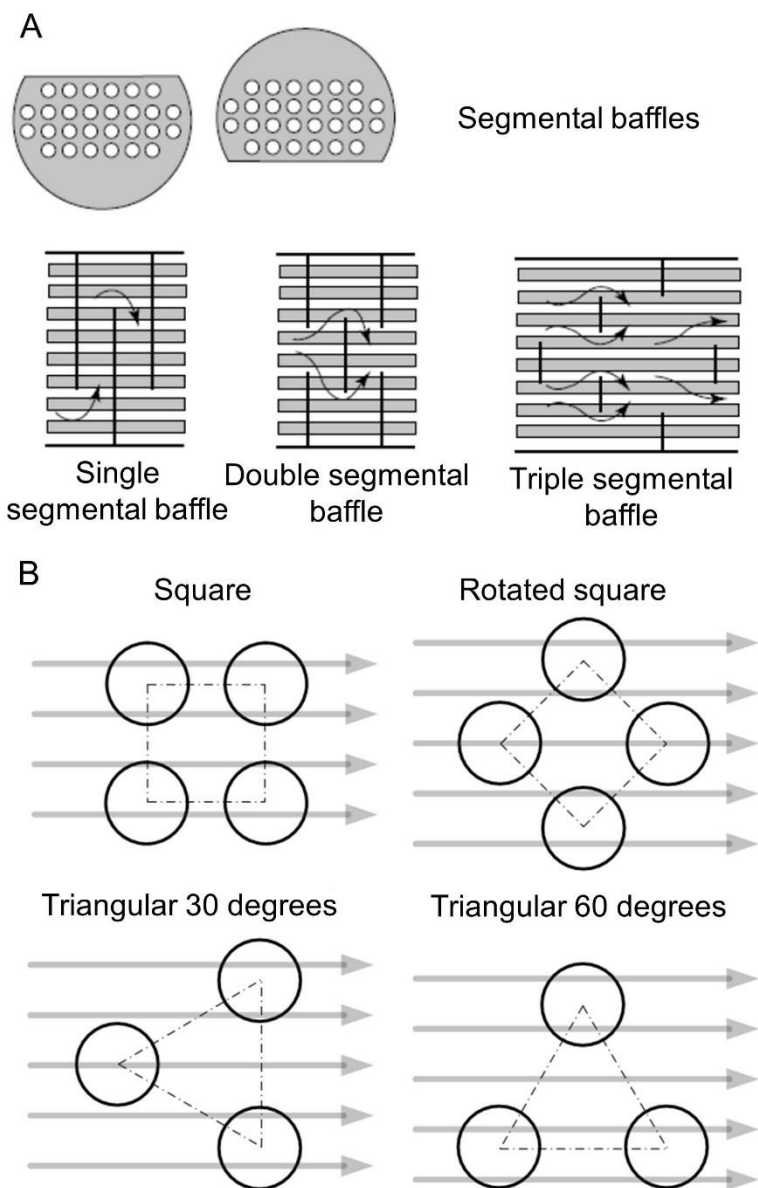


Figure 4-7. Possible baffles types in shell and tubes heat exchangers lay-out (A); possible pitch tube lay-outs (B).

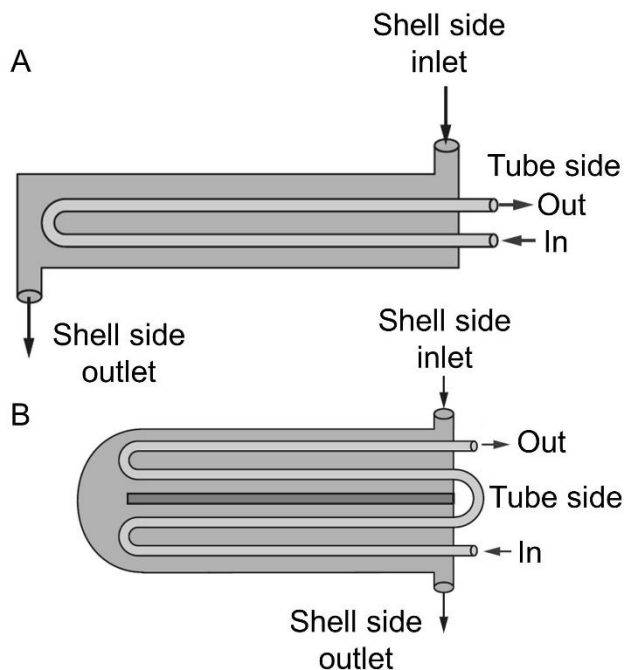


Figure 4-8. Multipass flow arrangement for shell and tubes heat exchangers. One shell-pass and two tube-passes (A); two shell-passes and 4 tube-passes (B).

TEMA provided a simple identification of the shell and tubes heat exchangers in function of their three main components, the front head, the rear head and the shell type. Figure 4-9 shows the TEMA types for this common classification of STHX.

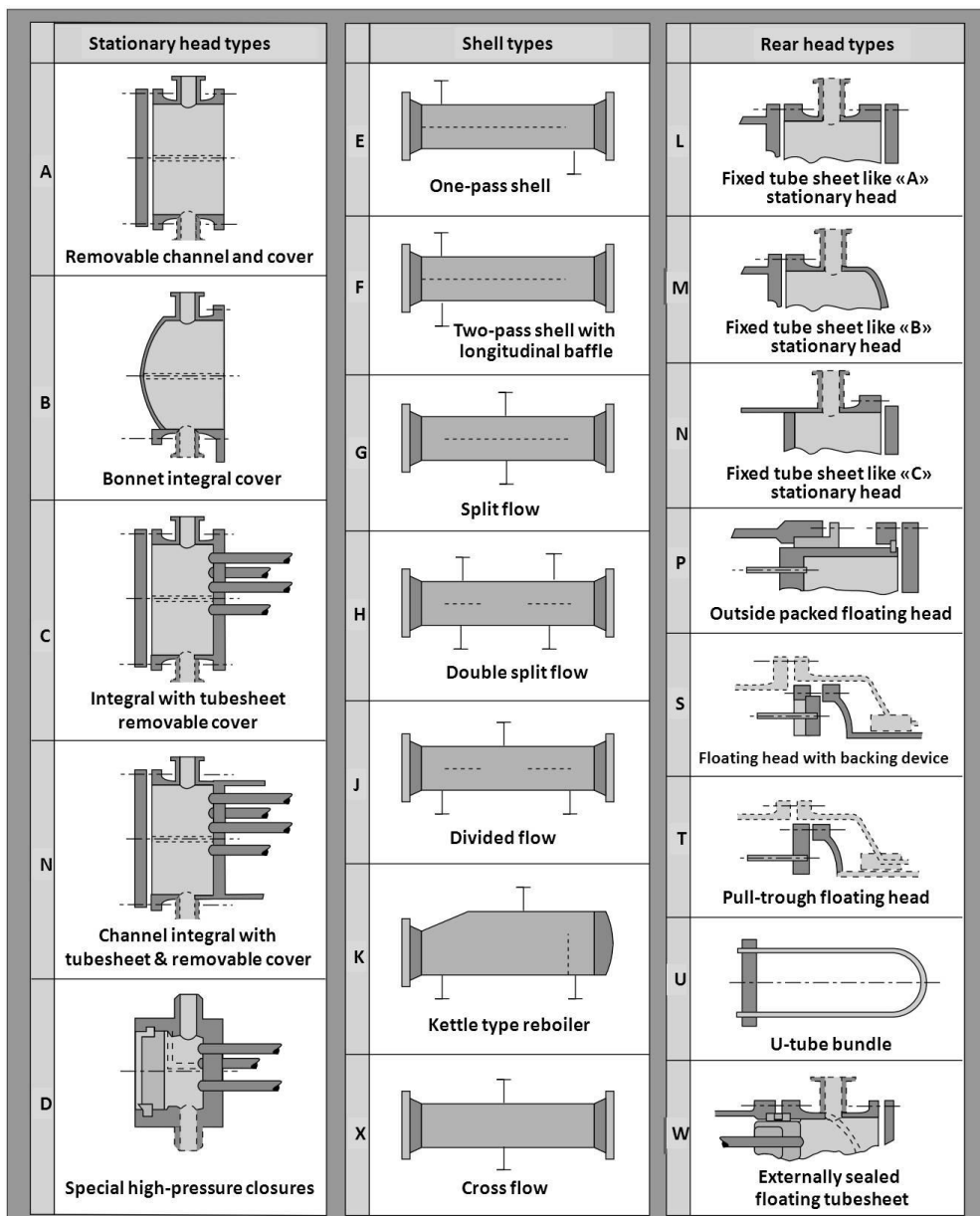


Figure 4-9. TEMA types for classification of shell and tubes heat exchangers.

The pilot plants were designed and built in collaboration with the company Special Tanks S.r.L. The simulation program Xchanger suite (v. 6.00) by HTRI was used for the dimensioning of the shell and tube heat exchangers constituting the pilot plant. During the PhD research, the pilot plant design was progressively implemented, thus two pilot plant layouts will be explained in the following sections. The first layout (I) was used to observe the fouling mitigation effect of the S10 and F10 coatings; while the second layout (II) was used for testing the anti-fouling activity of an organic-inorganic hybrid coating. Both the pilot plants were constituted by two heat exchangers, but the tube bundle of only one of them was coated, making the heat transfer surfaces hydrophobic; the second heat exchanger was not treated at all. During the experimentation the two heat exchangers worked in parallel and were alimented by the same operating fluids. Moreover, the operating conditions of the two heat exchangers were kept very similar during the whole experimentation. In that way, it was possible to use as a reference the uncoated heat exchanger and clearly observe the effect of the hydrophobic coating on the heat transfer efficiency of the coated heat exchanger, supposing that both the heat exchangers were involved in the same fouling phenomenon.

### 4.3.1 Pilot plant - I lay-out

Figure 4-10 is a picture of the first pilot plant lay-out (pilot plant I), the corresponding flowsheet is illustrated in Figure 4-11.

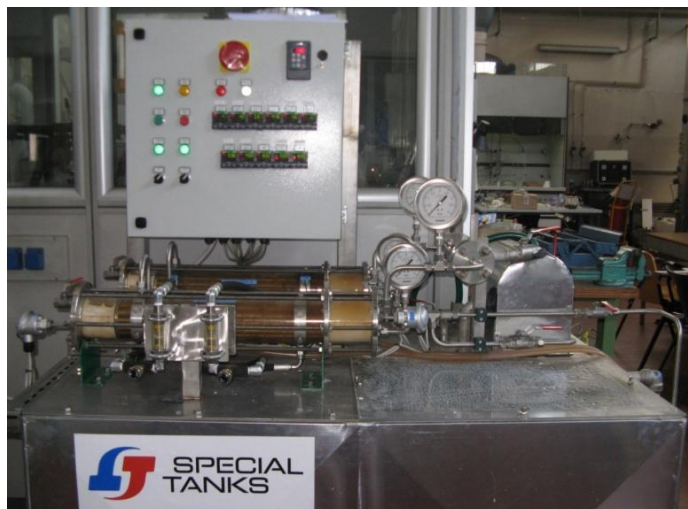


Figure 4-10. Picture of the pilot plant I.

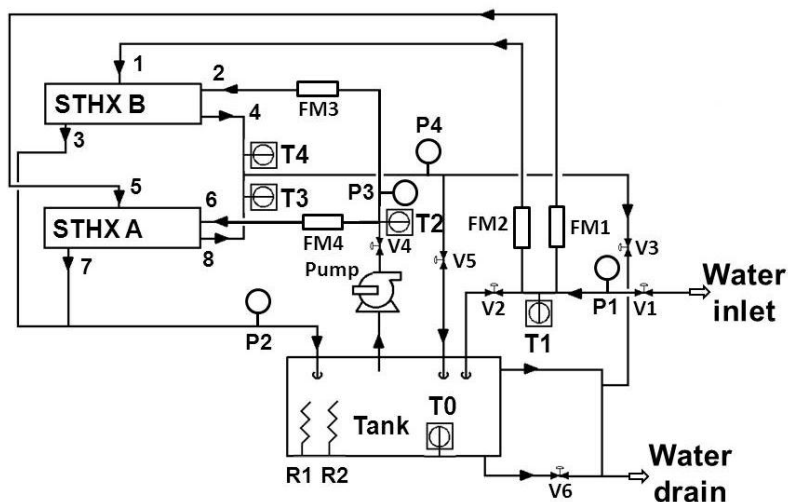


Figure 4-11. Schematic diagram of the pilot plant I. FM= flowmeter; P=manometer; R= Heating element; T=thermocouple; V= valve. STHX B= shell and tube heat exchanger B (not coated): 1= Shell side inlet; 2= tube side inlet; 3= shell side outlet; 4 =tube side outlet. STHX A= shell and tube heat exchanger A (coated): 5= shell side inlet; 6= tube side inlet; 7= shell side outlet; 8= tube side outlet.



The experimental equipment of pilot plant I consisted of two identical shell and tubes heat exchangers, TEMA type AEW, working in counter flow. The coated heat exchanger was named STHX A, while the uncoated one was named STHX B. The design settings of the two shell and tubes heat exchangers are reported in Table 4-3. The two heat exchangers were placed in horizontal position. We chose to use as operating fluid tap water (general composition reported in Table 4-1), since its supply was easy and unlimited, moreover, the content in salts is enough to permit fouling phenomena, namely, scaling. The tubes sides of both the heat exchangers were alimented from the same tank, where tap water was heated by two heating elements at a temperature of 313-323 K. The shell sides of the two heat exchangers were directly connected to the water system of the city of Milan through the same faucet; the temperature of the water entering in the shell side of the heat exchangers ranges from 290 K to 293 K. Thus, the hot fluid was positioned on the tube sides, while the cold fluid was placed on the shell sides. The temperatures of the inlet and outlet fluids of both shell sides and tubes sides were measured by flexible thermocouples (the thermocouples positions are illustrated in the flowsheet, Figure 4-11). The flowrate of the water, entering in the shell-sides of the heat exchangers, was regulated by float flowmeters (one flowmeter for each heat exchanger); the values of the flowrates varied from 60 L/h to 120 L/h. The flowrates of the tube sides inlet water were regulated by float flowmeters at values of 184 L/h or 330 L/h. The specific value or range of value adopted for each pilot plant experiment is reported in the corresponding results section (see Chapters 5 and 7). Further information about the operating units and all the measuring devices constituting the pilot plant I are reported in Table 4-4.

Table 4-3. Design specifications of the shell and tubes heat exchangers constituting the pilot plant I.

<b>Shell side</b>		<b>Tube side</b>	
Internal diameter	90 mm	Number of tubes	18
Outside diameter	102 mm	Number of passes per shell	6
Material	Glass	Tubes external diameter	10 mm
Lenght	500 mm	Tubes thickness (average)	1 mm
Number of passes per shell	1	Tubes lenght	500 mm
		Material	Stainless steel AISI 316
		Tubes pitch	12.5
		Tubes layout	30°
<b>Further specifications</b>			
Baffles cross	Single segmental	Baffle diameter	87 mm
Baffle spacing	41 mm	Flow regime	Counter flow

Table 4-4. Specifications of the operating units and of the measuring devices, working on the pilot plant I. The symbols used for referring to the devices are the same used in the flowsheet of the plant.

<b>Symbol and name</b>	<b>Specifications</b>
FM1/FM2 Float flowmeter	Parker, measure range: 12-120 L/h, standard accuracy: $\pm 5\%$ of full scale flow.
FM3/FM4 Float flowmeter	Key Instruments, measure range: 120-1200 L/h, standard accuracy: $\pm 5\%$ of full scale flow.
P1-P4 Manometer	INOX, measure range: 0-5 bar.
R1/R2 Heating elements	230 V, 3kW, alimented in series.
T0 Thermocouple	Immersion thermocouple, rigid, for temperature measurement in the hot water tank. Sensibility: $10-50 \mu\text{V}/^\circ\text{C}$ .
T1-T4 Thermocouples	Contact thermocouple, flexible, sensibility: $10-50 \mu\text{V}/^\circ\text{C}$ .
V1-V6 Valves	INOX ball valve, certified ISO 9001 and ISO 14001.

As previously mentioned, the two heat exchangers, STHX A and STHX B, were identical in dimensions, components, design settings and operation conditions. During the pilot plant operation, the flowrates values of the inlet fluids of the two heat exchangers were kept similar; also the temperatures of the inlet fluids were identical between the two heat exchangers. In that way, a comparison between the heat transfer efficiency of the coated and uncoated pilot plants was possible.

### 4.3.2 Pilot plant – II lay-out

Figure 4-12 and Figure 4-13 illustrate the picture of the second pilot plant lay-out (pilot plant II) and the flowsheet, respectively.



Figure 4-12. Picture of the pilot plant II.

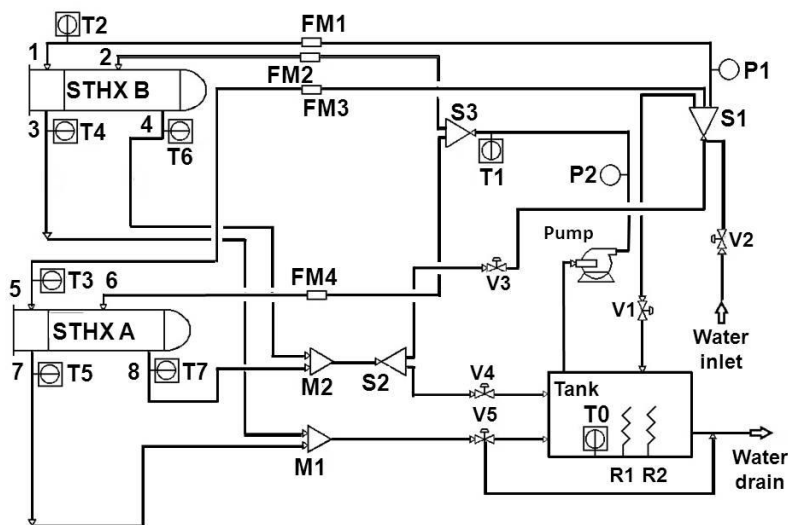


Figure 4-13. Schematic diagram of the pilot plant II. FM= flowmeter; P=manometer; R= Heating element; T=thermocouple; V= valve. STHX B= shell and tube heat exchanger B (not coated): 1= Shell side inlet; 2= tube side inlet; 3= shell side outlet; 4= tube side outlet. STHX A= shell and tube heat exchanger A (coated): 5= shell side inlet; 6= tube side inlet; 7= shell side outlet; 8= tube side outlet.

As in the previous lay-out, pilot plant II is constituted by two shell and tube heat exchangers, TEMA type NEW, working in parallel and designed identically. During the experimentation, only the tube bundle of STHX A was coated (specifically using the hybrid coating named  $\text{SiO}_2/\text{S10-20/80}_2$ ). The design specifications of the two heat exchangers operating in pilot plant II are listed in Table 4-5.

Table 4-5. Design specifications of the shell and tubes heat exchangers constituting the pilot plant II.

<b>Shell side</b>		<b>Tube side</b>	
Internal diameter	90 mm	Number of tubes	22
Outside diameter	102 mm	Number of passes per shell	6
Material	Alluminum	Tubes external diameter	10 mm
Lenght	700 mm	Tubes thickness (average)	1 mm
Number of passes per shell	1	Tubes lenght	700 mm
		Material	Stainless steel AISI 316
		Tubes pitch	12.5
		Tubes layout	30°
<b>Further specifications</b>			
Baffles cross	Single segmental	Baffle diameter	87 mm
Baffle spacing	27 mm	Flow regime	Counter flow

In respect to the first pilot plant lay-out, the second one is characterized by the presence of flexible thermocouples directly placed at the inlets and outlets of the shell side and tube side heat exchangers (see Figure 4-13). The operating units and the measuring devices remained unchanged (listed in Table 4-4).

During the experimentation with pilot plant II, tap water was used as operating fluid. The hot fluid, placed in the tube side, was heated at a temperature of 313-323 K. The cold fluid, flowing inside the shell, had a temperature varying from 290 K to 292 K. The flowrate of the shell side inlet fluid was kept stable between 108-120 L/h; the tube side flowrate of the inlet fluid was regulated at a value of 720 L/h. The operating conditions were kept very similar between the two heat exchangers during the experimental work, thus, one more time, it was possible to compare the heat transfer efficiency of the coated heat exchanger with the one of the uncoated heat exchanger.

### 4.3.3 Choice of the operating conditions

The operating conditions of the pilot plant were carefully chosen before the starting of each run. However, some variables were imposed by the pilot plant design, and we could not modify them. The temperature difference between the shell side and tubes side recurred in each pilot plant experiment, since it was impossible to modify the temperature of the water entering in the shell side, and the temperature of the water entering in the tube side as well. In fact, the first was directly provided from the city water system; the second was drawn from a tank, where the water was heated at a maximum temperature of 323 K, by two heating elements. During the pilot plant operation, however, the temperature of the water inside the supplying tank ranged from 313 K to 323 K. The fluid recirculating system, in fact, obliged the entering in the heated tank of at least a

part of the fluids coming out from the heat exchangers (characterized by a temperature varying from 303 K to 313 K. The continuous supplying of relatively cold fluids to the tank, however, made impossible the maintaining of a stable temperature in the tank itself. This problem could not be overcome since we could not provide further heating elements to the tank due to the excessive electrical demand. The fluid flowrates, on the other hand, could be regulated within the range of the float flowmeters, installed before the entrances in the shell and tubes. By modifying the flowrates, we could choose the flow regime inside the shell and the tubes. The flow regime is well expressed by the Reynold number, in particular, for  $Re < 2000$ , the flow regime is laminar, for  $Re > 3000$  the flow regime is turbulent, for  $2000 < Re < 3000$  the two regimes coexist (transitional regime) [4].

The Re number was introduced in Equation (1-4); therefore, the dimensions necessary for Re number calculations are the fluid velocity ( $u_m$ ), the fluid density ( $\rho$ ), the fluid viscosity ( $\mu$ ) and the tube diameter ( $D$ ).

The fluid velocity was calculated in the shell side considering the equivalent fluid velocity (Equation (4-1)):

$$u_{meq} = \overline{u_{mb} - u_{md}} \quad (4-1)$$

Where  $u_{mb} = \frac{W}{S_b}$  and  $u_{md} = \frac{W}{S_d}$ , where  $S_b$  is the free section calculated in correspondence of the baffle, while  $S_d$  is the free section in correspondence of the shell diameter. The value of  $S_b$  corresponds to  $\frac{1}{4}$  of the total free section of the mantle, the value of  $S_d$  can be calculated as follows:



$$S_d = \frac{D_{in}}{y_T} y_L x_p \quad (4-2)$$

where  $D_{in}$  is the internal diameter of the shell,  $y_T$  is the tubes pitch,  $y_L$  is the tube spacing and  $x_p$  is the baffle spacing.

The fluid velocity in the tubes was calculated in accordance with Equation (4-3).

$$u_m = \frac{W}{A_c N_T \rho} \quad (4-3)$$

$A_c$  is the cross sectional flow area of the tubes and  $N_T$  is the number of the tubes constituting the tubes bundle.

#### 4.3.4 Fouling conditions

Considering the composition of the water used as operating fluid in the pilot plant experiments, and the relative temperature (for the fluid 313-323 K and for the heat transfer surfaces 308-313 K), we supposed the formulation of scale deposits on the heat transfer surfaces, due to crystallization fouling. The depositions of salts for the heat exchanging solution can bring to the formation of hard scale deposits, which are difficult to be removed, or soft deposits (also defined as sludge) which are easier to be removed. Regardless the type of scale deposit, they are both responsible of a decrease of the heat transfer efficiency [1]. The mechanism of crystallization fouling is extremely complex, and many variables can influence the extent of the phenomenon. Beside the flow regime and the temperature, of both the solid surface and the bulk of the fluid, even the particular type of fluid involved, the features of the solid surface or the

particular area of the heat exchanger may be important, so it is difficult to generalize this phenomenon [68]. Anyway, it is interesting to point up that the fouling resistance progress in crystallization fouling, as in many other types of fouling processes, occurs in two steps. In the first step, called fouling induction period, the crystals form and grow on the heat transfer surfaces, without affecting consistently the overall heat transfer coefficient. Progressively the crystal coverage grows, increases in thickness and adhere more strongly on the solid surface, so that the removal process becomes negligible. In that step, which is called fouling period, or crystal growth period, it is possible to observe the increase of the fouling resistance [69].

## 5 RESULTS AND DISCUSSION: PERFLUOROPOLYETHERS COATINGS

*In the first section, the preparation and the deposition of PFPE coatings are discussed. The second section concerns the characterization results and the surface properties of the F10 and S10 coatings are compared. The resistance of the coatings against chemical and physical erosion is described in the third section. In view of these results, further tests on particulate fouling mitigation were performed and the results are briefly discussed in the fourth section. The anti-fouling efficiency of both the S10 and F10 coatings was investigated on the heat exchanger pilot plant. In the last section, the mitigation effect against crystallization fouling on the heat transfer surfaces was evaluated.*

## 5.1 Optimization of the formulation and of the deposition procedure

The first step in the development of the PFPE coatings was the assessment of the best formulation and best conditions for coatings deposition on stainless steel substrates.

According with the S10 technical sheet, we formulated the polymer in water, *iso*-propanol and acetic acid, varying the relative weight amount of each component as shown in Table 2-4. We observed that the maximum content of S10 in a water based formulation appeared to be the 5%, since for higher values the PFPE did not emulsified in the solvent mix. Best results in terms of emulsification, time stability and final processability, were obtained by formulating 1 wt % of S10 with 20 wt % of *iso*-propanol, 78 wt % of water and 1 wt % of acetic acid. The F10 polymer was formulated in a water based solution containing *iso*-propanol, as suggested in Table 2-4, following the indications of the technical data sheet. The best formulation implemented was composed by 10 wt % of F10, 20 wt % of *iso*-propanol and 70 wt % of distilled water. These two optimal formulations were used for the subsequent implementation of the deposition procedure.

The PFPE coatings were deposited on the stainless steel substrates by the dip-coating technique and successively heat treated in a static oven. The coatings were preliminarily deposited by using a dip-coater, following the procedure reported at pp. 46-47. In such a way, we obtained coatings with thickness at nanometer level, characterized by a surface contact angle varying from 114° to 118°. However, this coating procedure allowed the use of only small plain samples; moreover, the effective coating thickness was impossible to be measured by profilometer, or by other analytical techniques, due to the very

small thickness of the coatings combined with the high roughness of the stainless steel substrates. At last, the thickness was insufficient to confer a good mechanical stability to the coatings. For these reasons, we did not investigate further the coatings obtained with this procedure, but we implemented a different coating procedure, much available for bigger surfaces.

The second dip-coating procedure used for coatings deposition on stainless steel substrates is well described at pp. 47-48. A specific study was performed to obtain the optimal value of immersion time, and the optimal temperature and duration for the curing treatment, for both S10 and F10 coatings. To achieve this goal, we measured the static contact angle of each coating prepared varying or the deposition procedure or the heat treatment conditions, as reported in Table 5-1. The optimum deposition or curing procedure corresponded to the higher CA measured (higher hydrophobicity). The results are presented in Figure 5-1.

Table 5-1. Variables for the optimization of the coatings deposition and corresponding values used in the experimentation

<b>Time of immersion in dip-coating [min]</b>	<b>Temperature of the heat treatment [K]</b>	<b>Duration of the heat treatment [h]</b>
5	353	3
15	373	16
180	383	24
360	393	-
960	403	-
1440	413	-

Observing Figure 5-1a and Figure 5-1c, the increase of the immersion time, permitted to increase also the CA. The maximum value of CA was obtained for 1440 minutes (24 hours) of immersion of the substrates in the coating formulation; the CA of the S10 was 134° and of the F10 coating was 115° (the CA was measured after a standard heat treatment at 393 K for 3 hours). Regarding the thermal treatment conditions, the higher contact angle values (~150°) for S10 coatings (Figure 5-1b) were achieved by heating the samples at 393 K for 24 hours, or at 413 K for three hours. Even a thermal treatment at 383 K for 3 hours permitted the obtainment of very high contact angles (145°). Thermal treatments longer than 24 hours did not bring to sensitive improvements of the CA values. The best thermal treatment for the F10 coating

(Figure 5-1d) was instead the one performed at 413 K for 24 hours (CA=123°). In general we observed that, in the case of the F10 coatings, a prolongation of the thermal treatment time till 48 hours did not improve the CA value, however for shorter curing time the coating was not perfectly dried.

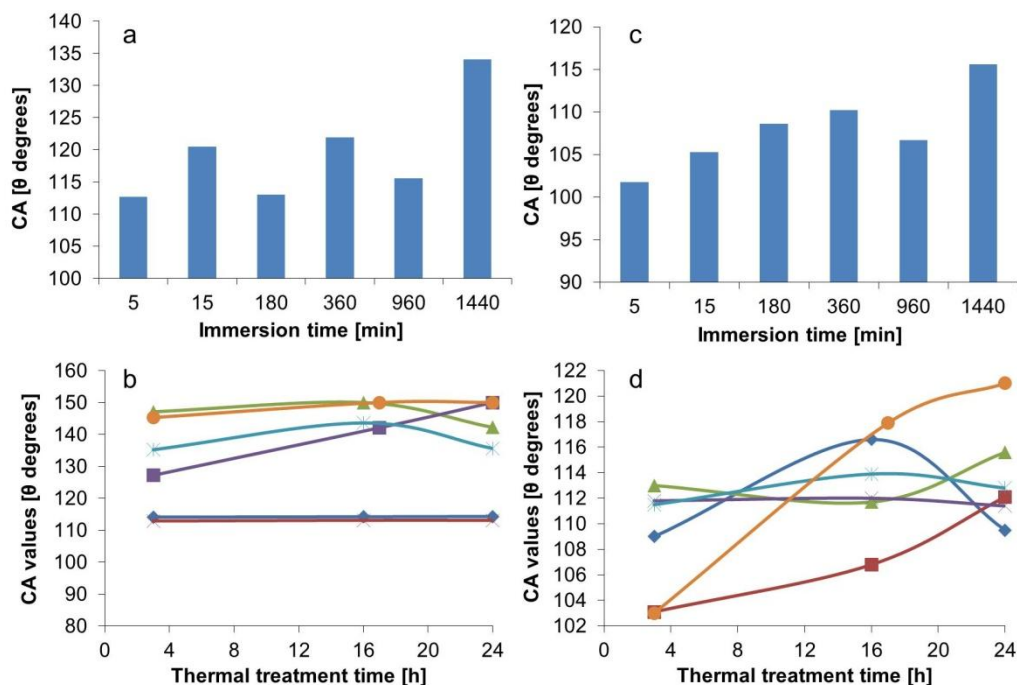


Figure 5-1. Optimization of the coatings deposition procedure for S10 (a, b) and F10 (c, d) coatings. a, c) variation of the immersion time, heat treatment performed at 393 K for 3 hours; b, d) variation of the temperature and duration for the heat treatment, immersion time 24 hours. Legend:  $\blacklozenge$  353 K;  $\blacksquare$  373 K;  $\blacktriangle$  383 K;  $\blacklozenge$  393 K;  $\blackstar$  403 K;  $\blacklozenge$  413 K.

Table 5-2 resumes the characteristics of the formulations and of the coating conditions that we adopted for the obtainment of the S10 and F10 coatings on

stainless steel substrates. The results discussed in the following sections are all referred to coatings obtained in such a way.

Table 5-2. Formulation and coating conditions adopted for the obtainment of the S10 and F10 coatings.

<b>Type of coating</b>	<b>Formulation</b>	<b>Coating conditions</b>
Fluorolink <sup>®</sup> S10	1 wt % S10;	Immersion time: 24 hours; thermal treatment at 383 K for 3 hours
	1 wt % Acetic acid;	
	20 wt % <i>iso</i> -propanol; 78 wt% distilled water	
Fluorolink <sup>®</sup> F10	10 wt % F10;	Immersion time: 24 hours; thermal treatment at 413 K for 48 hours.
	20 wt % <i>iso</i> -propanol;	
	70 wt% distilled water	

## 5.2 Characterization results

### 5.2.1 Morphology, composition and thickness

The surface morphology of the S10 and F10 coatings was assessed by SEM analyses. As a reference, a cleaned and uncoated stainless steel plain substrates was used and the corresponding images obtained by SEM are reported in Figure 5-2a-b. The S10 coating formed an inhomogeneous texture on the stainless steel substrate; the polymer in fact formed a first dark smooth layer on the substrate,



covered by second layer constituted by spheres of polymer (Figure 5-2c). A bigger magnification (Figure 5-2d) pointed out the presence of spots not perfectly coated; the grain of the stainless steel surface are in fact visible, indicating that the coating is not perfectly continuous on the surface. The F10 coating showed a different morphology in respect to the S10 one; it formed a homogenous and dark layer on the substrate, without assuming the spherical shape observed with the S10 polymer (Figure 5-2e). However, an uncovered part of the stainless steel surface is recognizable in Figure 5-2e (on the left); therefore, as confirmed by picture f in Figure 5-2, the coating is not continuous on the surface.

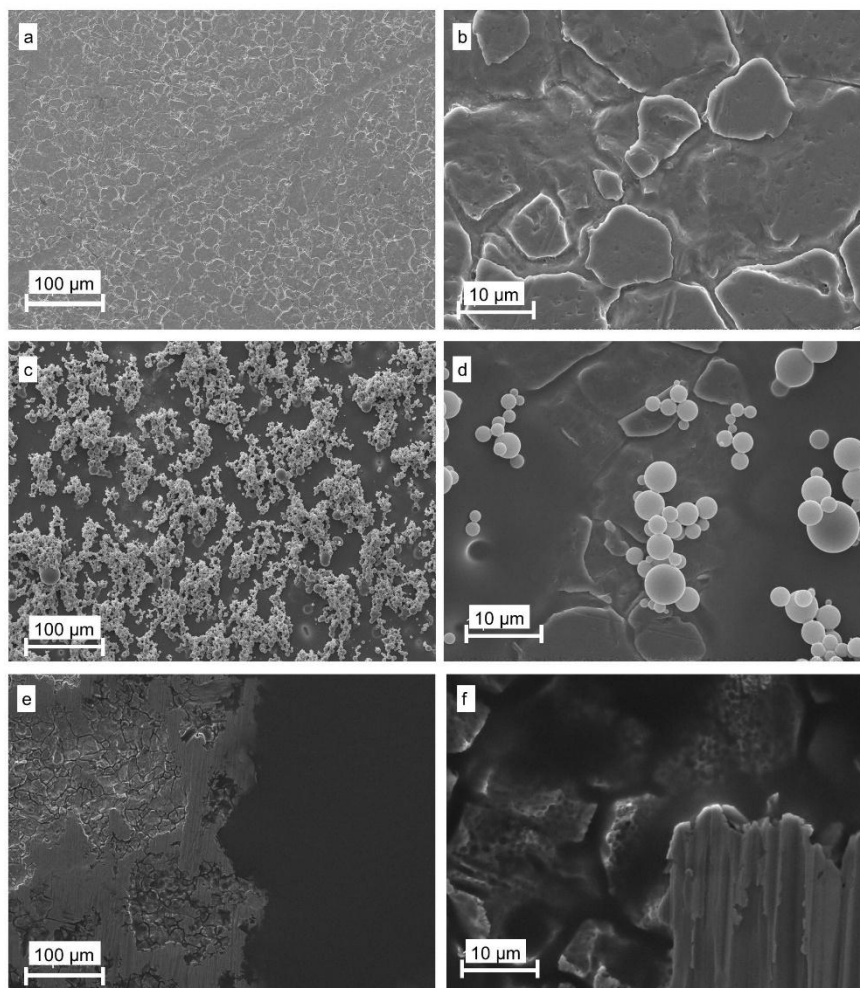


Figure 5-2. SEM pictures of a stainless steel plain substrate (a, b); S10 coating (c, d) and F10 coating (d, e). On the left magnification of 500X; on the right magnification of 2000X.

XPS analyses permitted to investigate the surface composition of the coatings. The relative atomic abundances of the element detected on stainless steel plain samples covered by S10 and F10 are listed in Table 5-3.

Table 5-3. Relative atomic abundance (%) of the S10 and F10 coatings, detected by XPS analyses.

Coating type	Elements [at. %]							
	C	F	O	Si	P	Na	Ca	Mg
Fluorolink®S10	30.4	40.4	22.8	3.5	-	0.4	0.4	2.1
Fluorolink®F10	23.9	56.2	19.5	-	0.4	-	-	-

Both the coatings showed a high atomic percentage of fluorine (40% and 56% respectively). The shape of the carbon C1s peak is the typical one of a fluoropolymer (double peak at 285-292 eV); in fact, the interaction between C and F generates a signal shifted on higher binding energy values, in respect to the normal binding energy of C1s (284.6 eV), which provokes the formation of a double peak due to the presence of a high content of F-C bonds (see Figure 5-3 and Figure 5-4). In the S10 coating was revealed the presence of Si, due to the triethoxysilane functional groups of the polymer; while in the F10 coating was detected P, related to the ammonium phosphate functional group. Cr, Mg and Ca atoms, detected in the S10 coated samples, were considered impurities; we suppose that the water used for the preparation of the S10 formulation used for covering the sample contained these ions.

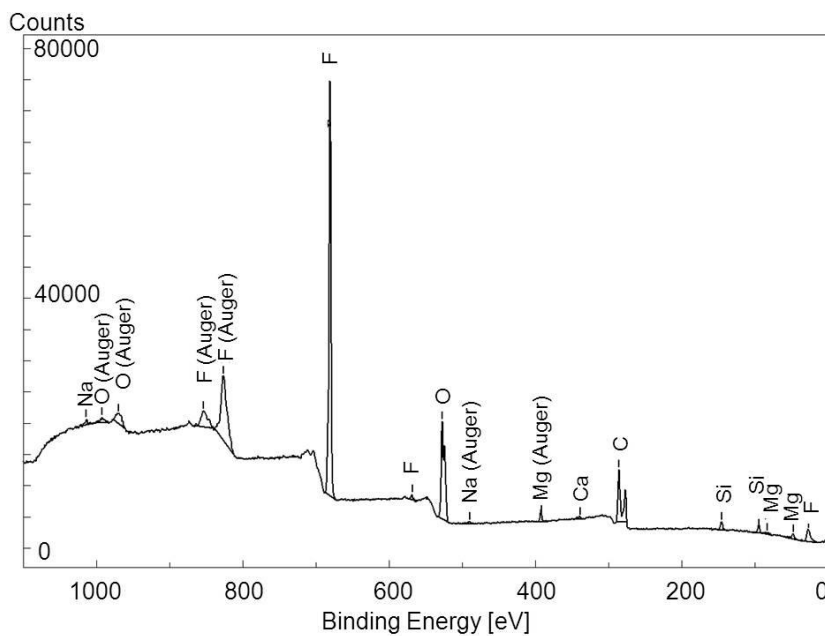


Figure 5-3. XPS survey spectrum for the S10 coating.

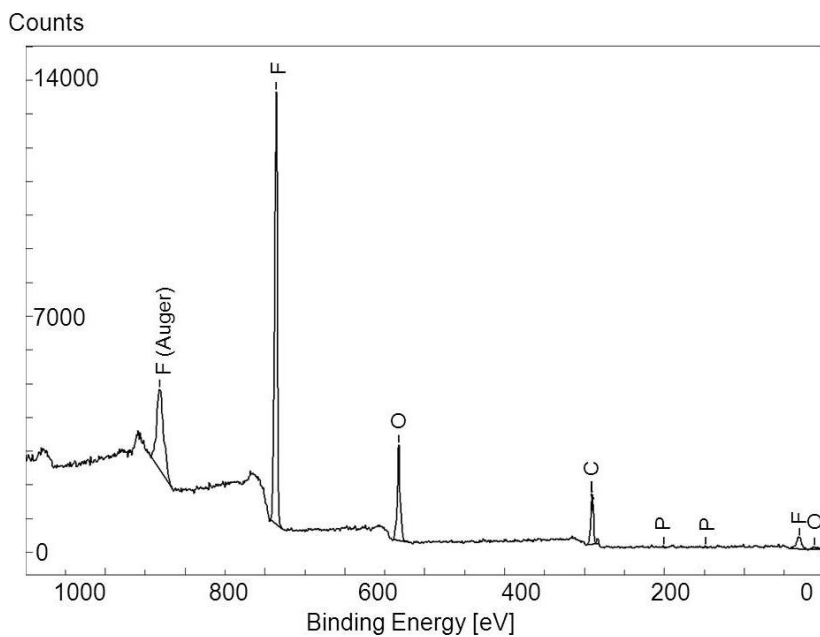


Figure 5-4. XPS survey spectrum for the F10 coating.

The thickness and roughness of the S10 and F10 coatings were measured by profilometry; the results are presented in Table 5-4. The thickness of the coatings was measured in correspondence of the cross-section, by depositing the coating on half a part of the plain sample. In that way it was possible also to measure the substrate roughness and the coating roughness on the same sample and compared them. The S10 coating had an average thickness of 2.7  $\mu\text{m}$  (calculated on 5 different points), the minimum value detected was 2.2  $\mu\text{m}$ , and the maximum 3.3  $\mu\text{m}$ . Regarding the average roughness (Ra) the measured value was 0.438  $\mu\text{m}$ ; in respect to the uncoated substrate, the roughness increment due to the coating is 0.246  $\mu\text{m}$ . The determination of the thickness and roughness of the F10 coating was difficult, due to the low continuity of this coating on the stainless steel substrate. The thickness of the coating was measured on a single point, and corresponded to 1.3  $\mu\text{m}$ . Moreover, it was impossible to determine the effective roughness of the coating, since the Ra value measured on the coating corresponded to the one measured on the uncoated substrate. Therefore, we can suppose that the presence of the F10 coating only slightly modified the roughness of the underlying substrate.

Table 5-4. Profilometry results for the S10 and F10 coatings deposited on stainless steel plain samples.

<b>Coating type</b>	<b>Average thickness [<math>\mu\text{m}</math>]</b>	<b>Min and max thickness [<math>\mu\text{m}</math>]</b>	<b>Ra [<math>\mu\text{m}</math>]</b>	<b>Ra increment [<math>\mu\text{m}</math>]</b>
Fluorolink <sup>®</sup> S10	2.7	2.2 -3.3	0.438	0.246
Fluorolink <sup>®</sup> F10	1.3*	-	-	-

\* thickness measured on a single point.

As discussed in the first chapter (pp. 22-23), the thickness and the roughness of the coatings play an important role in the modification of the heat transfer ability of the metal substrates, or in their propensity to foul. The obtainment of coatings with a thickness inferior than 5  $\mu\text{m}$  excludes the possibility to interfere with the heat transfer capacity of the substrate material [19]. Regarding the coating roughness, we observed that the S10 coating has a higher average roughness in respect to the uncoated starting substrate ( $R_a=0.192 \mu\text{m}$ ); the increase in surface roughness could enhance the tendency of the surface to foul, as demonstrated by Herz et al. [70]. The increment in roughness value should be thus considered in the view of a possible application of the coating on the heat transfer surfaces. However, the final  $R_a$  obtained on the S10 coated substrate was low, typically very rough surfaces have  $R_a > 1-1.5 \mu\text{m}$ .

### 5.2.2 Hydrophobicity assessment

Stainless steel substrates used for industrial practice are usually hydrophilic, therefore water contact angle value is low ( $<90^\circ$ ) and the surface free energy (SFE) is very high ( $>30 \text{ mN/m}$ ). The stainless steel surfaces used as substrates during this research were hydrophilic; as shown in Table 5-5, the static CA value ranged from  $66^\circ$  to  $76^\circ$ , in dependence from the polishing treatment. Accordingly, the SFE value was  $46 \text{ mN/m}$ , indicating the high wettability of the surfaces. The S10 and F10 coatings modified the wettability of the stainless steel substrates. All the perfluoropolyethers coatings had, in fact,  $CA > 90^\circ$ . The different wettability of the uncoated stainless steel surfaces and the PFPE coated ones are well illustrated in Figure 5-5 (the pictures were taken during the CA measurement).

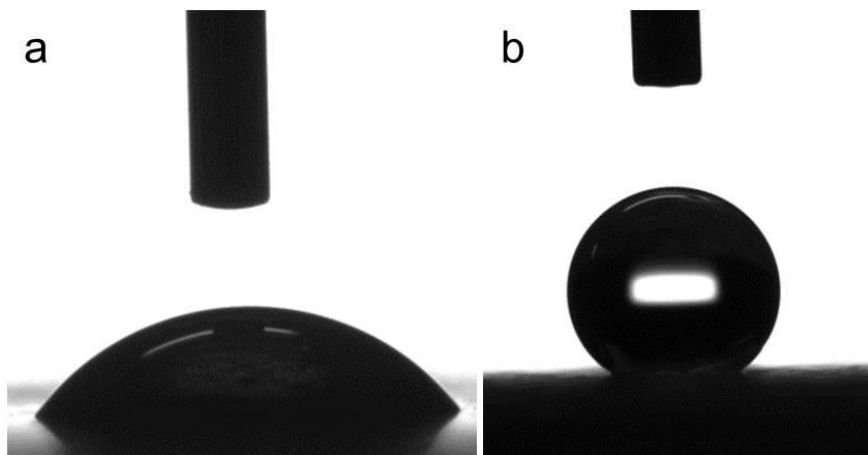


Figure 5-5. Images of water droplet deposited on an uncoated stainless steel surface (a), and a Fluorolink®S10 coated stainless steel surface (b).

The static CA values, reported in Table 5-5, correspond to the average of the medium CA calculated on 4 samples treated in the same way; thus the standard deviation correspond to the CA differences between different samples. The SFE and the advancing and receding contact angles correspond to the best results obtained between two repetitions of the same analyses; the standard deviation of the SFE values was calculated among the CA values measured by depositing the three standard liquids for the surface free energy determination. The S10 coating reduced the surface free energy until 3 mN/m, in accordance, the static contact angle was very high ( $147^\circ$ ); the surface was thus highly hydrophobic. The advancing and receding CA are very similar; the hysteresis value is 3, therefore it is possible to suppose that the interaction of the water drop with the S10 coated surface followed the Cassie-Baxter model. The F10 coating contributed to increase the substrate hydrophobicity as well, however the static CA is lower ( $118^\circ$ ) in respect to the S10 coating, and the surface free energy is

8 mN/m, therefore the surface is not completely repellent to water as observed for the S10 coating. We also observed a sensitive difference between the advancing and receding CA of the F10 coating, the hysteresis is in fact 15. We supposed that the interaction of water with the F10 surface can be described by the Wenzel model, however, is not to be neglected that the high discontinuity of the coating, observed with SEM analyses, could contribute to the high contact angle hysteresis. Figure 5-6 illustrates the difference between the advancing and receding contact angles for the S10 coating (a) and the F10 coating (b). The decrease in CA value that occurs during the step of contraction of the liquid is much more evident for the F10 coating, in respect to the S10 one.

Table 5-5. Wetting properties of the stainless steel plain samples before and after the coverage with S10 and F10.

Coating type	Static CA [θ°]	SFE [mN/m]	Advancing CA [θ°]	Receding CA [θ°]	Hysteresis
None (unpolished surface)	76 ± 5.5	46 ± 2.0	-	-	-
None (polished surface)	66 ± 4.7	-	-	-	-
S10 (polished substrate)	147 ± 2.6	3 ± 1.0	146	143	6
F10 (polished substrate)	118 ± 5.5	8 ± 1.0	113	98	15



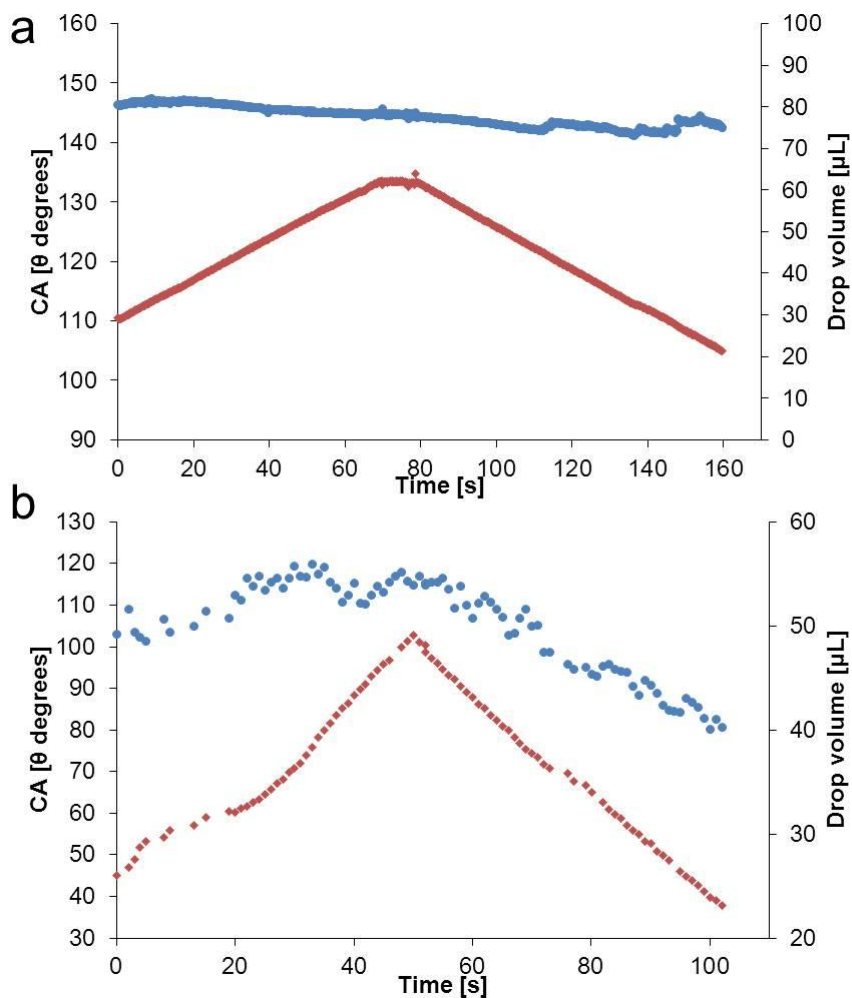


Figure 5-6. Illustration of the advancing and receding CA trend (●), compared with the volume of the water droplet (◆), which was increased and contracted accordingly. S10 coating (a); F10 coating (b).

### 5.3 Coatings resistance against erosion

Fluorolink<sup>®</sup>S10 and Fluorolink<sup>®</sup>F10 possess  $\alpha$ - $\omega$  inorganic functionalization, which promote the adhesion of the polymer on metal substrates. This property facilitates the formation of stable coatings on the stainless steel substrate, however the resistance of the coatings against chemical or physical stresses is not ensured. Indeed, we performed specific tests to determine the coatings stability when they are exposed to aggressive liquid environments or shear forces, in view of the specific application of the coatings for fouling mitigation in heat exchangers. Since the main effect of the coatings is the increase of the water contact angle of the stainless steel substrates, we used the CA value as an index to evaluate the integrity of the coating. The decrease in CA during the resistance tests is in fact indicative of a progressive deterioration of the coating, since without it, the normal hydrophilicity of the stainless steel substrate is restored. Each resistance test was performed at least two times and repeated until the final contact angles measured were similar ( $\pm 10^\circ$ ). The results presented correspond to the best results obtained.

Figure 5-7 resumes the results of the resistance tests performed on the S10 coatings. The initial CA value (water CA, measured in static conditions) was compared with the CA value measured after 7 days of immersion in a liquid aggressive environment. Moreover, the degradation trends of coatings deposited on polished or unpolished surfaces were compared, in order to assess if a polishing treatment could improve the adhesion of the polymeric coating on the stainless steel surface. Figure 5-8 illustrates the results of the same tests described in Figure 5-7, but the degradation trend is highlighted by reporting the CA values measured after 24 hours, 72 hours and 168 hours (7 days) of immersion.

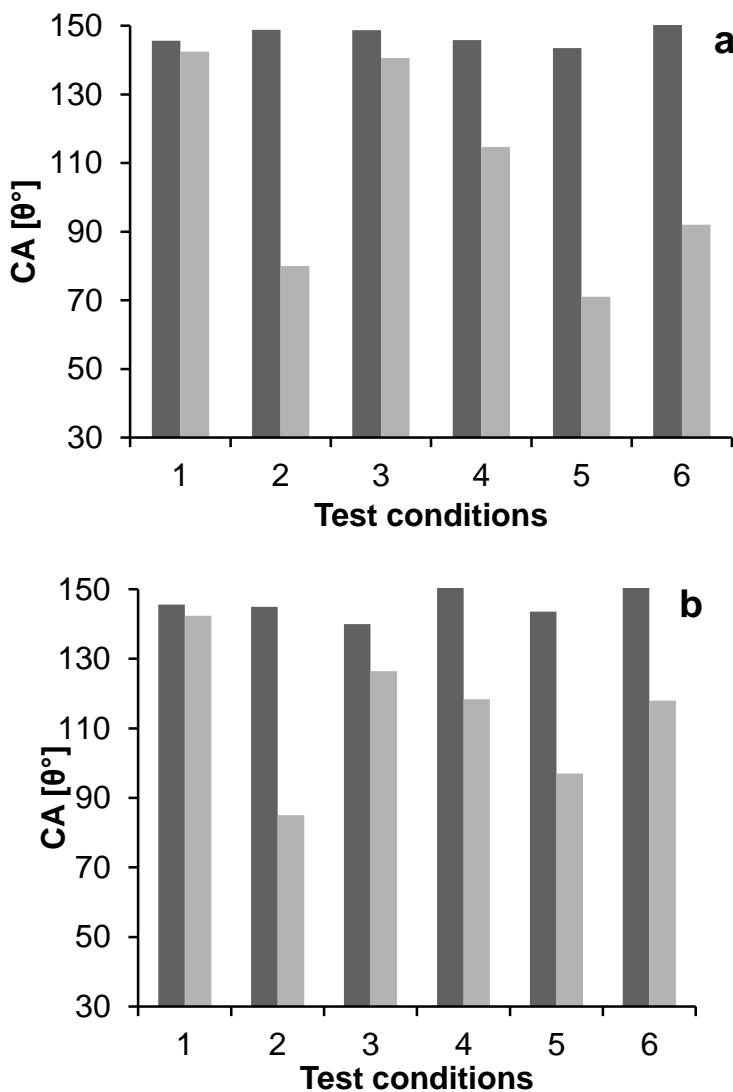


Figure 5-7. Coating resistance against erosion in liquid environments: comparison between the starting CA (■) and the CA at the end of the test (▒). S10 coating on unpolished stainless steel substrates (a); S10 coating on polished stainless steel substrates (b). 1=  $\text{NH}_2\text{Cl}/\text{NHCl}_2$  solution,  $T= 323 \text{ K}$ ; 2=  $\text{NaOH}$  solution,  $T= 323 \text{ K}$ ; 3=  $\text{HCl}$  solution,  $T=323 \text{ K}$ ; 4= water,  $T=298 \text{ K}$ ; 5= water,  $T=343 \text{ K}$ ; 6= water flux,  $T=313 \text{ K}$ , flowrate=0.13 m/s.

Alkaline solutions were the most detrimental liquid for the S10 coatings. In presence of a basic environment, in fact, occurs the hydrolysis of the covalent bonds generated between the functional groups of the polymer and the -OH functionalities of the substrate. Therefore, in a matter of 24 hours, the samples turned to be hydrophilic (Figure 5-8a-c), independently from the polishing treatment of the substrate. Acid environments were only slightly detrimental for the S10 coatings; the overall contact angle decrease, in 7 days, was the 5% for the coating deposited on the unpolished substrate (from 149° to 141°; Figure 5-7a) and the 10% for the coating deposited to the polished substrate (from 140° to 126°, Figure 5-7b). Disinfectant solutions provoked a decrease in CA of the S10 coatings of about the 15% (Figure 5-7a) on the unpolished substrate and the 10% on the polished substrate (Figure 5-7b). Hence, the degradation of the S10 coatings when deposited on the polished or unpolished substrates is very similar, as long as their exposed to these kinds of liquids. Tests performed in water highlighted the best differences between the use of polished or unpolished substrate. First, water, even at room temperature, was more aggressive for the S10 coatings than acidic or disinfectant solutions. Immersion in water at room temperature provoked an initial decrease of the CA (within 24 hours) of about the 13% for the S10 coating, deposited on both a polished or unpolished surface (Figure 5-8b-d). Then, the CA value remained almost stable until 72 hours of immersion, but after 168 hours, the CA decrease was about the 22 % on both polished and not polished samples. The final CA value was 114° for the S10 coating deposited on the unpolished surface, and 118° for the one deposited on the polished surface. The increase of the temperature of water until 343 K, determined a higher erosion of the S10 coatings. In particular, the one deposited on the unpolished substrate was completely removed in 7 days (CA<90°, Figure 5-7a). The polished surface coated with S10, instead,

remained hydrophobic after 7 days of immersion (final CA  $97^\circ$ , CA decrease is the 35%); however, the CA decrease trend suggested a possible further deterioration for longer immersion periods (Figure 5-8d). Also the shear stress tests (the water temperature was 313 K) highlighted a continuous decrease of the CA of the S10 coating deposited on the unpolished substrate, even if after 7 days of test the surface was still hydrophobic (CA =  $97^\circ$ , Figure 5-7a). Otherwise, the S10 coating deposited on the polished surface and exposed to water flow shearing, was mainly eroded within the 24 hours of exposition (21 % CA decrease), after the CA value remained almost stable (see Figure 5-8d). After 7 days the CA remained was  $118^\circ$ , suggesting a higher resistance of the S10 coating against shear stresses, when deposited on polished surfaces.

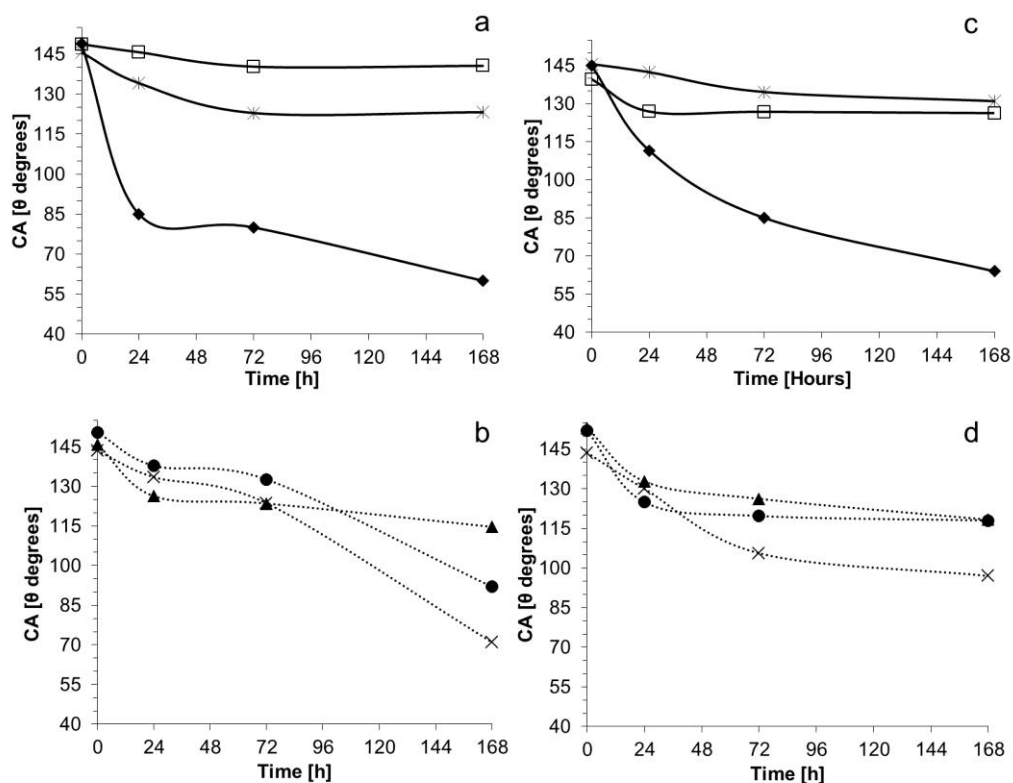


Figure 5-8. Trend of CA decrease during resistance tests for S10 coatings deposited on unpolished stainless steel surfaces (a,b) and polished surfaces (c,d). Legend:  $\ast$  = NH<sub>2</sub>Cl/NHCl<sub>2</sub> solution, T= 323 K;  $\blacklozenge$  = NaOH solution, T= 323 K;  $\square$  = HCl solution, T=323 K;  $\cdots\blacktriangle\cdots$  = water, T=298 K;  $\cdots\ast\cdots$  = water, T=343 K;  $\cdots\bullet\cdots$  = water flux, T=313 K, flowrate=0.13 m/s.

The initial CA value measured for the F10 coating deposited on polished or unpolished surfaces is quite inferior in respect to the S10 coatings (120°-125° vs 140°-147° respectively). However, at the end of all the resistance tests, the F10 coated surfaces were still hydrophobic (except from the tests in alkaline condition, which completely degraded the F10 coating). Moreover, any

significant difference was detected in coating deterioration, comparing the polished or unpolished substrates. Chloramines solutions were responsible of a CA decrease of about the 8%; similarly, the HCl solutions provoked a CA decrease of the 15% for the F10 coatings deposited on unpolished substrates, and the 7% for the ones deposited on the polished surfaces (Figure 5-9a-b). Even if the CA decrements were low and their values were comparable with the ones observed on the S10 coatings, the CA values measured on the F10 coatings at the end of the tests were much lower. After immersion in HCl, in fact, the samples were characterized by a CA of  $106^{\circ}$  (unpolished substrate) and  $108^{\circ}$  (polished substrate), while the final CA of S10 coated samples stressed in the same conditions assessed around  $140^{\circ}$  and  $126^{\circ}$ . Similarly, after the exposition to disinfectant solutions, the F10 coated samples had CA values of  $106^{\circ}$ , while the S10 coated samples maintained CA values higher than  $123^{\circ}$ . The degradation trends observed after immersion in water of the F10 coated samples are linear in respect to the S10 samples; the main deterioration of the coatings in fact occurred within 48 hours of exposition, then the CA remained unvaried (see Figure 5-10c-d). After immersion in water at room temperature, both the polished and the unpolished surfaces remained hydrophobic. The CA decrease were the 3% and the 8% respectively, but the CA values were about  $105^{\circ}$ . The immersion in water at 343 K brought to a higher deterioration of the F10 coatings, corresponding to the 23% for the unpolished substrate and the 17% for the polished one (CA value respectively of  $96^{\circ}$  and  $98^{\circ}$ ). Likewise, shear stresses were responsible of a deterioration of the coatings. The final CA decrease was the 12% on both the polished and unpolished samples (with a final CA of about  $98^{\circ}$ ).

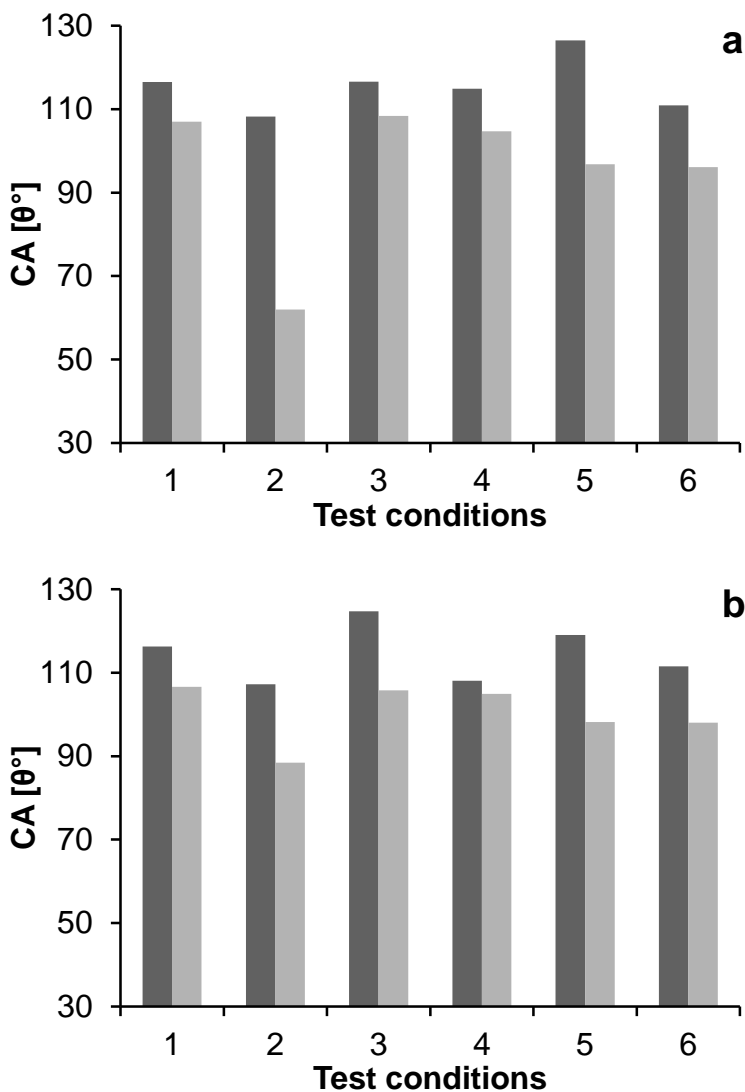


Figure 5-9. Coating resistance against erosion in liquid environments: comparison between the starting CA (■) and the CA at the end of the test (■). F10 coating on unpolished stainless steel substrates (a); F10 coating on polished stainless steel substrates (b). 1=  $\text{NH}_2\text{Cl}/\text{NHCl}_2$  solution,  $T= 323 \text{ K}$ ; 2=  $\text{NaOH}$  solution,  $T= 323 \text{ K}$ ; 3=  $\text{HCl}$  solution,  $T=323 \text{ K}$ ; 4= water,  $T=298 \text{ K}$ ; 5= water,  $T=343 \text{ K}$ ; 6= water flux,  $T=313 \text{ K}$ , flowrate=0.13 m/s.



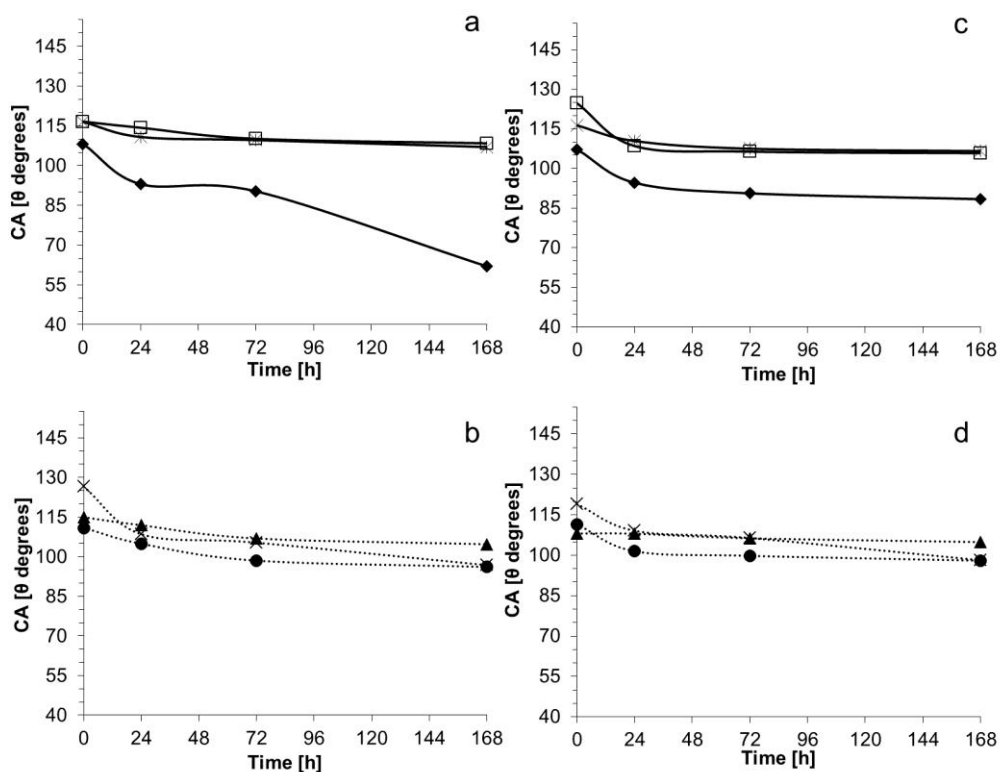


Figure 5-10 Trend of CA decrease during resistance tests of F10 coatings deposited on unpolished stainless steel surfaces (a,b) and polished surfaces (c,d). Legend: \* = NH<sub>2</sub>Cl/NHCl<sub>2</sub> solution, T= 323 K; ◆ = NaOH solution, T= 323 K; □ = HCl solution, T=323 K; ···▲··· = water, T=298 K; ···×··· = water, T=343 K; ···●··· = water flux, T=313 K, flowrate=0.13 m/s.

In conclusion, the PFPE coatings appeared to be low resistant against chemical aggression of alkaline environments, while acidic solutions or disinfectant solutions containing chlorine do not deteriorate the coatings in the conditions adopted for these tests. We observed a big difference between the S10 and F10 coatings after exposure to water, in particular at high temperature or in presence

of shear stresses induced by water flowing upon the coated surfaces. F10 coatings, in fact, emerged to be more resistant in respect to S10 coatings; however, the final CA values obtained on F10 coated surfaces are at the borderline with the hydrophilic behavior. As interesting point, we observed the improvement in S10 coatings adhesion, and therefore resistance, especially against water erosion and shear stresses, on polished stainless steel substrates. The pretreatment of the solid substrate for improving coatings adhesion is worth; however, in industrial application it could be expensive or even impossible.

Further resistance tests were performed by immersion of stainless steel coated samples in synthetic seawater. Since seawater is highly aggressive toward polymeric coatings, but also toward metal substrates, we applied the S10 and F10 coatings not only on stainless steel AISI 316 substrates, but also on other type of stainless steels (SMO and SAF). SAF and SMO are particular materials highly resistant against seawater corrosion. Before the coatings deposition, all the plain substrates were washed. The results obtained from these resistance tests are presented in Figure 5-11. F10 coatings, deposited on each type of metal surfaces, quickly deteriorated after immersion in seawater at room temperature; in 24 hours the normal hydrophilicity of the surfaces was restored. Even S10 coatings, when deposited on SAF substrates, were greatly eroded by the seawater at room temperature. Different results were obtained by depositing the S10 coatings on AISI 316 or SMO stainless steel substrates; after 7 days of immersion in seawater at room temperature, the surfaces were still hydrophobic. The CA decrease of the AISI 316 sample coated with S10 was the 23% (CA=101°) and the 30% (CA=95°) for the SMO coated sample (Figure 5-11a). Therefore, the S10 coatings deposited on these kind of stainless steels

were also immersed in seawater at a temperature of 323 K, in order to assess the effect of the increasing temperature on coating erosion. In 7 days the surfaces were hydrophilic (Figure 5-11b). In conclusion, PFPE coatings emerged to be extremely sensitive toward seawater, moreover, the pH of the environment was slightly alkaline (pH=8.1), this obviously contributed to a progressive detachment of the coatings from the substrates.

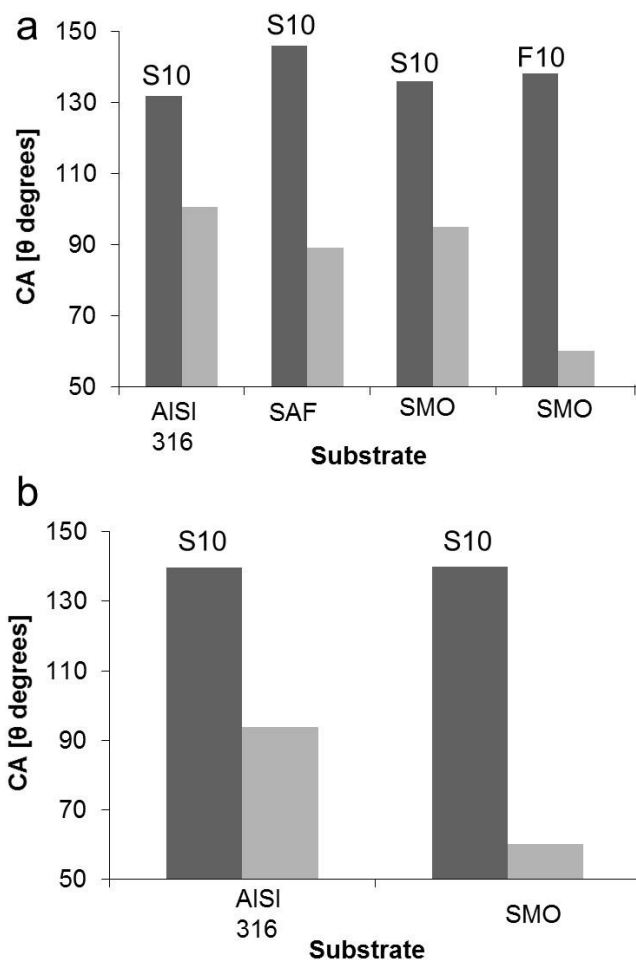


Figure 5-11. Results of coating resistance against erosion in synthetic seawater: test performed at room temperature (a); test performed at 323 K (b). ■ initial water CA; ■ water CA at the end of the test.

## 5.4 Particulate fouling mitigation

The particulate fouling test permitted to observe the ability of the hydrophobic coatings to reduce the deposition of solid materials dispersed in a fluidic media.

We used as foulant particles calcium sulphate, in a concentration which guarantees the precipitation of the particles in the aqueous operating fluid, kept at a moderate temperature of 313 K. The supersaturated solution of calcium sulphate used in this test was flowed inside the tubes sample at a moderate velocity ( $\approx 0.05$  m/s), to permit an easy gravitational settling of the foulant particles on the internal surface of the tube sample (maintained in horizontal position). In such a way, we could observed the formation  $\text{CaSO}_4$  deposits inside the tubes in a short time (48-72 hours). The fouling extent was quantified as mg of  $\text{CaSO}_4$  deposited on the internal surface area ( $\text{cm}^2$ ) of the sample with time (h). Table 5-6 compares the particulate fouling of an uncoated stainless steel tube, with the fouling calculated on the tubes coated with PFPE. After 48 hours test, we observed the formation of a  $\text{CaSO}_4$  layer on the internal surfaces

of the tube sample not coated (see

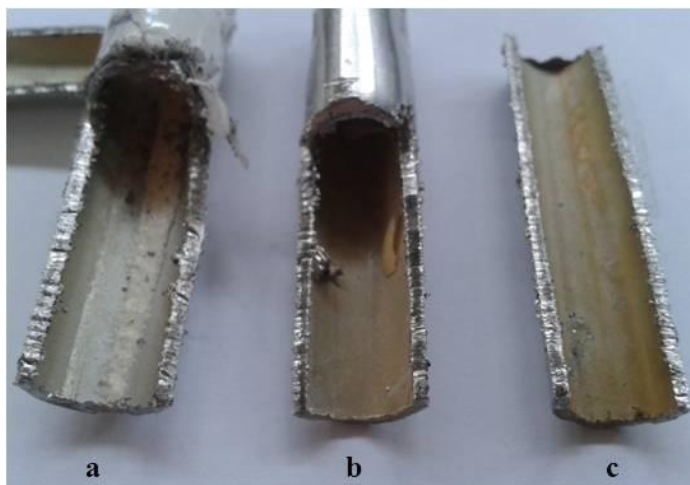


Figure 5-12a); the fouling quantified was  $9.2 \cdot 10^{-5}$  mg/cm<sup>2</sup> h. Prolonging the test for 72 hours, we observed a further increment of the weight of the sample, and the fouling value increased of one order of dimension. On the other hand, the weight increment of tubes samples coated with S10 or F10, after 48 hours of test, was zero. Therefore, we supposed that until 48 hours of test, fouling did not occur on the hydrophobic surfaces. After 72 hours, we detected a weight increase also for the coated samples, confirming the beginning of fouling. Anyway, the fouling value calculated after 72 hours test on the coated surfaces was lower than the one obtained for the uncoated surface even after 48 hours of test. If the fouling value measured for the uncoated tube, after 72 hours of particulate fouling test, corresponds to 100% of fouling, we estimated that the fouling occurred on the S10 coated sample was the 14% and the 3% on the F10 coated tube.

Table 5-6. CaSO<sub>4</sub> fouling deposits amounts, formed on uncoated tubes samples and on tubes samples coated with Fluorolink®S10 or F10.

<b>Coating type</b>	<b>Time [h]</b>	<b>Fluid velocity [m/s]</b>	<b>Fouling [mg/cm<sup>2</sup> s]</b>
None	48	0.05	$9.2 \cdot 10^{-5}$
None	72	0.05	$1.1 \cdot 10^{-4}$
S10	48	0.06	-
S10	72	0.05	$1.5 \cdot 10^{-5}$
F10	48	0.05	-
F10	72	0.06	$3.0 \cdot 10^{-6}$

The particulate fouling tests confirmed the ability of the PFPE coatings to delay particulate fouling in respect to hydrophilic surfaces. Therefore, we decided to observe the anti-fouling effect of the hydrophobic PFPE coatings on real heat transfer surfaces, i.e., on surfaces involved on localized temperature increments and wall shear stresses.



Figure 5-12. Pictures of tubes section after the fouling test (48 hours): Uncoated surface (a); S10 coated surface (b); F10 coated surface (c).

## 5.5 Pilot plant experimentation

Both Fluorolink<sup>®</sup>S10 and Fluorolink<sup>®</sup>F10 were used to coat the heat transfer surfaces of a heat exchanger in the pilot plant. The two experimentations ran separately, keeping, for each of them one of the two heat exchangers uncoated, in order to have reference data. The pilot plant lay out was the first one (pilot plant I, described at pp. 86-89) for both the experimentations.

### 5.5.1 Assessment of the anti-fouling effect of Fluorolink<sup>®</sup>S10 coatings

The S10 coating was deposited on the heat transfer surfaces of the heat exchanger, by dip-coating. The coating formulation, containing 1 wt% of S10, 1 wt% of acetic acid, 20 wt% of *iso*-propanol and distilled water was prepared in a quantity of 8 L. The tube bundle was dipped inside the coating formulation

using a tank of appropriate dimensions (about 8.5 L volume). The tube bundle was kept immersed in the S10 formulation for 20 minutes and consequently dried in a static stove at a temperature of 353 K for 19 hours. We could not perform characterization analyses on the coated tube bundle, due to its high dimensions; however, in view of the results obtained with small plain samples, coated with the same procedure, we supposed that, after the coating treatment, the heat transfer surfaces had a CA of 110°-120°. The coating thickness should varied from 3 to 5  $\mu\text{m}$ . Therefore, we can suppose that, even in the presence of the polymeric coating, a scarce alteration of the heat transfer capacity of stainless steel surface occurred.

The pilot plant worked in continuous conditions for about 5 months. The operating conditions maintained during the experimentation are summed up in Table 5-7. The operating conditions were kept mild; the temperature difference between the shell side and the tube side was in fact about 40 K, and the fluids velocity were low, with Reynold numbers attested a laminar flow in both shell and tubes.



Table 5-7. Operating conditions of the heat exchangers, maintained during the investigation of the fouling mitigation ability of Fluorolink®S10 coating.

<b>Operating condition</b>	<b>Numerical value</b>
Shell inlet fluid temperature [K]	291-293
Tubes inlet fluid temperature [K]	313 -333
Shell inlet flowrate [kg/h]	45-60
Tubes inlet flowrate [kg/h]	340
Fluid velocity inside the shell [m/s]	0.01-0.02
Fluid velocity inside the tubes [m/s]	0.1
Re number in shell	627-1150
Re number in tubes	1046-1113

The pilot plant worked continuously, 24/24 hours, for 180 days (about 5 months); however only the data collected from the 60<sup>th</sup> working day are discussed in this thesis. The lack of information related to the first period of operation of the plant, is mainly due to the necessity to set the best working conditions for the plant and to adjust the design of the plant in order to get the desired conditions. For this reason, the data collected from the 1<sup>st</sup> to the 59<sup>th</sup> day were considered inconsistent. A part of the data presented in this thesis (until

the 130<sup>th</sup> working day) were collected before the beginning of this PhD thesis [71], however, for the sake of clarity, all the data collected during this experimentation, before and during the PhD research, are presented.

During the experimentation, we monitored the flowrate values of the inlet fluids, and the temperatures of the water entering and coming out from the shells and the tubes of the two STHX. Data were collected 6 times per day, at time intervals of 2 hours, during the morning. The operating data were elaborated in order to define the heat transfer performances of the heat exchangers during the whole experimentation. The quantity of heat transferred ( $Q$ ), was calculated using Equation (5-1). The temperature difference ( $\Delta T$ ) was calculated on the shell side or on the tube side, in accordance with the value of the flowrate ( $W$ ).

$$Q = C_p W \Delta T \quad (5-1)$$

The overall heat transfer coefficient  $U$  was calculated in accordance with Equation (1-6), but considering the logarithmic mean of the external and internal heat transfer area ( $A_{lm}$ ), corrected by a factor  $Y$ , which consider that in a multi-pass flow arrangement, the heat exchanging fluid inside the shell flows in part in counter current in respect to the fluid contained in the tubes, and in part in parallel. The Equation (1-6) was therefore corrected in Equation (5-2):

$$U = \frac{Q}{A_{lm} \Delta T_{lm} Y} \quad (5-2)$$

The fouling resistance ( $R_f$ ) was calculated in accordance with Equation (1-9). For the hot side, or tube side film coefficient ( $h_H$ ), we used the relationship

provided by Sieder and Tate [4], valid for laminar flow regimes (i.e.,  $Re < 2000$  and  $1/Gz \leq 0.01$ ), expressed as in Equation (5-3):

$$Nu = \frac{h_H D}{k} = 1.86 G z^{\frac{1}{3}} \frac{\mu_b}{\mu_w}^{0.14} \quad (5-3)$$

The fluid viscosity in the bulk is expressed as  $\mu_b$ , while the viscosity in correspondence of the tube wall is expressed as  $\mu_w$ . Experimentally, the value of  $\frac{\mu_b}{\mu_w}$  varied in the range 0.69-0.78, since depends from the fluid temperature.

The cold side, or shell side film coefficient ( $h_C$ ) was calculated following the Equation (5-4), proposed by Gnielinski [72]:

$$Nu = \frac{h_C D}{k} = 0.664 Re_G^{0.5} Pr^{\frac{1}{3}} \quad (5-4)$$

The  $Re_G$  number, is the Reynold number defined by Gnielinski, expresses by Equation (5-5); this value experimentally ranged from 3000 to 6000. The Pr number varied from 5.9 to 6.2.

$$Re_G = \frac{W x_S}{\varepsilon_F D_S \mu_b x_p} \quad (5-5)$$

In Equation (5-5),  $W$  is the flowrate of the inlet fluid of the shell side,  $x_S$  is the length of the shell,  $\varepsilon_F$  is the shell void fraction,  $D_S$  is the shell internal diameter,  $\mu_b$  is the viscosity of the shell fluid in the bulk, and  $x_p$  is the baffle spacing.

The resistance imposed by the tubes wall ( $R_{wall}$ ) was determined in function of the wall thickness and the thermal conductivity of the stainless steel, using a table of correlation [73]. Therefore, the  $R_{wall}$  value was  $0.00005 \text{ m}^2\text{K/W}$ .

All the results corresponding to this experimentation on pilot plant appear on Figure 5-13, Figure 5-14, Figure 5-15 and Figure 5-16. For each working day, the heat transfer parameter ( $Q$ ,  $U$ ,  $h_H$ ,  $h_C$ , or  $R_f$ ) was calculated on the base of the average value of flowrates and temperatures, obtained from all the data collected during that day. The data presented in the Figures are highly dispersed due to the variability of the flowrates and of the temperatures during the pilot plant operation. The flowrates were kept similar between the two heat exchangers by using manual flowmeters, however it was impossible to kept constant such value day by day, due to fluctuations of the mass of water provided daily by the water network of the city. For example, the average flowrate value of the cold fluid entering in the shells determined for the 63<sup>rd</sup> working day was 59 kg/h, for the 64<sup>th</sup> day was 52 kg/h, and for the 65<sup>th</sup> day was 55 kg/h. Moreover, the temperature of the inlet fluid in the tubes varied in the range 313-323 K due to fluctuation of the water temperature inside the tank.

Figure 5-13 compares the films coefficients of the coated and the uncoated heat exchanger. The tube side film coefficient ( $h_H$ ) was kept almost stable during the whole experimentation; the values for STHX A (coated) varied in the range 939-941 W/m<sup>2</sup>K, while for STHX B (uncoated) the range was 938-941 W/m<sup>2</sup>K. Regarding the shell side film coefficients ( $h_C$ ), the range of values was wider, due to high fluctuation of the fluid flowrates. The values ranges from 455 to 623 W/m<sup>2</sup>K for STHX A, and from 450 to 606 for STHX B. Accordingly, the film coefficients  $h_H$  and  $h_C$  calculated for the coated exchanger were almost identical or very similar to the one of the uncoated heat exchanger, confirming that the two heat exchangers, working in parallel, maintained similar fluid dynamic conditions and similar operating conditions during the whole experimentation.

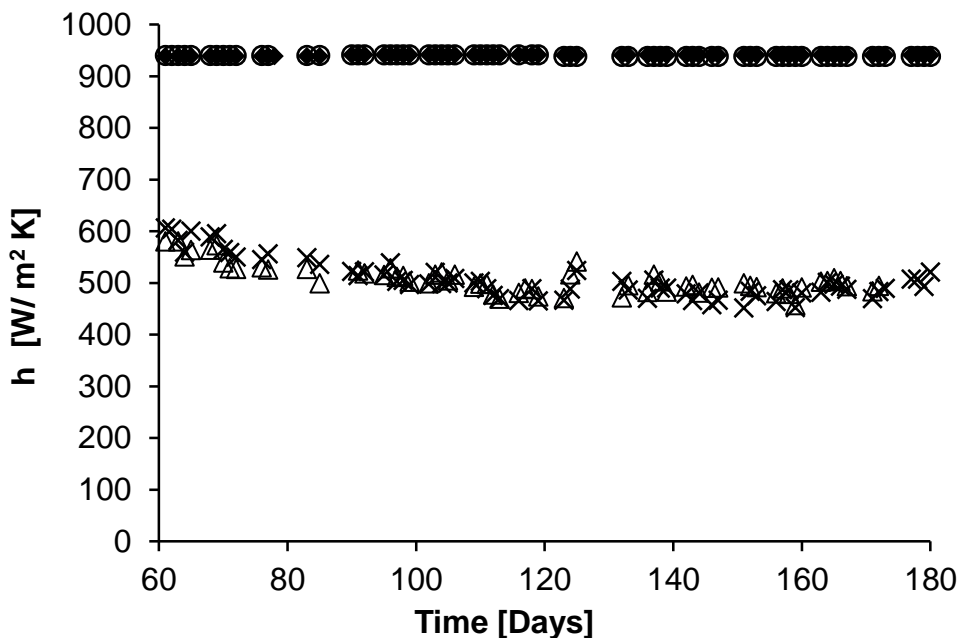


Figure 5-13. Shell-side and tube-side film coefficients of S10 coated (STHX A) and uncoated (STHX B) heat exchangers.  $\blacklozenge$   $h_H$  of STHX A;  $\circ$   $h_H$  for uncoated heat exchanger of STHX B;  $\triangle$   $h_C$  of STHX A;  $\times$   $h_C$  of STHX B.

Figure 5-14 illustrates the trend of the quantity of heat ( $Q$ ) transferred across the heat transfer surfaces. The  $Q$  value decreased with time in both STHX A and STHX B. The most significant reduction in the quantity of heat transferred occurred for both the exchangers between the 70<sup>th</sup> working day and the 100<sup>th</sup> day (about 46% decrease in respect to the starting value). However,  $Q$  values calculated for the coated heat exchanger were always higher than the ones calculated for the uncoated heat exchanger ( $\Delta q \approx 150$  W). We can suppose that, after 60 days of operation, fouling occurred on both coated and uncoated heat exchangers, thus the continuous decrease in the quantity of heat transferred can be explained. However, the fouling extent is different between the two heat

exchangers. It has been in fact estimated a total decrease in heat transfer capacity of 56% for the coated heat exchanger and of 61% for the uncoated one in the working period comprised between the 60<sup>th</sup> operating day and the 172<sup>nd</sup>. We can make the hypothesis of formation of a foulant deposit on the uncoated heat transfer surfaces earlier than on the coated surfaces. The hydrophobic coating permitted therefore a delay in the fouling layer formation and growth on the heat transfer surfaces. The same conclusions can be assumed observing Figure 5-15, which illustrates the trend of the overall heat transfer coefficient  $U$ , in respect to the time.

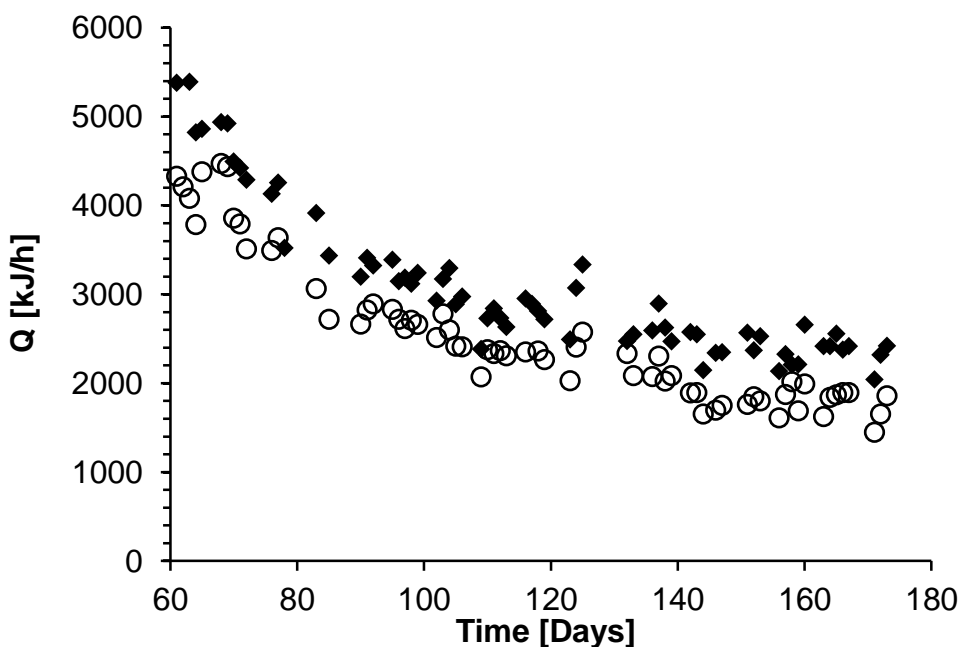


Figure 5-14. Absolute value of the heat transferred ( $Q$ ) vs time.  $\blacklozenge$  S10 coated heat exchanger (STHX A);  $\circ$  Uncoated heat exchanger (STHX B).

The overall heat transfer coefficient  $U$  decreased with time for both STHX A and STHX B, in agreement with the  $Q$  trend. However, one more time, the values determined for the coated heat exchanger were higher than the  $U$  values

obtained for the uncoated one. At the 60<sup>th</sup> operating day the value of  $U$  for STHX A was 319 W/m<sup>2</sup>K and 251 W/m<sup>2</sup>K for STHX B, confirming the hypothesis that the fouling phenomenon started before the 60<sup>th</sup> day of operation for both the heat exchangers, but later for the coated heat exchanger, hence creating a difference in the heat transfer efficiency. By the linear interpolation of the data, it is possible to compare the slopes of the linear trend of decrease of the  $U$  values of the two heat exchangers. The slope is -0.71 for the coated heat exchanger and -0.91 for the uncoated one, suggesting a higher decrease of heat transfer efficiency with time for the uncoated heat exchanger.

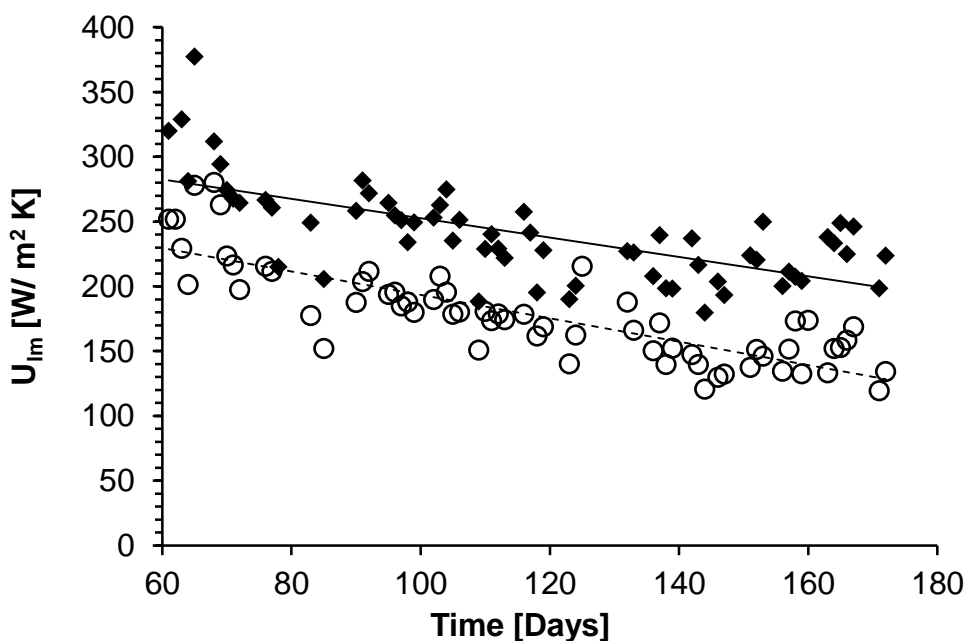


Figure 5-15. Overall heat transfer coefficient ( $U$ ) vs time.  $\blacklozenge$  S10 coated heat exchanger (STHX A);  $\circ$  Uncoated heat exchanger (STHX B); — linear trend STHX A; - - - - linear trend STHX B.

Table 5-8 directly compares the overall heat transfer coefficients of STHX A and STHX B. The total period of operation has been divided in 4 sub-periods,

each of them corresponding to about 30 days of operation. The average of all the  $U$  values collected during these sub-periods was calculated for both the heat exchangers and compared. In the first three sub-periods of operation, the difference in the overall heat transfer coefficient value was about  $60 \text{ W/m}^2 \text{ K}$ . During the last working sub-period the difference increased at  $74 \text{ W/m}^2 \text{ K}$ . Hence, observing the overall heat transfer coefficient trend, it is possible to confirm the hypothesis of formation of a thinner fouling deposit on the hydrophobic heat transfer surfaces. Moreover, in the last sub period of operation  $U$  consistently decreased for the STHX B, while the heat transfer coefficient values of the STHX A remained stable. This behavior suggested a thickening of the foulant deposits or an increase of the fouled heat transfer surface area on the uncoated heat exchanger, which did not occurred on the coated heat exchanger.



Table 5-8. Comparison between the average overall heat transfer coefficients and the average fouling resistance calculated (monthly) for the S10 coated heat exchanger and the uncoated heat exchanger.

Period	Coated heat exchanger STHX A		Uncoated heat exchanger STHX B	
	$U$ [W/m <sup>2</sup> K]	$R_f$ [m <sup>2</sup> K/ W]	$U$ [W/m <sup>2</sup> K]	$R_f$ [m <sup>2</sup> K/ W]
1	279	0.00098	217.4	0.0025
2	237	0.0017	177.9	0.0036
3	228	0.0018	167.3	0.0051
4	220	0.0021	146.1	0.0053

The trend of the fouling resistance  $R_f$  with time is described in Figure 5-16. The fouling resistance is expressed as the sum of the fouling resistance in correspondence of the external tubes surface and the internal tubes surface. In that case, the  $R_f$  trend of STHX A is quite different from the one of STHX B. The fouling resistance increased continuously within the 60<sup>th</sup> and the 150<sup>th</sup> working day in the uncoated heat exchanger. The fouling resistance increase for the coated heat exchanger, on the other hand, mainly occurred within the 60<sup>th</sup> and 110<sup>th</sup> working day, then, the value remained constant. Observing Table 5-8 and considering the uncoated heat exchanger (STHX B), the increase of  $R_f$  from the first to the second working sub-period was the 44%, from the second to the third sub-period was still the 40%, while in the last period, the  $R_f$  value was

only slightly different in respect to the one (4% total increment). Regarding STHX A, Table 5-8 highlights a consistent increase of the fouling resistance from the first to the second working sub-period (about the 70%). But in the third and fourth sub-periods the  $R_f$  value remained stable, indicating no further formations of foulant deposits. Moreover, it is worth to point out that the difference of fouling resistance values ( $\Delta R_f$ ) between STHX B and STHX A, was about 0.002-0.003  $\text{m}^2\text{K}/\text{W}$  in each sub period of operation.

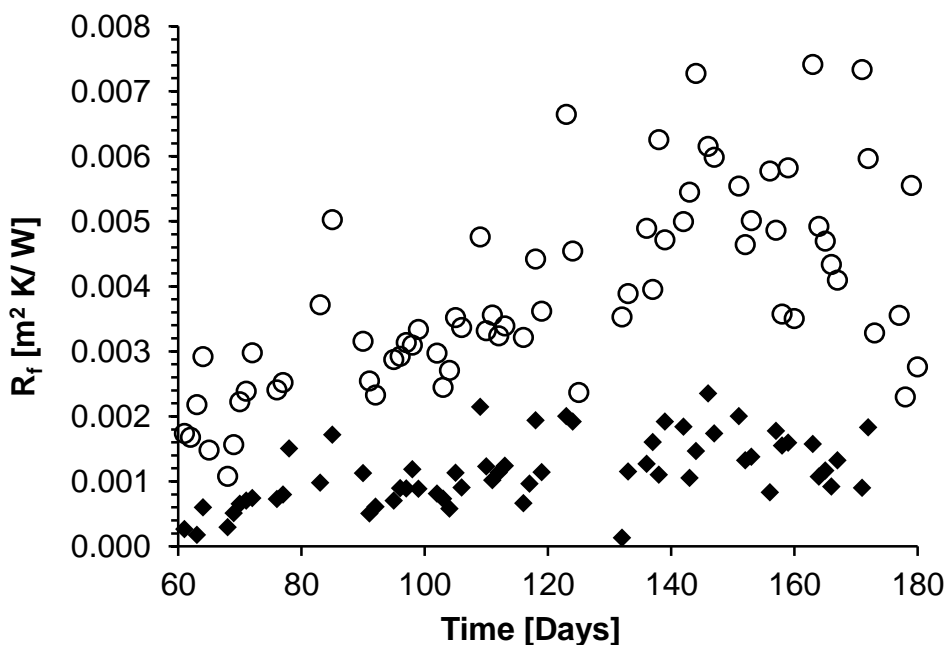


Figure 5-16. Fouling resistance *vs* time.  $\blacklozenge$  S10 coated heat exchanger (STHX A);  $\circ$  Uncoated heat exchanger (STHX B).

From the analysis of the heat transfer parameters and the fouling resistance values, we assumed a difference in fouling behaviour and extent on the hydrophobic heat transfer surfaces in respect to the normal one. In particular, we suppose that fouling started on both the heat exchangers before 60 days of working, but foulant deposits formed quicker on the uncoated heat transfer

surfaces, in respect to the coated ones. In fact, at the 60<sup>th</sup> working day the  $U$  value was higher for STHX A, while the  $R_f$  value was higher for the STHX B. Moreover, the fouling resistance increased continuously for the uncoated heat exchanger until the 150<sup>th</sup> working day, while in the coated heat exchanger the fouling resistance value increased only until the 110<sup>th</sup> day, then the value stabilized. These results can support the hypothesis of the fouling mitigation performed by the S10 coating, which reduced the rate of formation of fouling in the first working period, thus prolonging the phase of formation of the first deposit layers. Meanwhile, in the uncoated heat exchanger the fouling deposits were yet formed and began to thicken, thus provoking a reduction in the overall heat transfer coefficient and a consistent increase in the fouling resistance.

At the end of the pilot-plant run, the tube bundles were removed from the shells of the heat exchangers, in order to observe and investigate the fouling deposits formed on the heat transfer surfaces. Figure 5-17 is photograph of the tube bundle of the coated heat exchanger (A), in comparison with the tube bundle of the uncoated heat exchanger (B). The fouling deposits visible on the external side of the tubes appeared thicker and more continuous on the uncoated heat exchanger, compared to the ones formed on the hydrophobic tubes.

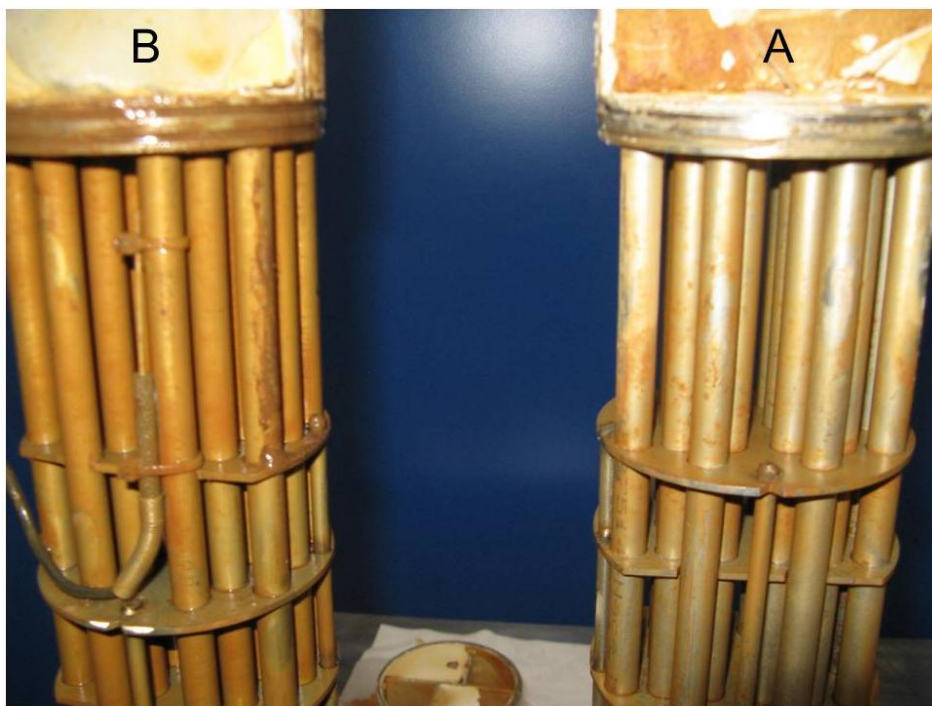


Figure 5-17. Pictures of the tube bundles of the heat exchangers at the end of the experimentation. A = tube bundle of the STHX A, coated with Fluorolink®S10; B = tube bundle of the STHX B, uncoated.

We also observed the deposits formed on the internal side of the tubes (Figure 5-18). During the cut of the tube sample collected from STHX A, part of the foulant layer pulled away, because of the mechanical stress imposed by the sample preparation; however we observed the presence of spots of foulant deposits, with a light brownish coloration. On the other hand, the tube sample collected from STHX B presented a sticking foulant deposit, in fact during the cut of the sample, only a small part of the foulant layer detached from the internal surface of the tube. Moreover, the fouling layer appeared brown and thick.

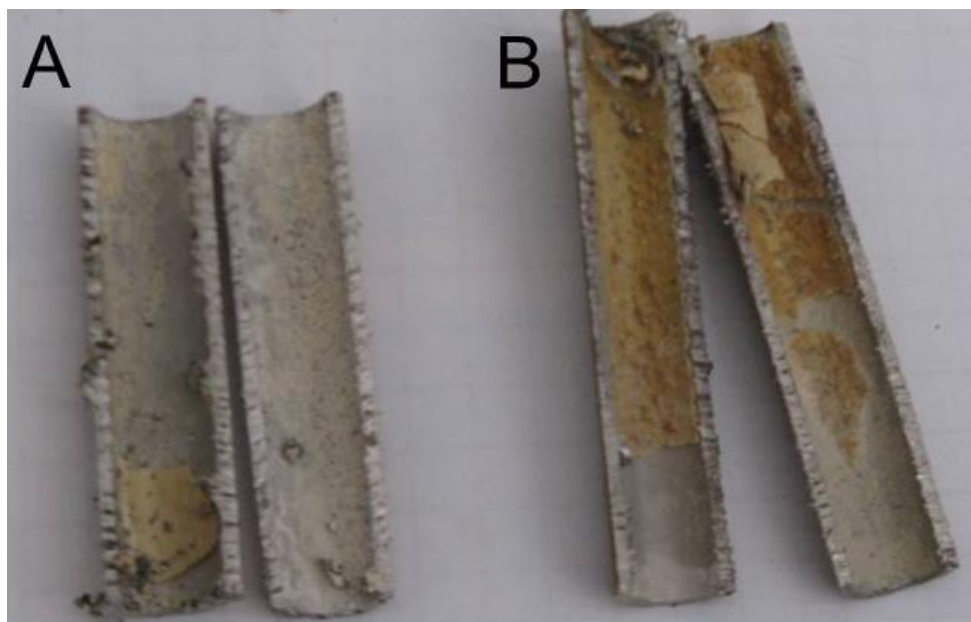


Figure 5-18. Sections of tube samples collected from the tube bundle of the heat exchangers at the end of the pilot plant operation. A = tube sample from the STHX A (coated with Fluorolink®S10); B = tube sample from STHX B (not coated).

A clear comparison between the fouling layers collected on STHX A and STHX B is shown in Figure 5-19.

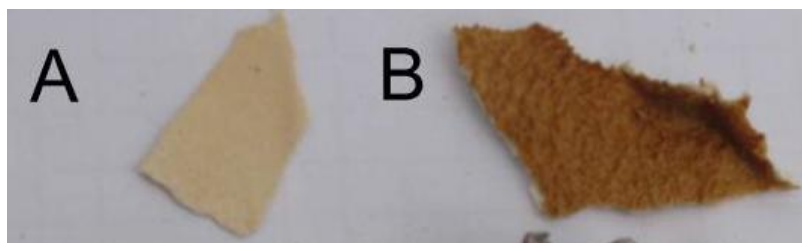


Figure 5-19. Fouling deposits collected from the rear heads of the heat exchangers. A = deposit collected on STHX A (coated with Fluorolink®S10); B = deposit collected in STHX B (uncoated).

The fouling deposits were collected from the rear heads of the heat exchangers (the stainless steel surfaces of the rear head of STHX A were coated as well as the tube bundle). The fouling deposits of STHX A appeared thin, with a light brownish coloration and slightly rough. On the other hand, the fouling deposits collected from STHX B were thicker, with a brown coloration, and highly rough. This difference in the appearance of the fouling deposits confirmed the earlier formation of scale on the hydrophilic heat transfer surfaces. Otherwise, the fouling deposits formed on the hydrophobic heat transfer surfaces were “younger”, in fact they are less thick and less rough, confirming that the fouling was still at the earlier stage on the coated heat exchanger.

As mentioned in Chapter 4, we supposed the formation of scale deposits on the heat transfer surfaces in accordance with the composition of the water used as operating fluid. However, we analyzed by SEM-EDX small tube samples collected from STHX A and STHX B, covered by a foulant layer, to confirm this hypothesis. The EDX analyses confirmed the formation of scale deposits, the most abundant elements are in fact C, O, Ca, and Mg (see Table 5-9). Hence, we can reasonably suppose the occurrence of crystallization fouling phenomena during the pilot plant operation.

Table 5-9. Elemental composition (relative atomic content %), obtained from EDX analyses, of foulant deposits on the stainless steel heat transfer surface of the coated (Fluorolink®S10) and uncoated heat exchanger.

<b>Atomic content [at %]</b>		
<b>Element</b>	Coated heat exchanger	Uncoated heat exchanger
Sulfur	0.2	0.04
Magnesium	8.5	8.2
Potassium	0.01	0.04
Calcium	2.18	1.41
Iron	2.9	6.3
Chromium	9.1	9.3
Nickel	1.5	3.1
Silicon	5.6	5.2
Carbon	14.4	10.6
Oxygen	54.9	54.0
Lead	0.0	0.11

The SEM magnifications are illustrated in Figure 5-20. The foulant deposit formed on the uncoated tube surface was constituted by crystals of scale of small dimension, which formed a compact layer on the stainless steel. The foulant deposit formed on the coated tube surface, on the other hand, was formed by crystals of bigger dimensions in respect to the ones observed on the uncoated surface, which are randomly distributed on the sample surface, without forming a compact layer. The different appearance of the two fouling deposits suggests a possible different mechanism of formation of the foulant layer on the uncoated stainless steel surface, in respect to the coated one, confirming the ability of the S10 coating to interfere with fouling.

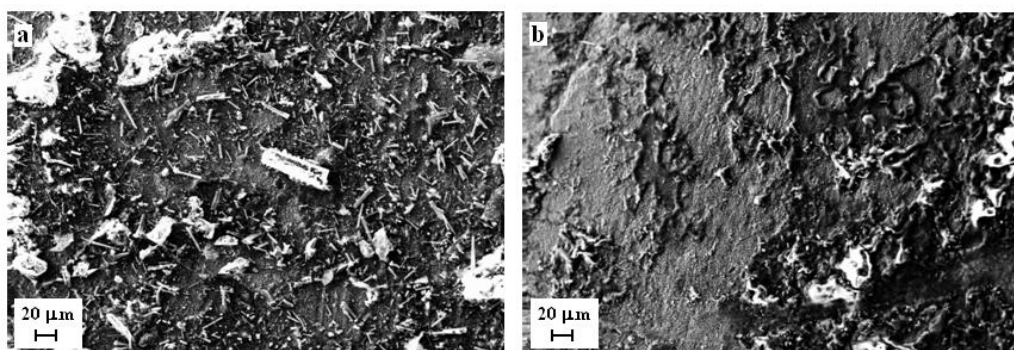


Figure 5-20 SEM pictures of fouling deposits formed on the internal tube surface of the S10 coated heat exchanger (a) and uncoated heat exchanger (b).

Eventually, a cleaning procedure of the internal surfaces of the tubes was performed, mechanically, by propelling foam projectiles inside the tube themselves. We observed an easier removal of the fouling deposits from the tubes of STHX A; on the other hand, the mechanical cleaning of the tubes internal surfaces of STHX B was more difficult. However, CA measurements performed on the internal surface of a cleaned tube samples, revealed the



complete detachment of the fluorinated coating. The surface was in fact completely hydrophilic.

### 5.5.2 Anti-fouling assessment of Fluorolink®F10

Fluorolink®F10 was deposited on a new tube bundle, carefully washed with water and acetone before the coating deposition. The coating formulation contained 10 wt% of the PFPE, 20 wt% of *iso*-propanol and distilled water. The tube bundle was kept immersed in the F10 formulation for 24 hours, and heat treated at 373 K for 24 hours. We suppose the formation of a F10 layer with thickness inferior than 5  $\mu\text{m}$ , and a static water contact angle of about 110°, as we observed on plain samples coated with the same procedures.

The pilot plant lay-out was the first one, the tube bundles, the front and rear heads and the glass shells were replaced with new ones after the experimentation with the S10 coating. The other plant components were kept identical. The operating conditions adopted for this experimentation are summed up in Table 5-10; the pilot plant worked in mild conditions, comparable to the ones maintained for the anti-fouling assessment of the Fluorolink®S10 coating. In that case, however, the experimentation ran for a period of 55 days (1320 hours), since we focused our attention on the effect of the hydrophobic coating on the fouling induction period. The pilot plant worked in continuous, the two heat exchangers operated in parallel, with the same conditions; the coated heat exchanger is named STHX A, the uncoated heat exchanger STHX B.

Table 5-10. Operating conditions of the pilot plant I used for the investigation of Fluorolink®F10 ability in fouling mitigation

<b>Operating condition</b>	<b>Numerical value</b>
Shell inlet fluid temperature [K]	290-293
Tubes inlet fluid temperature [K]	313 -323
Shell inlet flowrate [kg/h]	96-120
Tubes inlet flowrate [kg/h]	330
Fluid velocity inside the shell [m/s]	0.027-0.03
Fluid velocity inside the tubes [m/s]	0.09
Re number in shell	1880-2090
Re number in tubes	1075

During the plant operation, we checked the flowrates values and the temperatures of the inlets and outlets fluid of the shell side and the tube side of the two heat exchangers, collecting data 6/8 times per day at time intervals of 1 hour, during the morning. However, the plant worked in continuous, 24/24 hours. The heat transfer efficiency of the plant was assessed by calculating the quantity of heat transferred  $Q$ , the overall heat transfer coefficient  $U$  and fouling resistance  $R_f$ .

The fouling resistance was calculated according to Equation (5-6):

$$R_f = \frac{1}{U_t} - \frac{1}{U_0} \quad (5-6)$$

The term  $\frac{1}{U_t}$  expresses the overall heat transfer resistance at the generic time  $t$ , while the term  $\frac{1}{U_0}$  is the overall heat transfer resistance at time 0 (i.e., experimentally calculated in the first working day). The increase in the overall heat transfer resistance with time can be in fact related to an increase of the fouling resistance, since the film resistances ( $1/h$ ) and the wall resistance should be constant at constant working conditions. Moreover, considering that the experiment lasted for only a short time, we can suppose that fouling mainly occurred only on only one side of the heat transfer surfaces (the internal one), where the temperature was high enough to permit crystallization fouling phenomenon; therefore such a simplification in the determination of  $R_f$  is available [14].

Figure 5-21 illustrates the trend of the quantity of heat transferred during the plant operation. The starting  $Q$  value (average of the  $Q$  values calculated in the first working day) was 8003 kJ/h for the coated heat exchanger, and 7991 kJ/h for the uncoated heat exchanger. Therefore, the quantity of heat transferred by the two heat exchangers at the beginning of the experimentation was very similar, confirming the hypothesis that the coatings, thanks to their low thickness, did not alter the heat transfer properties of the stainless steel surface.  $Q$  decreased with time for both the heat exchangers, however the trends were different. The  $Q$  values of STHX B remained almost stable until the 10<sup>th</sup> working day; subsequently we observed a progressive decrease of the heat transferred. On the other hand, the quantity of heat transferred by STHX A only slightly varied until the 20<sup>th</sup> working day, then a consistent decrease was

observed. Until the 27<sup>th</sup> day of operation  $Q$  decreased similarly for both the heat exchangers, even if the values obtained for the coated heat exchanger remained always higher in respect to the ones calculated for the uncoated heat exchanger. After this period of operation, the  $Q$  value remained almost the same for STHX A, only slightly decreasing, while the heat transfer efficiency of STHX B continued to decrease until the end of the experiment. Interpolating the values of  $Q$  shown in Figure 5-21 with a linear equation, the slope of the line corresponding to the uncoated heat exchanger trend is -34, while for the coated heat exchanger is -29, confirming a different trend of decrease of the heat transferred by the coated heat exchanger.

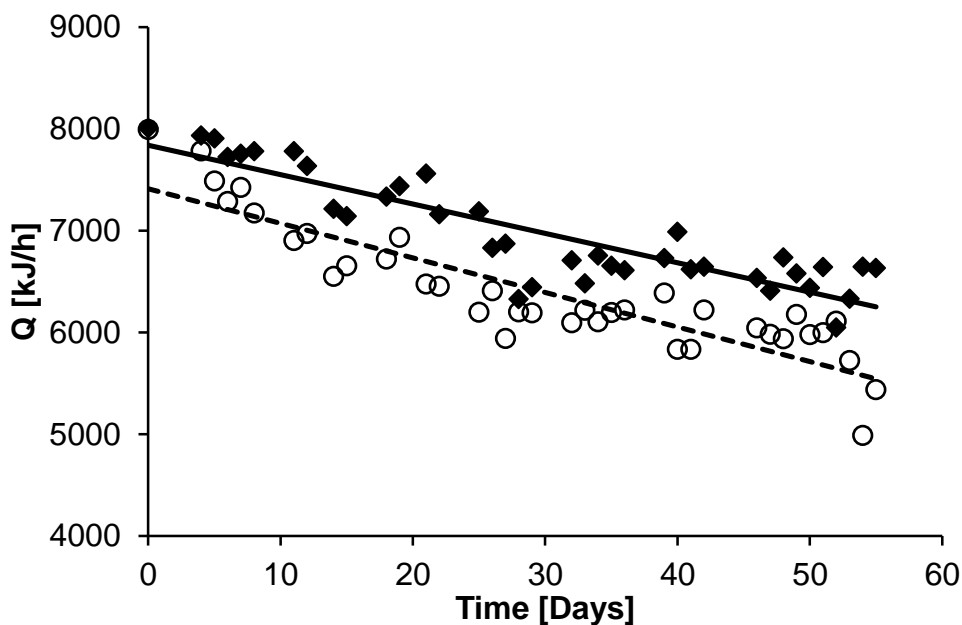


Figure 5-21. Absolute value of the heat transferred ( $Q$ ) *vs* time.  $\blacklozenge$  F10 coated heat exchanger (STHX A);  $\circ$  Uncoated heat exchanger (STHX B).

To better understand the differences in the heat transfer ability of the uncoated and F10 coated heat exchanger, during the experiment, consider Table 5-11,

where the average daily  $Q$  values of STHX A and B, of some selected days of operation, are compared.

Table 5-11. Comparison between the average daily values of  $Q$  of STHX A (coated by the F10 polymer) and STHX B, for some indicative days of working.

	<b>Coated heat exchanger STHX A</b>	<b>Uncoated heat exchanger STHX B</b>
Working day	$Q$ [kJ/h]	$Q$ [kJ/h]
1	8003	7991
7	7754	7423
19	7435	6933
28	6870	5939
36	6728	6218
41	6616	5833
55	6631	5436

In the first week of operation,  $Q$  decreased moderately in both the heat exchangers;  $\Delta Q$  from the first working day was 249 kJ/h for STHX A and 550 kJ/h for STHX B, corresponding to a decrease of the heat transfer efficiency of the 4% and the 7% respectively (Table 5-11). In the 19<sup>th</sup> day, the decrease of

the  $Q$  value was more consistent, in fact STHX B transferred the 13% less in respect to the first day, while STHX A the 7%. The  $Q$  value greatly diminished even for STHX A from the 19<sup>th</sup> to the 28<sup>th</sup> working day, the  $Q$  decrease in respect to the first working day was in fact the 14%. From the 28<sup>th</sup> day to the 41<sup>st</sup> working day, the quantity of heat transferred by STHX A remained almost stable, while at the 41<sup>st</sup> working day, the  $Q$  transferred by STHX B was the 27% less in respect to the first day. In the last working day (the 55<sup>th</sup>), the total decrease of  $Q$ , in respect to the first day, was the 17% for the coated heat exchanger and the 32% for the uncoated one.

The overall heat transfer coefficient  $U_{lm}$  was calculated considering the logarithmic mean of the total heat transfer surface area  $A_{lm}$ ; the trend is illustrated in Figure 5-22.

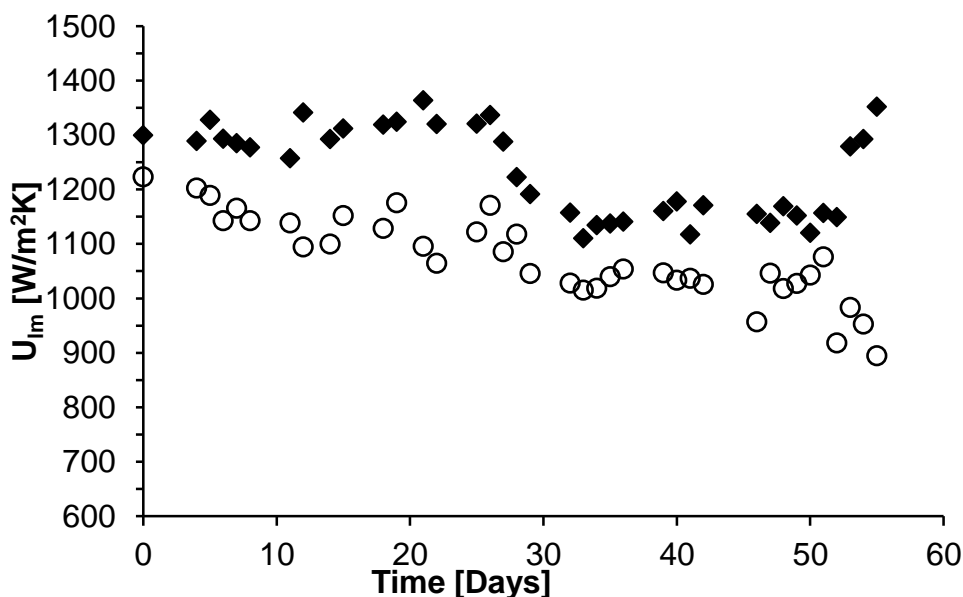


Figure 5-22. Overall heat transfer coefficient ( $U$ ) vs time.  $\blacklozenge$  F10 coated heat exchanger (STHX A);  $\circ$  Uncoated heat exchanger (STHX B).

The values of  $U$  diminished with time during the experimentation, suggesting the progressive formation of foulant deposits on the heat transfer surfaces for both the heat exchangers. However,  $U$  decreased progressively and continuously for the uncoated heat exchanger; on the other hand the trend of decrease for the coated heat exchanger was more complex. Regarding the trend of the overall heat transfer coefficient of the F10 coated heat exchanger, we observed that until the 27<sup>th</sup> working day, the  $U$  values remained almost stable, ranging from 1327 to 1300 W/m<sup>2</sup>K. At the 28<sup>th</sup> day the value of  $U$  started to diminish, reaching the minimum at the 33<sup>rd</sup> working day (1109 W/m<sup>2</sup>K). From that point, the overall heat transfer coefficient started to increase once more, and in the last working days the initial value of  $U$  was restored. Table 5-12 highlights the difference in the values of  $U$  calculated for STHX A and B in some selected days of operation (average daily values). In the first 19 days of operation the overall heat transfer coefficient decreased of the 4% in the uncoated heat exchanger, while remained unvaried in the coated one. In the 33<sup>rd</sup> working day, the percentage decrease of  $U$  in STHX A was identical to the one of STHX B (17%), even if the individual value of the coefficient was higher for the coated heat exchanger. In the last working period, from the 33<sup>rd</sup> day to the 50<sup>th</sup> day of operation,  $U$  slightly decrease in the uncoated heat exchanger, reaching the 27% of decrease in respect to the starting value. On the other hand the  $U$  values of the coated heat exchanger remained stable. After 50 days of work we had to shut down the plant for several hours, due to the necessity to replace the heating elements inside the tank with new ones. During this operation the heat exchangers were emptied. After the restarting of the experiment, we observed that progressively the initial  $U$  value of STHX A was restored, while, on the other hand, the coefficient increased more in STHX B. In view of these results, it is possible to suppose that the hydrophobic surfaces

started to foul later in respect to the hydrophilic surfaces (about 10 days later). Moreover, the deposits formed progressively on the coated surfaces from the 26<sup>th</sup> day until the 33<sup>rd</sup> day of operation, did not adhere strongly on the hydrophobic surfaces, hence, the wall shear stresses induced by the water flow in the restarting operation facilitated their removal, with a consequent restoring of the initial working conditions. This phenomenon, on the other hand, was not observed on the uncoated heat exchanger, the heat transfer surfaces in fact continued to foul.

Table 5-12 Comparison between the overall heat transfer coefficients ( $U_{lm}$ ) and the fouling resistance ( $R_f$ ) of Fluorolink®F10 coated heat exchanger (STHX A) and the uncoated heat exchanger (STHX B).

	<b>STHX A</b>	<b>STHX B</b>	<b>STHX A</b>	<b>STHX B</b>
Working day	$U_{lm}$ [W/m <sup>2</sup> K]	$U_{lm}$ [W/m <sup>2</sup> K]	$R_f$ [m <sup>2</sup> K/W]	$R_f$ [m <sup>2</sup> K/W]
1	1299	1223	-	-
19	1323	1175	$1.2 \cdot 10^{-5}$	$7.0 \cdot 10^{-5}$
33	1109	1014	$1.6 \cdot 10^{-4}$	$1.6 \cdot 10^{-4}$
55	1351	894	$-6.5 \cdot 10^{-6}$	$2.3 \cdot 10^{-4}$

The same hypothesis can be assumed observing the trend of the fouling resistance (Figure 5-23 and Table 5-12). Between the 26<sup>th</sup> and the 33<sup>rd</sup> working day it is possible to observe a consistent increase of the fouling resistance for both the heat exchangers, the  $R_f$  value was 0.00016 m<sup>2</sup>K/W for both STHX A



and STHX B. Afterwards, the  $R_f$  values stabilized for STHX B, while started to decrease for STHX A. At the 46<sup>th</sup> working day, the  $R_f$  value of STHX A was in fact 0.00012 m<sup>2</sup>K/W, and still 0.00016 m<sup>2</sup>K/W for STHX B. At the end of the experimentation, the fouling resistance increased until the value of 0.00027 m<sup>2</sup>K/W in the uncoated heat exchanger. The coated heat exchanger, on the other hand, had an  $R_f$  value, of two order of magnitude inferior in respect to the uncoated heat exchanger. Comparing this value with the ones measured in the first working days, we can observe a restoring of the initial conditions for the coated heat exchanger.

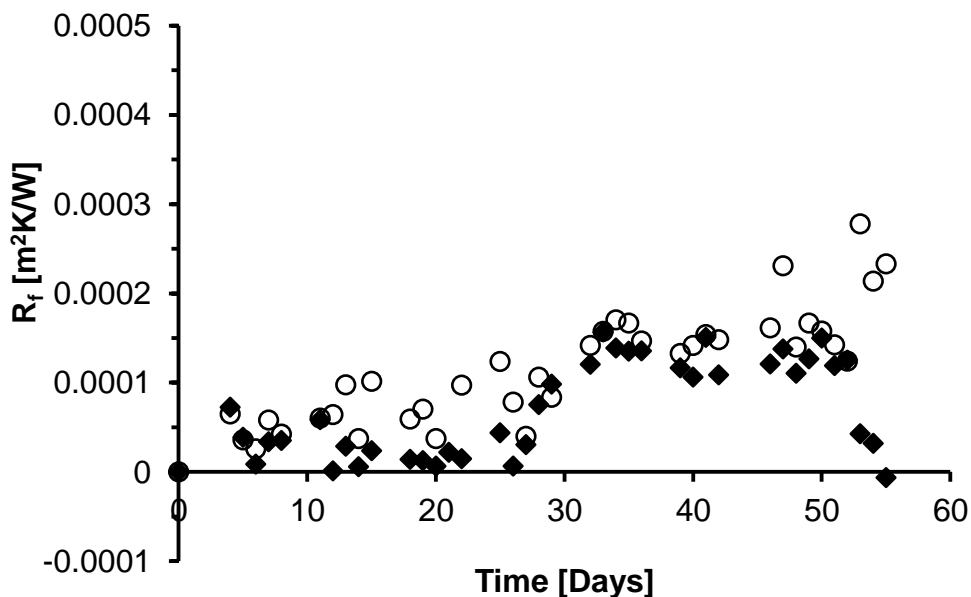


Figure 5-23. Fouling resistance *vs* time.  $\blacklozenge$  Coated heat exchanger;  $\circ$  Uncoated heat exchanger.

In conclusion, the trend of the fouling resistance confirmed the hypothesis previously made. The F10 coating prolonged the fouling induction period, in

the fouling conditions adopted, and facilitated the detachment of the foulant deposits from the stainless steel surfaces, under wall shear stresses.

At the end of the pilot plant experimentation, we took some photographs of the internal surfaces of the tubes, using a micro-camera. The presence of foulant deposits was assessed on both the coated and uncoated surfaces. In Figure 5-24 are illustrated two photographs, corresponding to the final section of a tube of STHX A or B, in correspondence of the rear head of the heat exchangers. Fouling deposits were observed in all the tubes examined with the micro-camera, but in general they were not uniform on the heat transfer surfaces. However, we noticed a higher presence of fouling deposits on the uncoated heat transfer surfaces in respect to the coated ones [74].

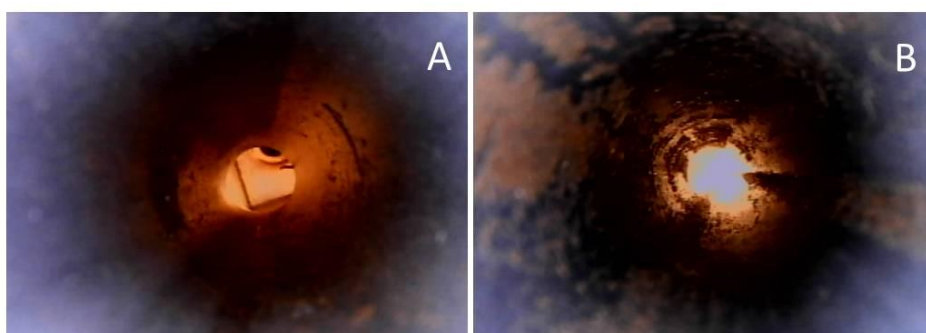


Figure 5-24. Pictures of internal tubes surfaces, collected in correspondence of the rear head. A) tube of the coated heat exchanger (STHX A); B) tube of the uncoated heat exchanger (STHX B).

The use of  $\alpha,\omega$ -functionalized perfluoropolyethers for the modification of the surface wettability of stainless steel emerged as a possible strategy for fouling mitigation in heat exchangers. The optimized coating procedure developed in this PhD research permitted the obtainment of PFPE layers with a thickness high inferior than 5  $\mu\text{m}$  and low roughness. The experimentation on the heat

exchanger pilot plant permitted to compare the fouling phenomenon occurring on a normal stainless steel heat transfer surface with the one of a hydrophobic heat transfer surface, coated with Fluorolink®S10 or F10. The fouling was in part mitigate, or either postponed in time in the specific working conditions adopted for these experimentations (very mild conditions). However, in view of the resistance tests results, is not possible to suppose a long term duration of the coatings, especially when exposed to very aggressive conditions, for example water at temperature higher than 323 K or turbulent flows. For this reasons, the attention was paid on the reinforcement of the PFPE hydrophobic coatings, in particular we tried to improve their mechanical and physical stability.

## 6 RESULTS AND DISCUSSION: MULTILAYER COATINGS

*The PFPE coatings suffered from erosion of aggressive liquids environments or shear stresses induced by water flow, hence compromising their long-term anti-fouling efficiency in real operating conditions. For this reason, we combined a PFPE layer with an inorganic layer, made of TiO<sub>2</sub> or ZrO<sub>2</sub> nanoparticles, obtaining multilayer coatings. In that way we preserved the hydrophobic behaviour of the coating (guaranteed by the PFPE), but at the same time we improved its resistance against mechanical stresses by adding a component characterized by high hardness and thermal stability. The first section of this chapter regards the characterization of the multi-layer coatings. In the second section, the results of the resistance tests are discussed, in comparison with the ones obtained from the simple PFPE coatings. The results of a preliminary assessment of the fouling mitigation ability of the multilayer coatings are presented at last.*

## 6.1 Characterization results

The multilayers coatings were prepared following the procedure reported at pp. 48-49. All the stainless steel substrates were washed with water and acetone before the coatings deposition. The characterization procedures were performed on stainless steel plain substrates, not polished before the coating deposition.

### 6.1.1 Morphology, composition and thickness

The surface morphology was investigated on the single layer of  $\text{TiO}_2$ -OTES or  $\text{ZrO}_2$ -OTES, deposited on the stainless steel substrate (Figure 6-1). The ceramic oxides coatings appeared continuous on the stainless steel surfaces, which was completely covered by the inorganic layer. However the morphology of  $\text{TiO}_2$ -OTES layer (Figure 6-1a) was quite different from the one of the  $\text{ZrO}_2$ -OTES layer (Figure 6-1d). The first one formed a homogeneous layer on the substrate (Figure 6-1c), however lower magnifications (Figure 6-1a-b) revealed the presence of crevices on the surface. The second coating was more compact (Figure 6-1d), but higher magnifications (Figure 6-1e-f) revealed an inhomogeneous texture, probably due to the formation of agglomerates of  $\text{ZrO}_2$  nanoparticles.

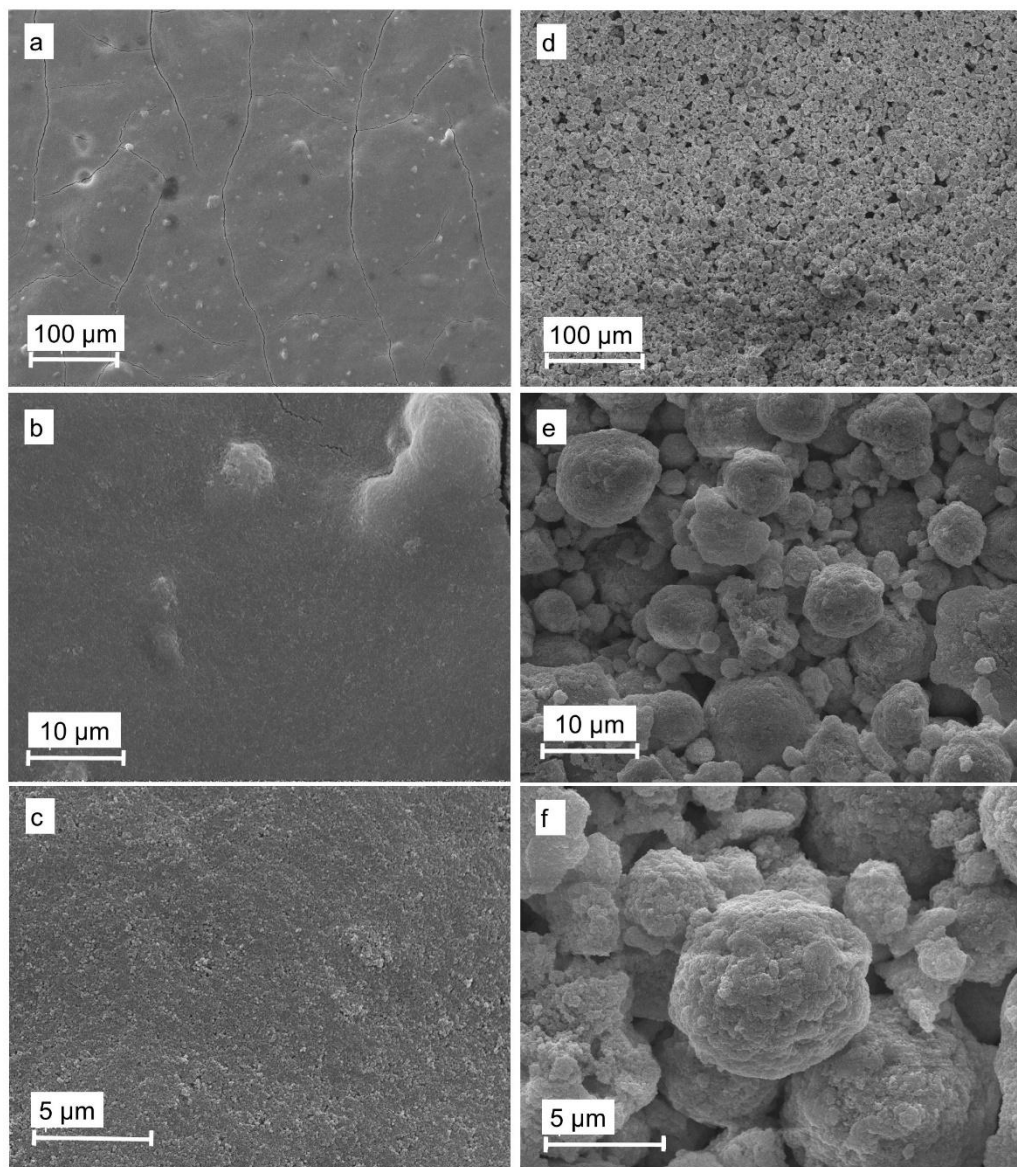


Figure 6-1. SEM images of a TiO<sub>2</sub>-OTES layer (a, b, c) and of a ZrO<sub>2</sub>-OTES layer (d, e, f). Magnification of 200X for pictures a and d, 2000X for pictures b and e; 5000X for pictures c and f.

The XPS analyses were performed only TiO<sub>2</sub>-OTES/S10 and ZrO<sub>2</sub>-OTES/S10 coatings, i.e., the coatings obtained by depositing a ceramic oxide film on the

stainless steel surface, and hence a S10 film on the previous one. The atomic composition of the coatings, revealed by XPS survey analyses is presented in Table 6-1.

Table 6-1. Atomic composition of the TiO<sub>2</sub>-OTES/S10 and ZrO<sub>2</sub>-OTES/S10 coatings, determined by XPS survey analyses.

Elements	Relative atomic abundance %					
	C	O	F	Si	Ti	Zr
TiO <sub>2</sub> -OTES/S10	22	28.3	41	3.7	5	-
ZrO <sub>2</sub> -OTES/S10	27.6	25.9	38	2.5	-	6

XPS high resolution analyses permitted to investigate the types of bonds generated by Ti and Zr and their chemical contour in the multilayer coating. The bonds region of Ti 2p and Zr 3d were analyzed. The Ti 2p doublet is reported in Figure 6-2 a, two components were recognized, identified by peaks A/C and B/D ( $\Delta E_V = 5.5$ ). The peaks named A and C corresponds to the Ti(IV) in the oxide, as reported in literature [75]. The peaks B and D identify a second Ti species; in particular the higher binding energies of these peaks suggested the interaction of Ti with a more electronegative species, usually this energy correspond to the interaction of titanium with fluorine [76]. Similarly, the typical doublet of Zr 3d appeared complex (Figure 6-2 b), and a two components peak fitting was used to correctly interpolate the shape of the doublet. The peaks named A and C ( $\Delta E_V = 2.7$ ) correspond to the species Zr(IV) in the oxide, while the peaks B and D, shifted to higher binding

energies, can be, one more time, explained by the presence of a very electronegative species in the chemical contour of Zr, which probably was fluorine [76]. Therefore, we can suppose that the PFPE layer interacted with the inorganic layer made by the metal oxide, but the type of interactions formed are not clear. Probably only weak interactions, such as electrostatic or Van der Waals interactions were formed.

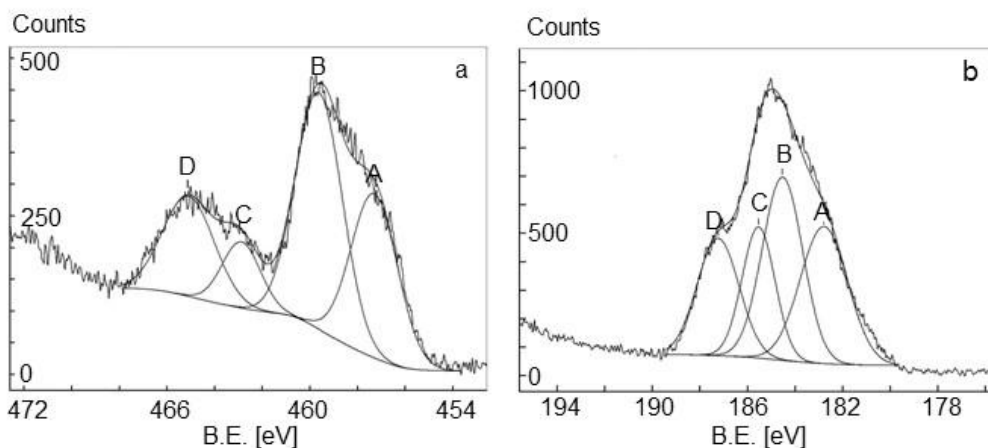


Figure 6-2. High resolution spectra of Ti 2p doublet (a) and Zr 3d doublet. Peak-fit table a: A=459.3, B=461.6, C=464.9, D=467.1; Peak-fit table b: A=182.8, B=184.5, C=185.5, D=187.2.

The profilometry analyses revealed the roughness and thickness of TiO<sub>2</sub>-OTES and ZrO<sub>2</sub>-OTES layers and of the multilayer coating ZrO<sub>2</sub>-OTES/S10. The ceramic oxides layers had an average thickness of 20-25 μm; the average roughness (Ra) was 0.786 μm for the TiO<sub>2</sub>-OTES layer and 0.717 for the ZrO<sub>2</sub>-OTES layer. In comparison, the Ra of the uncoated stainless steel substrate was 0.174 μm and 0.192 μm respectively, therefore the ceramic oxide layer was responsible of a consistent increase of the average roughness. As previously pointed out, the increase in roughness due to the presence of the coating could



be disadvantageous for application in fouling mitigation, since the more the surface is rough, the more increase the possibility of settlement of foulant particles in the asperities of the surface. Considering the results of profilometry analyses performed on the Fluorolink<sup>®</sup>S10 coating, we supposed that the thickness of a multilayer coating should range from 25 to 30  $\mu\text{m}$ . The analysis performed on the  $\text{ZrO}_2$ -OTES/S10 confirmed this hypothesis; however we observed also inhomogeneity in the coating distribution, corresponding to an inhomogeneous thickness. In fact, the measurements were performed on different spots of the sample, in correspondence of the coating section; we observed different value of thickness, varying from 10  $\mu\text{m}$  to 40  $\mu\text{m}$ . The Ra increased consistently also for the multilayer coating, reaching the value of 0.749  $\mu\text{m}$ .

### 6.1.2 Hydrophobicity assessment

Table 6-2 resumes the results of contact angle measurements. The single layers of  $\text{ZrO}_2$  and  $\text{TiO}_2$  nanopowders impregnated with siloxanes had the higher CA values ( $>150^\circ$ ), indicating a super-hydrophobic surface; accordingly, the surface free energy (SFE) is very low. The multilayer coatings composed by a layer of S10 overlapped with a layer of  $\text{TiO}_2$ -OTES or  $\text{ZrO}_2$ -OTES were super-hydrophobic too; the coatings  $\text{TiO}_2$ -OTES/S10, and  $\text{ZrO}_2$ -OTES/S10, characterized by the deposition of S10 as the upper layer, had CA respectively of  $141^\circ$  and  $153^\circ$ , slightly lower in respect to the other typology of multilayer coatings. The hysteresis of the advancing and receding contact angles was very low ( $<5$ ) for all the coatings considered in Table 6-2; the Cassie-Baxter model is therefore suitable to describe the interaction between water and the coated surface.

Table 6-2. Surface wetting properties of the ceramic oxides single layers deposited on stainless steel substrates and multilayer coatings.

Coating type	Static CA [°]	SFE [mN/m]	Advancing CA [°]	Receding CA [°]	Hysteresis
TiO <sub>2</sub> -OTES	152 ± 0.1	2 ± 0.3	149	148	1
S10/TiO <sub>2</sub> -OTES	151 ± 1.26	14 ± 0.7	151	146	5
TiO <sub>2</sub> -OTES/S10	141 ± 2.1	6 ± 0.4	146	143	3
ZrO <sub>2</sub> -OTES	156 ± 4.3	7 ± 1.0	150	146	4
S10/ZrO <sub>2</sub> -OTES	158.3 ± 2.15	1 ± 0.1	150	149	1
ZrO <sub>2</sub> -OTES/S10	153 ± 3.6	1 ± 0.1	150	148	2

## 6.2 Coatings resistance against erosion

Each resistance test was performed at least two times and repeated until the final contact angles measured were similar ( $\pm 10^\circ$ ). The results presented correspond to the best results obtained. The multilayers coatings were prepared on both unpolished and polished stainless steel plain samples. However, we observed that the deposition on polished substrates did not bring to better results in terms of adhesion or resistance of coatings, rather, we observed worsening in the resistance against chemical erosion. For this reason, here are

discussed only the results of the resistance tests performed on unpolished substrates, modified with the multilayer coatings.

Figure 6-3 summed up the results of resistance tests performed with multilayer coating obtained depositing a layer of S10 and, in the upper position, a layer of ceramic oxides nanopowders. The trend of CA decrease during these tests are, instead, illustrated in Figure 6-4. The deposition of the TiO<sub>2</sub>-OTES layer on a S10 layer did not improve the resistance of the polymeric coating. In seven days the samples turned to be hydrophilic when immersed in alkaline or disinfectant solutions containing chlorine, as well as when exposed to water at high temperature (343 K) or to shear stresses (see Figure 6-3a). We observed a limited erosion of the S10/TiO<sub>2</sub>-OTES multilayer coating only when immersed in water at room temperature (total decrease of CA is 23%) and HCl (12% CA decrease). These results, however were even worst in respect to the ones obtained with the single S10 layer. Moreover, we observed for the S10/TiO<sub>2</sub>-OTES coatings the inversion of wettability (from superhydrophobic to superhydrophilic) when exposed to solar light. This phenomenon is well documented in literature and is mainly due to the photocatalytic activity of titanium dioxide in the anatase phase [63]. The same phenomenon was observed also for the TiO<sub>2</sub>-OTES layers deposited on the stainless steel substrates.

The S10/ZrO<sub>2</sub>-OTES multilayer coatings, instead, showed an improved resistance in respect to simple S10 coatings when immersed in some aggressive liquids (Figure 6-3b). The immersion for 7 days in the NaOH solution did not erode completely the hydrophobic coating; at the end of the test the CA value was 124°, with a general decrease in CA of 18%. Moreover, the degradation trend (Figure 6-4c) suggested the possibility of no further degradation for

longer exposition. Similar results were obtained also after immersion in hydrochloric acid and chloramines solution; the CA decrease was the 15-20%, and the erosion occurred mainly in four days, then the CA remain stable at a value higher than  $115^\circ$ . Water at room temperature and the water flow only partially eroded the coating, the final CA decrease was 25-26%, and, at the end of the test, the CA was still higher than  $110^\circ$ . On the other hand, water at 343 K completely eroded the multilayer coating.

The multilayer coating obtained by depositing the  $ZrO_2$ -OTES layer on the S10 coating, had higher resistance against chemical or physical erosion in respect to the simple S10 coating. Only the high temperature was responsible of a degradation of the multilayer coating. On the contrary, the multilayer coating with  $TiO_2$  as the upper layer did not show resistance improvements.

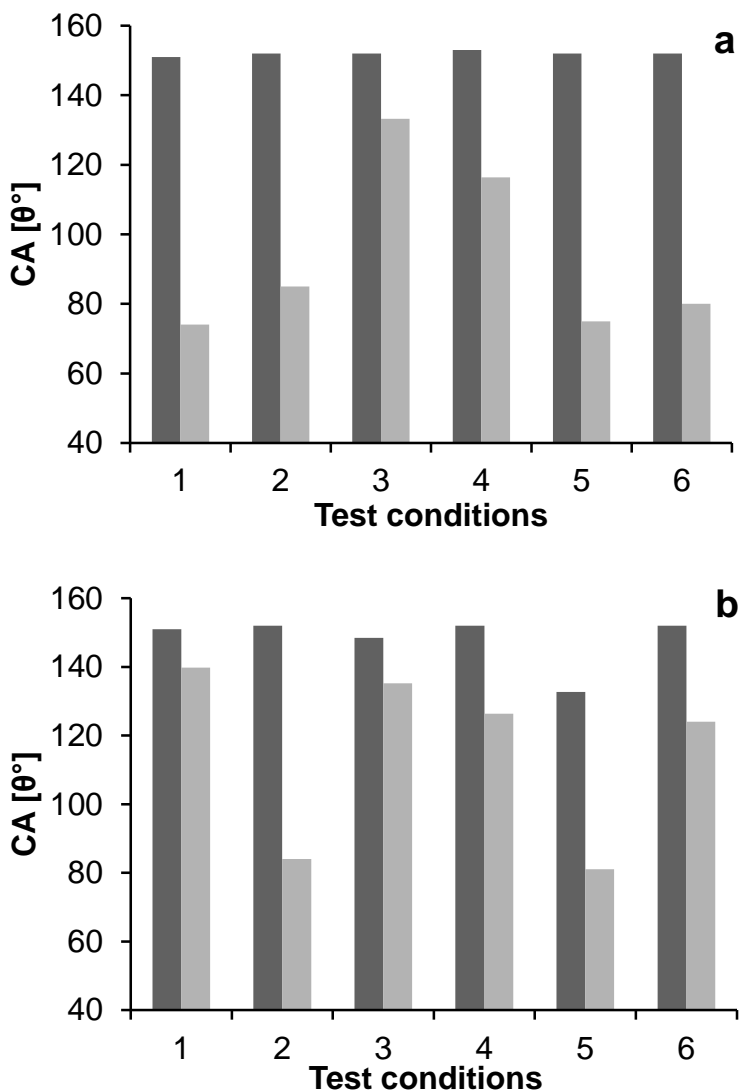


Figure 6-3. Coating resistance against erosion in liquid environments: comparison between the starting CA (■) and the CA at the end of the test (■). S10/TiO<sub>2</sub>-OTES multilayer coating (a); S10/ZrO<sub>2</sub>-OTES multilayer coating (b). 1= NH<sub>2</sub>Cl/NHCl<sub>2</sub> solution, T= 323 K; 2= NaOH solution, T= 323 K; 3= HCl solution, T=323 K; 4= water, T=298 K; 5= water, T=343 K; 6= water flux, T=313 K, flowrate=0.13 m/s.

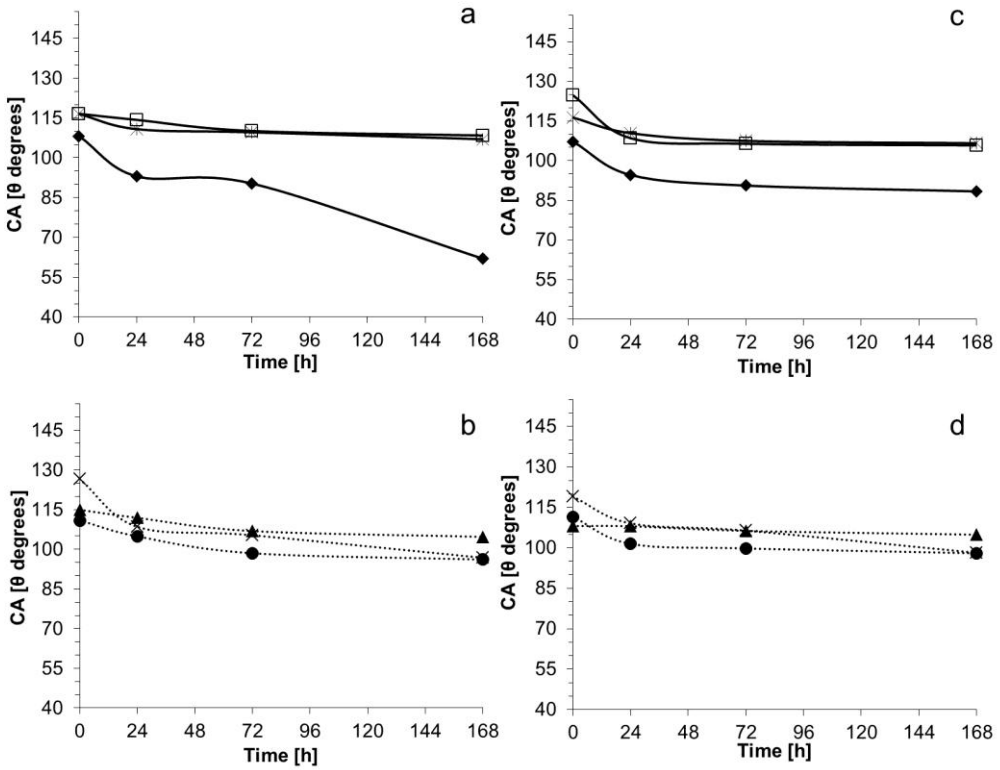


Figure 6-4. Trend of CA decrease during resistance tests. S10/TiO<sub>2</sub>-OTES multilayer coating (a, b); S10/ZrO<sub>2</sub>-OTES multilayer coating (c, d). Legend: \* = NH<sub>2</sub>Cl/NHCl<sub>2</sub> solution, T= 323 K; ◆ = NaOH solution, T= 323 K; □ = HCl solution, T=323 K; ▲ = water, T=298 K; × = water, T=343 K; ● = water flux, T=313 K, flowrate=0.13 m/s.

The multilayer coatings obtained by depositing a ceramic oxide layer on the stainless steel substrate and, in the upper position, a S10 layer, showed the best results in terms of erosion resistance (Figure 6-5). Both TiO<sub>2</sub>-OTES/S10 and ZrO<sub>2</sub>-OTES/S10 were resistant against chloramines and HCl erosion, the contact angle decreased mainly in the first four days of exposition (Figure 6-6a-

c); the final CA decrease was the 8% for TiO<sub>2</sub>-OTES/S10 coating and the 15-19% for ZrO<sub>2</sub>-OTES/S10 coating. The alkaline solution highly damaged the TiO<sub>2</sub>-OTES/S10 coating, in just one day (Figure 6-6a); the ZrO<sub>2</sub>-OTES/S10 coating, instead, was only partially eroded. At the end of the experimentation, the total CA decrease was the 18%, and the final CA value was 115° (Figure 6-5b). Regarding the water erosion, as previously observed the high temperature was particularly detrimental for the multilayer coatings, in 7 days, in fact, the surfaces were hydrophilic after immersion in water at 343 K; moreover, we observed a detachment of the coating in some part of the sample. Water at room temperature was not particularly aggressive for the ZrO<sub>2</sub>-OTES/S10 coating, the CA decrease was the 8% (Figure 6-5b) and the degradation occurred mainly between the 1<sup>st</sup> and the 4<sup>th</sup> day of immersion (Figure 6-6d). The immersion in water at room temperature was more aggressive for the TiO<sub>2</sub>-OTES/S10 coating, at the end of the experimentation, in fact, the CA value was 96°. On the contrary, the presence of the inorganic layer improved the resistance against shear stresses; the exposition to a water flux brought to a total contact angle decrease of the 19%, which mainly occurred within 24 hours of test for both the multilayer coatings (Figure 6-6b-d). Moreover, the final contact angle value was higher than 110°.

The multilayer coatings obtained by depositing on the stainless steel the layer of ceramic oxides nanopowders and, as the upper layer, the PFPE coating made of S10, emerged as the most resistant multilayer coatings. These coatings had improved resistance against alkaline solutions and shear stresses in respect to simple PFPE coatings, however, the exposition to high temperature liquid completely degraded the coating and the surfaces turned to be hydrophilic.

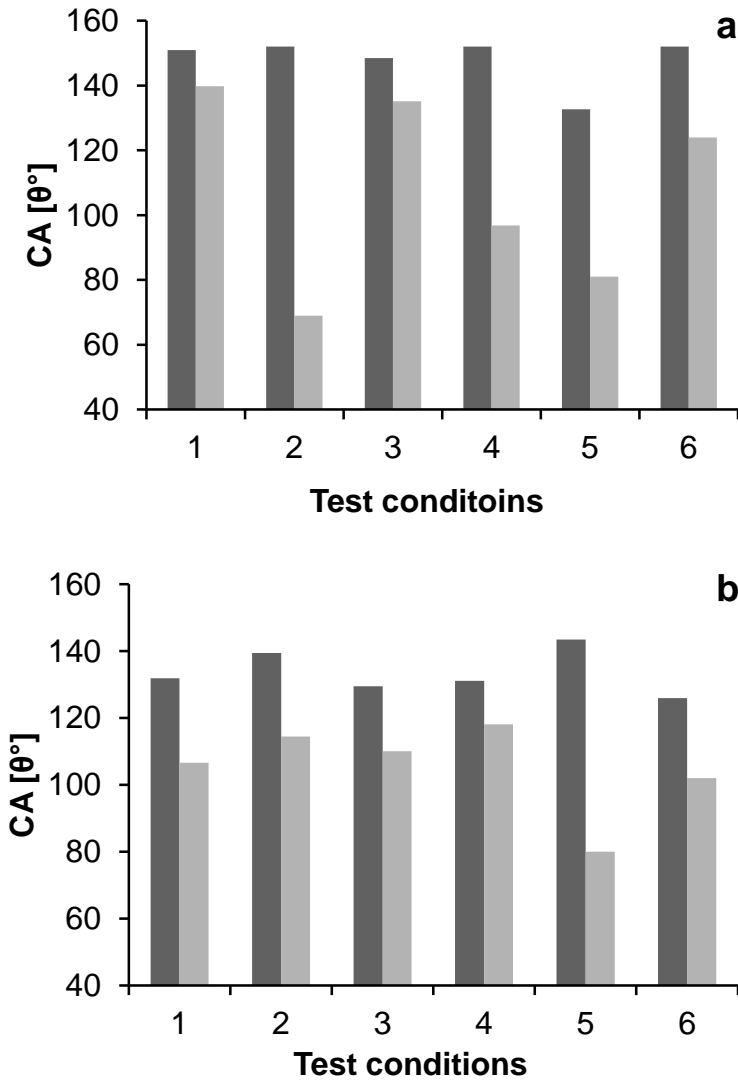


Figure 6-5. Coating resistance against erosion in liquid environments: comparison between the starting CA (■) and the CA at the end of the test (■). TiO<sub>2</sub>-OTES/S10 multilayer coating (a); ZrO<sub>2</sub>-OTES/S10 multilayer coating (b). 1= NH<sub>2</sub>Cl/NHCl<sub>2</sub> solution, T= 323 K; 2= NaOH solution, T= 323 K; 3= HCl solution, T=323 K; 4= water, T=298 K; 5= water, T=343 K; 6= water flux, T=313 K, flowrate=0.13 m/s.



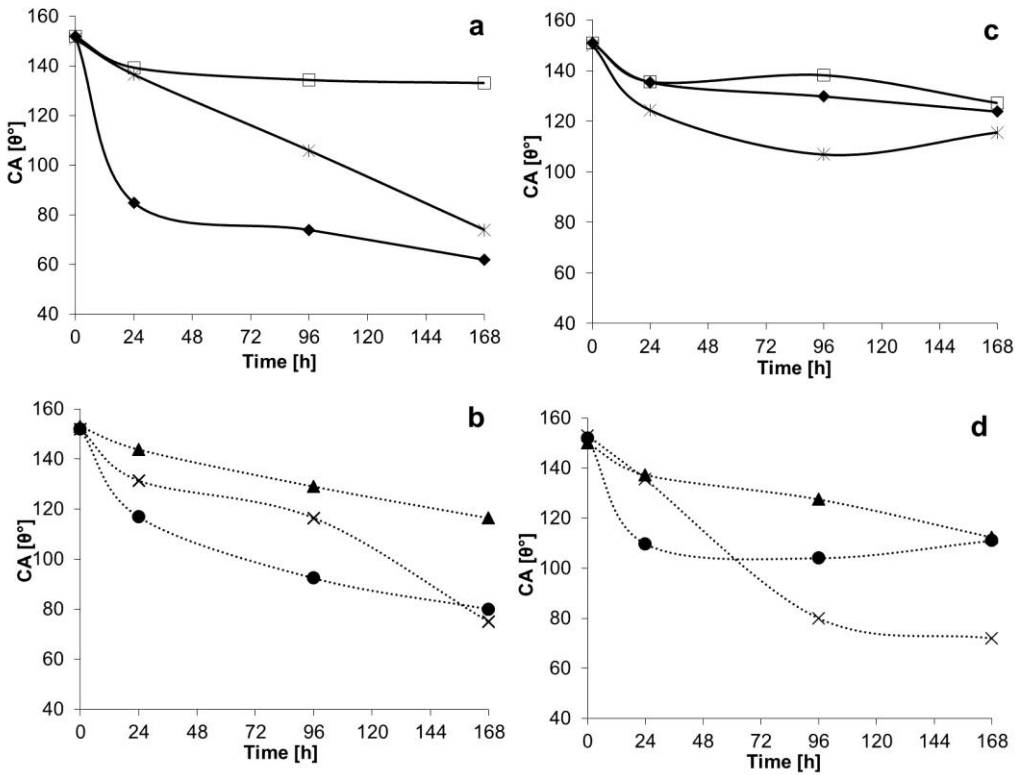


Figure 6-6. Trend of CA decrease during resistance tests. TiO<sub>2</sub>-OTES/S10 multilayer coating (a, b); ZrO<sub>2</sub>-OTES/S10 multilayer coating (c, d). Legend: \* = NH<sub>2</sub>Cl/NHCl<sub>2</sub> solution, T= 323 K; ◆ = NaOH solution, T= 323 K; □ = HCl solution, T=323 K; ▲ = water, T=298 K; × = water, T=343 K; ● = water flux, T=313 K, flowrate=0.13 m/s.

### 6.3 Particulate fouling mitigation

The anti-fouling ability of the multilayer coatings TiO<sub>2</sub>-OTES/S10 and ZrO<sub>2</sub>-OTES/S10 was assessed in the particulate fouling test-rig. The fouling was

quantified in terms of  $\text{CaSO}_4$  deposit on the internal surfaces of tubes samples, covered by the hydrophobic multilayer coatings, and normalized in respect to the total surface area exposed to the fouling phenomenon and the time of exposition. Table 6-3 summarizes the results obtained. The presence of  $\text{CaSO}_4$  deposits was observed after 48 hours test; the value calculated, however, was inferior in respect to the one measured on the uncoated tube sample, exposed to the same fouling conditions. Similarly, the fouling value calculated after 72 hours of tests, was inferior than the one calculated for the uncoated sample. We estimated that the fouling extent on the  $\text{TiO}_2$ -OTES/S10 coated tube was the 10% and on the  $\text{ZrO}_2$ -OTES/S10 coating the 2%, in comparison with 100% fouling extent for the uncoated tube sample after 72 hours of test. Interestingly, prolonging the test duration from 48 hours to 72 hours, the fouling grade on the multilayer coated surfaces diminished instead of increasing. These results can be explained by considering that particulate fouling is a phenomenon divided in a deposition step, and a re-entrainment step. The extent of the re-entrainment step depends from the competition between the surface-particles interaction and the fluid-particles interaction [65]. Possibly, the high hydrophobicity of the multilayer coatings altered the interactions between the fouling particles and the stainless steel surfaces, thus promoting the resuspensions of the  $\text{CaSO}_4$  particles settled on the stainless steel surface. Moreover, it is interesting to point out, that, in comparison with S10 coatings, the anti-fouling activity of  $\text{TiO}_2$ -OTES/S10 and  $\text{ZrO}_2$ -OTES/S10, was higher. The fouling value measured after 72 hours test, in fact, is lower than the one measured for the S10 coating (14%).

Table 6-3. CaSO<sub>4</sub> fouling deposits amounts, formed on uncoated tubes samples and on tubes samples coated with TiO<sub>2</sub>-OTES/S10 and ZrO<sub>2</sub>-OTES/S10 multilayer coatings.

Coating type	Time [h]	Fluid velocity [m/s]	Fouling [mg/cm <sup>2</sup> h]
None	48	0.05	9.2·10 <sup>-5</sup>
None	72	0.05	1.1·10 <sup>-4</sup>
TiO <sub>2</sub> -OTES/S10	48	0.04	2.6·10 <sup>-5</sup>
TiO <sub>2</sub> -OTES/S10	72	0.06	1.1·10 <sup>-5</sup>
ZrO <sub>2</sub> -OTES/S10	48	0.04	3.5·10 <sup>-5</sup>
ZrO <sub>2</sub> -OTES/S10	72	0.05	2.5·10 <sup>-6</sup>

Figure 6-7 illustrates the internal surfaces of the tubes samples, coated with TiO<sub>2</sub>-OTES/S10 or ZrO<sub>2</sub>-OTES/S10, after the particulate test. The surfaces were free from the presence of thick calcium deposits; however we observed the presence of a brownish layer on the TiO<sub>2</sub>-OTES/S10 coated sample. We supposed that the hydrophobic layer, which was white due to the presence of the TiO<sub>2</sub> nanopowder, turned in color because of the presence of iron oxides in the CaSO<sub>4</sub> solution, coming from the steel components of the mass flow meter. Moreover, we observed a partial detachment of the hydrophobic coating from the stainless steel surface, probably because of the wall shear stress induced by the water containing the CaSO<sub>4</sub> particles. In fact, the measurement of the CA highlighted a decrease in the hydrophobicity of the internal surfaces of the tubes

coated by both TiO<sub>2</sub>-OTES/S10 or ZrO<sub>2</sub>-OTES/S10, after the particulate fouling test (CA~110°) [77].

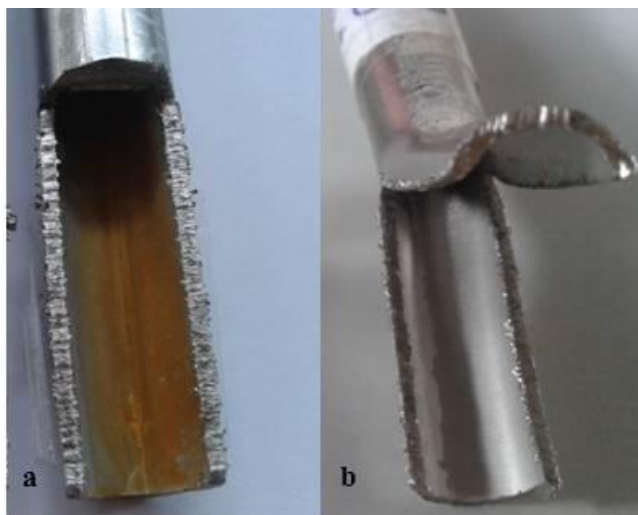


Figure 6-7. Internal surfaces of tubes samples after particulate fouling test lasted for 48 hours. TiO<sub>2</sub>-OTES/S10 coated sample (a) and ZrO<sub>2</sub>-OTES/S10 coated sample (b).

The use of ceramic oxides nanopowders, namely TiO<sub>2</sub> and ZrO<sub>2</sub>, impregnated with siloxanes, emerged as a possible way to reinforce and increase the anti-fouling ability of simple PFPE coatings. The presence of a ceramic oxide layer, in particular when deposited under the S10 layer, permitted the obtainment of a more continuous coating on the stainless steel substrate. The multilayer coatings thus obtained had higher resistance against alkaline environments and water erosion in respect to the simple PFPE coatings; moreover, the fouling mitigation ability was confirmed and we observed improvements in fouling deposits re-entrainment during the fouling phenomenon. However, the multilayer coatings are not particularly suitable for utilization on heat transfer surfaces. The high thickness and roughness of these coatings, in fact, can

compromise their utilization in real heat exchangers plant, since they can act as thermal insulators or favor some types of fouling due to their high roughness. Moreover, the reinforcement effect against erosion, both induced by high temperature water or shear stresses, was not was not enough to motivate further experiments with the pilot plant. For this reasons, we explored a different way to combine the metal oxides (used as reinforcing components) with the PFPE coatings.

## 7 RESULTS AND DISCUSSION: HYBRID COATINGS

*This Chapter deals with the preparation, characterization and use of the hybrid coatings. They were obtained by combining an inorganic network, made of  $\text{TiO}_2$ ,  $\text{SiO}_2$  or  $\text{ZrO}_2$ , with the commercial PFPE. Different hybrid coatings were obtained by varying the preparation methodology and the composition. The coatings were fully characterized in order to determine the surface morphology, the atomic composition and the wettability. Resistance tests pointed out a consistent improvement of the chemical and mechanical resistance of these coatings, in respect to the other typology of coatings previously examined. Particulate fouling tests confirmed the anti-fouling ability of the hydrophobic hybrid coatings. The best coating prepared, in terms of morphology, thickness and resistance, was tested in the heat exchanger pilot plant.*

## 7.1 Optimization of the formulation and of the deposition procedure

In respect to the previous typologies of coatings, we prepared a huge number of hybrid coatings by varying the ratio of organic and inorganic components, the typology of inorganic phase ( $\text{TiO}_2$  networks,  $\text{SiO}_2$  networks or  $\text{ZrO}_2$  networks) and even the type of polymeric component (Fluorolink<sup>®</sup>S10, or F10). However not all the coatings prepared emerged as interesting coatings for fouling mitigation in the heat exchangers. The aim of this section is to highlight the steps that we followed to prepare all the various types of coatings, and to explain how some of them were completely excluded from further investigations. The sections dealing with the coatings characterization, the resistance tests results, and the anti-fouling assessment, involve only the hybrid coatings most promising for fouling mitigation in heat exchangers.

In sol-gel organic inorganic hybrid coatings, the amount of the colloidal inorganic component is variable, but normally exceeds the 20% [78]. Therefore, three types of formulations were prepared varying the relative amount (weight percentage) of polymer and organometallic precursor for the sol-gel synthesis. The weight ratios selected were 50/50, 30/70 and 20/80, for the organometallic precursor and the PFPE respectively. The different types of coatings obtained by varying the components ratio, were compared each other in function of the CA value. The coatings were prepared on stainless steel plain substrates, and heated at 383 K for 3 hours and at 473 K for 1 hour. For the optimization of the coating formulation, only the S10 polymer was employed as organic component. Considering the results reported in Table 7-1, all the formulations prepared permitted the obtainment of hydrophobic coatings.

Table 7-1. Comparison between the static contact angle values of hybrid coating, prepared varying the relative weight composition of perfluoropolyether (Fluorolink®S10) and the organometallic precursor (TTIP, TEOS or ZP), for the preparation of the sol-gel inorganic network (TiO<sub>2</sub>, SiO<sub>2</sub> or ZrO<sub>2</sub> respectively).

Coating name	Component ratio (weight %)	CA (θ°)
TiO <sub>2</sub> /S10-50/50_2	TiO <sub>2</sub> /S10=50/50	117 ± 6.0
TiO <sub>2</sub> /S10-30/70_2	TiO <sub>2</sub> /S10=30/70	127 ± 2.1
TiO <sub>2</sub> /S10-20/80_2	TiO <sub>2</sub> /S10=20/80	135 ± 4.5
SiO <sub>2</sub> /S10-50/50_2	SiO <sub>2</sub> /S10=50/50	116 ± 5.4
SiO <sub>2</sub> /S10-30/70_2	SiO <sub>2</sub> /S10=30/70	113 ± 2.3
SiO <sub>2</sub> /S10-20/80_2	SiO <sub>2</sub> /S10=20/80	141 ± 0.9
SiO <sub>2</sub> /S10-50/50_1	SiO <sub>2</sub> /S10=50/50	140 ± 3.8
SiO <sub>2</sub> /S10-30/70_1	SiO <sub>2</sub> /S10=30/70	140 ± 6.0
SiO <sub>2</sub> /S10-20/80_1	SiO <sub>2</sub> /S10=20/80	146 ± 0.8
ZrO <sub>2</sub> /S10-50/50_2	ZrO <sub>2</sub> /S10=50/50	121 ± 2.3
ZrO <sub>2</sub> /S10-30/70_2	ZrO <sub>2</sub> /S10=30/70	118 ± 1.1
ZrO <sub>2</sub> /S10-20/80_2	ZrO <sub>2</sub> /S10=20/80	129 ± 0.8



ZrO <sub>2</sub> /S10-50/50_1	ZrO <sub>2</sub> /S10=50/50	123 ± 5.1
ZrO <sub>2</sub> /S10-30/70_1	ZrO <sub>2</sub> /S10=30/70	131 ± 4.7
ZrO <sub>2</sub> /S10-20/80_1	ZrO <sub>2</sub> /S10=20/80	121 ± 2.4

---

Regarding the coatings prepared by the two steps procedure, the best component ratio was the 20/80-inorganic precursor/PFPE, independently from the inorganic network typology. The CA was in fact, in general >130°, while for the other ratios the value was <130°. Considering instead the coatings obtained by the one-step procedure, we observed that for the SiO<sub>2</sub>/S10 coatings, all the compositions permitted the obtainment of coatings with CA >140°. On the other hand, the best ratios assessed for ZrO<sub>2</sub>/S10 coatings were 30/70 or 50/50, with CA>130°. The hybrid coatings prepared by the one step procedure and containing titania networks where not prepared. Anyway, since all the formulations prepared were hydrophobic, even at the lower percentage of polymer, the determination of the best component ratio was based on the results of some preliminary resistance tests. In Figure 7-1a, the results of the preliminary resistance test involving SiO<sub>2</sub>/S10 coatings and TiO<sub>2</sub>/S10 coatings, prepared with the two-steps procedure, are illustrated. The test consisted in the immersion for 7 days of the coated samples in water at 323 K. The only resistant coating was the SiO<sub>2</sub>/S10-20/80\_2; all the other coatings (i.e., coatings containing the TiO<sub>2</sub> sol gel network, and the SiO<sub>2</sub> network at 50 wt% or 30 wt%) degraded in short time. Hence, we excluded from further investigations these types of coatings, apart from the SiO<sub>2</sub>/S10-20/80 one. Figure 7-1b resumes the results of the preliminary resistance test involving the SiO<sub>2</sub>/S10

coatings prepared with the one-step procedure. In that case, all the coated samples remained hydrophobic at the end of the test; therefore, the three types of coatings, obtained by varying the organic/inorganic ratio, were employed for further experiments.

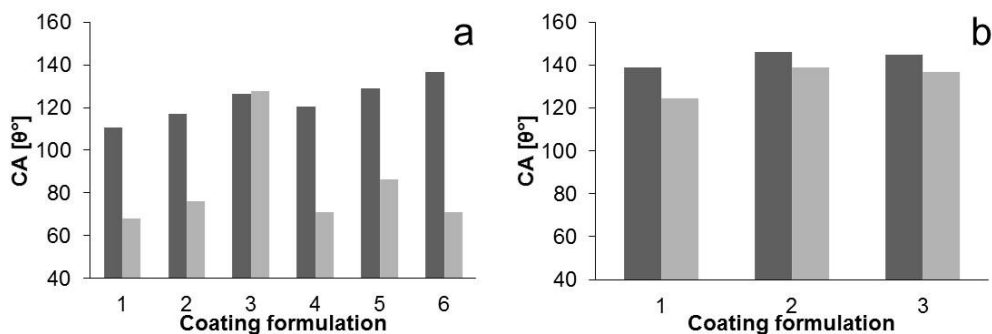


Figure 7-1. Coating resistance against erosion in water at 323 K: comparison between the starting CA (■) and the CA at the end of test (■). a) Hybrid coatings  $\text{SiO}_2/\text{S10}$  and  $\text{TiO}_2/\text{S10}$  prepared with the two-steps procedure: 1=  $\text{SiO}_2/\text{S10-50/50}_2$ ; 2=  $\text{SiO}_2/\text{S10-30/70}_2$ ; 3=  $\text{SiO}_2/\text{S10-20/80}_2$ ; 4=  $\text{TiO}_2/\text{S10-50/50}_2$ ; 5=  $\text{TiO}_2/\text{S10-30/70}_2$ ; 6=  $\text{TiO}_2/\text{S10-20/80}_2$ . b) Hybrid coatings  $\text{SiO}_2/\text{S10}$  prepared with the one step procedure: 1=  $\text{SiO}_2/\text{S10-50/50}_1$ ; 2=  $\text{SiO}_2/\text{S10-30/70}_1$ ; 3=  $\text{SiO}_2/\text{S10-20/80}_1$ .

Regarding the coatings containing the  $\text{ZrO}_2$  network, a preliminary test was performed only with the formulation  $\text{ZrO}_2/\text{S10-20/80}_2$ , which was the most hydrophobic. In 7 days the CA decrease was about the 20%, but the surface was still hydrophobic, therefore we proceed by preparing also the other typology of coatings with the one step procedure. The coatings prepared with the F10 polymer, maintained the same composition ratios selected for the hybrid

coatings containing S10. However, we excluded the combination with the TiO<sub>2</sub> network.

The second parameter considered in the optimization of the coating procedure, was the temperature and the time for the thermal treatment. In general, sol-gel inorganic coatings required heat treatments at temperature higher than 673 K, in order to get the desired properties in terms of hardness and strengthening. However, the organic-inorganic hybrid coatings cannot be heated at high temperatures, due to the possible thermal degradation of the polymeric part. For this reason, usually, the thermal treatment temperature does not exceed 473 K [78]. In order to get a sufficiently high temperature during the heat treatment stage, able to confer hardness to the inorganic part of the coating, without degrading the polymer, we operated this stage in 2 steps. The first heating step is similar to the heating treatment employed for PFPE coatings: samples were put in a static oven at 383K for 3 hours. In the second step, the temperature was raised at 473 K and the samples were kept for one more hour at that temperature in the oven. For the second heating step we explored the effect of different temperatures (from 673 K to 473 K), but we observed a loss in hydrophobicity for temperatures higher than 473 K. A longer time of heating for the second step did not bring, as well, improvements in the final CA value.

## 7.2 Characterization results

### 7.2.1 Morphology, composition and thickness

SEM analyses were performed with the aim to compare the coatings morphology of coatings prepared with the two-steps procedure and the one-step procedure. Moreover, we compared the surface features of coatings containing

the SiO<sub>2</sub> network with the ones of coatings containing the ZrO<sub>2</sub> network. Figure 7-2 illustrates the SEM images of some hybrid coatings prepared with Fluorolink® S10. The coating SiO<sub>2</sub>/S10-20/80\_2, prepared with the two steps procedure, appeared well distributed on the stainless steel substrate; the surface in fact was homogeneously coated and it was not possible to recognize the presence of uncoated spots of stainless steel. The coating looked like a black film, with white spots interspersed (Figure 7-2a); a further magnification in correspondence of the white spots, pointed out the presence of silica agglomerates (Figure 7-2b). Probably, a separation of the inorganic part from the organic one occurred during the preparation of the formulation, leading to the formation of silica crystals. The morphology and the texture of the coatings obtained by the one-step procedure were completely different from the ones observed on the coatings prepared in two-steps. Figure 7-2c-d correspond to the magnification of the coating SiO<sub>2</sub>/S10-30/70\_1. In that case, the black film was not recognizable, even if the coating was continuous on the substrate. The texture of the coating was composed by spheres of polymers connected each other (Figure 7-2c). A further magnification pointed out the presence of many overlapped layers of polymeric spheres, which probably incorporated the inorganic network. Moreover, we did not observe agglomerates of SiO<sub>2</sub> crystals. The SiO<sub>2</sub>/S10 coatings, either obtained from the two steps or the one step procedure, were microscopically cracks free. The appearance of the coating containing the ZrO<sub>2</sub> network was different from the coating containing SiO<sub>2</sub> networks. Figure 7-2e-f illustrate the magnification of the ZrO<sub>2</sub>/S10-30/70\_1 coating. Figure 7-2e highlights the presence of cracks on the surface of the coating; even if the stainless steel substrates was homogeneously coated. Thanks to a further magnification (Figure 7-2f), it was possible to recognize the same texture observed for coating SiO<sub>2</sub>/S10-30/70\_1; the polymer assumed a

spherical conformation, creating an overlapped structure which incorporated the inorganic part.

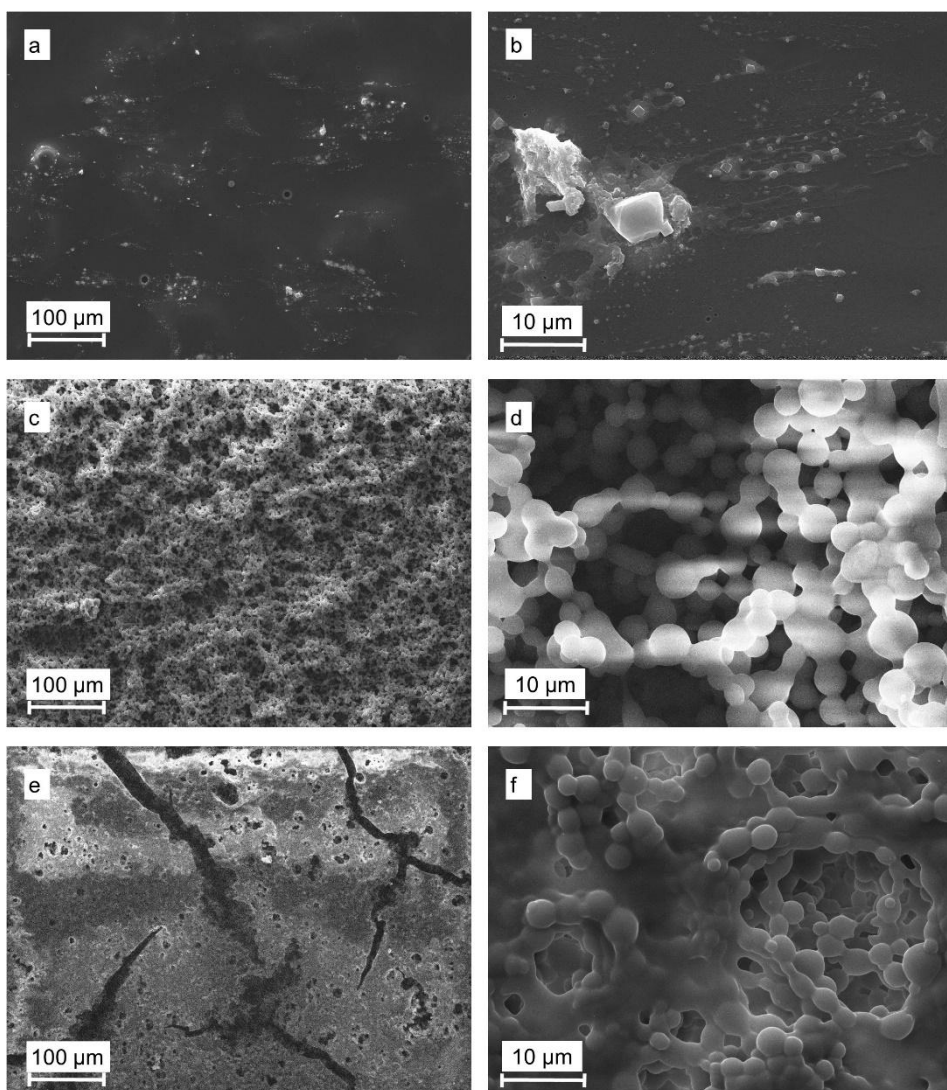


Figure 7-2. SEM images of hybrid coatings containing the polymer Fluorolink®S10. On the left magnification of 500X, on the right magnification of 2000X. Legend: SiO<sub>2</sub>/S10-20/80\_2 (a, b); SiO<sub>2</sub>/S10-30/70\_1 (c, d); ZrO<sub>2</sub>/S10-30/70\_1 (e, f).

Figure 7-3 regards the hybrid coatings containing Fluorolink<sup>®</sup>F10. In that case, the morphology changed in function of the inorganic network used. The SiO<sub>2</sub>/F10-20/80\_2 coating is shown in Figure 7-3a-b; the coating was not homogeneous, only a part of the substrate was covered by a dark layers of the polymer, having a texture very similar to the one observed on the simple F10 coating. The coating SiO<sub>2</sub>/F10-20/80\_1 (Figure 7-3 c-d), obtained with the one-step procedure, had a very similar morphology to the previous one. As observed for the simple F10 coating, even the hybrid coatings containing F10 are not perfectly continuous on the stainless steel surface; some uncoated spots of the stainless steel surface can be observed in both Figure 7-3a and Figure 7-3c. The appearance of the ZrO<sub>2</sub>/F10-20/80\_1 is instead quite different (Figure 7-3e-f). The coating was not homogeneous as well, but was continuous on the stainless steel surface. We observed the presence of emerging structures with a white colour (Figure 7-3e). A further magnification (Figure 7-3f) pointed out that these structures were not composed by separated crystals of ZrO<sub>2</sub>, but rather were formed by a polymeric structure incorporating the inorganic component (Figure 7-3fa).

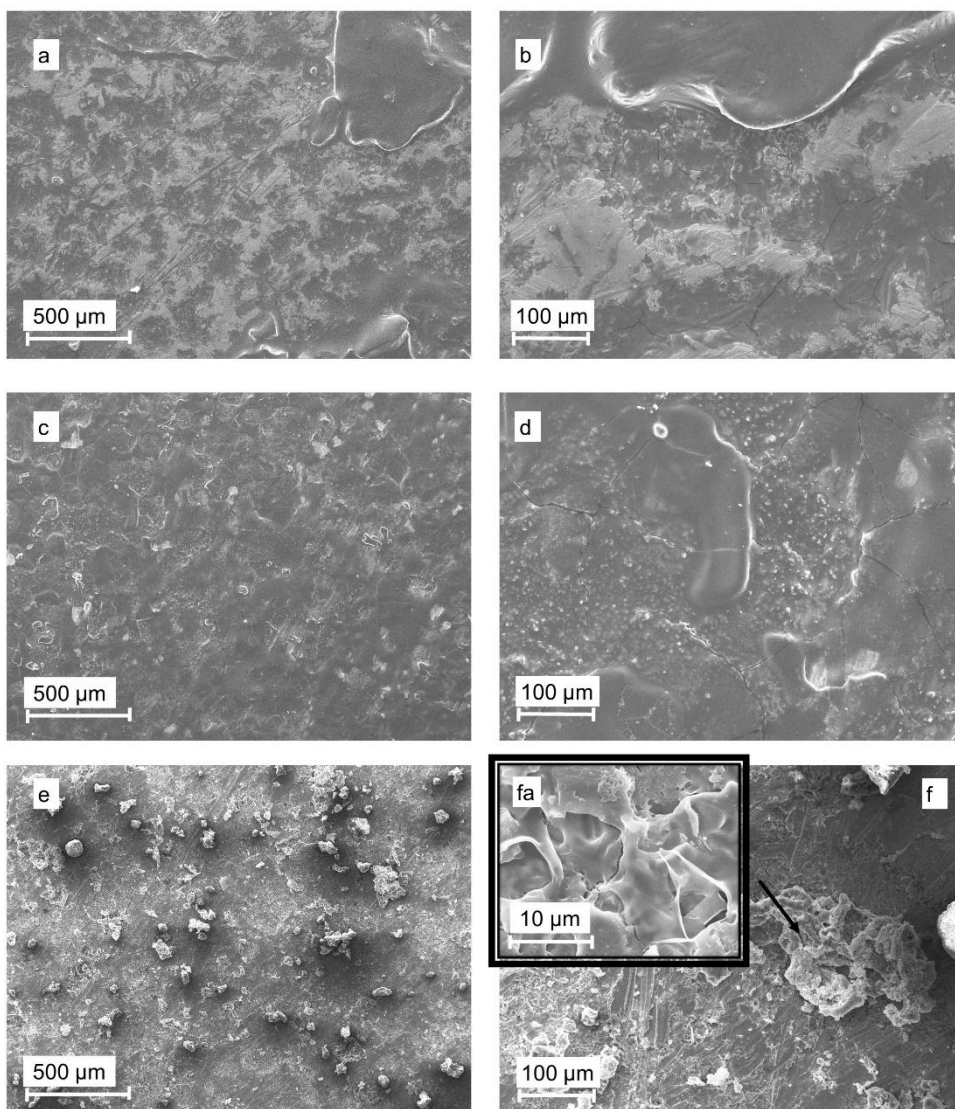


Figure 7-3. SEM images of hybrid coatings containing the polymer Fluorolink®F10. On the left, magnification of 50X, on the right magnification of 200X, in the framed picture magnification of 2000X. Legend:  $\text{SiO}_2/\text{F10-20/80}_2$  (a, b);  $\text{SiO}_2/\text{F10-20/80}_1$  (c, d);  $\text{ZrO}_2/\text{F10-20/80}_1$  (e, f).

The XPS analyses showed the surface composition of the hybrid coatings. One more time, we decided to focus our attention on the differences between the coatings prepared by the two-steps procedure and the one-step procedure. For this reason, the XPS analyses were performed on the following coatings: SiO<sub>2</sub>/S10-20/80\_2 and SiO<sub>2</sub>/S10-30/70\_1, ZrO<sub>2</sub>/S10-20/80\_2 and ZrO<sub>2</sub>/S10-30/70\_1, SiO<sub>2</sub>/F10-20/80\_2 and SiO<sub>2</sub>/F10-20/80\_1.

The coatings containing the SiO<sub>2</sub> network had a very similar composition, independently from the type of preparation method (consider Table 7-2). In both of them F (depending from the PFPE) and Si (deriving both from the inorganic network and the functional ending groups of the polymer) were detected. The atomic ratio F/C was 1.5 in the SiO<sub>2</sub>/S10-20/80\_2 coating, and 1.3 in the SiO<sub>2</sub>/S10-30/70\_1 coating. The weight content in polymer, in fact, was higher for the coating prepared in two steps (80 wt%) in respect to the coating prepared with the one-step procedure (70 wt%). Accordingly, the atomic ratio Si/C was 0.12 in the SiO<sub>2</sub>/S10-20/80\_2 coating, and 0.18 in the SiO<sub>2</sub>/S10-30/70\_1. Likewise, the atomic composition of the hybrid coatings containing the ZrO<sub>2</sub> network and the polymer S10 were very similar each other, even if two different preparation procedures were employed. As previously observed, the atomic ratio Zr/C was higher for the ZrO<sub>2</sub>/S10-30/70\_1 coating (0.23 *vs* 0.15). On the other hand, the ratio F/C was slightly higher for the ZrO<sub>2</sub>/S10-20/80\_2 coating, since the content of polymer was higher (1.6 *vs* 1.5).



Table 7-2. Relative atomic abundance (%) of the hybrid coatings containing the polymer Fluorolink®S10 and the inorganic network of SiO<sub>2</sub> or ZrO<sub>2</sub>, prepared with the two-steps or the one-step procedure.

Coating type	Elements [at. %]					
	C	F	O	Si	N	Zr
SiO <sub>2</sub> /S10-20/80_2	30.1	45.2	19.5	3.5	1.7	-
SiO <sub>2</sub> /S10-30/70_1	30.3	39.9	22.6	5.7	1.5	-
ZrO <sub>2</sub> /S10-20/80_2	25.3	40.0	28.8	2.1	-	3.8
ZrO <sub>2</sub> /S10-30/70_1	26	40.2	28	-	-	5.8

The high resolution analyses, performed in the bonds region of Si 1s and Zr 3d, pointed out some differences between the structures of the hybrid coatings prepared with the two steps or the one step procedure. Moreover, these analyses revealed the effective interaction of the polymeric part with the inorganic one in the hybrid coatings.

The Si 2p singlet had a complex shape in both SiO<sub>2</sub>/S10-20/80\_2 and SiO<sub>2</sub>/S10-30/70\_1 coatings (respectively Figure 7-4a, and Figure 7-4b). Three different Si species were thus identified in both the spectra; the Gaussian curve named A (at 102.3 eV) corresponds to a silane species, therefore we suppose is related to the presence of unreacted TEOS in the coating. The second peak, named B, at B.E.=103.8 eV is typical of the Si(IV) oxide, hence corresponds to the silica (SiO<sub>2</sub>) generated by the hydrolysis and condensation of TEOS in sol-gel

synthesis [75]. The last peak (C), at 105.4 eV, is shifted toward very high binding energy values, and is due to the interaction of the Si species with fluorine [79]. Thanks to these experimental evidences, we can assume an interaction between the fluorinated organic part of the coating and the inorganic SiO<sub>2</sub> network; however is not possible to ensure the formation of strong covalent bonds, indeed, probably, only weak interactions were formed. It is interesting to point out that the intensity of the peak A in the coating prepared with the one step procedure (SiO<sub>2</sub>/S10-30/70\_1; Figure 7-4b) was lower in respect to the one observed in the coating prepared in two-steps (Figure 7-4a). Hence, the hydrolysis of the organometallic precursor, and the consequent formation of the inorganic SiO<sub>2</sub> network, is more complete in the one-step procedure. In fact, the peak B, corresponding to the SiO<sub>2</sub> species, is more intense for SiO<sub>2</sub>/S10-30/70\_1 coating. The Zr 3d doublets were very similar between ZrO<sub>2</sub>/S10-20/80\_2 and ZrO<sub>2</sub>/S10-30/70\_1 coatings (Figure 7-4c-d). In that case, we can suppose that the coatings obtained by the two steps procedure were almost identical in terms of composition. Figure 7-4c is the high resolution spectra of Zr 3d of the ZrO<sub>2</sub>/S10-20/80\_2 coating; the peaks named A and C (B.E. = 182.5 eV and 184.9 eV respectively) correspond to the Zr (IV) in the oxide [75]; these peaks represent the ZrO<sub>2</sub> sol-gel network. The peaks B and D fall at higher B.E. (183.7 eV and 186 eV respectively), and confirmed the interaction between the Zr species with a more electronegative atom, i.e., fluorine [76]. The peaks highlighted in Figure 7-4d, referring to the ZrO<sub>2</sub>/S10-30/70\_1 coating, can be interpret in the same way, since the corresponding B.E. values are very similar to the ones observed in Figure 7-4c (A= 182.8 eV, B= 183.9, C= 185.2; D=186.4).

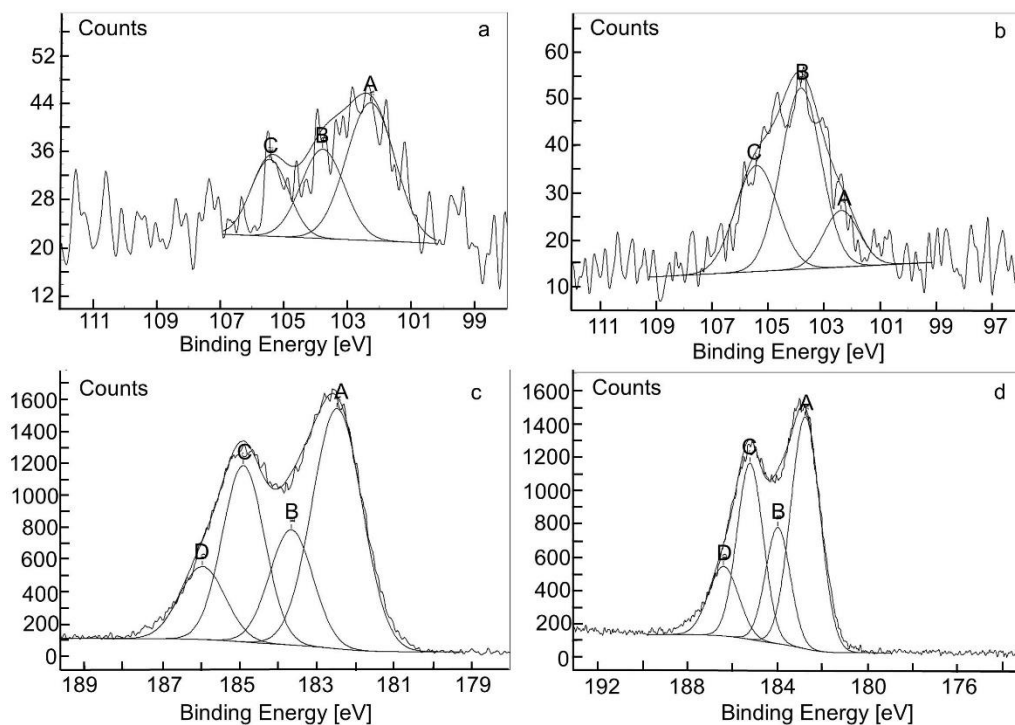


Figure 7-4. XPS high resolution spectra of Si 2p singlet (a, b) and Zr 3d doublet (c, d) of hybrid coatings containing Fluorolink®S10. SiO<sub>2</sub>/S10-20/80\_2 (a); SiO<sub>2</sub>/S10-30/70\_1 (b); ZrO<sub>2</sub>/S10-20/80\_2 (c); ZrO<sub>2</sub>/S10-30/70\_1 (d).

The results of XPS analyses involving hybrid coatings containing Fluorolink®F10 are illustrated in Table 7-3 (atomic composition). The atomic abundance of Si in both coatings containing the silica network was very low if compared with the corresponding coating containing S10. The atomic ratio Si/C was in fact 0.02 for SiO<sub>2</sub>/F10-20/80\_2 and 0.01 for SiO<sub>2</sub>/F10-20/80\_1. On the other hand, the atomic ratios F/C were very similar to the ones measured in the hybrid coatings containing S10 in the same weight proportion (1.7 and 1.8).

Table 7-3. Relative atomic abundance (%) of the hybrid coatings containing the polymer Fluorolink®F10, and the organic network of SiO<sub>2</sub> or ZrO<sub>2</sub>, prepared with the two-steps or the one-step procedure.

<b>Elements [at. %]</b>					
<b>Coating type</b>	<b>C</b>	<b>F</b>	<b>O</b>	<b>Si</b>	<b>Zr</b>
SiO <sub>2</sub> /F10-20/80_2	30.3	51.1	18.0	0.6	-
SiO <sub>2</sub> /F10-20/80_1	28.0	51.4	20.2	0.4	-

The profilometry analyses were performed only on some types of coatings; in that case, we decided to focus the attention on the difference between the SiO<sub>2</sub>/S10-20/80\_2 coating and the SiO<sub>2</sub>/S10-20/80\_1 coating. These two types of coatings, in fact, emerged as the most promising ones for possible application in fouling mitigation in heat exchangers. Table 7-4 sums up the profilometry results. The coatings were deposited on half a part of plain stainless steel sample and the thickness was measured in cross section.

Table 7-4. Profilometry results for the SiO<sub>2</sub>/S10-20/80\_2 and SiO<sub>2</sub>/S10-20/80\_1 hybrid coating deposited on stainless steel plain samples.

<b>Coating</b>	<b>Average thickness [μm]</b>	<b>Min and max thickness [μm]</b>	<b>Ra [μm]</b>	<b>Ra increment [μm]</b>
SiO <sub>2</sub> /S10-20/80_2	9.4	8.1-10.6	0.717	0.224
SiO <sub>2</sub> /S10-20/80_1	7.3	6-9.3	1.585	0.527

The average thickness of the hybrid coating prepared with the two-steps procedure was ~9 μm; the coating obtained with the one-step procedure had an average thickness of 7 μm. In general, the hybrid coatings were thicker in respect to the simple PFPE coatings (thickness of about 5 μm); however, in comparison with the multilayer coatings (thickness about 25 μm), the thickness was extremely reduced. Is not possible to exclude the insulator effect of the hybrid coatings when deposited on stainless steel surfaces; nevertheless, we can suppose that the negative effect could be negligible. Considering the increase in roughness related to the presence of the coatings, the SiO<sub>2</sub>/S10-20/80\_1 is responsible of a consistent increase of the roughness (>0.5 μm) when compared to the roughness of the uncoated part of the sample. This aspect could be particularly detrimental for application on fouling mitigation. On the contrary, the SiO<sub>2</sub>/S10-20/80\_2 coating provoked a restrained increase of roughness (~0.2 μm), comparable with the one determined by the simple PFPE coatings.

Profilometry analyses were not performed on hybrid coatings containing the  $ZrO_2$  network, in view of the results of resistance tests that will be discussed in the following section. However, the thickness was evaluated by cross-section SEM analyses on a  $ZrO_2$ /S10-30/70\_1 coated sample (Figure 7-5). The thickness measured on that sample was 53.3  $\mu m$ .

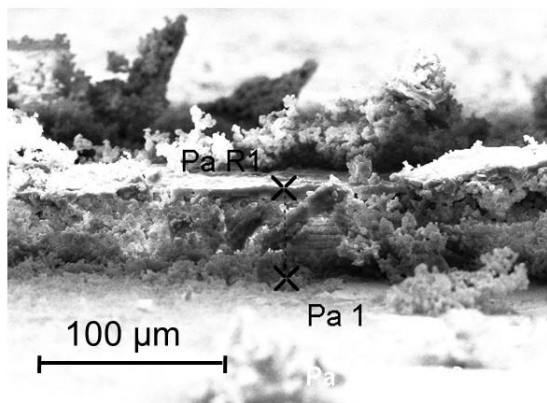


Figure 7-5. SEM magnification of a cut section of the coating  $ZrO_2$ /S10-30/70\_1, deposited on a stainless steel plain sample, for the determination of the coating thickness.

## 7.2.2 Hydrophobicity assessment

We investigated the wettability of the coatings prepared with the inorganic networks of  $SiO_2$  and  $ZrO_2$ , combined with the polymers S10 or F10. As it possible to observe from Table 7-5, not all the possible formulations were considered for the fully characterization with contact angle measurements; rather, we selected the coatings most interesting, in view of the results of the resistance tests.

Table 7-5. CA measurements of hybrid coatings containing the inorganic network based on SiO<sub>2</sub> or ZrO<sub>2</sub>, and the polymer Fluorolink®S10 or Fluorolink®F10.

Coating type	Static CA [θ°]	SFE [mN/m]	Advancing CA [θ°]	Receding CA [θ°]	Hysteresis
SiO <sub>2</sub> /S10-20/80_2	146 ± 0.8	7 ± 0.8	125	122	3
SiO <sub>2</sub> /S10-50/50_1	140 ± 3.8	7 ± 2.4	106	99	7
SiO <sub>2</sub> /S10-70/30_1	140 ± 6	8 ± 0.6	135	112	23
SiO <sub>2</sub> /S10-80/20_1	146 ± 0.8	2 ± 0.1	-	-	-
SiO <sub>2</sub> /F10-20/80_2	116 ± 2.8	16 ± 1.8	100	86	14
SiO <sub>2</sub> /F10-50/50_1	116 ± 4.4	12 ± 0.9	111	99	12
SiO <sub>2</sub> /F10-70/30_1	121 ± 1.9	12 ± 1.3	97	82	14
SiO <sub>2</sub> /F10-80/20_1	122 ± 1.8	10 ± 1.2	106	91	15

Coating type	Static CA [°]	SFE [mN/m]	Advancing CA [°]	Receding CA [°]	Hysteresis
ZrO <sub>2</sub> /S10-20/80_2	129 ± 0.9	9 ± 0.8	127	118	9
ZrO <sub>2</sub> /S10-50/50_1	131 ± 5.1	2 ± 0.5	138	132	6
ZrO <sub>2</sub> /S10-70/30_1	131 ± 4.6	4 ± 0.6	122	122	0
ZrO <sub>2</sub> /F10-80/20_1	111 ± 4.1	8 ± 1.9	122	118	4

The coating containing the SiO<sub>2</sub> network and the polymer S10, either prepared with the two-steps procedure or the one-step procedure, had water contact angles higher than 140° and very low contact angle hysteresis. The surface free energies were lower than 10 mN/m, confirming the very high hydrophobicity. The hysteresis of the SiO<sub>2</sub>/S10-80/20\_1 coating was not assessed, due to the impossibility to maintain the needle inside the water drop during the advancing CA measurements. The coatings containing the SiO<sub>2</sub> network and the polymer F10, had lower CA values (in the range 116°-122°), and surface free energies ranged from 10 mN/m to 16 mN/m. The hysteresis, however, were still low, indicating a probable interaction of water with the coated surface in accordance with the Cassie-Baxter model. The coatings containing the ZrO<sub>2</sub> network and the polymer S10, had a contact angle of about 130° and very low surface



energies ( $>10$  mN/m) and CA hysteresis. On the other hand, the ZrO<sub>2</sub>/F10-80/20\_1 coating, containing the polymer F10, had a CA value of 111°; however, surface free energy and CA hysteresis were low and comparable with the ones of the coatings containing the polymer S10.

### 7.3 Coatings resistance against erosion

The resistance tests, involving the hybrid coatings lasted for 30 days, instead of 7 days. Prolonging the duration of the resistance tests, we could assess the long term stability of these coatings when immersed in aggressive liquid environments. In respect to the other typologies of coatings, in fact, the hybrid coatings showed the best properties in terms of chemical and mechanical stability. We investigated the erosive effect of hydrochloric acid solutions, disinfectant solutions containing chloramines and water at temperature of 343 K. Some tests in alkaline environments were also performed, however the samples were highly damaged by the NaOH solutions, probably because of hydrolysis reactions which compromised the adhesion of the coatings on the stainless steel substrates. At last, we observed the effect of mechanical stresses induced by water flowing upon the coated surface; the flowrate imposed for these shear stress tests was 0.17 m/s, while the water temperature was 323 K. The results presented in this section correspond to the best result obtained. However, for each coating, at least two repetition of the same test were performed, until a good reproducibility of the data was obtained (difference in the final CA  $\pm 10^\circ$ ).

Figure 7-6 illustrates the results of resistance tests involving the SiO<sub>2</sub>/S10 coatings. Regarding the hybrid coatings prepared with the two-steps procedure, only the formulation named SiO<sub>2</sub>/S10-20/80\_2 (component ratio: 20/80-

inorganic precursor/S10) was considered, since the other formulations appeared scarcely resistant in the preliminary tests, previously discussed. On the other hand, all the coatings prepared with the one-step procedure, at the different component ratios, were investigated.

Acidic solutions degraded mostly the hybrid coatings characterized by the low content of polymer. In 30 days the SiO<sub>2</sub>/S10-50/50\_1 coated samples turned to be hydrophilic, while the CA of the SiO<sub>2</sub>/S10-30/70\_1 coated samples decreased of the 21%. On the other hand, coatings characterized by the higher content of polymer were highly resistant, in 30 days the CA decrease was about the 10%, and the final contact angles were still higher than 120° (Figure 7-6a). The SiO<sub>2</sub>/S10-50/50\_1 coating was low resistant even against disinfectant solutions (Figure 7-6b) The other coatings, instead, were only slightly eroded by chloramines; in particular the SiO<sub>2</sub>/S10-20/80\_1 and the SiO<sub>2</sub>/S10-30/70\_1 coatings maintained almost unaltered their initial value of CA (the final CA decrease was lower than 5%). Similar results were obtained also after immersion in water at 343 K (;Figure 7-6c). The only type of coating damaged by water was the one at the lower content of S10 (SiO<sub>2</sub>/S10-50/50\_1). Specifically, the coating prepared with the two-steps procedure had a contact angle decrease of the 11%, and the final CA value was 138°, thus, the surface was still highly hydrophobic after immersion for 30 days in water at high temperature. The coatings obtained by the one-step procedure were even more resistant, the CA decrease was in fact the 7-9% and the final CA values were always higher than 130°. Thanks to the presence of the inorganic network, all the hybrid coatings were highly resistant against shear stresses, as it possible to observe in Figure 7-6d. However, the most performing coatings were still the ones with the higher content of polymer (number 1 and 4 in the Figure 7-6d).

The contact angle decrease for SiO<sub>2</sub>/S10-20/80\_2 coating was the 5%, and for the SiO<sub>2</sub>/S10-20/80\_1 coating the 12%; the CA measured at the end of the test were about 130°.

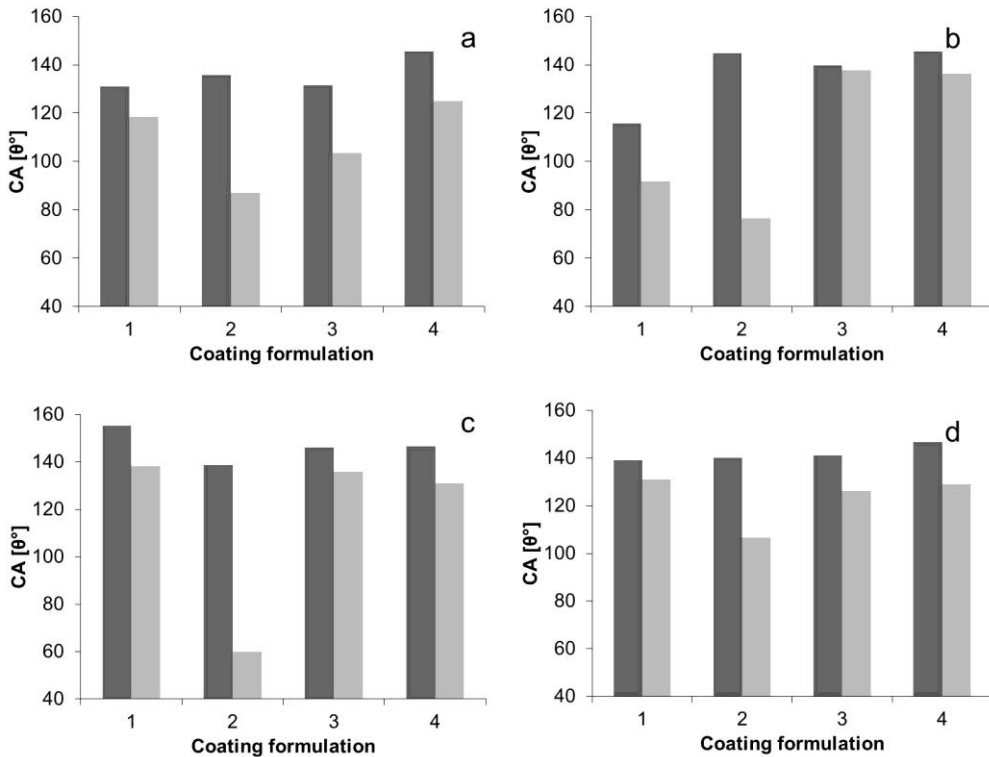


Figure 7-6. Coating resistance against erosion in liquid environments: comparison between the starting CA (■) and the CA at the end of the test (■). Coatings: 1= SiO<sub>2</sub>/S10-20/80\_2; 2= SiO<sub>2</sub>/S10-50/50\_1; 3= SiO<sub>2</sub>/S10-30/70\_1; 4= SiO<sub>2</sub>/S10-20/80\_1. Legend: a) HCl, pH=2, 323 K; b) NH<sub>2</sub>Cl-NHCl<sub>2</sub>, pH=7, 323 K; c) water at 343 K; d) water flux, 0.17 m/s, 323 K.

Figure 7-7 compares the degradation trend of the CA values of coatings SiO<sub>2</sub>/S10-20/80\_2 and SiO<sub>2</sub>/S10-20/80\_1, in all the aggressive conditions adopted for these tests. Interestingly, we observed that the most aggressive

environment for both the coatings was represented by the hydrochloric acid solution (Figure 7-7a-c). Moreover, in all the aggressive liquids, the erosion mainly occurred within 120 hours of test (5 days). The linear trend observable in Figure 7-7 confirmed the long-term stability of these coatings, even when exposed to very aggressive liquid environments.

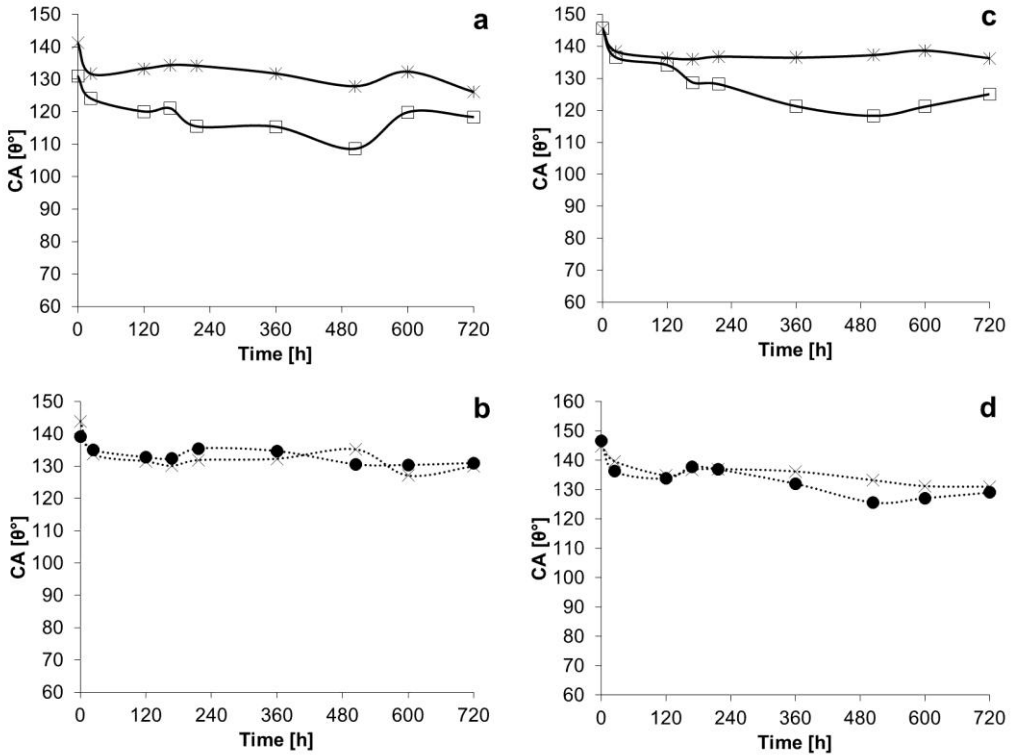


Figure 7-7. Trend of CA decrease during resistance tests. Coatings: SiO<sub>2</sub>/S10-20/80\_2 (a, b); SiO<sub>2</sub>/S10-20/80\_1 (c, d). Legend: \* = NH<sub>2</sub>Cl/NHCl<sub>2</sub> solution, T= 323 K; □ = HCl solution, T=323 K; \*·\* = water, T=323 K; ·●· = water flux, T=343 K, flowrate=0.17 m/s.

Coatings prepared with the SiO<sub>2</sub> sol-gel network and the polymer F10 appeared resistant to all the aggressive liquid environments selected for the resistance

tests, however the CA measured at the end of the test were very low (90-100°). Figure 7-8 resumes the results obtained. Regarding the erosion due to exposition to acidic solution (Figure 7-8a), the most resistant coatings were the ones prepared with the one-step procedure, in particular SiO<sub>2</sub>/F10-20/80\_1 and SiO<sub>2</sub>/F10-30/70\_1. The CA decrease was in general the 10%, and the final CA value was about 110°. On the other hand, the SiO<sub>2</sub>/F10-20/80\_2 coatings were progressively eroded by the acid, and at the 21<sup>st</sup> day of immersion, the surface was hydrophilic. After immersion in a chloramines solution for 30 days, all the hybrid coatings here considered had CA values comprised between 90° and 105°, therefore they were still hydrophobic. However the CA decrease ranged from the 10% to the 25% (consider Figure 7-8b). Water at 343 K was the less aggressive environment; after 30 days of immersion, the coatings were still hydrophobic, with contact angle values ranging from 105° to 115°. The most resistant coatings were the SiO<sub>2</sub>/F10-30/70\_1 and SiO<sub>2</sub>/F10-20/80\_1, with a final CA decrease of 4% and 10% respectively. The CA decrease of the samples coated by SiO<sub>2</sub>/F10-20/80\_2, on the contrary, was the 22%. Concerning the resistance against shear stresses (Figure 7-8d), all the coatings prepared remained hydrophobic at the end of the test. In general the CA decrease ranged from 15% to 20%, and the final contact angle values were about 95°. These results surely proved an improvement of the mechanical resistance of the hybrid F10 coatings in respect to the simple F10 coatings (the final degradation of the coating was similar, but occurred in 7 days instead of 30 days of test). However, we could not observe the same great improvement in mechanical resistance observed in the hybrid coating containing S10. These results can be explained considering the results of SEM and XPS analyses, which pointed out a scarce continuity of the F10 hybrid coatings on the stainless steel substrate,

and even a very low content of the inorganic phase (Si), which is the main responsible of the increase of the mechanical stability of the hybrid coatings.

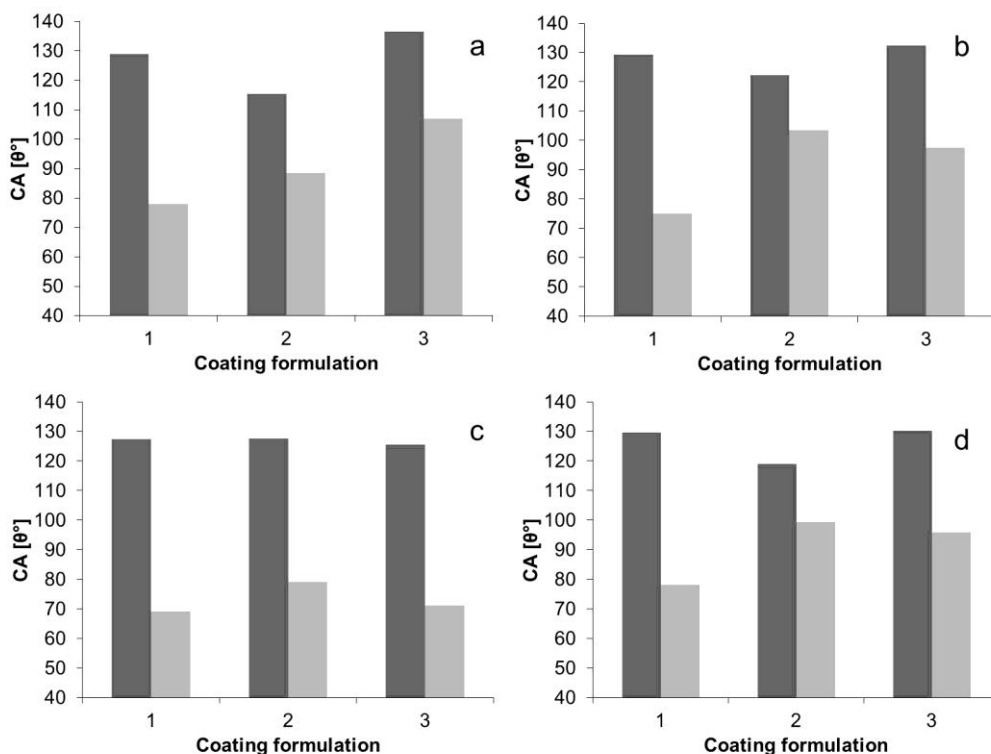


Figure 7-8. Coating resistance against erosion in liquid environments: comparison between the starting CA (■) and the CA at the end of the test (■). Coatings: 1= SiO<sub>2</sub>/F10-20/80\_2; 2= SiO<sub>2</sub>/F10-50/50\_1; 3= SiO<sub>2</sub>/F10-30/70\_1; 4= SiO<sub>2</sub>/F10-20/80\_1. Legend: a) HCl, pH=2, 323 K; b) NH<sub>2</sub>Cl-NHCl<sub>2</sub>, pH=7, 323 K; c) water at 323 K; d) water flux, 0.17 m/s, 323 K.

In Figure 7-9 we compared the trend of CA decrease of the SiO<sub>2</sub>/F10-20/80\_2 coating with the SiO<sub>2</sub>/F10-20/80\_1 coating. For both the coatings, HCl and chloramines solutions were the most aggressive liquids. The HCl solution mostly eroded the SiO<sub>2</sub>/F10-20/80\_2 coating; within 500 hours of test the CA

value was  $<90^\circ$  (Figure 7-9a). On the other hand, the chloramines solution was more aggressive for SiO<sub>2</sub>/F10-20/80\_1 coating, and in the last 5 days of immersion in the disinfectant solution, we observed a consistent decrease (20%) of the CA value (Figure 7-9c). Regarding the exposition to water at high temperature, the CA only slightly decreased for both the types of coatings, (Figure 7-9 b-d), confirming a long term stability of these hybrid coatings when exposed to high temperature liquids. The erosion due to shear stresses mainly occurred within 10 days of exposition to the water flow for both the coated samples; the final CA decrease was the 12% for SiO<sub>2</sub>/F10-20/80\_2 coating, and the 23% for SiO<sub>2</sub>/F10-20/80\_1.

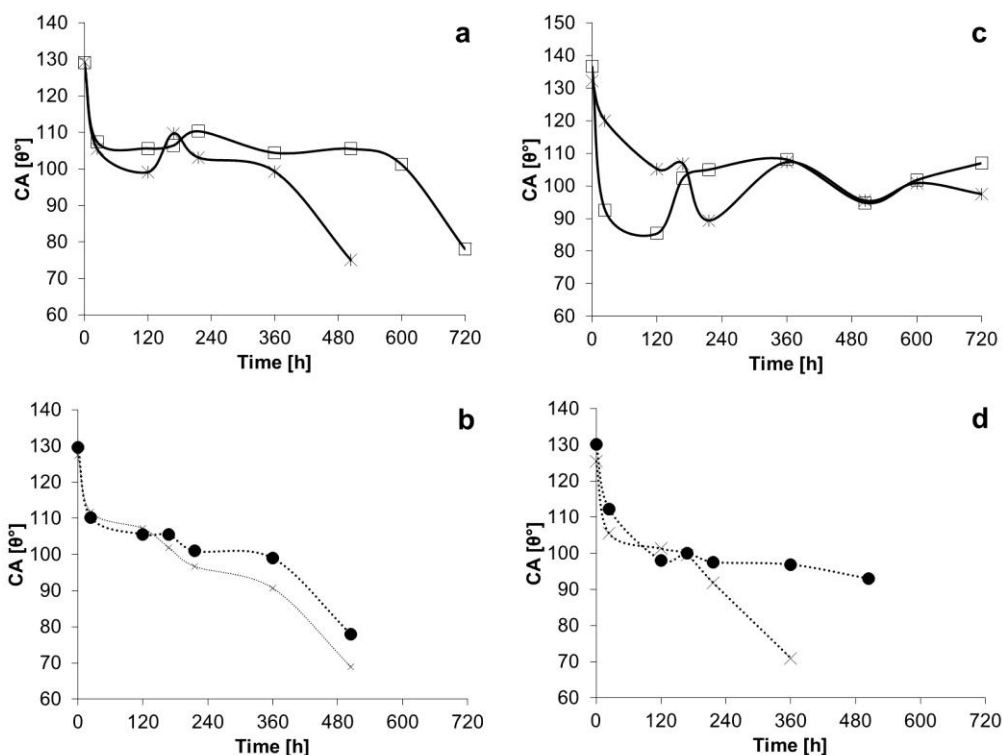


Figure 7-9. Trend of CA decrease during resistance tests. Coatings: SiO<sub>2</sub>/F10-20/80\_2 (a, b); SiO<sub>2</sub>/F10-20/80\_1 (c, d). Legend: \* = NH<sub>2</sub>Cl/NHCl<sub>2</sub> solution, T= 323 K; □ = HCl solution, T=323 K; ···x··· = water, T=343 K; ···●··· = water flux, T=323 K, flowrate=0.17 m/s.

The combination of silica network with the PFPE, permitted to increase the coating resistance against chemical or mechanical stresses, in respect to the simple PFPE coatings or the multilayer coatings prepared with metal oxides nanopowders. The best results were obtained by coatings composed by 20 wt% of inorganic component and 80 wt% of PFPE, either using the two-steps or the one-step procedure. Comparing the hybrid coatings containing S10 and F10, we can conclude that the resistance against chemical aggressive liquid environments was very similar in terms of CA decrease during a 30 days test.



However, the contact angle values measured at the end of the tests involving hybrid coatings containing F10 were at the borderline with hydrophilicity ( $\sim 90^\circ$ ). On the contrary, we observed a scarce increment of the mechanical resistance of the  $\text{SiO}_2/\text{F10}$  hybrid coatings, if compared with the  $\text{SiO}_2/\text{S10}$  hybrid coatings. The better performances of the  $\text{SiO}_2/\text{S10}$  hybrid coatings probably lies on the morphological homogeneity of these coatings, highlighted by SEM, and the better interspersions of the inorganic phase in the organic one observed by XPS analyses.

The combination of the  $\text{ZrO}_2$  network with the PFPE did not bring to the same interesting results obtained with the  $\text{SiO}_2$  network. We observed that, within 7 days of test, the coated samples were still hydrophobic, however, prolonging the tests duration until 20 or 30 days, the coatings were greatly eroded by the liquid environments. Figure 7-10 illustrates the results of resistance tests involving the  $\text{ZrO}_2/\text{S10}$  hybrid coatings. The  $\text{ZrO}_2/\text{S10-20/80}_2$  coating, prepared with the two-steps procedure, was resistant neither against aggressive chemical environments, nor water at high temperature or fluxed upon the surface. As it is possible to observe from Figure 7-11a-b, that the main degradation of the coating occurred from the 10<sup>th</sup> to the 20<sup>th</sup> day of test. The coatings prepared with the one-step procedure appeared more resistant, at least against chemical aggressive environments. After 30 days of immersion in the HCl solution (Figure 7-10a), the CA decrease was the 22% (final CA  $107^\circ$ ) for the  $\text{ZrO}_2/\text{S10-30/70}_1$  coating. On the other hand, the samples coated with the  $\text{ZrO}_2/\text{S10-50/50}_1$  coating were completely degraded within 15 days. Chloramines solution was less aggressive toward  $\text{ZrO}_2/\text{S10-50/50}_1$  coating; in 30 days, the CA decrease was the 15%. Regarding  $\text{ZrO}_2/\text{S10-30/70}_1$  coating, the CA decrease was the 26%. Even if after 30 days of immersion in the

chloramines solution the surfaces were still hydrophobic, the CA values measured at the end of the tests were about  $100^\circ$  (see Figure 7-10b). Water at high temperature was responsible of a complete deterioration of the hybrid coatings containing  $ZrO_2$  (Figure 7-10c). Observing the trend of CA decrease in Figure 7-11d, the erosion started from the 10<sup>th</sup> immersion day and at the 20<sup>th</sup> day of test, the surfaces were hydrophilic. The exposition to a water flow, at a temperature of 323 K, did not provoke a complete erosion of the coatings (Figure 7-10d). The CA decrease for  $ZrO_2/S10-50/50_1$  coating was the 15%, and for the  $ZrO_2/S10-30/70_1$  was the 26%. Anyway, the final CA value was about  $95^\circ$ , attesting a scarce resistance even against shear stresses.

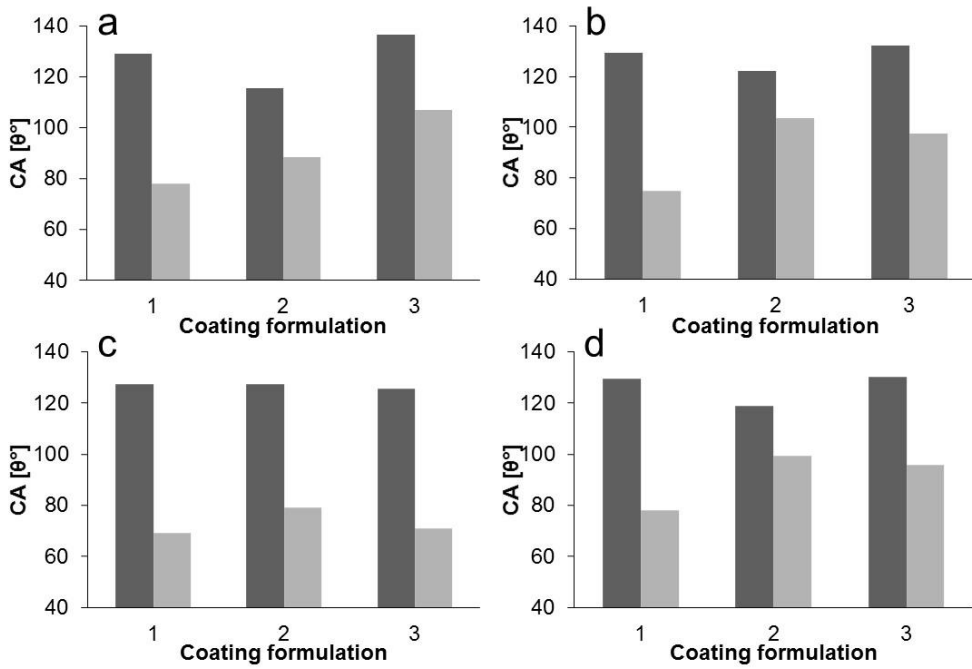


Figure 7-10. Coating resistance against erosion in liquid environments: comparison between the starting CA (■) and the CA at the end of the test (▒). Coatings: 1= ZrO<sub>2</sub>/S10-20/80\_2; 2= ZrO<sub>2</sub>/S10-50/50\_1; 3= ZrO<sub>2</sub>/S10-30/70\_1. Legend: a) HCl, pH=2, 323 K; b) NH<sub>2</sub>Cl-NHCl<sub>2</sub>, pH=7, 323 K; c) water at 343 K; d) water flux, 0.17 m/s, 323 K.

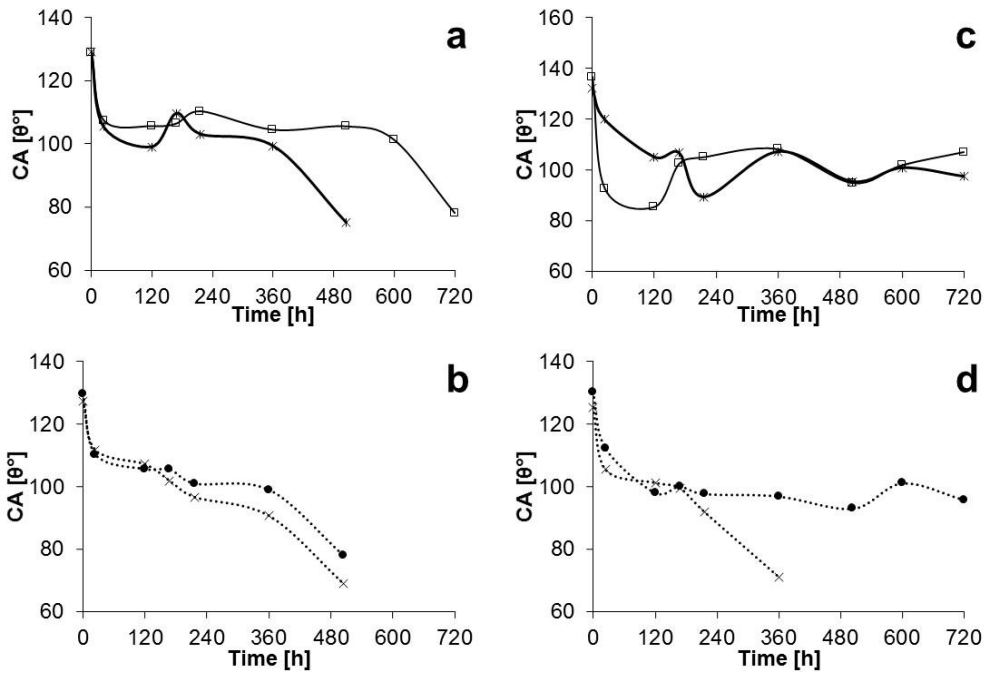


Figure 7-11. Trend of CA decrease during resistance tests. Coatings: ZrO<sub>2</sub>/S10-20/80\_2 (a, b); ZrO<sub>2</sub>/S10-30/70\_1 (c, d). Legend: \* = NH<sub>2</sub>Cl/NHCl<sub>2</sub> solution, T= 323 K; □ = HCl solution, T=323 K; × = water, T=323 K; ● = water flux, T=343 K, flowrate=0.17 m/s.

The low resistance of the ZrO<sub>2</sub>/S10 hybrid coatings can be mainly explained in function of the morphology characteristics observed by SEM analyses. The surfaces, in fact, appeared full of cracks at microscopic level.

The combination of the ZrO<sub>2</sub> sol-gel network with polymer F10 did not improve the resistance of the hybrid coatings. The exposition to all the aggressive liquid environments was responsible of a progressive deterioration of the coatings and a consequent restoration of the initial wettability of the stainless steel substrates. As an example, the resistance tests results of the coating ZrO<sub>2</sub>/F10-20/80\_1 are reported in Figure 7-12.

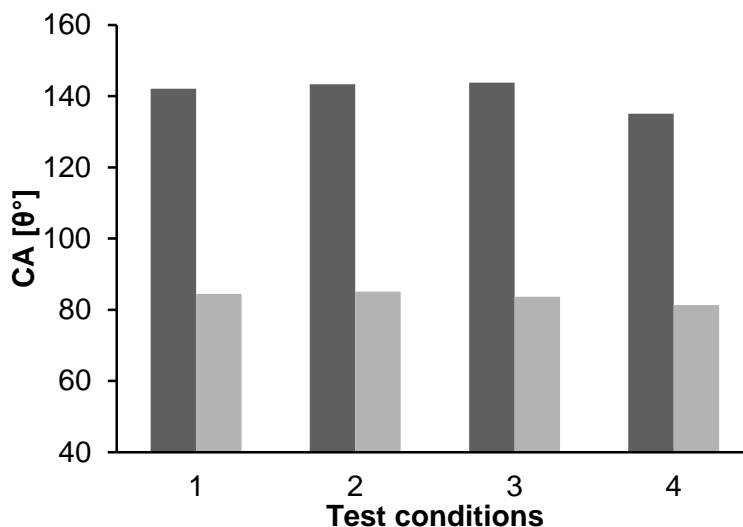


Figure 7-12. Coating resistance against erosion in liquid environments: comparison between the starting CA (■) and the CA at the end of the test (■). Coating:  $\text{ZrO}_2/\text{F10-20/80}_1$ . Test conditions: 1= water flux, 0.17 m/s, 323 K; 2= water, 323 K; 3= HCl, pH=2, 323 K; 4=  $\text{NH}_2\text{Cl-NHCl}_2$ , pH=7, 323 K.

The hybrid coatings containing the  $\text{SiO}_2$  sol-gel network and the polymer S10 emerged as the most resistant ones, in respect to the other typology of hybrid coatings prepared during this PhD research. In particular, the  $\text{SiO}_2/\text{S10-20/80}_2$  and the  $\text{SiO}_2/\text{S10-20/80}_1$  formulations showed the best results in terms of resistance against chemical stresses and mechanical stresses. Hence, further resistance tests were performed, involving these two types of coatings, by exposition to synthetic seawater, which is in particular detrimental for PFPE coatings. The samples were immersed in the synthetic seawater solution, heated at 323 K, for a period of 30 days. Figure 7-13 highlights the good resistance of the coating  $\text{SiO}_2/\text{S10-20/80}_1$  against seawater erosion. After 30 days, the

SiO<sub>2</sub>/S10-20/80\_1 coated samples were still hydrophobic and the CA decrease was the 18% (the final CA value was about 110°). On the other hand, the sample coated by SiO<sub>2</sub>/S10-20/80\_2 turned to be hydrophilic in 30 days of immersion. Considering the Figure 7-14, it is possible to observe that the erosion of both the coatings occurred mainly after 20 days of immersion in the synthetic seawater solution. Nevertheless, after 30 days of immersion the SiO<sub>2</sub>/S10-20/80\_1 coated sample was still hydrophobic. However, we cannot exclude a possible complete deterioration of the coating for longer exposure to this extremely aggressive environments, observing the progressive trend of decrease of the CA value.

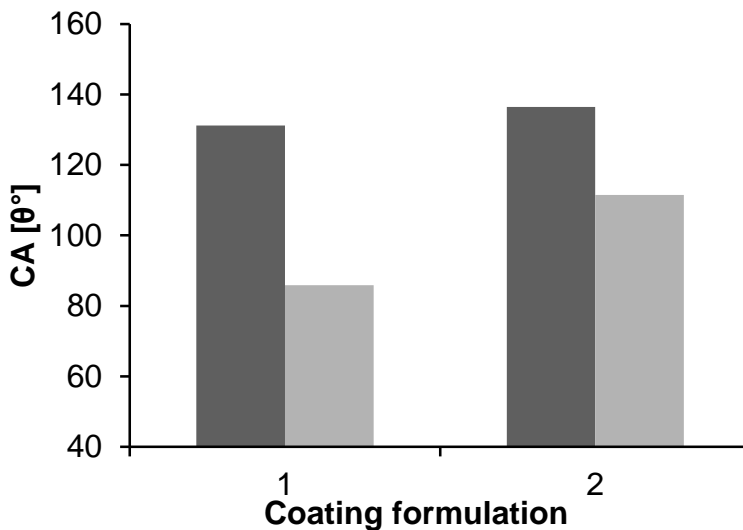


Figure 7-13. Coating resistance against erosion due to synthetic seawater: comparison between the starting CA (■) and the CA at the end of the test (■). Coating: 1= SiO<sub>2</sub>/S10-20/80\_2; 2= SiO<sub>2</sub>/S10-20/80\_1.

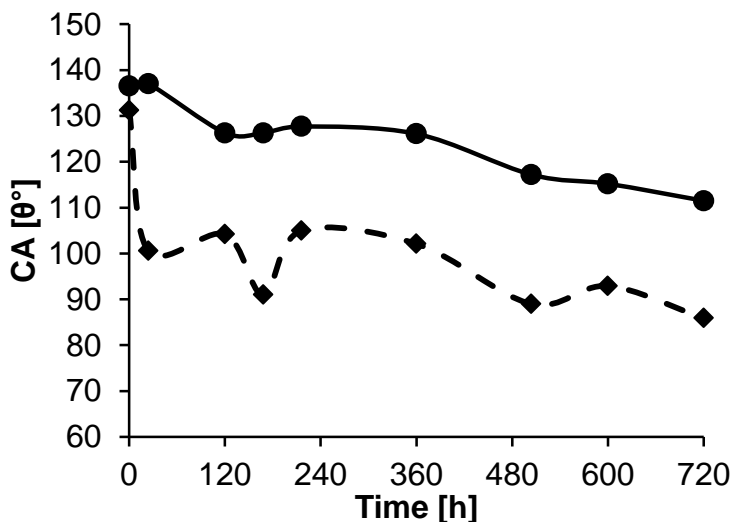


Figure 7-14. Trend of CA decrease during immersion in synthetic seawater. Legend:  $\blacklozenge$  SiO<sub>2</sub>/S10-20/80\_2 coating;  $\bullet$  SiO<sub>2</sub>/S10-20/80\_1 coating.

The results obtained from the seawater test confirmed once more the possibility to greatly improve the chemical and mechanical stability of the PFPE coatings, by combining them with inorganic compounds. The reinforcement obtained by the preparation of hybrid coating was the most effective one. The formulation named SiO<sub>2</sub>/S10-20/80\_1, prepared by the one-step procedure and containing 20 wt% of inorganic precursor and 80 wt% of S10, permitted to obtain very resistant coatings on stainless steel substrates. From the results of resistance tests, we can suppose a possible utilization of the hybrid coatings in heat exchangers working in mild conditions, for example sweet water at 323 K, supposing even a long term durability of the coatings.

## 7.4 Particulate fouling mitigation

Tubes samples for particulate fouling tests were coated using the formulations SiO<sub>2</sub>/S10-20/80\_2 and SiO<sub>2</sub>/S10-20/80\_1. These two hybrid coatings, in fact, demonstrated to have the higher stability when immersed in aggressive liquids, even at high temperature, or exposed to shear stresses. Some parameters of the particulate fouling tests were modified in respect to the conditions adopted with the PFPE or multilayer coatings. The flowrate was increased in the range 0.15-0.16 m/s (vs 0.05 m/s in the previous tests), with the aim to increase the shear stresses across the coated surfaces, and observe the fouling mitigation ability of the hybrid coatings in more drastic conditions. Since the flowrate was increased, we had to prolong the duration of the tests in order to observe the formation of foulant deposits. In fact, the high shear stresses contributed to a continuous removal of the particles settled by gravity on the internal surface of the tubes. For this reason, the tests lasted for 240-1032 hours (from 10 to 42 days).

The fouling grade on the SiO<sub>2</sub>/S10-20/80\_2 coated tube, after 120 hours of test, was higher in respect to the one measured on the uncoated tube sample, as Table 7-6 highlights. However, after 240 hours of test, the fouling value decreased of one order of magnitude (from  $3 \cdot 10^{-5}$  to  $2 \cdot 10^{-6}$ ), and was inferior to the one measured on the uncoated tube sample, exposed to fouling for the same period of time. We can assume that the fouling phenomenon on the uncoated surface is progressive, the more the surface was exposed to the CaSO<sub>4</sub> flow, the more it fouled. On the other hand, the hydrophobic surfaces permitted a continuous re-entrainment of the CaSO<sub>4</sub> particles, therefore, after 240 hours, the fouling grade was inferior in respect to the one measured 100 hours before. A similar phenomenon was observed with the SiO<sub>2</sub>/S10-20/80\_1 coating; the



fouling grade measured at 1032 hours of test was slightly inferior in respect to the value measured at 400 hours of test ( $1.8 \cdot 10^{-6}$  vs  $1.2 \cdot 10^{-6}$ ). Interestingly, before 400 hours of test it was not possible to detect the presence of foulant deposit on the SiO<sub>2</sub>/S10-20/80\_1 coated tube. After 1032 hours of test, the fouling grade measured on the SiO<sub>2</sub>/S10-20/80\_1 coated tube was one order of magnitude inferior than the fouling grade measured on the uncoated sample after 360 hours of test.

Table 7-6. CaSO<sub>4</sub> fouling deposits amounts, formed on uncoated tubes samples and on tubes samples coated with SiO<sub>2</sub>/S10-20/80\_2 and SiO<sub>2</sub>/S10-20/80\_1 hybrid coatings.

Coating type	Time [h]	Fluid velocity [m/s]	Fouling [mg/cm <sup>2</sup> h]
None	120	0.15	$6.9 \cdot 10^{-6}$
None	240	0.15	$1.2 \cdot 10^{-5}$
None	360	0.15	$5.5 \cdot 10^{-5}$
SiO <sub>2</sub> /S10-20/80_2	120	0.15	$2.7 \cdot 10^{-5}$
SiO <sub>2</sub> /S10-20/80_2	240	0.15	$1.8 \cdot 10^{-6}$
SiO <sub>2</sub> /S10-20/80_1	400	0.15	$1.8 \cdot 10^{-6}$
SiO <sub>2</sub> /S10-20/80_1	1032	0.16	$1.2 \cdot 10^{-6}$

At the end of the test, the SiO<sub>2</sub>/S10-20/80\_2 coated tube used in the 240 hours test and the SiO<sub>2</sub>/S10-20/80\_1 coated tube used in the 1032 hours test were cut,

in order to expose the internal surface of the tubes. The surfaces were washed with distilled water and characterized by CA measurements. We measured the static water contact angle with the circle fitting method, imposing a manual baseline with curve fitting. The average CA measured on the SiO<sub>2</sub>/S10-20/80\_2 coated sample (5 measurements by depositing the water drops on different areas of the sample) was 124°±4.6; the average CA of SiO<sub>2</sub>/S10-20/80\_1 was instead 128°±5.2 (see Figure 7-15). These results confirm the long term stability of these coatings even when they are exposed to liquids containing foulant particles, at relative high temperature (423 K) and responsible of consistent wall shear stresses (fluid velocity 0.15 m/s).

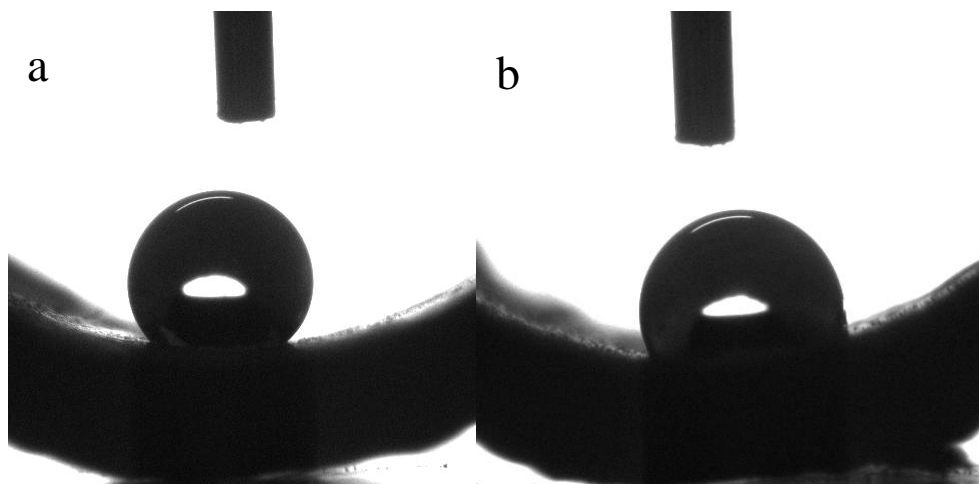


Figure 7-15. Photographs of the water droplet deposited on the internal surfaces of the tubes after the particulate fouling test. SiO<sub>2</sub>/S10-20/80\_1 (a); SiO<sub>2</sub>/S10-20/80\_2 (b).

## 7.5 Pilot plant experimentation

We selected the SiO<sub>2</sub>/S10-20/80\_1 formulation to coat the tubes bundle of the heat exchanger A in the pilot plant. The lay-out of the pilot plant is described at pp. 91-93 (lay-out II). The tube bundle and the shell (in aluminium) were new, and, before the coating deposition, they were rinsed with water and acetone. The amount of coating formulation prepared was 8 L; in order to get the total amount, we prepared smaller amounts of formulation (500 mL or 1 L) following the procedure described on pp. 57-59. Once 8 L of formulation were prepared, we collected the whole amount inside an appropriate tank; then the solution was mechanically stirred for several hours. Consequently, the tube bundle was dipped inside the solution, and kept immersed for 3 hours. Heat treatment consisted in 3 hours heating at the temperature of 383 K, and 1 hour heating at 473 K. The high temperatures of the heat treatment could be responsible of a thermal expansion of the metal constituting the tube bundle. The linear thermal expansion coefficient ( $\lambda$ ) of stainless steel AISI 316 is  $16 \cdot 10^{-6}$  m/mK. If a stainless steel tube (length 700 mm) is exposed to a thermal gradient of 85 K (I heating step) or 90 K (II heating step), the linear expansion of the metal corresponds to 0.1 mm, which is a negligible value. Moreover, the tube bundle designed for the pilot plant was equipped with a floating head, which permits the thermal expansion of the stainless steel tubes, without inducing mechanical stresses to the structure.

The pilot plant worked continuously for a period of 580 hours. The STHX A (coated) and STHX B (uncoated) operated in parallel at the same conditions (Table 7-7). The working conditions were mild, but the fluid velocity inside the tubes was slightly increased in respect to the other pilot plant experimentations, to increase the fluid turbulence. Anyway, we obtained a transient flow regime

in both the shell and tubes of the heat exchangers (flow regime in part laminar and in part turbulent). Due to technical impediments, related to the dimension of the plant and the energetic supply required, it was not possible to reach a turbulent flow regime in the tubes (Re number > 3000).

Table 7-7. Operating conditions of the pilot plant II used for the investigation of the fouling mitigation ability of the hybrid coating named SiO<sub>2</sub>/S10-20/80\_1

<b>Operating condition</b>	<b>Numerical value</b>
Shell inlet fluid temperature [K]	290-293
Tubes inlet fluid temperature [K]	312 -314
Shell inlet flowrate [kg/h]	108-120
Tubes inlet flowrate [kg/h]	720
Fluid velocity inside the shell [m/s]	0.03-0.04
Fluid velocity inside the tubes [m/s]	0.2
Re number in shell	1880-2092
Re number in tubes	2346

During the operation, the temperature values and the flowrates of the inlet and outlet fluids were collected at time intervals of one hour during the morning. The quantity of heat transferred ( $Q$ ), the overall heat transfer coefficient ( $U$ ) and

the fouling resistance  $R_f$ , were calculated as reported in Chapter 5, pp.143-144. The results, illustrated in Figure 7-16, Figure 7-17, and Figure 7-18 correspond to the average daily value. As observed in the previous pilot plant experimentations, the data collected are dispersed, due to variation of the temperatures and flowrates of the inlet fluids in the range specified in Table 7-7.

The average values of the quantity of heat transferred, daily, by the two heat exchangers, are shown in Figure 7-16. At the beginning of the experimentation, the  $Q$  values of STHX A and STHX B were very similar (8627 and 8418 kJ/h respectively). This first observation is very interesting, since we can suppose that the presence of the hybrid coating on the stainless steel surfaces did not alter the heat transfer capacity of the metal heat transfer surface. Within 200 hours of operation,  $Q$  remained almost identical between the two heat exchangers. After that time, the quantity of heat transferred began to decrease for both the heat exchangers, but the trend of decrease was different. In Figure 7-16 the  $Q$  values were interpolated in a linear equation; the slope of the resulting line has a value of -1.9 for the coated heat exchanger and -3.2 for the uncoated one.

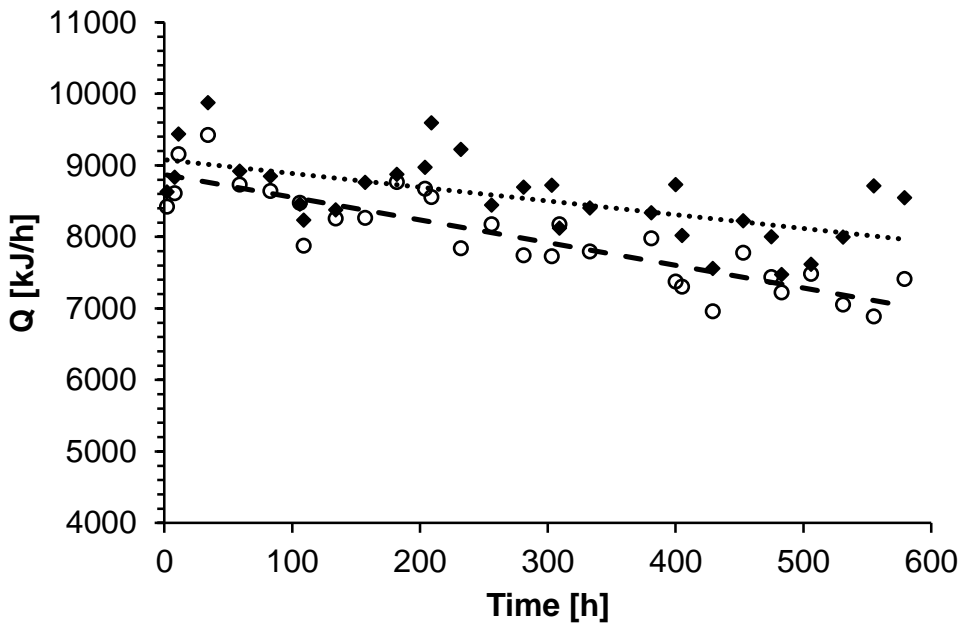


Figure 7-16. Quantity of heat transferred ( $Q$ ) vs time.  $\blacklozenge$  Heat exchanger coated by the hybrid  $\text{SiO}_2/\text{S10}$  formulation (STHX A);  $\circ$  Uncoated heat exchanger (STHX B); — linear trend STHX A; - - - - linear trend STHX B.

The differences between the heat transfer efficiency of the two heat exchangers can be observed also from Table 7-8, which highlights the average daily value of  $Q$  at 200, 400, 500 and 600 hours of operation. From 200 to 400 hours we observed a consistent decrease of  $Q$  for the uncoated heat exchanger, in fact the value diminished of about 1000 kJ/h. On the other hand, the value of the coated heat exchanger only slightly decreased ( $\Delta Q=240$  kJ/h) in that period of operation. After 400 hours of operation, until 500 hours, the  $Q$  value of the uncoated heat exchanger decreased more, but we observed a consistent decrease in the heat transfer ability also for the coated heat exchanger. The same decrease in  $Q$  values observed for STHX B after 200 hours of operation,

occurred for the STHX A, but after 400 hours of operation. Moreover, the quantity of heat transferred by the coated heat exchanger remained higher. In the last period (from 500 to 600 working hours), the quantity of heat transferred increased once more for both STHX A and STHX B. This phenomenon was probably related to a short shut-down of the plant (2 days) necessary for permitting the cleaning of the heating elements inside the tank. During this period, the water inside the two heat exchangers was completely drained; is it possible that in absence of water, the fouling deposits formed on the internal surfaces of the tubes have dried, and consequently, they were easier removed from the heat transfer surfaces at the restart of the plant, because of a shear stress effect, induced by the water flow. However, we observed a restoring of the initial heat transfer performances for the coated heat exchanger (Q increased until 8500 kJ/h); on the contrary, the Q value of the uncoated heat exchanger only slightly increased (7400 kJ/mol) and the initial heat transfer conditions were not restored at all. These experimental evidences suggested the ability of the hydrophobic coating to favor the removal of foulant deposits once deposited on the heat transfer surfaces.

Table 7-8. Comparison between the average daily Q value of the heat exchanger coated by SiO<sub>2</sub>/S10-20/80\_1 (STHX A) and the uncoated heat exchanger (STHX B), at selected time of operation.

Time	Q [kJ/h] STHX A	Q [kJ/h] STHX B
0	8627	8418
200	8969	8672
400	8728	7373
500	7471	7219
600	8544	7409

The ability of the hydrophobic hybrid coating to delay the formation of foulant deposits during the fouling induction period can be observed considering the trend of the overall heat transfer coefficient  $U_{lm}$  (Figure 7-17). Considering the first working period, until 200 hours of operation, the  $U$  values of STHX A and STHX B were very similar each other. From 200 hours to 500 hours, the overall heat transfer coefficient of the uncoated heat exchanger progressively decreased, reaching the minimum (454 W/m<sup>2</sup> K) at 506 hours of work. On the contrary, the  $U$  values of STHX A remained almost stable until 400 working hours; hence, the  $U$  coefficient began to decrease, reaching the minimum at 483 hours of operation (537 W/m<sup>2</sup> K).



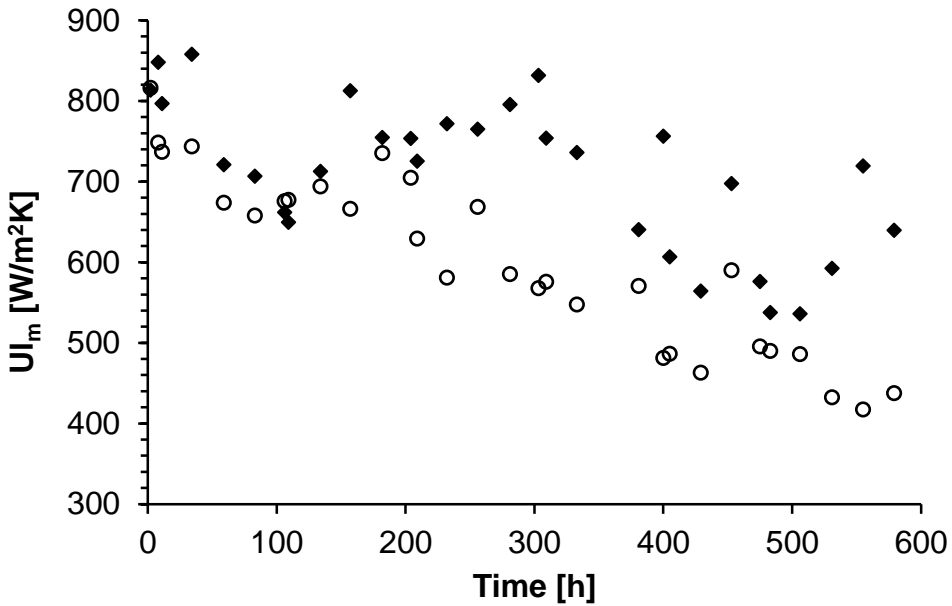


Figure 7-17. Overall heat transfer coefficient ( $U_{lm}$ ) vs time.  $\blacklozenge$  Heat exchanger coated by the hybrid  $\text{SiO}_2/\text{S10}$  formulation (STHX A);  $\circ$  Uncoated heat exchanger (STHX B).

Table 7-9 compares the average  $U_{lm}$  value corresponding to the following sub-period of operation: from 0 to 200 hours, 200-400, 400-550 and 550-600. In the first sub-period, the average  $U$  coefficient of STHX A was higher in respect to the one of STHX B, but the difference was negligible ( $50 \text{ W/m}^2 \text{ K}$ ). In the second period, on the contrary, the overall heat transfer coefficient calculated for the uncoated heat exchanger was much more lower in respect to the coated heat exchanger ( $\Delta U$  between STHX A and B was  $166 \text{ W/m}^2 \text{ K}$ ). In fact, while  $U$  remained almost the same from the first to the second sub-period of operation for STHX A, the one of STHX B decreased of  $90 \text{ W/m}^2 \text{ K}$ . In the third sub-period, the  $U$  value of the coated heat exchanger decreased with the same extent observed for the uncoated heat exchanger in the previous sub-period.

Interestingly, the average  $U$  value of STHX A, measured in the third sub-period, corresponded to the  $U$  value of STHX B measured in the second sub-period. Hence, the passage from the fouling induction period to the fouling period occurred for the coated heat exchanger about 200 hours later in respect to the uncoated heat exchanger. Furthermore, in the third sub-period, the  $U$  value of the uncoated heat exchanger kept on decreasing ( $U$  was  $100 \text{ W/m}^2 \text{ K}$  inferior to the value measured in the second sub-period). At the end of the experimentation, in the last 50 hours of operation (involving the 2 days of shut down of the plant), the overall heat transfer coefficient of STHX A increased once again, reaching a value very similar to the one measured in the first 200 hours of operation. On the other hand, the average value of  $U$  calculated for the uncoated heat exchanger (STHX B) in the last period of operation, were even inferior to the previous one ( $\Delta U = -68 \text{ W/m}^2 \text{ K}$ ).

Table 7-9. Comparison of the average  $U_{lm}$  and  $R_f$  values, corresponding to three sub-periods of operation of the pilot plant, between the coated heat exchanger (STHX A) and the uncoated heat exchanger (STHX B).

<b>Working period [h]</b>	<b><math>U_{lm}</math> STHX A [W/m<sup>2</sup> K]</b>	<b><math>U_{lm}</math> STHX B [W/m<sup>2</sup> K]</b>	<b><math>R_f</math> STHX A [m<sup>2</sup> K/ W]</b>	<b><math>R_f</math> STHX B [m<sup>2</sup> K/ W]</b>
0-200	771	716	$6.5 \cdot 10^{-5}$	$1.1 \cdot 10^{-4}$
200-400	769	598	$7.0 \cdot 10^{-5}$	$4.2 \cdot 10^{-4}$
400-550	599	494	$5.1 \cdot 10^{-4}$	$7.9 \cdot 10^{-4}$
550-600	687	425	$2.5 \cdot 10^{-4}$	$1.2 \cdot 10^{-3}$

The hypothesis assumed observing the trend with time of  $Q$  and  $U_{lm}$ , can be confirmed by the analysis of the fouling resistance values. Figure 7-18 illustrates the trend of  $R_f$  with time. Until 200 hours of operation, the fouling resistance was very low for both the heat exchangers. From 200 hours the  $R_f$  value increased only for the uncoated heat exchanger, while was still almost zero for the coated one. Hence we can suppose that the fouling period started for the uncoated heat exchanger from that time, while the coated heat exchanger was still in the fouling induction period. The first increase in fouling resistance for STHX A was observed after 400 hours of operation, hence, the fouling induction period was prolonged of about 200 hours.

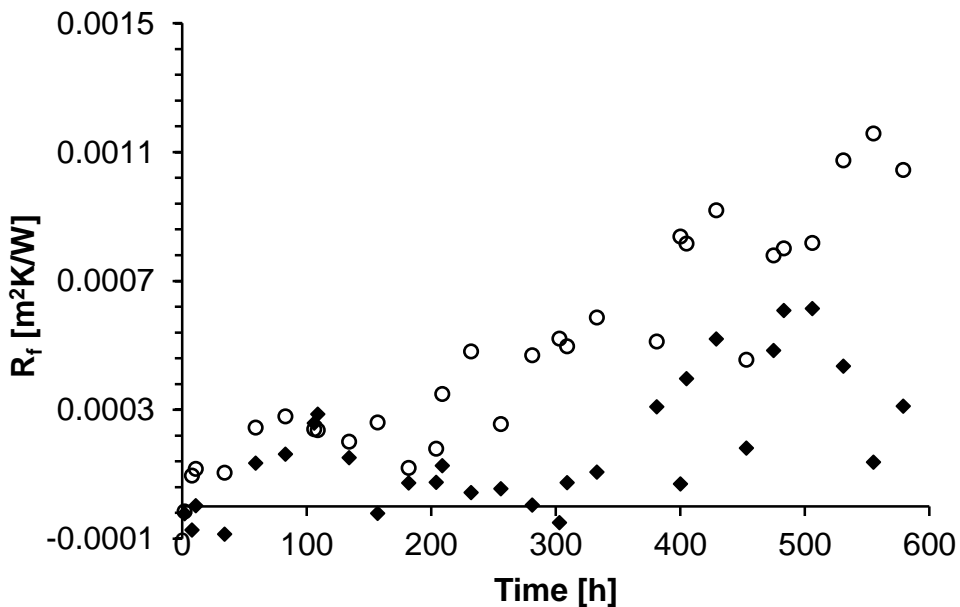


Figure 7-18. Fouling resistance ( $R_f$ ) vs time. ♦ Heat exchanger coated by the hybrid  $\text{SiO}_2/\text{S10}$  formulation (STHX A); ○ Uncoated heat exchanger (STHX B).

Considering Table 7-9, the differences in  $R_f$  between the coated and uncoated heat exchanger in the four sub-periods of operation is clearer. From 0 to 200 hours of operation, the average  $R_f$  value of the coated heat exchanger was very similar to the  $R_f$  value of the uncoated one. On the contrary, from 200 hours of operation, the  $R_f$  values of the uncoated heat exchanger began to increase, while the fouling resistance remained very low for the coated heat exchanger. In the third sub-period we observed a consistent increase of the fouling resistance for STHX A,  $R_f$  value was in fact one order of magnitude higher in respect to the previous one. The average  $R_f$  value measured in the third operation period of STHX A was comparable to the one measured for the uncoated heat exchanger in the second sub period. Indeed, we can assume the formation of foulant layers on the hydrophobic heat transfer surfaces about 200 hours later than the normal heat transfer surfaces. The further increase of fouling resistance on the uncoated heat exchanger during the last sub-period suggests that the uncoated heat transfer surfaces continued to foul (see Table 7-9), even after the shutdown of the plant. On the other hand, in the last period of operation, the fouling resistance of the coated heat exchanger decreased, thanks to the fact that the fouling deposit did not adhere strongly on the hydrophobic surfaces, and therefore were easily removed by shear stresses.

.



## 8 COMPARISON BETWEEN PFPE COATINGS AND COMPOSITE COATINGS

The simple  $\alpha,\omega$ -substituted PFPE coatings (5  $\mu\text{m}$  thickness) were inhomogeneous, and the substrates were only partially covered by the polymer. Anyway, the wettability of the stainless steel substrate was completely changed, and the PFPE coated surfaces appeared hydrophobic (CA range: 120-140°). The PFPE coatings appeared chemically resistant against water or acidic solutions, and mechanically resistant against shear stresses, even if we observed a progressive deterioration of the coatings with time. We experimentally observed the fouling mitigation ability of the PFPE coatings on a heat exchanger pilot plant. Regarding the PFPE coatings based on the Fluorolink<sup>®</sup>S10, in the last period of experimentation (5 month of operation) the fouling resistance value was much inferior for the coated heat exchanger compared to the uncoated one (0.0018 vs 0.0051  $\text{m}^2\text{K/W}$ ). Regarding the polymer Fluorolink<sup>®</sup>F10, we observed the ability of the hydrophobic coating to prolong the fouling induction period and facilitate the foulant removal process. At the end of the experimentation (50 days of operation), in fact, the fouling

resistance values measured for the coated and uncoated heat exchangers were, respectively, 0.000031 m<sup>2</sup>K/W and 0.00027 m<sup>2</sup>K/W. The PFPE coatings effectively limited scale deposits formation on the heat transfer surfaces, however their low resistance against erosion induced by hot water and shear stresses was not sufficient to permit the maintenance of hydrophobic condition for long periods of operation. For this reason we explored the reinforcing effect played by inorganic components, namely metal oxides, which can impart mechanical resistance and hardness to the coatings.

Multilayer coatings had very high contact angle values (>150°). The one prepared by overlapping a Fluorolink<sup>®</sup>S10 film to a film of ZrO<sub>2</sub> nanoparticles impregnated with a silane, showed an improved resistance against mechanical erosion induced by water, in respect to the simple PFPE coatings (the CA decrease was 15-20% higher for the latter after exposition to the same aggressive liquid environments). However, multilayer coatings had very high thickness (~30 μm), which inhibits their application for fouling mitigation in heat transfer surfaces due to their insulator effect.

Hybrid coatings were prepared by the physical combination of the commercial PFPE with a metal oxide network, prepared by sol-gel synthesis, leading to an interspersed structure of the two phases. The preparation of hybrid coatings emerged as the most practical way to combine the hydrophobic properties of the PFPE with the hardness and mechanical resistance of metal oxides. Hybrid coatings containing Fluorolink<sup>®</sup>S10 and the silica network, in particular, possessed the best properties in terms of chemical and mechanical stability, together with high hydrophobicity (CA>130°). Moreover, they formed a homogeneous and continuous layer on the stainless steel substrates, with an average thickness of 7-9 μm. The resistance tests highlighted a CA decrease of less than 10% after

immersion for one month in chemical aggressive liquids or water at high temperature (343 K) and when exposed to wall shear stresses. These results are much better in respect to the ones obtained with the other typologies of coatings. In the pilot plant experimentation, the first increase in fouling resistance, due to formation of scale deposits on the internal surface of the tubes, occurred on the coated heat exchanger about 200 hours later than a normal (not coated) heat exchanger, operating in the same conditions. Therefore, we assumed the effective ability of the hydrophobic hybrid coating to mitigate fouling in heat exchangers. The insulator effect of the hybrid coating, and the influence on surface roughness were not investigated in deep; however, we observed that the heat transfer efficiency of the coated heat exchanger was not compromised by the presence of the coating. These results confirmed the observation made by coating the pilot heat exchanger with the simple PFPE coatings, therefore confirming the interesting properties  $\alpha,\omega$ -functionalized perfluoropolyethers for applications in the field of fouling protection. The great advantage of the combination of the fluoropolymer with inorganic components for the obtainment of a new type of formulation, is the improvement in mechanical resistance, which is key step in the development of an effective industrial coating.





## 9 CONCLUSIONS

In the present PhD research, a particular family of polymer, the organic/inorganic  $\alpha,\omega$ -functionalized perfluoropolyethers, was considered and successfully employed in the field of fouling mitigation in heat exchangers, thus contributing to enrich the current state of the art regarding the utilization of these kind of fluorinated polymers. We prepared a novel type of coating formulation composed by a silica sol-gel network able to interact, physically, with the commercial PFPE. The hybrid coatings obtained showed improved resistance against chemical and physical erosion induced by water, in respect to the simple commercial PFPE coatings. The pilot plant experimentation surely represents an important test bench to determine the possible applicability on larger scale of the coating technology investigated. The design and use of the heat exchanger pilot plant contributed to make more interest and innovative this PhD research, since is not common to find in literature long term experiments performed on pilot heat exchangers of such a dimension, working in continuous conditions. Thanks to the experimentations on the pilot plant, we could observe not only the real influence of the hybrid coating in foulant deposition on heat transfer surfaces, but also we could demonstrate the possibility to produce in large scale the coating formulation developed. Clearly, the working conditions

adopted in the experiments with the pilot plant cannot ensure the applicability of these coatings in every type of industrial plant. However, in view of the results obtained from resistance tests and pilot plant, we can suppose the ability of the hybrid coatings to control fouling on heat transfer surfaces, together with other fouling mitigation strategies, on those pilot plant working in not severe conditions, for example with water as heat exchanging fluid and with temperature varying from 323 to 343 K.

## BIBLIOGRAPHY

- [1] T. R. Bott, Fouling of heat exchangers, T. R. Bott, Ed., The Netherlands: Elsevier Science and Technology Book, 1995.
- [2] H. Muller-Steinhagen and H. Zettler, Eds., Heat exchanger fouling. Mitigation and cleaning technologies, Israel: PP Publico Publications, 2011.
- [3] D. Q. Kern, Process heat transfer, International student edition a cura di, Tokio: McGraw-Hill Book Company, 1983.
- [4] L. Forni and I. Rossetti, Fenomeni di trasporto, F. L. and R. I., Eds., Milano, Italy: Libreria Cortina Milano, 2009.
- [5] H. Muller-Steinhagen, M. Malayeri and A. Watkinson, "Heat exchanger Fouling: mitigation and cleaning strategies," *Heat Transfer Engineering*, Vols. 32(3-4), pp. 189-196, 2011.
- [6] H. Muller-Steinhagen and M. W. A. Malayeri, "Fouling of heat exchangers-New approaches to solve an old problem," *Heat Transfer Engineering*, vol. 26, pp. 1-4, 2005.
- [7] C. Magin, S. Cooper and A. Brennan, "Non-toxic antifouling strategies," *Material Today*, vol. 10, pp. 36-44, 2010.
- [8] R. Baier, "Modification of surfaces to reduce fouling and/or improve cleaning," in *Proceedings of Fundamentals and Applications of Surface*

*Phenomena Associated with Fouling and Cleaning in Food Processing*, Tylosand, 1981.

- [9] R. Baier, “Surface behaviour of biomaterials: the theta surface for biocompatibility,” *Journal of Material Science: Material Medicine*, vol. 17, pp. 1057-1062, 2007.
- [10] M. Żenkiewicz, “Methods for the calculation of surface free energy of solids,” *Journal of Achievements in Materials and Manufacturing Engineering*, vol. 24, pp. 137-145, 2007.
- [11] K. Grundke, “Wetting, spreading and penetration,” in *Handbook of Applied Surface and Colloid Chemistry*, vol. 2, Great Britain: Holmberg K., 2001, pp. 119-138.
- [12] A. Marmur, “Super-hydrophobicity fundamentals: implications to biofouling prevention,” *Biofouling: The Journal of Bioadhesion and Biofilm Research*, vol. 22, pp. 107-115, 2007.
- [13] Q. Zhao, Y. Liu, C. Wang, S. Wang and H. Müller-Steinhagen, “Effect of surface free energy on the adhesion of biofouling and crystalline fouling,” *Chemical Engineering Science*, vol. 60, p. 4858 – 4865, 2005.
- [14] M. R. Malayeri, A.-J. A. and H. Muller-Steinhagen, “Application of nano-modified surfaces for fouling mitigation,” *International Journal of Energy Research*, vol. 33, p. 1101–1113, 2009 .
- [15] R. Oliveira, “Understanding adhesion: a means for preventing fouling,”

- Experimental Thermal and Fluid Science*, vol. 14, pp. 316-322, 1997.
- [16] M. Forster and M. Bohnet, "Influence of the interfacial free energy crystal/heat transfer surface on the induction period during fouling," *International Journal of Thermal Science*, vol. 38, pp. 944-954, 1999.
- [17] M. Forster and M. Bohnet, "Modification of molecular interactions at the interface crystal/heat transfer surface to minimize heat exchanger fouling," *International Journal of Thermal Science*, vol. 39, pp. 697-708, 2000.
- [18] G. Bixler, A. Theiss, B. Bhushan and S. Lee, "Anti-fouling properties of microstructured surfaces bio-inspired by rice leaves and butterfly wings," *Journal of Colloid and Interface Science*, vol. 419, p. 114-133, 2014.
- [19] H. Muller-Steinhagen and Q. Zhao, "Investigation of low fouling surface alloys made by ion implantation technology," *Chemical Engineering Science*, vol. 52, pp. 3321-3332, 1997.
- [20] A. Bornhorst, H. Muller-Steinhagen and Q. Zhao, "Reduction of scale formation under pool boiling conditions by ion implantation and magnetron sputtering on heat transfer surfaces," *Heat Transfer Engineering*, vol. 20, pp. 6-14, 1999.
- [21] H. Muller-Steinhagen, Q. Zhao, A. Helali-Zadeh and R. X., "The effect of surface properties on CaSO<sub>4</sub> scale formation during convective heat transfer and subcooled flow boiling," *The Canadian Journal of Chemical Engineering*, vol. 78, pp. 12-20, 2009.

- [22] R. Rosmaninho, O. Santos, T. Nylander, M. Paulsson, M. Beuf, T. Benezech, S. Yiantsios, N. Andritsos, A. Karabelas, G. Rizzo, H. Muller-Steinhagen and L. Melo, “Modified stainless steel surfaces targeted to reduce fouling – Evaluation of fouling by milk components,” *Journal of Food Engineering* , vol. 80, p. 1176–1187, 2007.
- [23] Cheng, Y.H.; Chen, H.Y.; Zhu, Z.C.; Jen, T.C.; Peng, Y.X., “Experimental study on the anti-fouling effects of Ni-Cu-P-PTFE deposit surface of heat exchangers,” *Applied Thermal Engineering* , vol. 68, pp. 20-25, 2014.
- [24] Y. Takata, S. Hidaka and U. T., “Boiling feature on a super water-repellent surface,” *Heat Transfer Engineering*, vol. 27, pp. 25-30, 2006.
- [25] Y. W. Cai, M. Y. Liu and L. F. Hui, “CaCO<sub>3</sub> Fouling on microscalenascale-nanoscale hydrophobic Titania-Fluoroalkylsilane films in pool boiling,” *AIChE Journal* 2013, vol. 59, p. 2662–2678, 2013.
- [26] Y. Cai, M. Liu and L. Hui, “Observations and mechanism of CaSO<sub>4</sub> fouling on hydrophobic surfaces,” *Industrial Engineering Chemical Research* , vol. 53, p. 3509–3527, 2014.
- [27] Q. Yanga, Y. Liu, A. Gua, J. Ding and Z. Shen, “Investigation of induction period and morphology of CaCO<sub>3</sub> fouling on heated surfaces,” *Chemical Engineering Science* , vol. 57, pp. 921-931, 2002.
- [28] Y. Wang, L. Wang and L. Ming-yan, “Antifouling and enhancing pool boiling by TiO<sub>2</sub> coating surface in nanometer scale thickness,” *AIChE*

*Journal*, vol. 53, pp. 3062-3076, 2007.

- [29] R. Thomas, "Material properties of fluoropolymers and perfluoroalkyl-based polymers," in *Fluoropolymers 2 - Properties*, G. Hougham, P. Cassidy, K. Johns and D. T., Eds., Online version, Springer Link, 1999, pp. 47-67.
- [30] M. Vecellio, "Opportunities and developments in fluoropolymeric coatings," *Progress in Organic Coatings*, vol. 40, p. 225–242, 2000.
- [31] M. Fowzy, «PFPE, a unique lubricant for a unique application,» Downers Grove, Illinois, 1998.
- [32] J. Yarbrough, J. Rolland, J. DeSimone, M. Callow, J. Finlay and J. Callow, "Contact angle analysis, surface dynamics, and biofouling characteristics of cross-linkable, random perfluoropolyether-based graft terpolymers," *Macromolecules*, vol. 39, pp. 2521-2528, 2006.
- [33] S. Kwon, H. Kim, J. Ha and S. Lee, "Prevention of protein and polymeric nanoparticles adsorption using perfluoropolyethers," *Industrial & Engineering Chemistry*, pp. 259-263, 2011.
- [34] C. Tonelli, P. Gavezotti and S. E., "Linear perfluoropolyether difunctional oligomers: chemistry, properties and applications," *Journal of Fluorine Chemistry*, vol. 95, pp. 51-70, 1999.
- [35] G. Gu, X. Shen and F. Qing, "Preparation and tribological performance of perfluoropolyether derived coatings," *Applied Surface Science*, vol. 253,



p. 6980–6986, 2007.

- [36] D. Mitzi, “Thin film deposition of organic-inorganic hybrid materials,” *Chemistry of Materials*, vol. 13, pp. 3283-3298, 2001.
- [37] D. Wang and G. Bierwagen, “Sol–gel coatings on metals for corrosion protection,” *Progress in Organic Coatings*, vol. 64, p. 327–338, 2009.
- [38] D. Del Angel-Lopez, D.-C. M. A., T.-H. A.M., F.-V. A., J. Andraca-Adame and D.-R. H., “Analysis of degradation process during the incorporation of ZrO<sub>2</sub>:SiO<sub>2</sub> ceramic nanostructures into polyurethane coatings for the corrosion protection of carbon steel,” *Journal of Material Science*, vol. 48, p. 1067–1084, 2013.
- [39] K. Strzelek and P. P., “Improvements of mechanical properties and electrical conductivity of polythiourethane-modified epoxy coatings filled with aluminium powder,” *Progress in Organic Coatings*, vol. 63, pp. 133-138, 2008.
- [40] X. Ji, J. Hampsey, Q. Hu, J. He, Z. Yang and Y. Lu, “Mesoporous silica-reinforced polymer nanocomposites,” *Chemistry of Materials*, vol. 15, pp. 3656-3662, 2003.
- [41] H. Fischer, “Polymer nanocomposites: from fundamental research to specific applications,” *Materials Science and Engineering*, vol. 23, p. 763–772, 2003.
- [42] I. Kartsonakis, E. Koumoulos, A. Balaskas, G. Pappas, C. Charitidis and

- K. G.C., “Hybrid organic–inorganic multilayer coatings including nanocontainers for corrosion protection of metal alloys,” *Corrosion Science*, vol. 57, p. 56–66, 2012.
- [43] P. Zurlini, A. Lorenzi, I. Alfieri, G. Gnappi, A. Montenero, N. Senin, R. Groppetti and F. P., “Titanium and zirconium hard coatings on glass substrates prepared by the sol-gel method,” *Thin Solid Films*, vol. 517, p. 5881–5887, 2009.
- [44] O. Carp, C. Huisman and A. Reller, “Photoinduced reactivity of titanium dioxide,” *Progress in Solid State Chemistry*, vol. 32, p. 33–177, 2004.
- [45] X. Li, R. Song, Y. Jiang, C. Wang and D. Jiang, “Surface modification of TiO<sub>2</sub> nanoparticles and its effect on the properties of fluoropolymer/TiO<sub>2</sub> nanocomposite coatings,” *Applied Surface Science*, vol. 276, p. 761–768, 2013.
- [46] F. Milanesi, G. Cappelletti, R. Annunziata, C. L. Bianchi, D. Meroni and A. ., “Siloxane-TiO<sub>2</sub> hybrid nanocomposites. The structure of the hydrophobic layer,” *Journal of Physical Chemistry*, vol. 114, p. 8287–8293, 2010.
- [47] J. Wen and G. Wilkes, “Organic/Inorganic hybrid network materials by the sol-gel approach,” *Chemistry of Materials*, vol. 8, pp. 1667-1681, 1996.
- [48] R. Suriano, V. Oldani, C. Bianchi and S. Turri, "AFM nanomechanical properties and durability of new hybrid fluorinated sol-gel coatings,"

*Surface and Coatings Technology*, vol. 264, p. 87–96, 2015.

- [49] S. Pandey and S. Mishra, “Sol–gel derived organic–inorganic hybrid materials: synthesis, characterization and applications,” *Journal of Sol-Gel Science and Technology*, vol. 59, p. 73–94, 2011.
- [50] K. Yoshinaga, “Functionalization of inorganic colloidal particles by polymer modification,” *Bulletin of the Chemical Society of Japan*, vol. 75, pp. 2349-2358, 2002.
- [51] M. Wouters, C. Rentrop and P. Willemsen, “Surface structuring and coating performance. Novel biocidefree nanocomposite coatings with anti-fouling and fouling-release properties,” *Progress in Organic Coatings* , vol. 68, pp. 4-11, 2010.
- [52] M. Berglin, K. Wynne and P. Gatenholm, “Fouling-release coatings prepared from  $\alpha,\omega$ -dihydroxypoly(dimethylsiloxane) cross-linked(heptadecafluoro-1,1,2,2-tetrahydrodecyl)triethoxysilane with,” *Journal of Colloid and Interface Science* , vol. 257, p. 383–391, 2003.
- [53] a. Singh, P. Singh, S. Mishra and V. Shahi, “Anti-biofouling organic-inorganic hybrid membrane for water treatment,” *Journal of Material Chemistry*, vol. 22, pp. 1834-1844, 2012.
- [54] S. Kermadi, N. Agoudjil, S. Sali, M. Boumaour, S. Bourgeois and M. Marco de Lucas, “Sol-gel synthesis of  $x\text{TiO}_2(100 - x)\text{SiO}_2$  nanocomposite thin films: structure, optical and antireflection properties,”

*Thin Solid Films*, vol. 564, p. 170–178, 2014.

- [55] Outo Kumpo, “Thecnical sheet Data”.
- [56] Solvay-Solexis, «Fluorolink surface treatments agents. Product Data Sheet,» [www.solvaysolexis.com](http://www.solvaysolexis.com), 2002.
- [57] W. Navarrini, T. Brivio, D. Capobianco, M. Diamanti, M. Pedefferri, L. Magagnin and G. Resnati, “Anti-fingerprints fluorinated coating for anodized titanium avoiding color alteration,” *Journal of Coatings Technology Research*, vol. 8, pp. 153–160,, 2011.
- [58] E. Fabbri, P. Fabbri, M. Messori, M. Montecchi and F. Pilati, “Perfluoropolyethers-silica hybrids: preparation and surface characterization,” *Journal of Sol-Gel Science and Technology*, vol. 34, pp. 155-163, 2005.
- [59] C. Bianchi, S. Ardizzone, G. Cappelletti, G. Cerrato, W. Navarrini and M. Sansotera, “Nanostructured TiO<sub>2</sub> modified by perfluoropolyethers: gas phase photocatalytic activity,” *Journal of Materials Research*, vol. 1, pp. 96-103, 2010.
- [60] A. Kessman, K. Ramji, N. Morris and D. Cairns, "Zirconia sol–gel coatings on alumina–silica refractory material for improved corrosion resistance," *Surface & Coatings Technology*, vol. 204, p. 477–483, 2009.
- [61] Kruss, Software for drop shape analysis DSA 1 - User Manual, Hamburg, 2012, pp. 166-170.

- [62] Y. Yuan and T. Lee, "Contact angle and wetting properties," in *Surface Science Techniques*, vol. 51, G. Bracco and B. Holst, Eds., Berlin Heidelberg, Springer Series in Surface Sciences, 2013.
- [63] D. Meroni, S. Ardizzone, G. Cappelletti, M. Ceotto, M. Ratti, R. Annunziata, M. Benaglia and R. L., "Interplay between chemistry and texture in hydrophobic TiO<sub>2</sub> hybrids," *The Journal of Physical Chemistry C*, vol. 115, pp. 18649-18658, 2011.
- [64] C. van Oss, R. Good and M. Chaudhury, "Additive and non-additive surface tension components and the interpretation of contact angles," *Langmuir*, vol. 4, pp. 884-891, 1988.
- [65] C. Henry, J. Minier and G. Lefèvre, "Towards a description of particulate fouling: From single particle deposition to clogging," *Advances in Colloid and Interface Science*, vol. 185-186, p. 34-76, 2012.
- [66] A. Dimian, C. Bildea and A. Kiss, *Integrated design and simulation of chemical processes*, Second Edition ed., Amsterdam: Elsevier, 2014, pp. 780-784.
- [67] A. Costa and E. Queiroz, "Design optimization of shell-and-tube heat exchangers," *Applied Thermal Engineering*, vol. 28, p. 1798-1805, 2008.
- [68] B. Hasan, G. Nathan, P. C. R. Ashman and R. Kelso, "The effects of temperature and hydrodynamics on the crystallization fouling under cross flow conditions," *Thermal Applied Engineering*, vol. 36, pp. 210-218,

2012.

- [69] T. Geddert, W. Augustin and S. Scholl, "Induction time in crystallization fouling on heat transfer surfaces," *Chemical Engineering & Technology*, vol. 34, pp. 1303-1310, 2011.
- [70] A. Herz, M. Malayeri and H. Müller-Steinhagen, "Fouling of roughened stainless steel surfaces during convective heat transfer to aqueous solutions," *Energy Conversion and Management*, vol. 49, pp. 3381-3386, 2008.
- [71] V. Oldani, *Usa di coating perfluorurati per la protezione dal fouling delle superfici metalliche di scambiatori di calore*, 2012.
- [72] V. Gnielinski, "Equation for calculating heat transfer in single tube rows and banks of tubes in transverse flow," *International Journal of Chemical Engineering*, vol. 19, pp. 380-400, 1979.
- [73] W. Rohsenow, J. Hartnett and Y. Cho, Eds., *Handbook of heat transfer*, 3rd. ed., United States of America: McGraw-Hill, 1998.
- [74] V. Oldani, C. Bianchi, S. Biella, C. Pirola and G. Cattaneo, "Perfluoropolyethers coatings design for fouling reduction on heat transfer stainless steel surfaces," *Heat Transfer Engineering*, 2015.
- [75] J. Moulder, W. Stickle, P. Sobol and K. Bomben, *Handbook of X-ray photoelectron spectroscopy*, J. Chastainc, Ed., United States of America: Perkin-Elmer Corporation Publication, 1992.

- [76] D. Briggs and M. Seah, Practical surface analysis, 2nd ed., vol. 1, John WILEY & SONS, 1993.
- [77] V. Oldani, R. del Negro, C. Bianchi, R. Suriano, S. Turri, C. Pirola and B. Sacchi, "Surface properties and anti-fouling assessment of coatings obtained from perfluoropolyethers and ceramic oxides nanopowders deposited on stainless steel," *Journal of Fluorine Chemistry*, vol. 180, pp. 7-14, 2015.
- [78] J. MacKenzie and E. Bescher, "Physical properties of sol-gel coatings," *Journal of Sol-Gel Science and Technology*, vol. 19, pp. 23-29, 2000.
- [79] H. Ebert, M. Knecht, M. Muhler, O. Helmer and W. Bensch, "Experimental and theoretical bandstructure of the layer compound ZrSiTe," *Journal of Physical Chemistry*, vol. 99, pp. 3323-3330, 1995.

## LIST OF PUBLICATIONS

### Publications on peer reviewed journals

**V. Oldani**, R. del Negro, C.L. Bianchi, R. Suriano, S. Turri, C. Pirola, B. Sacchi, Surface properties and anti-fouling assessment of coatings obtained from perfluoropolyethers and ceramic oxides nanopowders deposited on stainless steel, *Journal of Fluorine Chemistry*, vol. 180, p. 7-14, 2015.

**V. Oldani**, C.L. Bianchi, S. Biella, C. Pirola and G. Cattaneo, Perfluoropolyethers coatings design for fouling reduction on heat transfer stainless steel surfaces, *Journal of Heat Transfer Engineering*, DOI: 10.1080/01457632.2015.1044417.

R. Suriano, **V. Oldani**, C.L. Bianchi, S. Turri, AFM nanomechanical properties and durability of new hybrid fluorinated sol-gel coatings, *Surface & Coatings Technology*, vol. 264, p. 87-96 (2015).

C. de Marco, **V. Oldani**, C.L. Bianchi, M. Levi, S. Turri, A biomimetic surface treatment to obtain durable omniphobic textiles, *Journal of Applied Polymer Science*, vol. 132, p. 42404-42412 (2015).

R. Djellabi, M.F. Ghorab, G. Cerrato, S. Morandi, S. Gatto, **V. Oldani**, A. di Michele, C.L. Bianchi, Photoactive TiO<sub>2</sub>-montmorillonite composite for degradation of organic dyes in water, *Journal of Photochemistry and Photobiology A: Chemistry*, vol. 295, p- 57-63, 2014.



### **Publications in conference proceedings (peer reviewed)**

V. Oldani, C.L. Bianchi, S. Biella, C. Pirola and G. Cattaneo, Use of perfluoropolyether coatings to mitigate fouling on heat exchanger metal surfaces, Proceedings of Heat Transfer Fouling and Cleaning X Conference, 2013.

## COMMUNICATIONS AT CONGRESSES

V. Oldani, C.L. Bianchi, S. Biella, C. Pirola, G. Cattaneo, Use of perfluoropolyethers coating to mitigate fouling on heat exchanger metal surfaces, **X Heat Transfer Fouling and Cleaning Conference**, June 9-14, 2013, Budapest (poster presentation).

V. Oldani, C.L. Bianchi, S. Biella, C. Pirola, G. Cattaneo, Perfluoropolyethers coatings whit hydrophobic properties for fouling protection on heat transfer metal surfaces, **IX Convegno Nazionale INSTM sulla Scienza e Tecnologia dei Materiali**, June 30 – July 3, 2013, Bari (oral presentation).

V. Oldani, C.L. Bianchi, C. Pirola, R. del Negro, G. Cattaneo, Hydrophobic coatings obtained from perfluoropolyethers and metal oxides for fouling mitigation on heat transfer surfaces, **X Coatings Science International**, June 23 – 27, 2014, Noordwijk (oral presentation).

V. Oldani, G. Sergi, C.L. Bianchi, C. Pirola, Reinforcement of perfluoropolyethers coatings by ceramic oxides sol-gels for fouling mitigation on metal surfaces, **X Convegno Nazionale INSTM sulla Scienza e Tecnologia dei Materiali**, June 28 – July 1, 2015 Favignana (oral presentation).